THE UNIVERSITY *of* EDINBURGH

Reaction Force Control Implementation of a Linear Generator in Irregular Waves for a Wave Power System

Bin Li

Submitted in satisfaction of the requirements
for the degree of *Doctor of Philosophy* in

THE UNIVERSITY OF EDINBURGH

October 2012

Abstract

Most designs for wave energy converters include a hydraulic (or pneumatic) interface between the wave device and the generator to smooth electricity production, but a direct drive power take-off system is a possible way of increasing the power transfer efficiency and the reliability, which was first adopted by Archimedes Wave Swing. Direct drive wave energy systems normally include a low speed linear generator directly coupled with the wave device. With no mechanical interface, the mechanical energy loss and maintenance requirements can, in theory, be significantly reduced.

To maximize the energy capture, the motion of the wave energy converter must be controlled to achieve mechanical resonance so that the velocity is in phase with the incoming waves. So far, a number of control methods have been proposed, but few of them have been tested experimentally. For direct drive linear generators in real sea conditions, reaction force control is shown to be an effective way to achieve control where knowledge of future wave could not be required.

Different reaction force control methodologies are suggested where the force is provided directly from the linear generator. Among these methodologies, complex conjugate control is regarded as the optimal control and can be used to achieve mechanical resonance. When resonance occurs, some system parameters such as the system excursion and required power take-off force become extremely large, and may exceed the design parameters. In this thesis, the system is modelled under reaction force control taking into account practical considerations which are based on design parameters.

A novel control scheme for a direct drive linear generator to achieve such reaction force control in irregular waves is proposed, where a voltage-source rectifier is employed as the bridge between the linear generator and the dc bus. The application of linear generator in real wave conditions not only has inherent advantages, but also present a big challenge for controller design in order to obtain maximum power production. For

a linear generator in real sea states, reaction force control idea can be implemented to adjust the velocity of motion, hence to maximize the power production, where the required currents in the generator coils to provide the desired force are constantly varying in frequency and amplitude. The control strategy of the active rectifier is developed based on the derived three-phase currents and the dynamic response of the system to determine varying modulation indices. The unknown situations and some unmeasurable parameters in the system degrade the performance of the control system, hence the current feedback and PI controller are both adopted to reject the effect of the disturbance. Simulation verifications are included for the proposed control idea.

Acknowledgements

I offer my first and foremost sincerest gratitude to my supervisor, Dr Ewen Macpherson, who had supported me throughout my PhD work with his patience and knowledge whilst allowing me the room to work in my own way. I attribute the level of my PhD degree to his encouragement and effort. I would also like to express much gratitude to Professor Markus Mueller who has offered much advice and his experience throughout my work.

In the beginning of my PhD course, Ally Price and David Forehand provided great help to let me get my PhD started very quickly. Due to their help, I could finish my first part in a reasonable time period. I also would like to offer my sincere gratitude to my colleagues, Jonathan Shek, Estanislao JuanPablo Echenique Subiabre, Ozan Keysan, Ahmad Zaki Annuar, Yew Chong and Isaac Portugal Rosas, for their on call help and talking to me during my spare time which made boring PhD time fly.

Finally, I would like to thank my parents Li Zhenzhong and Zhang Yingchun for there continued financial support and care. Also, I would like to thank my wife Wei Wei for her love and support. In particular, I would like to thank my little daughter. Her arrival gave me a lot courage to finish this thesis.

Declaration

I declare that this thesis was composed by myself, that the work contained herein is my own except where explicitly stated otherwise in the text, and that this work has not been submitted for any other degree or professional qualification except as specified.

Bin Li

Contents

Figures and Tables

Figures

Tables

Chapter 1

Introduction

1.1 Introduction to Wave Energy

Global research into renewable energy began in the early 1970s in response to the imminent oil crisis. To date various types of renewable energy have been developed and introduced such as wind power, hydropower, solar energy, biomass, biofuel and geothermal energy. Wave energy can be considered a type of ocean energy which is another form of solar energy. In the late 1970s, several European countries, including the UK, Sweden and Norway initiated their research on wave energy under the Research and Development (R&D) program. However, in the following decade between the early 1980s and 1990s, this research was dramatically curtailed or even abandoned due to falling petrol prices [1]. The last decade has been an incredibly exciting time for wave energy research due to the ever-increasing concerns over air pollution and global warming. It has been estimated that 65% of the world's greenhouse-gas emissions come from energy production [2]. In addition, surging oil and gas prices force wave energy researchers to find a solution of raising power production in order to supply the world's growing energy needs. In 2003, the International Energy Agency (IEA) received an agreement on international co-operation in developing wave and tidal energy technologies from Canada, Denmark, Ireland, Japan, Portugal and United Kingdom [3]. During the past five years, the technology of wave energy has been transferred from academic research to real commercial installations. In late 2008 the world's first commercial wave farm was estabilished by Pelamis Wave Power in Portugal. To date, approximately 100 wave energy concepts have been proposed and tested all over the

world but among them Portugal and the United Kingdom are two leading countries in prototype development [4].

The work presented in this thesis concerns the control of a direct drive linear generator to generate the most power that can be extracted from irregular waves. Computer-aided simulation is applied to analyse the control process and power output. Experimental work which was done in Shek's work [5] is not available anymore to this work. In Shek's work, linear generator was placed on a test rig and was driven by a rotating motor to provide a regular motion as in regular waves. However, such a rotating motor is not able to provide an irregular motion which is the same as that a linear generator experiences in irregular waves. Therefore, in this thesis, experiment verification is not included due to the prohibitive cost of an irregular waves experimental platform which cannot be built in the lab, and immature control technology, therefore, further work must be carried out in the real sea conditions.

1.1.1 Wave Energy Resource

Wave energy can be regarded as a specific type of solar energy, where wind is considered the transmission medium carrying energy from solar energy and transferring some of its energy to generate sea waves. The amount of power transferred to the waves is mainly determined by wind speed, time and distance the winds blow across the oceans [6]. Waves can carry the stored energy, travelling thousands of kilometres until head winds are encountered or they reach the coastline [7]. In contrast, energy stored in waves can be intensified by fair winds that blow over existing waves. In general, offshore waves hold more energy than either nearshore or shoreline waves. Data in [8] shows annual wave energy production offshore can be 25 times greater than nearshore and 125 times greater than shoreline.

An enormous amount of wave energy is unevenly distributed worldwide, and its energy density is the highest among renewable energy sources with available energy per square metre reaching 15-20 times more than either wind or solar [9]. The estimated market potential is in excess of 2,000 TWh which could supply 10 % of total global electricity

consumption [6]. Most of the wave energy resource spreads over several countries with long coastlines such as South Africa, Australia, United Kindom, Norway, United States and Canada. However, not all countries with a long coastline have high wave energy. China, for example, has about 14,500 kilometres coastline but the wave energy power per metre is only 1/14 of that of the United Kindom, due to waves originating in the east being dispersed or decreased by the islands of Japan and the Korean Peninsula.

1.1.2 Current Status and Future Development of Wave Energy

Wave energy has the potential to become one of the most competitive renewable resources providing energy in the future due to its high energy density. So far a range of different technologies and their corresponding devices have been developed, with as yet no clear winner emerging. A number of methods are proposed to classify wave energy devices, with emphasis on three principal categories which are the positions, power take-off (PTO) types and device types. Firstly, devices can be installed either onshore, near shore and off shore with their own advantages and disadvantages. The further out the device is installed the more wave energy might be obtained but installation and maintenance will become more difficult. Secondly, if wave energy devices are classified according to PTO systems, there are hydraulic, pneumatic and direct drive PTO systems. Currently, most wave energy developers are focusing on either a hydraulic or pneumatic PTO system as their preferred energy conversion method, which does not mean that direct drive systems are not suitable for wave energy. As within the thesis scope that only off shore wave energy devices are considered, it can be finally broken down into several types below:

- Point Absorber was first proposed in [10] with a floating buoy (the shape can be designed based on the designer's criterion) having a much smaller horizontal dimension compared to wave length. Based on present knowledge, a point absorber is the only device that a direct drive linear generator can be fixed on in wave energy.
- Attenuator/Contouring device with a number of identical components linked

together which lies on the sea surface. Power is generated due to the relative motion between each section.

- Overtopping device is constructed with a reservoir filled by ocean waves that are higher than the device. A turbine is mounted under the reservoir and driven by seawater flowing out of the device.

Figure 1.1 [6], shows the proportion of different types of wave energy devices that have been suggested so far. The point absorber is the most widely used device because of its smaller structure which contributes to a larger ratio between potentially converted power and structural volume [11], as well as its simple installation and ease of connection to different types of energy conversion systems.

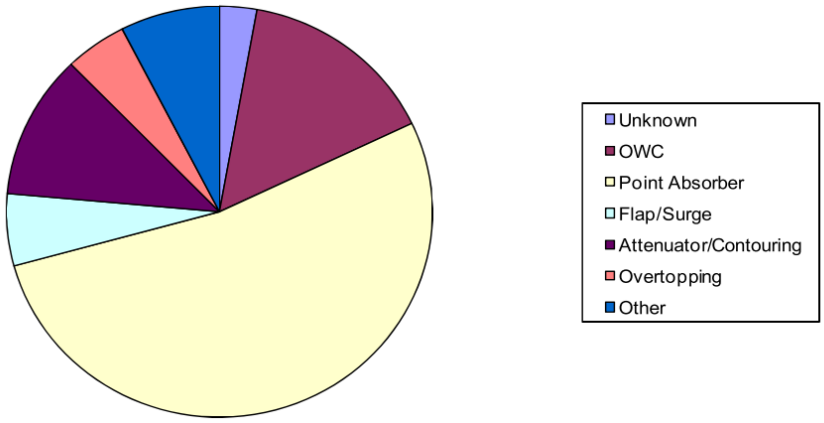

Figure 1.1: Breakdown of current wave energy devices by type.

Wave energy cannot become a predominant energy supplier in the next few years, because most wave energy technologies are currently immature and still at the R&D stage. Investment for manufacturing and installation is very high, so that the payback period is extended. However, high energy density of the resource is one of the reasons wave energy could become one of the major renewable energy technologies in the future. Wave energy is a clean energy; greenhouse gasses or other atmospheric pollutants are not produced while generating electricity. Low amount of emissions do exist during the whole life-cycle of wave energy devices such as in manufacture, transport and installation [12]. Other environmental impacts such as biological and noise related are technically solvable by increasing the investment during projects.

1.1.3 European Wave Energy Policies and Plans

Europe has the world's most abundant wave energy resource that attracts several developed countries to exploit their own technologies to increase energy production. Wave energy technology development can be also regarded as a potential solution to the financial crisis of 2008/09, which is attributed partly to volatile oil prices [13]. Hence some device developers could receive considerable financial and political support in becoming leading wave energy industries in the world. In return, these companies can directly or indirectly contribute to economic recovery. For some countries with a slightly more mature wave technology, such as Ireland, Portugal, Spain and UK, long term plans (to 2020) have been proposed in innovation, manufacturing and deployment. As a leader in global wave energy, the Scottish government announced a Wave and Tidal Energy Support Scheme (WATES) with £ 13 million capital and revenue grant. Maritime communities are very interested in developing several projects in the future on Islay, Shetland and Orkney [14]. In order to stimulate technology development, a £ 10 million Saltire Prize was announced on 23rd March 2010, which will be awarded to a winning company with the final goal to produce a continuous 100 GWh electrical output in Scottish waters for 2 years before 2017 [15]. In Ireland, a funding scheme has reached its third stage, a full scale pre-commercial array between 2011-2015 whose investment is about € 11.15 million. Portugal had a PRIME-DEMTEC (Incentive Scheme for the Implementation of Pilot Projects Related to Technologically Innovative Products, Processes and Systems) scheme between 2000 and 2006 which has been replaced by QREN (a Portugal Organization) running between 2007-2013. In Denmark, a financial support from RTD (a Danish Company) with € 13 million was completed at the end of 2011 [16]. Other device developers are seeking further technology development with the aid from government support and policy. Edinburgh-based Aquamarine Power unveiled its second Oyster wave energy device in the summer of 2011 to capture 800 kW power, followed by two further identical devices in Orkney in 2012 and 2013 [17]. Another Scottish company, Archimedes Wave Swing (AWS) Ocean Energy, has just secured £ 2 million for developing its AWS- III with generating

capacity between 2.4 MW and 4 MW. A full-system prototype was created in 2011 which will result in a pre-commercial demonstrator plant in 2013 [18].

1.2 Motivations and Objectives

Various types of WECs have been developed, among which heaving point absorbers are deemed as the simplest and most promising concepts. This up and down motion point absorber can employ an energy conversion system based on either a hydraulic PTO or an electrical direct drive PTO. The hydraulic system is the most widely used and has been tested on many devices in the last decade due to its capability of short term energy storage for smoothing power flow. Energy extraction can be amplified by simply opening the accumulators mechanically to provide an acceleration increase on the buoy when the peak of the wave excitation force is detected, hence the so called phase control can be achieved [19], [20].

The use of a linear generator simplifies the whole system by eliminating the mechanical interface such that the power transfer efficiency and reliability can be improved. A range of different control strategies that have been tested or simulated for hydraulic systems can also be applied to such systems. There is no common consensus on a clear "winner" yet as the choice of control method partly depends on the size of the buoy and the sea state [21]. Reaction force control uses the force from the linear generator, thus mechanical interaction can be further removed, such as in latching control which requires brake pads or friction brakes. Also by taking the reaction force control to the limit, known as full complex conjugate control, absolute mechanical resonance can be achieved. However, due to the limitations on linear generator design and drawbacks of this control strategy, perfect reaction force control, in reality, has not been achieved so far. Hence, reaction force control of a linear generator in irregular waves with realistic considerations is of great interest in terms of extracting maximum power.

Different from a conventional rotary machine where the rotating speed can be operated at a constant speed most of time to produce a regular back EMF with unique peak

voltage and frequency, the output of a linear generator varies in both amplitude and frequency due to its linear motion. This leads on to a difficulty of how to implement the proposed control method into the system. To date, power converter control to achieve reaction force control can only be achieved on a conventional rotary machine, such as in [22] or on a linear generator in regular ocean waves [5]. Hence, this thesis is motivated by finding a solution to implementing reaction force control onto a direct drive linear generator in irregular waves. In this work, irregular waves interacting with a direct drive WEC with reaction force control is focused upon which is followed by the implementation of reaction force control by controlling the power converter. There are several objectives listed below that need to be achieved.

- Random ocean waves are required as the preliminary input for the system model. The frequency domain energy spectrum is converted to time domain ocean waves by applying an Inverse Fourier Transform. Different random waves can be generated by giving a different peak frequency and random phases.
- The complex conjugate control, which is also called sub-optimal mass-spring-damping control, method is simulated to extract maximum power. In this work, ocean wave prediction is not included, hence only near mechanical resonance can be achieved by supplying the peak frequency to the control system.
- There are four different reaction force control methods. Three of them are reactive force control which uses the reactive power to amplify the velocity. The method which does not apply reactive force is called real control. Therefore, the comparison of power production of a specific linear generator by these four control methods is introduced.
- The system becomes unrealistic when complex conjugate control is applied so that the displacement exceeds the design draft of the floating buoy. Apart from that, the PTO force required is so large that existing linear generators can not provide it. As large currents are required, the electrical losses are significant which need to be considered. Therefore, practical constraints are modelled to analyze net power production.
- The required currents in the generator coils to provide the force are constantly

varying in frequency and amplitude which presents a challenge for a traditional power converter control method. Hence, novel control algorithms are introduced to demonstrate how to implement reaction force control by controlling the power converter.

1.3 Thesis Statement and Contribution to Knowledge

The central thesis of this work is that reaction force control is able to be implemented onto a direct drive linear generator to extract more power from irregular waves and maximum power can be obtained when complex conjugate control is applied. In addition, the power converter is able to be controlled to supply appropriate currents to get the desired force to achieve reaction force control. However, this control algorithm has to be different from traditional control algorithms. Therefore in this work it will be proven that power production by using complex conjugate control onto a linear generator under practical considerations, such as motion displacement, generator rating and electrical loss, is higher than working passively. Additionally, a novel control algorithm to control the power converter to achieve irregular currents control will be developed.

There are four main contributions in this thesis. It continues Shek's work [5] in which reaction force control method was used to control the linear generator in regular waves. Control becomes more complicated when the system is placed in irregular waves. Price [23] had done a lot of work to develop control methods in irregular waves, but no work was done to implement reaction force control method onto a linear generator in irregular waves. Therefore, this work brings Shek's work and Price's work together to implement reaction force control on a direct drive linear generator to extract maximum possible power from irregular waves. In addition, a lot of work had been done to implement latching control in irregular waves under the assumption that future wave prediction is available. This work proposed an idea on how to implement latching control without future wave prediction. Traditional PWM control idea is not available

anymore to this work to control the active rectifier to get highly varying currents. Two new methods based on carrier based PWM are proposed to achieve reaction force control. Therefore, in this thesis, a complete model, including ocean wave generation, hydrodynamic analysis, reaction force control, linear generator simulation and power converter control is designed to describe the whole process of controlling direct drive linear generator.

1.4 Review of Previous Research

Much of the research into ocean WEC control has focused on mechanical control, such as latching control which applies mechanical braking pads to lock the buoy to achieve mechanical resonance [24], [25], [26]. Such control methods require the knowledge of future waves to decide the specific timing, and the natural frequency of the floating buoy has to be designed to be higher than the predominant wave frequency to achieve best performance.

Reactive force control, also known as continuous control, is widely discussed by researchers but little progress has been made to implement this control for a WEC [27], [28]. The complex conjugate control, which is the reactive force control taken to the limit, is regarded as the optimal control method to extract maximum power from ocean waves. As this control is inherently unstable, it was rarely implemented until NeBel [29] used an open loop control on the Salter's duck to achieve almost 100 percent efficiency curve. Due to the rapid development of direct drive linear generators in the last decade [30], [31], [32], reaction force control is of particular interest because power conversion is directly from the mechanical wave movement to electricity by the direct drive system and reaction force control can be achieved by only controlling the currents which would eliminate additional mechanical systems.

Reaction force control implementation to a linear generator was first carried out by Shek [33], [5] in regular waves and multi-frequency waves and later it was also tested experimentally [34]. In his work, a large reactive force is required to control the WEC

unless the natural frequency of the buoy is designed to be the same as the wave frequency. The large force will be produced by high coil currents in the linear generator which therefore needs overrating. In this thesis, work is carried out to implement the reaction force control on a linear generator in real sea conditions. Detailed information of optimal complex conjugate control has been given by Price [35], [23] which is the main control theory used in this thesis.

1.5 Chapter Breakdown

Chapter 2 gives all the specific background information which is used in this thesis. It begins with the definitions and descriptions of ocean waves. To obtain the time domain ocean waves, the frequency domain energy spectrum is used and converted by using the Inverse Fourier Transform, hence the Fourier Transform technique is presented. Hydraulic and direct drive PTO systems are two important energy conversion systems that can be applied on point absorber WECs. Working principles of these two systems and a comparison indicating their advantages and disadvantages are provided in Section 2.4. In Section 2.5 different types of linear machines are introduced. Electrical power converters which are directly connected to the linear machine to control the phase current and dc link voltage are also introduced in Section 2.6.

Chapter 3 explains the hydrodynamic characteristics of the interaction between ocean waves and the WECs. Firstly, random wave elevations are modelled by using the random phase method, and the random wave excitation force is also simulated later on in this chapter. The electrical analogue of a simple mass-spring-damper is discussed. The original frequency domain WEC representation is given followed by the time domain representation after applying the Inverse Fourier Transform. The system can be divided into four different types: memoryless system, causal system, acausal system and anticausal system. Detailed analyses of these four systems are introduced.

Chapter 4 presents the control strategies of point absorber WECs. Reaction force control is focused on in this chapter and four different reaction force control meth-

ods, along with the relevant simulation results, are provided. By applying complex conjugate control, displacement of the oscillating buoy is large and may exceed the design draft. Hence, mechanical constraint is considered.

In Chapter 5, linear causal sub-optimal mass-spring-damper control, where the PTO force consists of mass, spring and damping terms, and causal indicates the unavailability of future wave information, applies mechanical impedance matching to calculate the PTO force required to perform the control. With this method, a large amount of reaction force is needed which can be much greater than the generator can provide. Therefore the generator force must be limited, which results in a nonlinear system and off-resonance between the WEC and the wave excitation force. Furthermore, electrical losses will be significant if this control method is applied. Hence, this chapter focuses on the simulation of reaction force control under practical constraints.

Chapter 6 explains two control algorithms for the active rectifier. The required currents in the generators to provide the force are constantly varying in frequency and amplitude, which presents a challenge to traditional control algorithms. In this chapter, a continuous varying average voltage method and a various modulation index method are presented to control the currents to follow the required currents. A feedback current loop and PI controller are both employed to upgrade the performance.

Chapter 7 summarises the key points from the simulation results. Several important comparisons between different control methods are provided. In addition, the feasibility of reaction force control in irregular waves and some future improvements are discussed.

Chapter 8 draws conclusions from the simulation results provided in the previous chapters. Finally, several suggestions for future work and proposals for future research are provided.

Chapter 2

Background

2.1 Introduction

The main purpose of this thesis is to implement control methods for a direct drive linear generator which is operating in real ocean waves. The following chapters describe each specific step to achieve reaction force control. The present chapter provides the basic knowledge required for preparing to model the whole process. Real ocean waves, from which power will be extracted, play a critical role in this work. Therefore, the first part of this chapter introduces different definitions of ocean waves and wave energy spectrum. To simulate real ocean waves, the Fourier Transform technique has to be studied in order to achieve time domain ocean waves from the frequency domain wave spectrum as discussed in the second part of this chapter. There are several different PTO systems which require different control strategies and power conversion systems. A detailed comparison between these PTO systems is presented in the following sections.

The linear generator is the only electrical machine that can be used for direct drive wave energy systems. Unlike conventional high speed rotating machines, the linear machine has a similar reciprocating velocity to ocean waves. Due to the low speed of the sea waves, a large force is required to generate the desired power which requires a bulky and heavy linear generator. Several different topologies of linear machines are introduced without a common consensus as to which one is the optimum. Fluctuating power is generated from a linear generator, so that an electrical power converter with a smoothing capacitor should be added between the linear machine and electricity network to achieve very short-term energy storage and power smoothing. The aim of

this chapter is to provide a basic understanding by the reader of what is simulated in this work.

2.2 Ocean Waves

Oceans cover approximately 71% area of the planet with an infinitely varying surface. Ocean waves, also referred to as wind waves, are generated by wind blowing over a vast sea surface. Waves carry a vast amount of energy that travel thousands of kilometres before reaching the shoreline. This attracts wave energy engineers to intercept and capture some of the energy during its transmission path. Before any prototype is placed in real seas to operate, computer aided simulation is an effective technique to reduce the risk of investment. Hence, for wave energy engineering, simulation of real sea waves is of primary importance to further modeling tasks. It is necessary to present two different expressions of real ocean waves and their relationship because they can be converted mutually using the Fourier Transform and the Inverse Fourier Transform.

2.2.1 Ocean Wave Definition

Ocean waves are formed by wind blowing over the sea surface. However, each wave is not only created by local wind speed, but also affected by neighbouring waves and small ripples. Because of the existence of upcoming waves and small ripples, some newborn waves can be enlarged or diminished depending on their relative travelling direction. There are some very important parameters to describe a wave.

- Wave height: Vertical distance between the bottom of a trough and the top of a nearby crest.
- Wave length: Horizontal distance between one top of a crest and the next top of a crest.
- Wave amplitude: Distance between the top of a crest and sea level or distance between the bottom of a trough and sea level.
- Wave elevation: Distance between any point of the wave and the sea level.

There is another very important definition to describe a series of waves which is known as significant wave height. If we look closely at a wind-driven sea, sea waves have various heights, and some of them have significantly larger amplitudes than others. Hence, a practical definition of significant wave height is the average height of the largest 1/3 waves in a measured time period. For instance, ocean waves might be measured in a few minutes where 120 wave crests are picked up. In these wave crests, the 40 largest waves are picked to calculate the average height which is known as the significant wave height.

There are several ways to classify sea waves, but the most well-known method is to categorize the waves based on their directional spreading as listed below. In this project, long-crested waves are considered because the WEC is assumed to be a point absorber.

- Long-crested waves: Waves travel in the same direction with long crests.
- Short-crested waves: Waves travel in different directions with relatively short crests.

2.2.2 Time and Frequency Domain Definition of Waves

In the context of computer aided simulation, ocean waves are analyzed by using digital signal processing (DSP). The word *domain* is a mathematical definition, which specifies the function of signal description. A time domain function describes how a signal changes over time; similarly, a frequency domain function describes a signal as a function of frequency.

Time domain waves

In the time domain, a series of wave elevations with respect to time are used to describe a wave during the chosen time period. The time domain wave signal can be expressed as a continuous wave or a discrete wave. The continuous wave is used to describe a function which contains no gaps between all of the values. In practical experiments, wave elevation is measured and plotted from a fixed point to form a continuous wave.

If a measured wave is recorded into a computer system, data will be read in with very small time intervals, which indicates that the wave stored in a computer is discrete. Figure 2.1 shows a random wave in both continuous form and discrete form. In this figure, T_e and T_k represent two random complete wave periods. In this context, the wave period is defined as the time distance between two successive zero up-crossings. In other cases, a wave period can also be defined as the time between two successive zero down-crossings or the time distance between two successive peaks. The first two definitions are suitable for random waves, because several peaks can occur during a time period but without any zero crossing. For instance, in the period T_k in Figure 2.1, there are two positive peaks but no zero crossings. A wave height is the distance between a positive peak and its adjacent negative peak as indicated by H_m in the figure. What should be noticed is that the measurement should be considered in one complete wave cycle. Here, one wave period is the time between the start of one zero up-crossing to the next zero up-crossing. Wave height can be different depending whether the signal is continuous or discrete. If a continuous signal is considered, wave height is as introduced above. If a discrete signal is taken into account, wave height is the distance between the positive top point and the negative bottom point in one wave cycle. However, these two points are possibly not the peaks. In a discrete time domain wave signal, every specific time corresponds to a wave elevation $\eta[t_n]$.

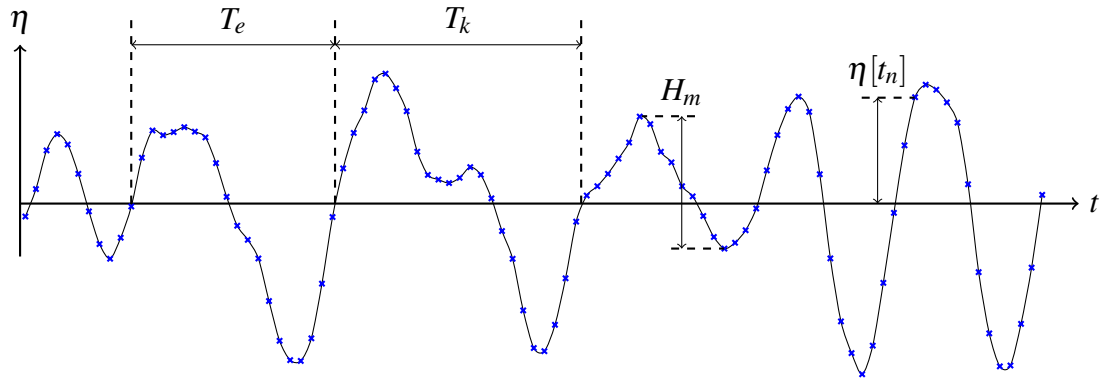

Figure 2.1: Important parameters of a random wave

Frequency domain waves

Any type of wave can be expressed in two primary ways; either in the time domain, or in the frequency domain. Frequency domain describes how a wave can be decomposed into different single frequency waves. Each individual wave has its unique phase information that can be applied to recombine the frequency components to generate the original time domain signal. To demonstrate, a time domain wave which consists of three sinusoidal waves with different amplitudes, frequencies and phases is shown in Figure 2.2. It is a contrived example, as the integrated signal is composed of three simple sinusoidal signals. In fact, any integrable parametrically continuous signal can be decomposed into a finite number of sinusoidal signals with their own amplitude, frequency and phase information that can be found in the frequency domain expression.

If the frequency information of a signal is required, it can be obtained by applying the Fourier Transform as introduced in Section 2.3. For example, Figure 2.3 is the frequency domain representation of the time domain wave shown in Figure 2.2. It is shown that the integrated signal is composed of three different sinusoids with angular frequencies π rad/s, 2π rad/s and 4π rad/s as shown in the top trace in Figure 2.3. Each amplitude shown represents its corresponding amplitude in the time domain. Phase information can also be obtained in the bottom figure where positive, zero and negative phase shifts exist in the three decomposed signals.

2.2.3 Wave Energy Calculation

Wave power has greater power density than either wind power or solar power. The correct calculation of the available power from a wave plays an important role in designing a WEC, so that the dimensions of the floating buoy can be determined. Other than that, the knowledge of power possessed by ocean waves provides an assessment on the performance of the WEC by comparing the power extracted with the power existing in the waves.

Wave power is calculated by supposing the water depth is much larger than the wave-

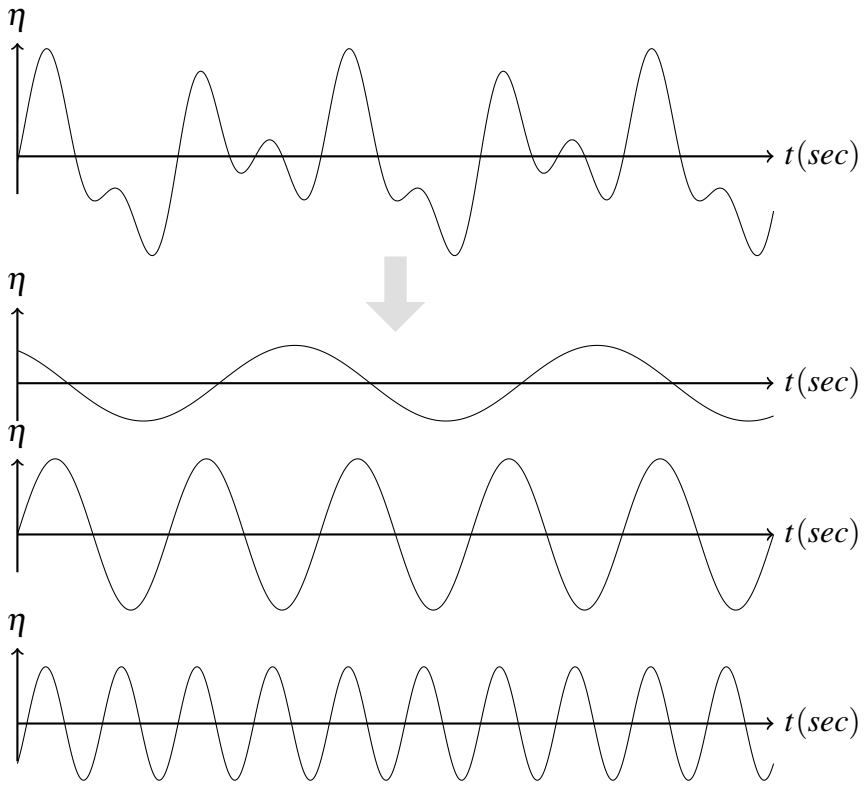

Figure 2.2: Time domain wave.

length and is shown in Equation 2.1:

$$P = \frac{\rho g^2}{64\pi} H_s^2 T \tag{2.1}$$

where, P is wave energy flux per unit of wavefront length (wave-crest length) with the units W/m, ρ is water density, g is gravity acceleration, H_s is the significant wave height and T is one wave period. Thus wave energy flux is proportional to wave period and the square of significant wave height.

Another measurement of wave energy is wave energy density per unit horizontal area with unit J/m^2, as expressed in Equation 2.2. The wave's power density is calculated using the wave energy density divided by wave period which is given in Equation 2.3.

$$E = \frac{1}{16} \rho g H_s^2 \tag{2.2}$$

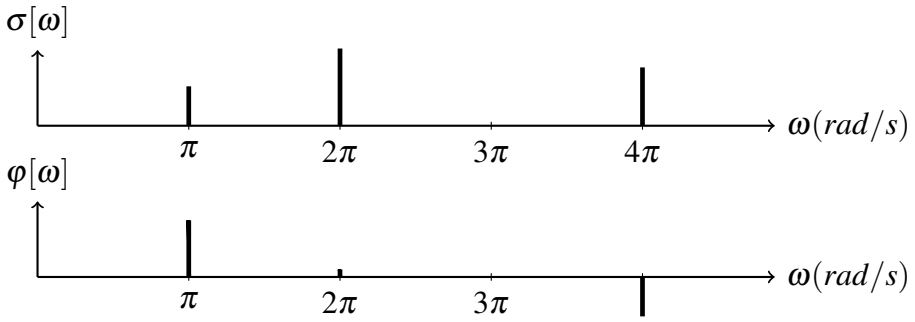

Figure 2.3: Frequency domain wave.

$$P = \frac{1}{16}\rho g H_s^2 / T \tag{2.3}$$

2.2.4 Wave Energy Spectrum

Ocean waves are produced by the wind passing over the surface of the sea. The amplitude, frequency and the energy of waves depend on the wind. Bigger waves are created by either stronger wind or by it blowing for a longer time. In marine engineering, the biggest waves produced by a specific wind speed plays a critical role in designing ships or offshore structures. Hence, a wave energy spectrum, which can indicate energy distribution with a range of frequencies at a given wind speed, is an effective method for analysing ocean waves at a specific location [36].

PM spectrum

Pierson and Moskowitz [37] first proposed the PM (Pierson-Moskowitz) spectrum by assuming wind speed is constant for a long time over a long distance of sea surface. This type of sea is known as a fully developed sea. To obtain data, an anemometer mounted on weather ships is used to provide wind speed and take the wave observations. Then a relationship between wave energy density and wind speed is obtained as shown in Equation 2.4.

$$S(\omega) = \frac{\alpha g^2}{\omega^5} exp\left[-\beta\left(\frac{\omega_0}{\omega}\right)^4\right] \tag{2.4}$$

Wave energy density is represented using $S(\omega)$ with the units m^2/Hz. In the PM spectrum, angular frequency $\omega = 2\pi f$,where f is the wave frequency in Hertz, $\alpha = 8.1 \times 10^{-3}$, $\beta = 0.74$, $\omega_0 = g/U_{19.5}$ and $U_{19.5}$ denotes the wind speed measured by an anemometer on the weather ship at the height of 19.5 m above the water level.

Equation 2.4 cannot be used to illustrate at what frequency the waves have the most energy. Hence, it can be simplified by choosing the peak frequency. Peak frequency is obtained by making $\frac{dS}{d\omega} = 0$ which is shown in Equation 2.5. Full details for calculating peak frequency ω_p can be found in Appendix A, and the PM spectrum can be rewritten in Equation 2.6 by applying the peak frequency ω_p instead of ω_0.

$$\omega_p = 0.877\omega_0 = 0.877 \cdot g/U_{19.5} \tag{2.5}$$

$$S(\omega) = \frac{\alpha g^2}{\omega^5} exp\left[-\frac{5}{4}\left(\frac{\omega_p}{\omega}\right)^4\right] \tag{2.6}$$

JONSWAP spectrum

In 1973, the Joint North Sea Wave Project (JONSWAP) proposed a new wave energy spectrum by analyzing data collected from the Island of Sylt (North Germany) in the North Sea [38]. It was found the ocean could not be fully developed because of nonlinear energy transfer between waves and wave interactions, and the interactions between very short waves and longer waves. To get JONSWAP spectrum, γ is introduced into the PM spectrum as shown in Equation 2.7 and Equation 2.8. It is used to represent wind-wave growth state with the value range between 1.5 and 6, and it is normally called peak enhancement factor [39].

$$S(\omega) = \frac{\alpha g^2}{\omega^5} exp\left[-\frac{5}{4}\left(\frac{\omega_p}{\omega}\right)^4\right] \gamma^r \tag{2.7}$$

$$r = exp\left[-\frac{(\omega - \omega_p)^2}{2\sigma^2\omega_p^2}\right] \tag{2.8}$$

where, $\gamma = 3.3$, $\sigma = 0.07$ when $\omega \leq \omega_p$ and $\sigma = 0.09$ when $\omega > \omega_p$. In the JONSWAP spectrum, the constant α and peak frequency ω_p are determined as given in Equation 2.9 and Equation 2.10 by measuring U_{10} which is the wind speed 10 metres above sea level. The fetch F is the distance over which the wind blows with a constant velocity.

$$\alpha = 0.076 \left(\frac{U_{10}^2}{Fg} \right)^{0.22} \tag{2.9}$$

$$\omega_p = 22 \left(\frac{g^2}{U_{10}F} \right)^{1/3} \tag{2.10}$$

2.2.5 Wave Prediction and Measurement

Ocean wave forecasting has been widely applied in Naval ship design processes and naval operations for a long time. With the help of radar techniques, real-time observations of ocean waves can be achieved [40]. For the past few years, 48 to 96 hours accurate wave forecasting has been provided by the Naval Research Laboratory [41]. Although being an effective way of forecasting the general ocean waves' situation, it cannot accurately predict detailed information wave by wave. With the rapid development of wave energy, detailed wave by wave prediction, such as wave frequency, wave height and wave speed, several seconds into the future is increasingly important for real seas wave energy device control. As is described in Section 4.3, both latching control and reaction force control rely on the information on future waves. For latching control, one wave period into the future prediction is used to determine when to lock and unlock the wave energy device to make it move in phase with the waves. For reaction force control as is discussed in Section 4.5, optimal control can only be achieved if future waves are known.

Since the late 1980s, a number of contributions to future waves prediction have been made. The autoregressive (AR) model is regarded as an effective way to attempt to predict waves based on the previous outputs. Forsberg first developed the AR model by adding a Moving Average to the AR formulation (ARAM) to describe ocean waves

off the coast of Sweden [42]. In the last few years, Fusco [43–45] proposed Linear Autoregressive models to predict up to 20 seconds future waves with very good accuracy. It has proved to be a promising approach for predicting future wave elevations only from its past history. However, the application of AR models results in increased instrumentation costs because several distant observations are required to reconstruct a new wave field.

2.2.6 Wave Power Transmission

For wave energy, energy is carried by incident waves to travel a long distance to a wave energy device. Subsequently, power extraction and transmission can be carried out by intercepting, capturing and delivering the energy.

Intercepted power

The first process is called power interception which occurs between incident waves and the primary interface. There are several different WECs with different primary interfaces that result in different ways of power interception. In this work, a reciprocating motion buoy connected to a linear machine is used, so that power interception is introduced based on a floating type wave device.

As an incident wave reaches the buoy, the buoy starts to move which can be regarded as power being intercepted by the floating buoy to make it move up and down. If a PTO system is not connected, the reciprocating motion generated by incident waves can generate other waves that carry the same amount of power as the buoy intercepted. Therefore, all the power is returned to the ocean, which is radiated power. In most cases, energy carried by the incident waves cannot be fully intercepted by the buoy leaving the rest of the energy to continue to travel, diffracted by the buoy. The diffracted small waves can travel in many directions. Some of these small waves that travel in the same direction as the incident wave possess an amount of power known as transmitted power. The power carried by other waves that travel in all other different directions

is called diffracted power. Hence, the energy leaves the buoy in the form of waves associated with diffracted, transmitted and radiated power.

Captured power

The intercepted power used to move the floating buoy can be captured by an electrical machine to generate electricity. As explained above, if no PTO system is connected, all the power will be returned to ocean waves, and the sum of diffracted power, transmitted power and radiated power equals the power possessed by the incident wave. If a PTO system is connected (damping force), some of the intercepted power can be captured. The rest of the intercepted power still needs to be returned to the ocean. Hence, for wave energy engineers, the main tasks are to design a good structure for the primary interface to intercept as much power as possible from the incident waves, and to design control strategies for the buoy to capture as much power as possible from the intercepted power. This power normally cannot be directly connected to a load (e.g., rotating electrical motor) or electricity grid due to its unstable nature. A power conditioning device, accumulator for a hydraulic system or power converter for a direct drive system, is required to smooth power production before connecting to the user interface or electricity network (as is introduced in Section 2.6).

2.3 Fourier Transforms in Random Waves

In wave engineering, both the time domain and frequency domain are widely used to describe signals. For any specific signal, the time domain is used to describe the signal variation with respect to time and its equivalent representation as a function of frequency is used to describe the frequency information of the signal. As long as either time domain or frequency domain is known, the other domain function can be obtained using the Fourier Transform or the Inverse Fourier Transform. The Fourier Transform is a mathematical calculation based on decomposing signals into sinusoids. The goal of the decomposition is to make the original signal more simple to analyze. The original signal may be random and not have sinusoidal properties.

Because of the importance of the Fourier Transform in this thesis, it is necessary to review this theory. This section first introduces the Discrete Fourier Transform and then the Fast Fourier Transform is presented for use in computer aided simulation.

2.3.1 Discrete Fourier Transform

The Fourier Transform can be divided into four categories depending on whether the signal is continuous or discrete, and periodic or aperiodic, as illustrated in Figure 2.4 [46].

- Continuous and Aperiodic: Signals are continuous and exist in both positive and negative infinity. Signals do not have periodic patterns. The Fourier Transform applied to these kinds of signals is called the Fourier Transform (FT).
- Discrete and Aperiodic: Signals are made up of an infinite number of values without repeating in a period cycle. This type of Fourier Transform is called the Discrete Time Fourier Transform (DTFT).
- Continuous and Periodic: Signals are changing continuously with periodic patterns. The Fourier Transform for this type of signal is called the Fourier Series (FS).
- Discrete and Periodic: Discrete signals change with a periodic pattern. The Discrete Fourier Transform (DFT) is used for these types of signals.

As continuous signals cannot be dealt with in a digital computer, they have to be changed into discrete form. Also, any completely aperiodic signal can be decomposed into an infinite number of sinusoids, but it is impossible for a computer to solve. Therefore, only discrete and periodic signals can be transformed by a Fourier Transform in a computer-aided system, which is known as the DFT.

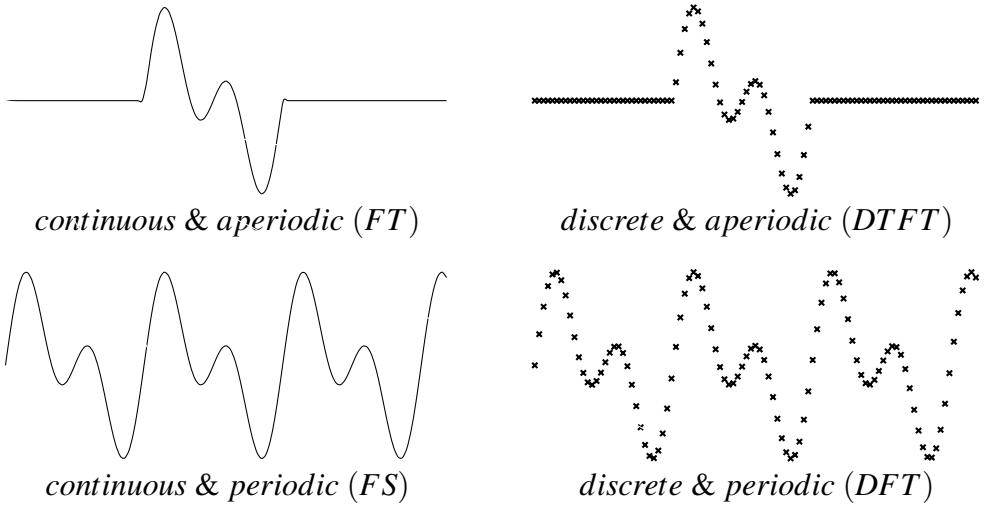

Figure 2.4: Four categories of Fourier Transform

2.3.2 Real Discrete Fourier Transform

The input of the DFT is the original function, normally a function in the time domain. By sampling a continuous function, the function is expressed in discrete form with a number of samples. In the real DFT, if N samples are chosen as the input, the output after the DFT consists of $N/2+1$ cosine waves and $N/2+1$ sine waves. The amplitudes for both cosine and sine waves are stored in the frequency domain. The mathematical calculation from time domain to frequency domain is shown in Equation 2.11.

$$\begin{aligned} ReX[k] &= \frac{2}{N}\sum_{n=0}^{N-1} x[n]cos(2\pi kn/N) \\ ImX[k] &= -\frac{2}{N}\sum_{n=0}^{N-1} x[n]sin(2\pi kn/N) \end{aligned} \tag{2.11}$$

Here, we use lower case letters $x[n]$ to represent the time domain and the upper case letter $X[k]$ to represent its corresponding frequency domain representation. Complex numbers are used where the real part is considered to be the cosine wave amplitudes, while the imaginary part is considered to be the sine wave amplitudes. The application of complex numbers does not mean it is the complex DFT, but for the purpose of expressing cosine and sine waves' amplitudes. Here, n runs from 0 to $N-1$, and k

which can be regarded as frequency runs from 0 to $N/2$.

2.3.3 Complex Discrete Fourier Transform

The Fourier Transform can be carried out on either real numbers or complex numbers. In the real DFT, the input time domain signal is treated as real, whereas it is treated as complex in the complex DFT. For instance, if an ocean wave is modelled, the wave elevation is the real part of the complex number so the imaginary part is zero. In the real DFT as stated in Section 2.3.2, an N samples signal can be broken down into $N/2+1$ cosine waves and $N/2+1$ sine waves. However, by applying the complex DFT, an N samples signal which has N imaginary samples with value zero, can be transformed into N real values and N complex values. The forward transform of the complex DFT is given in Equation 2.12.

$$X[k] = \frac{1}{N}\sum_{n=0}^{N-1} x[n](cos(2\pi kn/N) - jsin(2\pi kn/N)) \tag{2.12}$$

At first glance, the complex DFT in Equation 2.12 seems to be identical with the real DFT in Equation 2.11, except for the constant factor. But differences do exist between them and are extremely important. The frequencies in the complex DFT have both positive frequencies and negative frequencies running from $-(N-1)/2$ to $(N-1)/2$. The real part in the frequency domain has an even symmetry and the imaginary part has an odd symmetry. Also with the real DFT, the real part represents the amplitude of cosine waves and the imaginary part represents the amplitude of sine waves. However, the amplitudes for both of these two parts in the complex DFT are half of the amplitudes in the real DFT. That explains why the constant factor is half of the factor in the real DFT.

$$e^{jx} = cos(x) + jsin(x) \tag{2.13}$$

$$X[k] = \frac{1}{N}\sum_{n=0}^{N-1} x[n]e^{-j2\pi kn/N} \tag{2.14}$$

Based on Euler's relation given in Equation 2.13 the complex DFT can be rewritten as shown in Equation 2.14. In ocean wave engineering, the complex DFT is widely used unless otherwise specified. In this thesis, wave generation is achieved by using a computer aided system based on the theory of the complex DFT.

There are several ways to solve the DFT, but normally with a large amount of calculation. The Fast Fourier Transform (FFT), which was originally introduced by Cooley and Tukey, is another method to produce the same result as the DFT based on the complex DFT, but in a more efficient way which can reduce the computation time by a factor of several hundred [47]. The FFT technique is now widely used in computer aided systems to achieve fast computing of the Fourier Transform. In this work, the FFT based on the Matlab software is applied to simulate random ocean waves as is introduced in Section 3.2.3.

2.4 Direct Drive Systems

In power systems, direct drive mechanisms have already been widely used in wind power. Turbines are divided into three types according to the rating ranges, which are micro-turbines (less than 3 kW), small wind turbines (less than 30 kW) and large wind turbines. Almost 90% of micro-turbines use direct drive permanent magnet generators for low power systems such as remote telecommunications, domestic systems and electric fences. Most of the small direct drive wind turbines use permanent magnet generators, except for the Atlantic Orient Corporation which uses a switched-reluctance generator [48]. In April 2011, Siemens announced that the first 3 MW direct drive wind turbine will be installed on the new Millour Hill Community Windfarm in the UK to power 14,000 homes in the local area. Six of these wind turbines will produce 18 MW of green electricity to displace about 20,340 tonnes of carbon dioxide per annum [49].

2.4.1 Direct Drive Systems for Wave Power

A WEC is a combination of a wave device and an electrical generator. So far, a number of types of WECs have been proposed throughout the world such as the OWC, the point absorbers, the flap devices such as the Oyster (from Aquamarine Power), the attenuators such as Pelamis (from Pelamis Wave Power) and overtopping devices such as the Wave Dragon (from Wave Dragon ApS) as introduced in Section 1.1.2. Apart from the OWC and the overtopping device, all other types of WEC use the reaction to the ocean force to generate electricity. Most designs for WECs include a hydraulic interface between the wave device and the electrical generator to smooth electricity production. However, this mechanical interface will reduce the power transfer efficiency and reliability [50], which are of prime importance for wave engineering in a harsh offshore environment. A direct drive PTO system is an alternative method which was first proposed in the 1970s. In the late 1990s, it was first adopted by AWS, a commercial company, to achieve higher energy conversion efficiency [51]. A typical direct-drive WEC normally may include a low speed linear generator directly coupled with the wave device. With no mechanical interface, mechanical energy loss is zero and maintenance requirements can be significantly curtailed [52]. A WEC consisting of a floating buoy and a linear generator utilizing a direct drive PTO system is detailed in Figure 2.5 [5]. The floating buoy is designed to move with the ocean waves to drive the moving part of a linear generator, referred to as the translator. The translator is the only moving part, increasing the reliability.

Floating buoy

This typical configuration of direct drive system has been proposed in two different versions by several wave energy companies, depending on the floating buoy's position. The concept of a fully submerged floating buoy as described in Figure 2.6 was developed and built in 2004 by AWS to produce 2 MW peak power and 1 MW average power [31]. The figure on the left in Figure 2.6 is a sketch describing how the fully submerged device works; however, it has not yet progressed to the testing

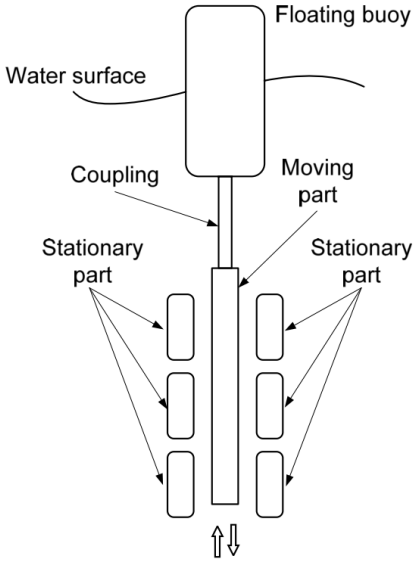

Figure 2.5: A WEC consists of a floating buoy and a linear generator.

stage. Instead, this prototype has been designed in another way by fixing the floating buoy and linear generator on a stable structure as shown in the right figure in Figure 2.6 [53], in a pilot plant. The chamber is fully air-filled and is covered by a lid. The lid can move vertically based on the water pressure. As a crest passes over the device, the added height of the water depth causes higher pressure to force the device to fall. The crest is followed by a wave trough to reduce the pressure inside the chamber to make the device rise under the force of the air. Power is generated by this reciprocating linear motion.

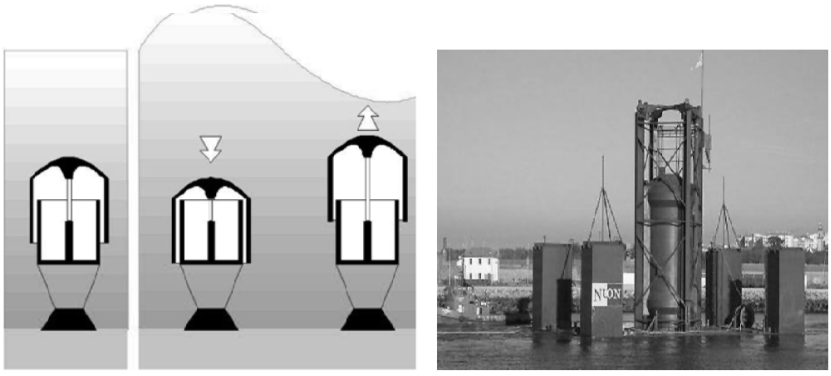

Figure 2.6: A direct drive linear generator configuration with fully submerged floating buoy.

Another concept, known as the semi-submerged floating buoy, was developed by Trident Energy Limited in 2009 to demonstrate the 30 kW device detailed in Figure 2.7 [54]. This fully functional test rig was planned to be located in the North Sea off England's east coast, however, it finally capsized while towing to the test site [55]. In contrast to the AWS pilot plant, the motion of the device has the same direction as the ocean waves, so the motion amplitude can be obtained based on the wave elevation which is much easier than with the AWS pilot plant. The advantage of this concept is that it has the linear generator 3 metres out of the water which reduces the requirement of being watertight. Hence, maintenance requirements are significantly reduced.

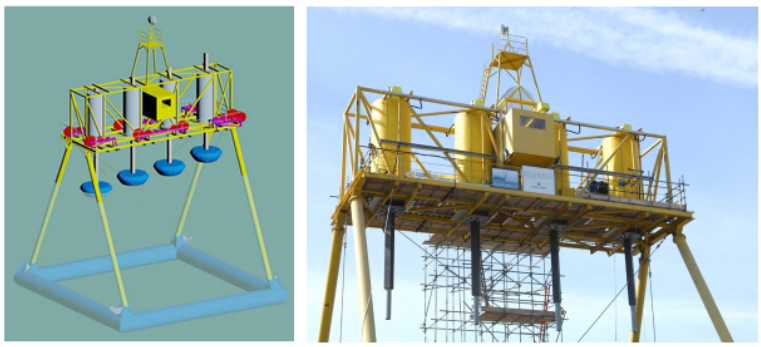

Figure 2.7: A direct drive linear generator configuration with semi-submerged floating buoy.

Inter project service buoy

The Inter Project Service (IPS) buoy had been proposed to be connected to a linear generator in 2001 [30]. The IPS device is constructed with a semi-submerged float and a fully submerged hollow tube, open to the sea at both ends as shown in Figure 2.8 [30]. As an ocean wave passes, the float, the entire tube and cylinder move together according to the sea surface. The piston is the only stationary part and establishes relative motion with the cylinder. This relative motion of the piston forces high pressure sea water to drive a turbine [56]. Hence, to eliminate the hydraulic PTO system, the other end of the piston can be connected to the translator of the linear generator.

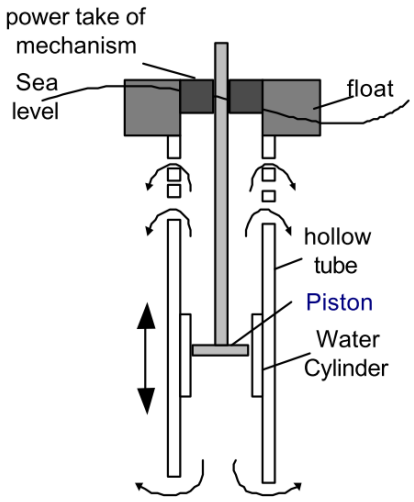

Figure 2.8: Cross section of an IPS device.

Edinburgh Duck

Floating buoys can be divided into two different types, the heaving buoy type with linear motion or the nodding device which produces a circular motion. The first wave energy device, the Edinburgh duck, which is also the best known, uses rotary movement to generate power, shown in Figure 2.9 [57]. A nodding cam is placed on the water surface to react with the force. It can then be directly coupled to a stationary spine which has permanent magnets and copper coils on it. Because of the shape of the floating buoy, ideally 100% energy from ocean waves can be absorbed [30], hence, if the Edinburgh duck is designed to be a direct drive system, efficiency will be very high.

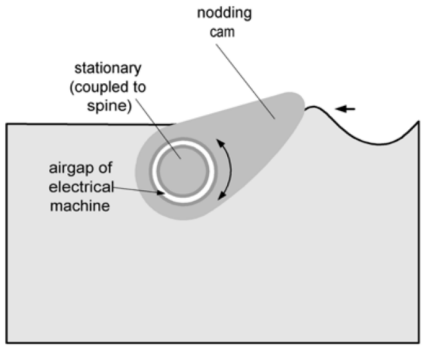

Figure 2.9: Concept of a direct drive Edinburgh duck.

2.4.2 Hydraulic and Pneumatic Systems for Wave Power

Apart from direct drive PTO systems, there are also two other important systems which are widely used in wave engineering. One of them is a hydraulic system such as is used by Pelamis Wave Power, and the other is a pneumatic system which is used by OWC.

The Pelamis WEC as shown in Figure 2.10 [52], a semi-submerged, articulated structure, consists of several cylindrical sections and power modules. Pairs of cylindrical sections are linked together by a swaying hinged joint. In every coupled cylindrical section, two hydraulic rams are constructed to react to the wave induced relative motion between them. In these hydraulic rams, high pressure oil is generated and pushed into high pressure accumulators for short term energy storage, also smoothing power flow into the electricity network. Finally, electricity is generated from the hydraulic motors which are driven by high pressure oil.

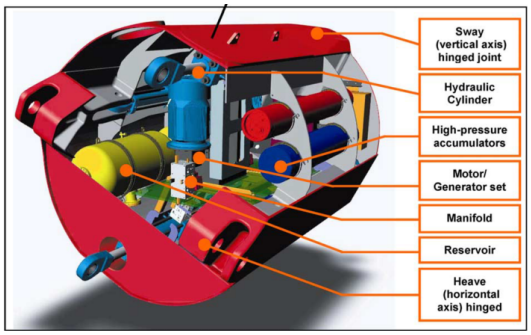

Figure 2.10: Internal view of a Pelamis power conversion module.

An existing 40 kW OWC wave power pilot plant built on the island of Pico, Azores, Portugal, is a turbine type shoreline WEC which has been demonstrated and tested to be a successful wave energy capture device [58]. It operates by compressing air filled in a big chamber to drive a Wells Turbine under the motion of the ocean waves as shown in Figure 2.11 [59]. Air flow is bidirectional based on the motion of the water level. As the waves come to the device, the water level rises to push air out of the chamber, whereas as waves leave the device, air is sucked into the chamber as the water level drops. However, the rotating Wells Turbine has been designed to rotate in only one direction irrespective of the direction of air flow.

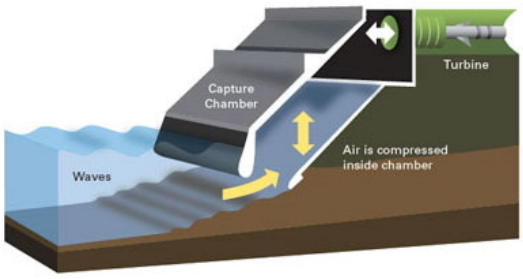

Figure 2.11: Working principle of an OWC WEC.

2.4.3 Comparisons Between Direct Drive and Other Systems

As described in Section 2.4.1 and Section 2.4.2, three different energy conversion methods are widely used in modern WEC technologies, with no clear winner yet emerging from these choices. The purpose of this section is to clarify the advantages and disadvantages of a direct drive system, a pneumatic system and a hydraulic system for improving future development to achieve satisfactory performance with the aim to reduce cost and to increase reliability.

The most significant advantage of direct drive systems is that they have fewer moving parts resulting in higher energy conversion efficiency. If a floating buoy is directly coupled with a linear generator, the only moving part is the translator which removes complex mechanisms such as oil-based hydraulics and a gearbox. Without these mechanisms, energy losses on mechanical parts can be significantly reduced; in addition, the risk of mechanical failure is reduced which lowers the requirements of maintenance. Maintenance for WECs is always likely to be costly and time consuming. This is because most of the devices will be located offshore in a harsh environment where big ocean waves pose high risks for maintenance, and sometimes large lifting equipment must be transported by a large vessel to carry out the maintenance. Hence, a direct drive with fewer moving parts and mechanical systems is more competitive than a hydraulic system both in terms of reducing energy losses and increasing reliability. However, for wave engineering, another essential feature which must be taken into account is thrust capacity. It is well known that power extracted is proportional to force and velocity.

Therefore, to achieve a satisfactory output power, either the force or the velocity of the motion has to be large. For a floating buoy located on the surface of the water, its oscillating velocity depends on the speed of the ocean waves which are normally very slow. Therefore, to obtain a relative high output power, a higher reaction force is required. For a direct drive system, induction machines and reluctance machines are not suitable due to small airgaps which cannot be maintained in very large machines as is explained in Section 2.5, so that only permanent magnet machines are normally considered. Permanent magnet machines use rare earth materials such as Neodynium-Iron-Boron (Nd-Fe-B) to increase the remnant flux density from 0.4T for ferrite to 1.2T, hence the force. However, the increasing price of such material has compromised the higher force it can offer. Hence, for both direct drive and hydraulic systems, neither design is fully optimized to meet both basic requirements. However, developments in permanent-magnet materials and in new machine topologies offer the prospect of a direct drive system able to achieve high forces.

As described above, mechanical moving parts and thrust capacity are two important features in choosing a PTO system device. Apart from these two important features, there are further differences between direct drive and hydraulic systems as listed below [60].

- Machine cost

  The cost of a linear generator is much higher than a hydraulic motor with similar thrust capacity. However, a direct drive system requires fewer moving parts such as watertight enclosure and speed reducing mechanism, so the overall cost of a direct drive system is likely to be similar to the cost of a hydraulic system.

- Mass

  The direct drive system is much heavier than a hydraulic system, normally five times greater. Most of the mass of the direct drive system comes from copper, stator and translator, which are much smaller in a hydraulic system. The heaviest part in a hydraulic system is the accumulator which has roughly the same mass as the translator in a direct drive system.

- Efficiency

  The system's efficiency is affected by, mechanical loss and electrical loss. With no mechanical parts in a direct drive system, the mechanical loss is significantly reduced. Hence, the efficiency of a direct drive is slightly higher than a hydraulic system.

- Power quality and storage

  In a hydraulic system, the generator is driven by a hydraulic motor. Hence, continuous rotation to achieve smooth power relies on continuous flow to the hydraulic motor. This is achieved by placing two accumulators in both the high and low-pressure lines from the cylinder to the motor. Energy can then be stored in a short time in the high pressure accumulator to provide reasonably smooth water flow. Because of the variation of ocean waves, the accumulator normally has sufficient capacity (at least 10 times the working volume of the cylinder) to deal with irregular waves. Direct drive systems have little (or no) storage, therefore, they have relatively worse power quality as a result.

- Sealing

  The hydraulic system must have a perfectly watertight enclosure to prevent water penetrating the system and mixing with the oil, as well as to prevent oil leaking. Unlike the hydraulic system, the gap between the stator and the translator does not have to be kept watertight, but the electrical circuitry must be perfectly sealed [61].

The whole energy conversion for pneumatic, hydraulic and direct drive systems is shown in Figure 2.12, which shows that several mechanical linkages in both pneumatic and hydraulic systems can be eliminated in the direct drive system. However, small mechanical loss does not mean a direct drive system is much better than the other two PTO systems. The use of an accumulator in a hydraulic system can smooth power production and is replaced by a power converter in a direct drive system. The existence of the large power converter with complex control system increases the cost of the system significantly and reduces the power transfer efficiency due to electrical losses in the power converter. So far, it is hard to conclude which type of PTO system is the

best because each has advantages and disadvantages.

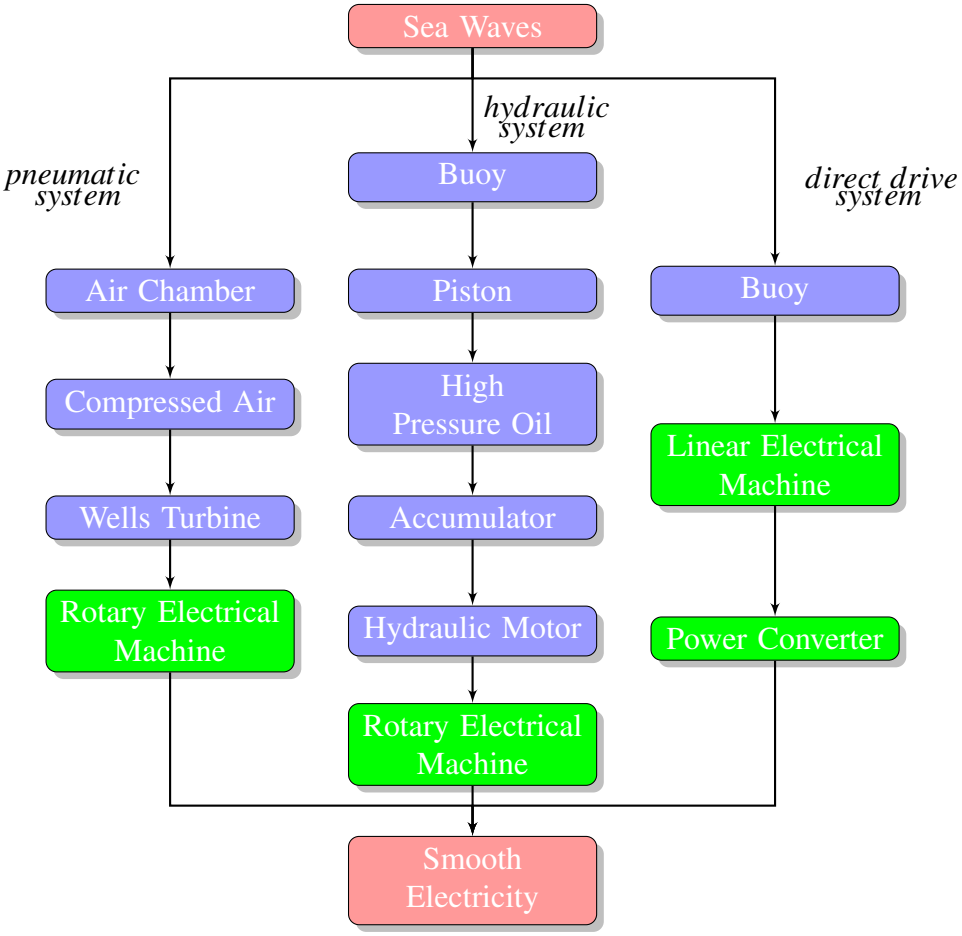

Figure 2.12: Energy conversion of three PTO systems; pink blocks show the source and electricity conversion, purple blocks show mechanical connection, and green blocks show electrical conversion.

2.5 Linear Machines for Direct Drive Systems

Conventional off-the-shelf electrical generators, which are driven by rotating air or hydraulic turbines, can be adopted into a heaving motion WEC to produce power. Due to significant losses on the mechanical moving parts, linear machine topologies that only apply linear motion to generate electricity become more interesting to the device design engineer.

Conventional machines are mostly of a rotary configuration and are used in a very wide range of applications. For wave energy engineering, the low speed reciprocating motion of the buoy can be connected to a conventional machine, via a hydraulic system or pneumatic system, to convert the low speed reciprocating motion into a high speed rotary motion, typically 1500 rpm, to produce electricity [32]. The concept of a linear machine, which is directly coupled to the floating device with slow reciprocating motion, offers the opportunity to simplify the system and to increase the energy conversion efficiency. As in conventional electrical rotary machines, the linear machine has two basic parts, the stator and the rotor, and can be perceived as a flattened rotating machine. The torque produced by a conventional rotary machine is replaced by a straight-line force along its length in a linear machine. Instead of calculating the power by using the torque multiplied by the shaft speed, the power for a linear generator is calculated by multiplying the linear force by the linear velocity. Therefore, to achieve a high power production, a high shear force is required for linear machine due to low linear velocity. A major challenge emerges for engineers to design a better machine topology with higher shear stress, which is the force per unit area of the active airgap.

Linear generators with a number of different topologies are available so far, with no clear "winner" yet emerging from these choices. All these designs include an unrolled rotor and stator, falling into three major categories, conventional machines, variable reluctance permanent magnet machines and tubular machines [62]. In this section, all of these linear machine topologies are introduced and a comparison of their behaviour is presented.

2.5.1 Conventional Linear Machines

Some of the topologies of linear machines, such as the linear induction machine, the linear synchronous machine and the permanent magnet synchronous machine, are derived directly from rotating machines, so are referred to as conventional machines which are the basis for designing direct drive linear generators. Consequently, the induced emfs within the translator are obtained by the motion of the translator.

Linear induction machine

The general principles of the well-known rotary induction machine can be applied to a linear induction machine which is designed to produce linear motion. A linear machine has an active three-phase winding as the stator which sets up a magnetic field between the stator and translator. The linear induction machine performs either as a generator or a motor depending on the speed of the translator, like a rotary induction machine. So far, the linear induction machine has been widely used on metro trains due to its simple structure and low cost [63]. In addition, to further reduce the cost a longer translator and relative shorter stator can be used.

Synchronous machine

The synchronous machine is another conventional machine in which the rotary version is widely used in power systems. In a synchronous machine, a magnetic field is established by feeding a direct current (dc) that is supplied by a dc source, to the rotor by, typically, brushes and slip rings, and the armature winding is fixed on the stator. In contrast to the induction machine, the behaviour of the synchronous machine depends on the angle between rotor-mmf axis and the stator mmf axis rather than the speed of the rotor. The machine operates as a generator when the angle is greater than zero, and operates as a motor conversely [64].

For a synchronous machine to produce linear motion, there are two important topologies, the *field wound synchronous machine* and the *permanent magnet synchronous machine*. The linear field wound synchronous machine can be envisaged as a rotary synchronous machine which has been cut and flattened, where the working principle is very similar. This field wound synchronous machine is rarely used due to durability issues. The brushes or slip rings are physically in contact with the translator; therefore, failure inspections should be included which will increase the maintenance requirements. Hence, a permanent magnet synchronous machine in which magnetized material is applied to create a magnetic field is more attractive than a field wound linear synchronous machine and was first adopted by AWS in 2004 [53].

2.5.2 Variable Reluctance Permanent Magnet Machines

The variable reluctance permanent magnet (VRPM) machine produces high specific force by converting low speed motion of the translator into a high speed flux change as described in Figure 2.13. Permanent magnets are mounted on each arm of the stator with the magnetic poles for each magnet placed in the opposite direction to its adjacent magnet. The toothed translator moves forth and back to make the teeth approach different position magnets. As the translator moves to the position in the top figure, the flux flow direction is shown by the dashed line in the figure. When the translator moves one tooth forward, the direction flux flow is reversed as shown in the bottom figure. Hence, the frequency of the direction of flux flow is four times that of non-toothed designs. However, the translator can only interact with two of the four stator poles at any one time which reduces the flux by half. Hence, the overall specific force is two times bigger than a non-toothed design.

A linear generator which is operating in ocean waves has a low velocity: normally, its peak lies between 0.5 m/s and 2 m/s without control and around 10 m/s under optimal reaction force control. To obtain a relatively high power, the reaction force needed should be very high which requires either high shear stress or a large active surface area (thus leading to a big machine). A high energy permanent magnet material, Nd-FE-B, seems to be the best choice which can provide shear stresses in the air gap up to 200 kN/m^2 [65]. There are two common variation of the VRPM machines as introduced below.

Transverse Flux Machine

There are several topologies for VRPM with the same basic principle of operation; one of them is known as the transverse flux permanent magnet (TFPM) machine. The first prototype was proposed in the late 1980s in which the permanent magnets are mounted on the translator. Stator coils are mounted on each side of the translator. Flux is established inside the stator and hence, the motion of the translator is perpendicular to the flux path. A comparison was made between the TFPM machine and the conventional

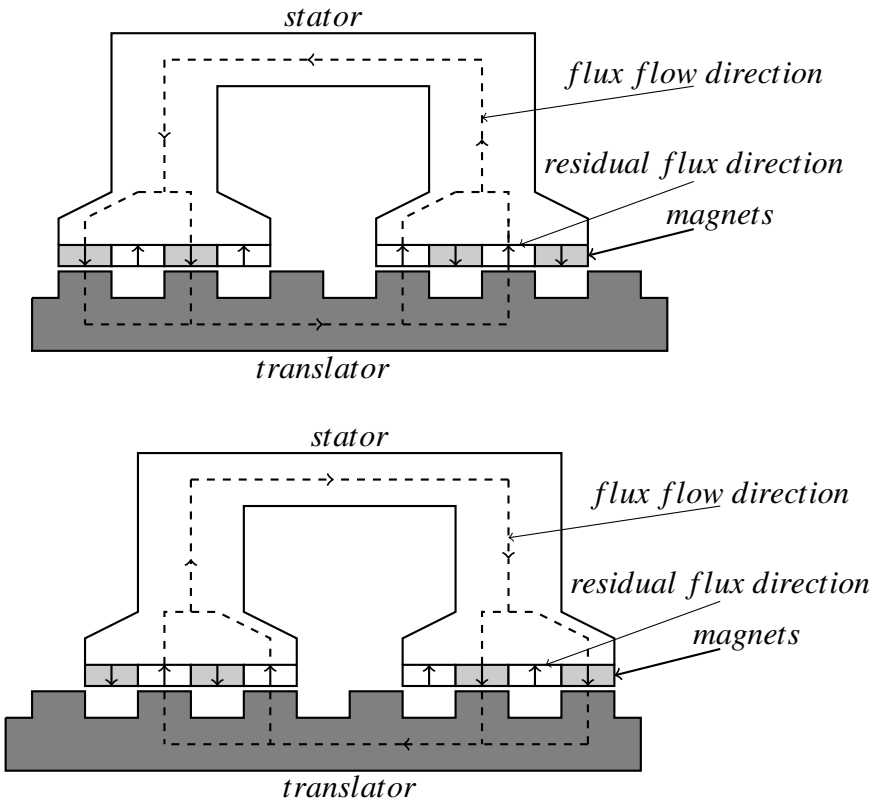

Figure 2.13: Working principle of VRPM where the stator is kept stationary and the translator is moving.

machine by Mueller that showed the mean shear stress produced by the TFPM machine is 3.5 times greater than the conventional machine with the same airgap [32]. Also, if the same shear stress is produced, the stator length needed for the TFPM is 1/4 of the stator length needed for a conventional machine. Therefore, the total size and mass can be significantly reduced.

Vernier Hybrid Machine

The vernier hybrid machine (VHM) has the typical structure of the VRPM as described above. Figure 2.14 shows two opposite C core stators with four permanent magnets and two coils fixed on each arm which represents one phase. The magnets interact with the purely iron toothed translator to produce a flux path in the two stators and the translator. As the translator moves in either direction in the middle of the stators, flux flow direction changes quickly to generate emfs inside the coils. Due to the toothed

design of the translator, flux density on the translator cannot be kept as a constant value. When the tooth is exactly aligned with the magnetic pitch, flux can flow evenly to the translator. In contrast, some flux may be formed in the slot region to generate an opposite force when the tooth is not fully aligned with the magnetic pitch. To achieve three phase emfs, another two identical structures are included so that when one stator pitch is fully aligned with the translator teeth, the other two stator pitches should not be fully aligned to achieve the appropriate phase shifts.

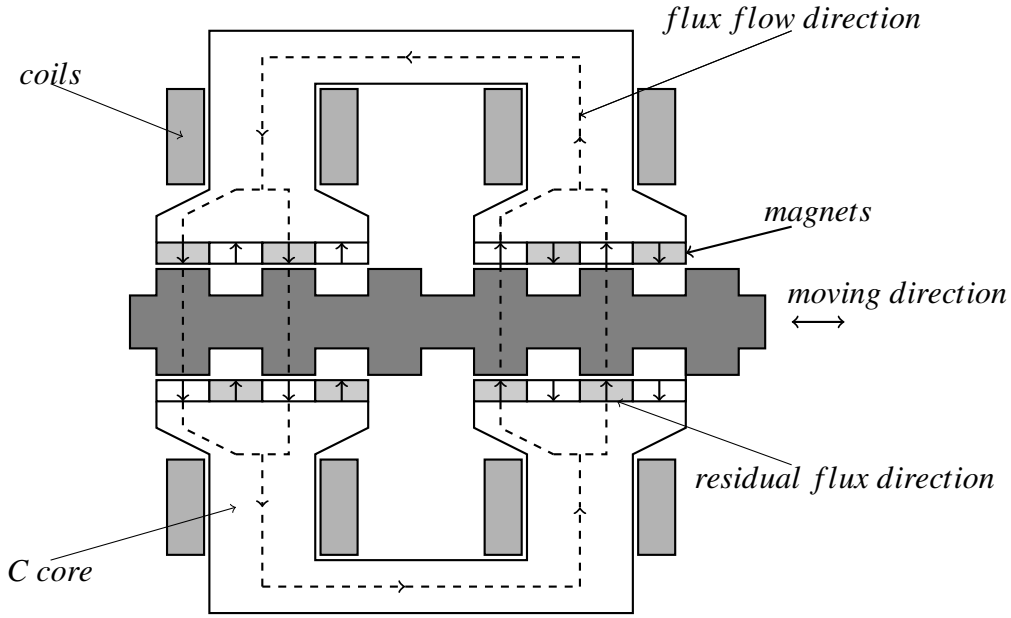

Figure 2.14: Typical configuration of VHM.

2.5.3 Tubular Machines

The prototype of the linear permanent magnet machine which was used by AWS is over 10 metres long and can produce an average power output of only about 400kW. This large machine resulted from high investment but achieved lower power generation than expected; furthermore, it increased the difficulty of construction. Technological innovation in a new type of linear generator such as the VRPM, described in Section 2.5.2, has overcome the difficulties which existed in conventional machines. The application of new magnetic materials along with the toothed design has significantly increased the specific force.

Design of a linear generator can be improved by making the stationary copper coils tubular and surrounding the magnetized translator. The translator is made up of a series of axially magnetized permanent magnet discs with alternating polarity, separated by steel discs mounted on a central shaft as shown in Figure 2.15. This slots into a second cylinder made up of circumferentially wound copper coils. For a linear generator operating in ocean waves, a large machine which can provide a large force must be designed to cancel out the low speed motion. This also produces a significant force of attraction between stator and translator which needs additional mechanical structure to support it and an appropriate lubrication system. In tubular machines, design of the stator is ironless to reduce the force between the two parts. A detailed description of this air cored tubular machine is found in [62, 66]. In this thesis, a specific design of a tubular machine is used which was fully tested and validated by Richard Crozier, researcher at the Institute for Energy Systems, University of Edinburgh.

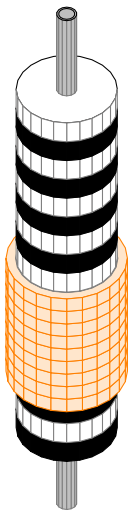

Figure 2.15: 3D representation of the tubular machine.

2.5.4 Comparison of Linear Generators

Cost comparison

The synchronous and induction linear machines require only iron and copper to construct its stator and translator which simplifies the structure and greatly reduces the cost of materials. In contrast, due to the requirement for permanent magnets, the costs of the linear permanent magnet synchronous machine, the VRPM machine and the tubular machine are dramatically higher. The tubular machines use much more magnetic material than VHM and TFM machines, because the permanent magnets have to cover half the length of the translator; hence, the longer the translator is designed, the more magnetic material is used. The VHM machine uses fewer magnets to cover its stator area. The TFM topology has a very complicated structure compared to a tubular machine which must also be taken into account as an extra cost for assembly.

Suitability for wave energy

Ocean waves can only produce slow velocity which requires a bulky linear machine to provide higher forces. To successfully handle and locate such a large device in harsh environments is difficult and costly. Therefore, the best design should aim to obtain a high force but to reduce size and weight. Permanent magnet machines seem to be more competitive than conventional electrical machines due to higher Maxwell shear stress between the translator and stator. From all types of machines previously discussed, the TFM can provide the highest shear stress, but has the disadvantages of complex structure and high cogging torque. To further increase the relative velocity between the stator and translator, a novel Snapper generator is under investigation [67]. This Snapper generator can use any type of linear generator introduced above, but with an additional set of springs attached between the armature and the sea bed. Here, the term stator is no longer used because the armature can move under the attraction force. As the armature is attracted to move, the springs are compressed or extended to store energy. Eventually, the armature can accelerate rapidly in the opposite direction to the translator movement when the spring forces are strong enough. Such a high relative

motion produces a pulse output power which can be used to reduce the size of the device.

Slip rings are used in conventional electrical machines (linear induction machine or field wound synchronous machine) for transferring currents to the translator. This mechanical contact increases the opportunity of failure and need for routine maintenance which is not favourable in ocean wave energy, especially for offshore deep water. However, it is easy to instantly switch off the output power by cutting off the field current to make the whole process neutral. This cannot be achieved for a permanent magnet machine. Instead, the outputs from the translator have to be shorted together to stop power flowing to the grid [62]. Large currents are hence created inside the coils. To prevent serious damage to the device, an extra large inductance should be included in the short circuit to limit the currents.

Another disadvantage of VRPM machines is that both the TFM and the VHM suffer from low power factor between 0.35 and 0.55 [68]. To obtain a high specific force, the VRPM machine is designed to change flux flow direction in a very short distance which is the width of one translator tooth. To prevent rapid current change in the coils, a large inductance has to be included which is a contributor to the low power factor. Hence, a power converter with active rectifier is connected to the electrical circuit to adjust the current to be in phase with the voltage to get as higher power factor as possible.

2.6 Introduction to Power Converters

2.6.1 Electrical Power Converter

A power converter is an electrical device to convert electrical energy from alternating current (ac) to dc or from dc to ac, or from ac to ac but with different frequency or even from dc to dc. The device that converts ac to dc is called a rectifier, and the device which does the opposite is called an inverter. The device that converts one dc voltage level to another dc voltage level is called a dc-to-dc converter or dc chopper.

There are several semiconductor devices used in power converters. The diode and thyristor are two typical one-way devices where current can only flow in one direction. These two types of devices can allow a high voltage up to 12,000 V and a high current up to 8,000 A. The power MOSFET device has the highest switching frequency which can reach 10 MHz, but with a very low voltage and current limitation. The insulated gate bipolar transistor (IGBT) and integrated gate-commutated thyristor (IGCT) are the most commonly used devices with different advantages and disadvantages. The IGCT can conduct up to 40 kA current which is much bigger than the 3,000 A which is the limitation of the IGBT. However, the IGBT can have a switching frequency up to 100 kHz which is much bigger than the 25 kHz of the IGCT. Currently, the IGBT is most widely used for medium to high power conversion systems due to its fast switching and low conduction losses [69].

2.6.2 Wave Energy Application

Recent research in wave energy is focusing on ways to create a successful device to interact best with ocean waves, and significant progress has been made by a handful of companies and organizations in designing wave energy structures for maximum power extraction. The power conversion process also plays a vital role in converting wave energy to useful electricity that can be integrated into the grid. Technology for power conversion in wave power systems is still very much in its infancy and its further development will have a major influence on both device performance, so that the device can be controlled by the power conversion system to move in phase with the incoming waves to extract maximum power, and power quality, so that unity power factor is achieved for connecting the system to the network.

Variability of ocean waves naturally results in varying output power after the primary interface. This output appears in different ways based on the different PTO systems. The variable outputs are high pressure oil for a hydraulic system, compressed air for a pneumatic system and electrical output for a direct drive system. In the first two PTO systems, the electrical machines are driven by either a hydraulic motor or a Wells

turbine. If these two mechanical systems are not controlled, the electrical output from the generators will have a varying frequency and amplitude which cannot be integrated into the electricity grid. For a hydraulic system, such as Pelamis, a high pressure accumulator is applied to smooth the electrical output. As the sea waves are big and produce high oil pressure in the accumulator, energy is stored which will be released when the sea waves are not big enough to meet the output power requirement. For a pneumatic system, such as the OWC, there is no effective way to achieve mechanical power conditioning, thus a power converter is included.

A direct drive system does not use any mechanical linkage and power generation is directly from the linear generator so that power storage can only be achieved by an electrical method. A comparison of output power generation after the electrical generators among three PTO systems are simulated by Shek [70], showing that power generation is smoothed for a hydraulic system, but further control is required for both of the other two systems. Unlike a rotating machine where energy can be stored based on the inertia of the machine, whereby the machine can keep rotating even when the air flow or fluid flow is zero, a linear generator has to move according to the oscillating of a heaving buoy, which means the translator has to stop for an instant and change its moving direction, resulting in zero power generation during that small period. To achieve power storage and good power quality, a power converter which consists of two back-to-back inverters provides the only solution for a direct drive system. The whole system from a floating buoy to electricity gid is shown in Figure 2.16. This is a traditional ac/ac converter with a dc rail to achieve short-term energy storage. The capability of reducing the power fluctuation depends on the capacitor chosen: the bigger size of the capacitor, the better smoothing can be achieved but at a significant cost. If a 100kW WEC is taken as an example, almost over 200 normal size capacitors are required which adds an extra cost of about £ 16,000 to the power converter [71]. In this typical system in Figure 2.16, an active rectifier is used to control either the device performance or the power quality, and an inverter is implemented to maintain the constant voltage of the dc link. Therefore, power flow is potentially bi-directional.

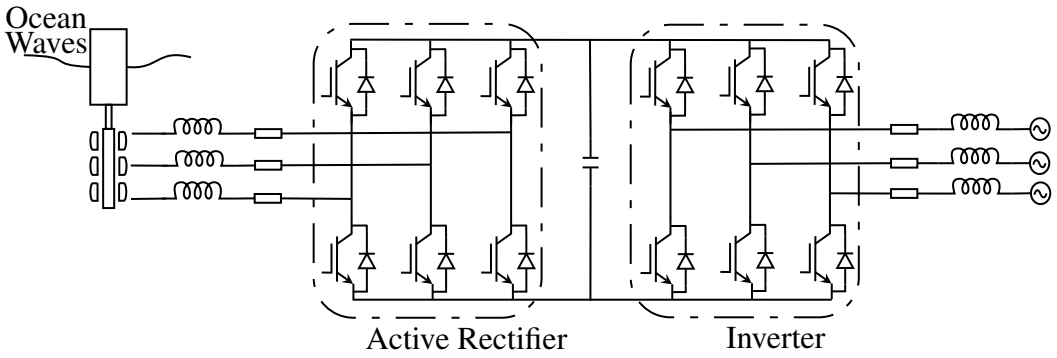

Figure 2.16: Direct drive linear generator interacts with ocean waves with a power converter connected between it and the grid to achieve power conditioning.

2.6.3 Pulse Width Modulation

Pulse width modulation (PWM) is commonly used for controlling modern electronic power switches. There are two commonly used methods which are carrier based PWM and space vector modulation and the relationship between these two methods is detailed in [72]. The carrier based PWM uses a reference waveform compared with a high frequency triangular carrier to obtain the control signal.

Figure 2.17 shows a three phase bridge converter which is controlled by carrier based PWM. In this figure, the dc link voltages is presumed to be constant with the value V_{dc}. The voltages at the midpoint of each leg $(v_a^{'}, v_b^{'}, v_c^{'})$ can be adjusted by controlling the six IGBT gates. For the sake of completeness, an inductance is included in the circuit but can be ignored in this analysis. A reference voltage is generated (as shown in red line) to be compared with the triangular carried voltage (as shown in blue line) to generate the control signals. The phase voltage can then be obtained by calculating the average value that is described in Equation 2.15.

$$v_i = \frac{V_{dc}}{2} \cdot \frac{\hat{v}_{ref}}{\hat{v}_{car}} \ (i = a, b, c) \tag{2.15}$$

Here, the expression of $\hat{v}_{ref}/\hat{v}_{car}$ is called the modulation index which is represented by m. Therefore, the phase voltage, phase rms value and line rms value are described in Equations 2.16, 2.17 and 2.18, where, $\hat{v}_i$, $\hat{v}_{ref}$ and $\hat{v}_{car}$ indicates the maximum value.

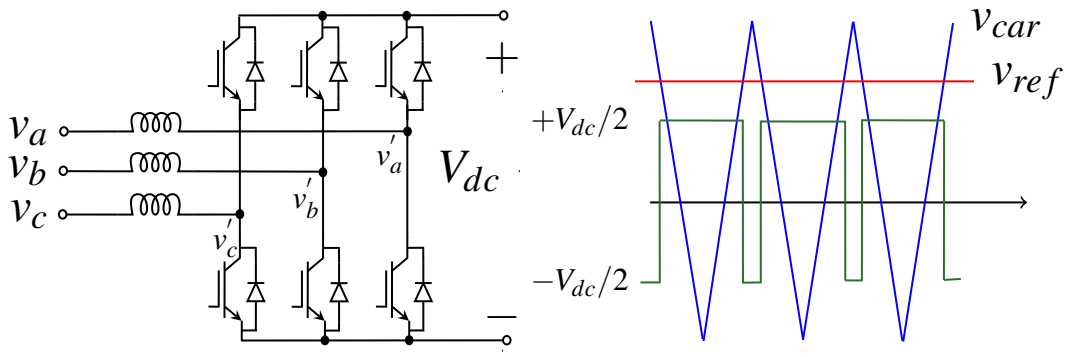

Figure 2.17: Three phase bridge converter with its PWM control method

$$\hat{v}_i = m \cdot \frac{V_{dc}}{2} \ (i = a,b,c) \tag{2.16}$$

$$v_{i-rms} = m \cdot \frac{V_{dc}}{2\sqrt{2}} \ (i = a,b,c) \tag{2.17}$$

$$v_{l-rms} = m \cdot \frac{\sqrt{3} \cdot V_{dc}}{2\sqrt{2}} \tag{2.18}$$

2.7 System Consideration

The dimensions of the buoy chosen in this thesis follows the typical buoy size which is fully described in [73]. It is a cylindrical buoy due to linear response. The draft of the buoy is 1.88 times the radius of the cross section and hence, all the hydrodynamic parameters can be obtained based on the curves described in Chapter 3.4. Indeed, as the buoy's draft cannot be maintained exactly the same, the hydrodynamic parameters may vary during the operation. In this work, the draft is assumed to be same which gives an approximation results. The generator design was based on the output of an optimisation routine for the generator operating with a similar sized buoy but with no control system, just working passively. In this work it was found that this was insufficiently large to provide the necessary force for control without overheating. For this reason two generators are used to supply the force. It is possible to make the generator longer, but such a generator would be impractically long for structural reasons. It should be

noted that in the future, a generator should be designed specifically for the system including the control method. As this thesis is a study on the application of reaction force control onto linear generator, doing extensive design work on the generator for this application is though to be outside the scope of the work. The rating of the power converter is based on the peak value of the output voltage and current. As a large force is required to achieve reaction force control, a big power converter is selected in this thesis which is assumed to be able to provide enough current required. In fact, this configuration is not economic due to a very high peak-to-average ratio.

2.8 Chapter Summary

This chapter provides background introducing the basic knowledge required in this thesis. There are three main areas in a wave energy conversion system, which are power intercepted by the wave energy device, power captured by a linear generator and power delivered and conditioned by the power converter. The comparison between different PTO systems is highlighted and the advantages and disadvantages of a direct drive system are presented. Section 2.2 and 2.3 give information on ocean waves and ocean wave generation. The Fourier Transform technique is applied to wave generation according to computer aided software. Section 2.4 and 2.5 introduce power capture by a linear generator and classifications of linear generators. Section 2.6 introduces the electrical power converter for energy storage and smoothing.

Chapter 3

Linear Wave Energy Converter Dynamics

3.1 Introduction

This chapter presents the linear dynamics of a WEC which is operating on a real ocean surface. The dynamic model created in this chapter is a preparation for the following chapters. Ocean wave generation is the first step for not only this chapter but is also the beginning of the entire simulation work. Unlike multi-frequency waves, real ocean waves are not periodic and vary continuously in frequency and amplitude. An empirical energy spectrum as well as Fourier analysis are applied to generate the time domain irregular waves. An immersed, heave motion only, WEC interacts with the generated irregular waves according to the basic theory of a traditional mass-spring-damper system, so that the acceleration, velocity and displacement of the oscillating body can be simulated. However, due to the interaction between the water and the oscillating buoy, a radiation force is created that makes the whole system different from traditional mass-spring-damper systems. The radiation force consists of two parts; (a) added mass which can be regarded as physical inertia, and (b) added damping which needs to be considered for the determination of the optimal damping force to achieve high power capture. Both the added mass coefficient and the added damping coefficient are functions of frequency and non-dimensional graphs are provided to calculate different values according to different frequencies. In addition a non-dimensional impulse response graph is also given to provide an accurate hydrodynamic model.

3.2 Ocean Wave Generation

This thesis aims to implement control methods for direct drive linear generator WECs in irregular waves. Random waves simulation thus plays a key role in starting the whole model simulation. A number of techniques for generating random ocean waves with specified characteristics have been developed. All of them can be categorized into two main approaches, deterministic approach and non-deterministic approach [74]. The deterministic approach for wave generation produces random waves within a finite time period. The irregular waves generated in this period follow exactly the information of the wave energy spectrum in the frequency domain. As for the non-deterministic approach, an infinite time series wave can be produced. During its time span, there should be a period of waves following the required information provided by the spectrum. A debate as to which approach is better is ongoing, but as yet there is no wide universal consensus. The random phase method, which belongs to the deterministic approach, is widely used to produce irregular waves. Based on the Inverse Discrete Fourier Transform (IDFT), wave elevation can be derived from a desired spectrum by providing random phase values. As for the non-deterministic approach, there are two important methods for generating waves: the random complex spectrum method, and the white noise filtering method. The random complex spectrum method also relies on the IDFT but with Gaussian distributed amplitude spectra. The white noise filtering method applies a digital filter to convolute with spectral values from the desired spectrum. In this work, the random phase method is introduced to generate random waves based on PM spectrum.

3.2.1 Wave Energy Spectrum Generation

The spectrum of waves describes the changes of wave energy density with frequency. To generate time domain ocean waves, a specific wave energy spectrum has to be selected and modelled. As introduced in Section 2.2.4, two types of wave energy spectrum can be selected, the PM spectrum and the JONSWAP spectrum. The PM spectrum is obtained and used by assuming that the wind blows over a fully developed sea. It

is regarded as a one-parameter spectrum as its generation relies on only one input, either wind speed, peak frequency or significant wave height. As for the JONSWAP spectrum, five parameters are needed to obtain the spectrum, which is, therefore, a more realistic spectra. It can be seen from Figure 3.1 that wave spectral density is normally non-stationary which implies the spectrum changes with time due to weather change. In fact, JONSWAP spectrum is used to describe non-stationary spectral density because all factors are related to the wind speed. In this thesis, non-stationary wave spectral density is not considered and the PM spectrum provides acceptable accuracy for modelling fully developed waves, therefore, it is selected for irregular wave generation.

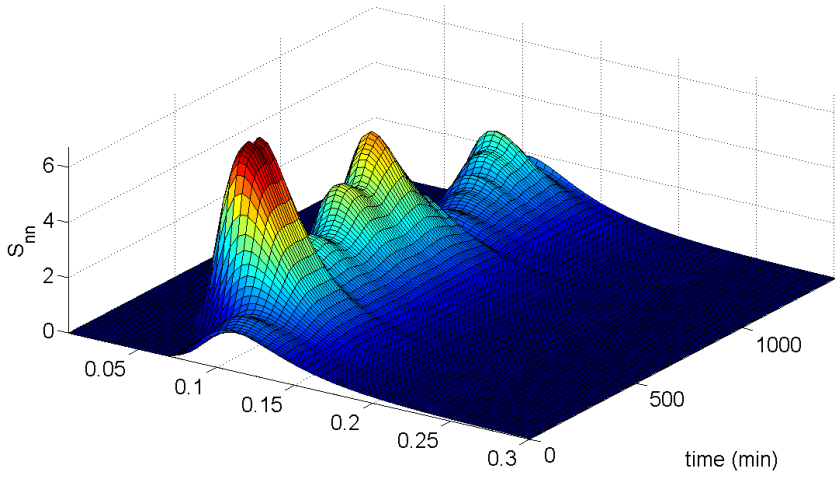

Figure 3.1: Non-stationary wave spectral density.

The PM spectrum is given in Equation 2.6 by using angular frequency which can be rewritten in Equation 3.1.

$$S(f) = \frac{5}{16} H_s^2 f_p^4 f^{-5} exp\left[-\frac{5}{4}\left(\frac{f_p}{f}\right)^4\right] \tag{3.1}$$

Two parameters are used in the above equation to determine the spectrum, f_p (peak frequency) and H_s (significant wave height), which is contradictory to what has been presented before. Indeed, for every peak frequency, there should be a unique corre-

sponding significant wave height. The relation between them is given in Equation 3.2 [36], therefore, the frequency domain wave energy spectrum can be obtained by only giving the value of the peak frequency, which can be calculated by a measured wind speed at the 19.5 m above the sea surface according to Equation 2.5.

$$H_s = 0.162g/(2\pi f_p)^2 \tag{3.2}$$

Figure 3.2 shows different PM spectra by giving different peak frequencies. It can be seen from the figure that wave energy density decreases as the peak frequency increases. For every energy spectrum, the maximum energy density occurs at the peak frequency and dramatically reduces when frequency moves away from the peak point. In addition, the figure shows that most energy is held by the waves that are near the peak frequency, and thus control should be focused on extracting power from these ocean waves.

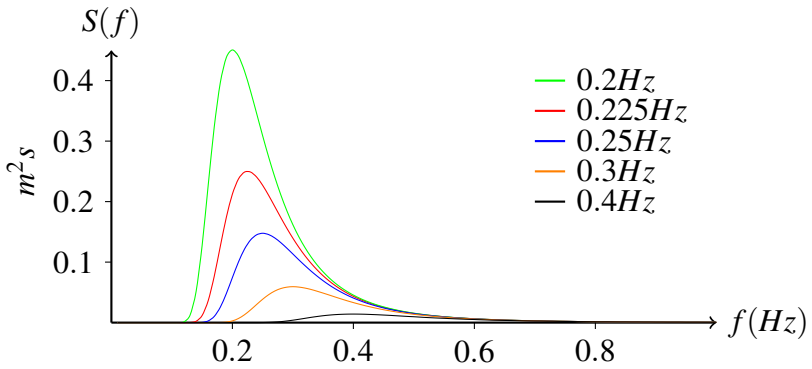

Figure 3.2: Wave energy distribution (wave energy density) at different peak frequencies.

3.2.2 Discrete Wave Energy Spectrum

This section introduces the basic knowledge required to obtain the discrete wave energy spectrum as the basis of the proceeding Inverse Discrete Fourier Transform to convert the frequency domain PM spectrum to the time domain wave elevation. Hence, it is important to review the Fourier Transform to clarify some important parameters.

If there is a time series waveform running for the period T, irrespective of the number of zero-crossing points during that period, the frequency of the waveform is $1/T$. On this selected waveform, N points are chosen with equal time interval during one period to be decomposed into N sine waves. Here, N is called the resolution of the spectrum, which is half the number of Fourier Components. The selection of these N points results in the time interval $\Delta t = T/N$, so the sample frequency (known as samples per second) is $f_s = N/T = 1/\Delta t$. All the parameters stated above are shown in Figure 3.3.

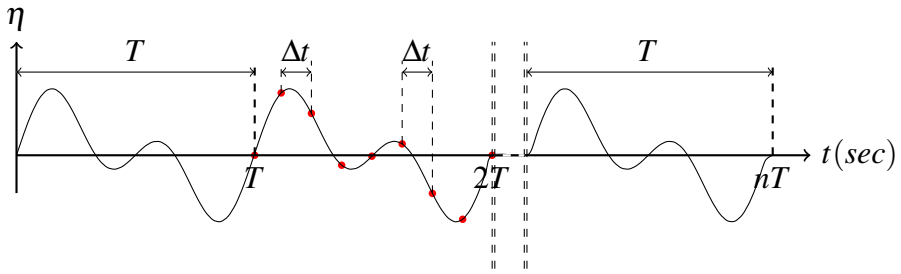

Figure 3.3: Fourier explanation.

In the frequency domain, N sine waves are described according to their amplitudes against frequencies. All these N sine waves have frequencies running from $1/T$ to N/T, hence, the frequency interval, which is also called the frequency domain resolution, $\Delta f = 1/T = 1/(N \cdot \Delta t) = f_s/N$.

Before we can obtain the wave elevation in the time domain, using the IDFT, the units in the wave energy density spectrum need to be converted. The wave elevation in the time domain has units in metres (or centimetres), and the units in the frequency domain should correspond. Hence, the continuous wave energy density spectrum in Equation 2.6 can be discretized in Equation 3.3. In this equation the wave energy density is multiplied by the frequency domain resolution Δf to achieve the correct unit (metres squared).

$$\sigma^2(f_i) = S(i \cdot \Delta f) \cdot \Delta f \tag{3.3}$$

where $\sigma^2(f_i)$ indicates the wave energy at an individual frequency and i represents

every sine wave running from 1 to N. The discrete wave energy is shown in Figure 3.4 based on the equation introduced above.

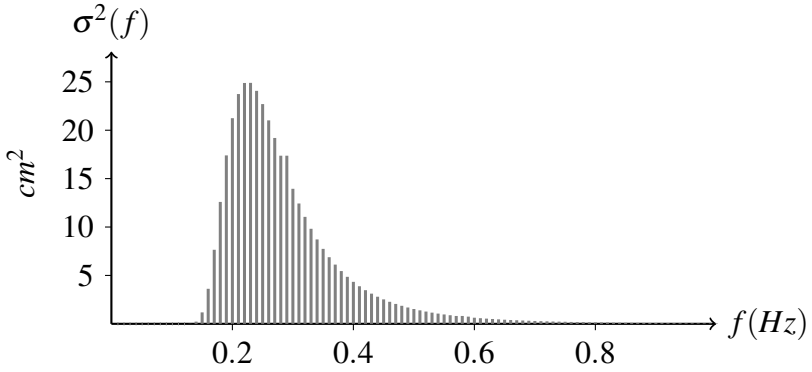

Figure 3.4: Discrete wave power distribution (discrete wave power density) of the PM spectrum.

3.2.3 Ocean Wave Generation

Irregular waves are generated by applying the IDFT to the discrete wave energy spectrum according to the random phase method. Random phases $\varphi(f)$ are generated randomly between 0 and 2π, which are subsequently allocated to all the frequencies from 1 to N to establish the real part A_i and the imaginary part B_i of the complex Fourier coefficients $C_i = A_i + j \cdot B_i$ as shown in Equation 3.4 and 3.5. The root of the discrete wave energy represents the magnitude of ocean waves in the frequency domain.

$$A_i = cos(\varphi(f_i)) \cdot \sqrt{\sigma^2(f_i)} \tag{3.4}$$

$$B_i = sin(\varphi(f_i)) \cdot \sqrt{\sigma^2(f_i)} \tag{3.5}$$

The calculation of the complex IDFT is based on the illustration in Section 2.3.3 where the negative frequencies have to be established in the proper format so that the imaginary part after the complex IDFT is zero. In this case, the real part value at point $N+1$ should be the same as the real part value at point $N-1$, whereas the imaginary part value at point $N+1$ should be the same as the negative imaginary part value at

point $N-1$. This relation can be simply achieved by the complex conjugate theory as shown in Equation 3.6.

$$C_{N+i} = C^*_{N-i} \tag{3.6}$$

From the above analysis, the length of the complex Fourier coefficients is $2N-2$ which determines the period in the time domain as introduced in Section 3.2.2. By applying the Inverse FFT (IFFT), the time domain wave elevation by giving the peak frequency 0.225 Hz is shown in Figure 3.5.

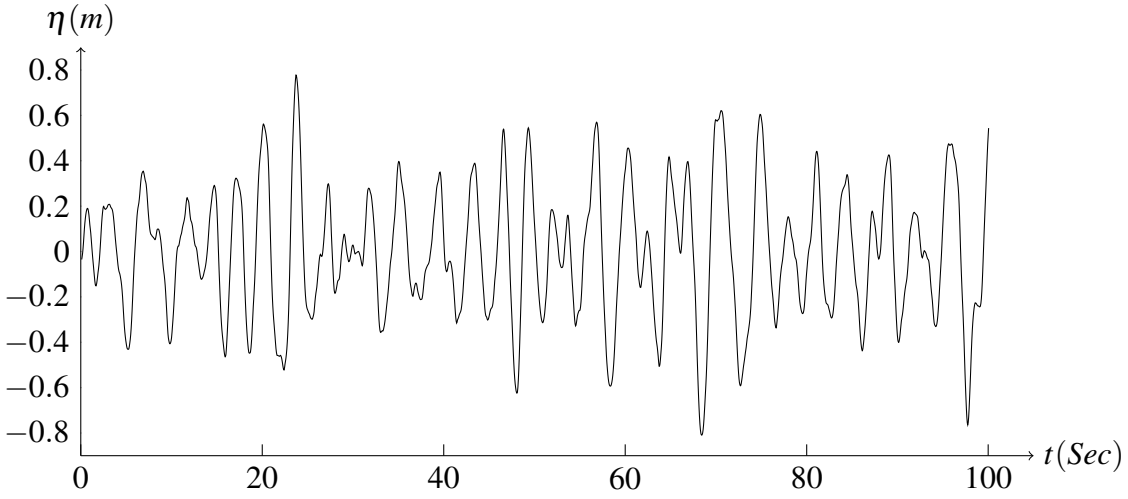

Figure 3.5: Time domain wave elevation by applying the IFFT to the PM spectrum with peak frequency 0.225 Hz.

3.3 Oscillating Systems

A floating buoy on the ocean surface moves with the ocean waves. This up and down oscillation is effectively a simple mass-spring-damper system which can be analysed using Newton's Second Law. This section introduces the basic working principle of two concepts of simple mechanical mass-spring-damper systems, free oscillation and forced oscillation. Force analysis of this mechanical system can be interpreted using electrical analogies. The frequency domain representation of a floating buoy is provided as preparation for time domain analysis. A convolution term which includes

an impulse response emerges after applying an IDFT to the frequency domain representation to get the time domain representation. Depending on the impulse response transfer function, such a system can be classified as either a memoryless system, a causal system, an anticausal system or an acausal system.

3.3.1 Traditional Oscillator and Electrical Analogue

Figure 3.6 shows a typical mass-spring-damper system where the left figure shows a free oscillating system and the right figure shows a forced oscillating system. It is assumed a mass m is suspended from a ceiling by a mechanical spring k_m and a mechanical damper b_m. If the mass is forced to a position x from its equilibrium position under an external force which is then removed to let the mass move freely, the equation of motion is given by Equation 3.7:

$$m\ddot{x} + b_m\dot{x} + k_m x = 0 \tag{3.7}$$

where the product of mass and acceleration is inertia force, the product of damping coefficient and velocity is damping force, and the product of spring stiffness and displacement is spring force. If the external force on the mass is still present during motion, the equation can be rewritten as shown in Equation 3.8.

$$m\ddot{x} + b_m\dot{x} + k_m x = f(t) \tag{3.8}$$

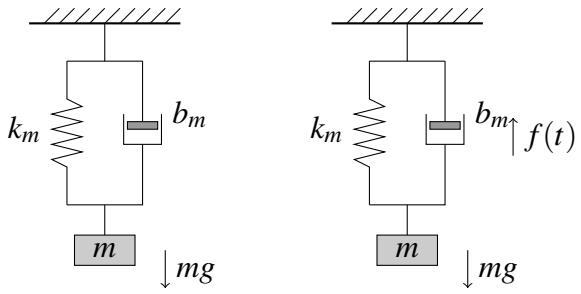

Figure 3.6: Traditional mass-spring-damper system.

To investigate the maximum power transfer, the mechanical system can be represented

using an electrical circuit [75]. In the mechanical oscillating system, a differential equation describes the relationship between the external force and the displacement. Similarly, in a simple RLC (resistor, inductor and capacitor) series circuit as shown in Figure 3.7, a differential equation can be used to create a relationship between the source voltage and charge on the capacitor. Hence, in order to relate the electrical system to the mechanical system, some physical equivalencies between the mechanical system and electrical system can be described as below, and the corresponding electrical equation is given in Equation 3.9.

- external force $\longrightarrow$ source voltage
- mass $\longrightarrow$ inductance
- damping coefficient $\longrightarrow$ resistance
- spring stiffness coefficient $\longrightarrow$ 1/capacitance
- displacement $\longrightarrow$ charge

$$L\ddot{q} + R\dot{q} + \frac{1}{C}q = e(t) \tag{3.9}$$

In the above equation, $\dot{q}$ is the current which corresponds to velocity in the mechanical system. The damper in the mechanical system and the resistor in the electrical system are both used to dissipate energy. The spring and inertia in the mechanical system, and the capacitor and inductor in the electrical system are both used to store energy.

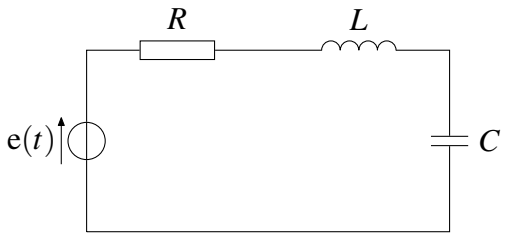

Figure 3.7: RLC series circuit representation.

3.3.2 Linear Dynamic Model of WECs

This thesis aims to create a mathematical model to represent the behaviour of the real WEC system in irregular waves. A linear dynamic system modelled by computer-aided simulation based on common theory is never linear in real conditions. Systems such as a mass-spring-damper and an RLC circuit are nearly linear, thus a linear system model can provide a good approximation. However, the physical system of a WEC operating in ocean waves is highly non-linear due to non-linear hydrodynamic response and non-linear PTO. As the floating buoy is operated under heave, surge and pitch, the motion of the buoy cannot be exactly vertical, hence the hydrodynamic response is non-linear. However, this non-vertical motion is not the only cause of non-linearity of the hydrodynamic response, there are several other possible causes, including steep waves, large motions to hit end-stop systems or non-linear PTO force. The non-linear PTO force is normally caused by the variable pressure of the hydraulic circuit and the end-stop devices. Here, a linear model is provided which is only appropriate for a sub-set of the behaviour [23].

To simplify the system, a linear equation is applied to describe the WEC where wave excitation is the input and motion is the output. The system governing equation of motion is given in Equation 3.10, which is Newton's second law, $f = ma$. The total force consists of wave excitation force, force due to energy loss, radiation force, spring force and PTO force.

$$f_e - f_{loss} - f_r - f_s - f_{pto} = ma \tag{3.10}$$

where,

f_e is the wave excitation force

f_{loss} is the net force due to energy losses

f_r is the radiation force

f_s is the buoyancy spring force

f_{pto} is the force from PTO system

Equation 3.10 is only for force analysis and is only suitable for a subset of the behaviour of the WEC. This force analysis can be rewritten in both time domain and frequency domain equations. The frequency domain expression is introduced first, in Section 3.3.3, as it is directly derived from the force analysis in Equation 3.10 and is much easier to understand. All of the parameters in the frequency domain are functions of frequency and can be changed into functions of time by applying an Inverse Fourier Transform. The corresponding time domain equation is easier to implement into computer aided software such as Matlab/Simulink. In addition, the time domain expression can be better used to explain causality as is discussed in Section 3.3.5. In this thesis, an upper case letter is used to describe a frequency domain equation and lower case is used to describe a time domain equation. A Fourier Transform and Inverse Fourier Transform are applied to make the conversion between them, such as the transformation of displacement, velocity and acceleration from the time domain to the frequency domain as shown in Equations 3.11,3.12 and 3.13.

$$X(\omega) = \mathscr{F}x(t) \tag{3.11}$$

$$i\omega X(\omega) = \mathscr{F}\dot{x}(t) \tag{3.12}$$

$$-\omega^2 X(\omega) = \mathscr{F}\ddot{x}(t) \tag{3.13}$$

3.3.3 Frequency Domain Representation of WECs

The easiest way to describe linear motion is in the frequency domain and Equation 3.10 can be expressed as shown in Equation 3.14.

$$F_e(\omega) = mA(\omega) + F_{loss}(\omega) + F_r(\omega) + F_s(\omega) + F_{pto}(\omega) \tag{3.14}$$

Acceleration against frequency is defined as $A(\omega)$. It is normal to use the Fourier Transformation of velocity to replace acceleration and displacement due to the simple calculation of power transfer. As the WEC oscillates with ocean waves, it operates as

a normal mass-spring-damper system and can be interpreted by using the knowledge of the electrical circuit introduced in Section 3.3.1. The wave excitation force F_e can be regarded as the source voltage, the mass term is represented by the inductance, the loss and radiation force are represented by the resistor, and the buoyancy spring force is represented by the capacitor. Hence, we can borrow the term *impedance* from an electrical circuit to describe a mechanical WEC system.

The loss term in Equation 3.14 is contributed to by fluid losses and mechanical losses. Fluid loss is caused due to the existence of viscosity and drag forces, whereas, mechanical loss is regarded as the energy losses due to the mechanical force between mechanical linkages, such as, the linkage between the floating buoy and the translator. Normally, the loss force is very small compared to other forces, such as the wave excitation force and the PTO force, therefore it is not included in the following work of this thesis as shown in Equation 3.15.

$$F_e(\omega) = j\omega m U(\omega) + Z_r(\omega)U(\omega) + \frac{c}{j\omega}U(\omega) + Z_{pto}(\omega)U(\omega) \tag{3.15}$$

where,

$Z_r(\omega)$ is the radiation impedance

c is the buoyancy spring stiffness

$Z_{pto}(\omega)$ is the PTO impedance

$U(\omega)$ is the velocity in frequency domain

The difference between Equation 3.15 and Equation 3.8 is that the damping coefficient is replaced by radiation impedance, because the oscillating mass has been changed from a suspended object in the air to an immersed WEC in the water. The oscillating motion of the immersed buoy results in motion of the surrounding water and some of the energy is taken away by radiated waves. However, some of the energy is stored in the form of kinetic energy due to the velocity of the water. In addition, there is also some potential energy, cause by gravity, stored in the water because of the height change of the water surface. Both the stored kinetic energy and potential energy will

be eventually added to the mechanical oscillating system. Hence, a new term *radiation reactance* $X_r(\omega)$ is introduced here related to the difference between the average added kinetic energy and the added potential energy, which is indicated in Equation 3.16 [73],

$$X_r(\omega) = \omega M_{add}(\omega) \tag{3.16}$$

where $M_{add}(\omega)$ is the so-called added mass. It is usually positive unless the added potential energy is larger than the added kinetic energy.

As $Z_r(\omega)$, here named radiation impedance, is equivalent to electrical impedance, hence it should be a complex value. The imaginary part is the added mass coefficient and the real part should be the real damping coefficient (also called added damping coefficient), hence it can be written in Equation 3.17.

$$Z_r(\omega) = B_{add}(\omega) + jX_r(\omega) = B_{add}(\omega) + j\omega M_{add}(\omega) \tag{3.17}$$

where $B_{add}(\omega)$ is the added damping coefficient. Both the added mass and added damping are functions of frequency. To simplify the equation, the subscript *add*, which makes the equation more complicated and difficult to read, can be replaced by using $M(\omega)$ and $B(\omega)$, hence Equation 3.17 can be written as shown in Equation 3.18.

$$Z_r(\omega) = B(\omega) + jX_r(\omega) = B(\omega) + j\omega M(\omega) \tag{3.18}$$

Replacing $Z_r(\omega)$ in Equation 3.15 by Equation 3.18 and combining the physical mass term and added mass term together, we can obtain the final equation of the WEC in Equation 3.19. Hence, it can be seen that the total mass of an immersed oscillating buoy is increased due to the radiation force.

$$F_e(\omega) = j\omega[m + M(\omega)]U(\omega) + B(\omega)U(\omega) + \frac{c}{j\omega}U(\omega) + Z_{pto}(\omega)U(\omega) \tag{3.19}$$

If we refer to our understanding of electrical circuits again, wave excitation force is the

source voltage, the PTO impedance can be deemed to be the load impedance, and thus the other three parts in Equation 3.19 constitute the intrinsic impedance, so the final equation can be written as shown in Equation 3.20.

$$F_e(\omega) = Z(\omega)U(\omega) + Z_{pto}(\omega)U(\omega) \tag{3.20}$$

Here, $Z(\omega)$ can be regarded as the intrinsic impedance and is given in Equation 3.21 by sorting out all the terms in Equation 3.19.

$$Z(\omega) = B(\omega) + j\left([m + M(\omega)] - \frac{c}{\omega}\right) \tag{3.21}$$

3.3.4 Time Domain Representation of WECs

The frequency domain representation of WECs can be simply converted into the time domain by applying the Inverse Fourier Transform. As it is linear in the frequency domain, each term can be transformed individually and combined together to generate the new time domain equation. The Inverse Fourier Transform does not change a constant value. For the term which is the multiplication of a fixed coefficient and a frequency domain function, the Inverse Fourier Transform can be applied by keeping the coefficient the same and changing the frequency domain function into the time domain function. However, for the term which is the multiplication of two frequency domain functions, the prerequisite of applying the Inverse Fourier Transform is that at least one of the frequency domain functions must have a zero value when the frequency approaches infinity. Furthermore, the Inverse Fourier Transform on the multiplication of two frequency domain functions gives a convolution term in the time domain as explained in Equation 3.22.

$$\mathscr{F}^{-1}[G(\omega)H(\omega)] = g(t) * h(t) \tag{3.22}$$

Equation 3.19 has two multiplication of two frequency function products, $j\omega[m +$

$M(\omega)]U(\omega)$ and $B(\omega)U(\omega)$. As is shown in Section 3.4.3, the added mass coefficient tends to a value which is not zero as the frequency tends to infinity, thus it is not possible to apply the Inverse Fourier Transform on the first term. If that was possible, the two convolution terms in the equation would increase the computer calculation work considerably. Hence, the solution is to combine the two products together as a radiation force term as shown in Equation 3.23.

$$F_e(\omega) = j\omega mU(\omega) + [j\omega M(\omega) + B(\omega)]U(\omega) + \frac{c}{j\omega}U(\omega) + Z_{pto}(\omega)U(\omega) \quad (3.23)$$

Although two products of frequency functions are combined together to be only one term, the added mass term still exists that indicates the Inverse Fourier Transform is unavailable. If we assume that the added mass converges to a constant value m_∞, as well as the added damping coefficient converging to zero when the frequency approaches zero, m_∞ can be subtracted from the radiation impedance to obtain a new response function $K(\omega)$ as given in Equation 3.24 which tends to zero when the frequency approaches infinity.

$$\begin{aligned} K(\omega) &= Z_r - j\omega m_\infty \\ &= B(\omega) + j\omega[M(\omega) - m_\infty] \end{aligned} \quad (3.24)$$

The subtracted m_∞ is then added to physical mass to generate a new frequency domain equation as given in Equation 3.25. In this equation, the response function $K(\omega)$ converges to zero when the frequency approaches infinity as discussed in Section 3.4.3, which implies the Inverse Fourier Transform can be applied to obtain a convolution term in the time domain.

$$F_e(\omega) = j\omega[m + m_\infty]U(\omega) + K(\omega)U(\omega) + \frac{c}{j\omega}U(\omega) + Z_{pto}(\omega)U(\omega) \quad (3.25)$$

The Inverse Fourier Transform is then applied to Equation 3.25 to obtain the time

domain representation of WECs in Equation 3.26.

$$f_e(t) = [m + m_\infty]\ddot{x}(t) + k(t) * \dot{x}(t) + cx(t) + f_{pto}(t) \tag{3.26}$$

The convolution term indicates the radiation force and is a particular kind of integral transform defined as shown in Equation 3.27.

$$\begin{aligned}(k * \dot{x})(t) &= \int_{-\infty}^{\infty} k(\tau)\dot{x}(t-\tau)d\tau \\ &= \int_{-\infty}^{\infty} k(t-\tau)\dot{x}(\tau)d\tau\end{aligned} \tag{3.27}$$

The radiation impulse response $k(t)$ is only affected by present and past inputs and states, as is discussed in Section 3.3.5, which means the system has memory. This results in the impulse response zero when time is less than zero. Therefore, $\int_t^\infty k(t-\tau)u(\tau)dt = 0$, and Equation 3.26 can be rewritten as:

$$f_e(t) = [m + m_\infty]\ddot{x}(t) + \int_0^t k(\tau) * \dot{x}(t-\tau)d\tau + cx(t) + f_{pto}(t) \tag{3.28}$$

3.3.5 Systems Analysis

System analysis is a special terminology used in the field of electrical engineering to define electrical systems and also to characterize the system properties. Memoryless and causality are two important concepts to distinguish the systems. In wave energy engineering, the electrical system analysis is used to define the mechanical systems. Under this system analysis, the oscillating systems can be classified into two different categories, wet oscillators and dry oscillators.

Memoryless system

The definition of a memoryless system is a system in which past information does not affect the present value or state. This can be simply explained using an electrical circuit example which has only a voltage source and a resistor. The current can be regarded as the output of the system and is only affected by the instantaneous voltage value. If either an inductor or a capacitor is connected into the circuit, energy is stored in this component, so that the current depends not only on the source voltage but also on the energy that has previously been stored in the inductor or the capacitor. Hence, this type of system has memory in which the past information determines the present state. For a mechanical system, such as a mass-spring-damper system, the mass term plays the role of an inductor, and the spring term plays the role of a capacitor. The past value of acceleration contributes to inertia while the past displacement contributes to spring force. Therefore, the present velocity is not only affected by the present value of the external force, but also by the energy stored in the inertia and the spring. In this analysis, a mechanical memoryless system is when only damping is applied under an external force.

In wave energy engineering, the term memoryless does not fit the standard definition because a system with a convolution term is often described as a causal system with memory (as introduced later). Hence, a mass-spring-damper system with no convolution term, in wave energy, is considered to be a memoryless system where the present state is only affected by the instantaneous excitation force.

Causality

The term causality in systems analysis refers to three different types of system: causal system, acausal system and anticausal system. A causal system is a system whose output is dependent on past input and present inputs. An acausal, or non-causal, system is a system in which the output depends on past, present and future inputs, and a system that depends solely on future inputs is called an anticausal system.

The systems analysis introduced above is used for analyzing the system in this thesis.

$k(t-\tau)$ type	Requirements	System
Instantaneous term	$k(t-\tau) \neq 0$ when $t-\tau = 0$ $k(t-\tau) = 0$ when $t-\tau \neq 0$	Memoryless
Memory term	$k(t-\tau) \neq 0$ when $t-\tau \geq 0$ $k(t-\tau) = 0$ when $t-\tau = \infty$ or $t-\tau < 0$	Causal
Premonition term	$k(t-\tau) \neq 0$ when $t-\tau \leq 0$ $k(t-\tau) = 0$ when $t-\tau = -\infty$ or $t-\tau > 0$	Anticausal
Memory/Premonition term	$k(t-\tau) \neq 0$ when $-\infty < t-\tau < \infty$ $k(t-\tau) = 0$ when $t-\tau = \pm\infty$	Acausal

Table 3.1: The influence of the impulse response for four different systems

If we refer to Equation 3.26 but exclude the PTO force, it can be rewritten as Equation 3.29.

$$f_e(t) = [m+m_\infty]\ddot{x}(t) + k(t-\tau) * \dot{x}(\tau) + cx(t) \tag{3.29}$$

In this equation, the mass and spring stiffness terms are regarded as two memoryless terms which depend only on the present excitation force, whereas $k(t-\tau) * \dot{x}(\tau)$ is the convolution term and the impulse response $k(t-\tau)$ determines whether the system is a memoryless system, a causal system, an acausal system or an anticausal system which are defined in in Table 3.1. Therefore, the time domain representation of WECs described in Equation 3.28 is a causal system. This can be explained in that the radiation force is affected by the past motion state and plays a key role in affecting the present state of motion.

Wet and dry oscillators

The oscillators in wave energy engineering can be divided into wet oscillators and dry oscillators as was first proposed by Price [23], to better distinguish the motion behaviour of a WEC in both regular and irregular waves. A dry oscillator can be regarded as a simple mass-spring-damper system in air or in regular waves with the damping coefficient a constant value and not affected by past values. In contrast, a wet oscillator can be regarded as an oscillator buoy that is operating in irregular waves, thus the damping coefficient is affected by past values. It is possible to describe these two types of oscillating systems by using the knowledge of system analysis introduced

above. For simplicity, PTO force is not included in the following analysis.

The wet oscillator model has a memory damping term which indicates it is a causal system. The mass term is directly proportional to the instantaneous acceleration and the spring term is directly proportional to the instantaneous displacement. However, the damping term has a convolution between impulse response and velocity which implies the damping term is affected not only by the present input but also by the past state. The equation expression of a wet oscillator can be simply obtained from Equation 3.28 but without PTO force, and is shown in Equation 3.30.

$$f_e(t) = [m + m_\infty]\ddot{x}(t) + \int_0^t k(\tau) * \dot{x}(t-\tau) + cx(t) \tag{3.30}$$

The dry oscillator is defined as a simple mass-spring-damper which operates in regular waves with single frequency, say ω_s. The radiation force can be simply obtained by calculating the added mass and radiation damping according to this given frequency. As the radiation force is no longer a function of frequency, there is no convolution term in the equation, which indicates that the dry oscillator model is a memoryless system with a frequency domain equation as given in Equation 3.31,

$$F_e(\omega) = j\omega[m + M(\omega_s)]U(\omega) + B(\omega_s)U(\omega) + \frac{c}{j\omega}U(\omega) \tag{3.31}$$

where, $M(\omega_s)$ and $B(\omega_s)$ are the added mass and the added damping at the specific frequency. Therefore, a time domain expression can be obtained using the Inverse Fourier Transform as shown in Equation 3.32.

$$f_e(t) = [m + M(\omega_s)]\ddot{x}(t) + B(\omega_s)\dot{x}(t) + cx(t) \tag{3.32}$$

3.4 Hydrodynamic Parameters

Hydrodynamics is a branch of science that deals with the dynamics of fluids. In wave energy engineering, hydrodynamics is more complicated as it can be interpreted as the interaction between a floating WEC and the incoming ocean waves. Hence, research on hydrodynamics for wave energy can be divided into three parts; fluid hydrodynamics which describes the motion characteristics of waves, floating device hydrodynamics which deals with the motion of a buoy under a wave excitation force, and the hydrodynamics of the relative motion between them. The floating device hydrodynamic parameters are regarded as intrinsic and thus are fixed as soon as the floating device has been designed. Apart from that, all other hydrodynamic parameters, such as wave excitation force and radiation force, are functions of frequency. Therefore, in regular waves, defining any of these hydrodynamic parameters is relatively simple due to the unique frequency of waves. This becomes more complicated when dealing with a floating WEC in irregular waves, because frequency is constantly varying.

3.4.1 Intrinsic Parameters

The basic hydrodynamic parameters for a WEC in ocean waves are its physical parameters, such as physical mass and buoyancy spring stiffness. These parameters are fixed once the floating buoy has been designed. If it is assumed that the semi-submerged buoy is freely sitting on the ocean surface, the mass of the body can be calculated by the mass of water displaced by the body. If the radius of the buoy is a metres and the draft is h metres, the total mass can be calculated using Equation 3.33, where, m is the total mass of the floating body.

$$m = \rho h \pi a^2 \tag{3.33}$$

In this thesis, this total mass is calculated by summing all physical masses together, including the buoy, the generator etc. A typical cylindrical buoy is selected to give a linear response which is fully described in [73].

All oscillating systems on ocean waves suffer from a buoyancy spring stiffness force

(referred as spring stiffness force later). For example, if a float is pushed down under the water surface, a vertical force is required. Once this force is removed, the float moves upwards due to its buoyancy and oscillates for a while until it returns to its original position. Hence, mechanical energy is stored in the buoyancy similar to a compressed spring. This buoyancy force is proportional to the cross sectional area of the oscillator and the distance it is pushed down. As distance changes when it oscillates, the spring stiffness force is expressed as the product of the constant spring stiffness coefficient given in Equation 3.34 and the displacement.

$$c = \rho g \pi a^2 \tag{3.34}$$

3.4.2 Wave Excitation Force

There are various ways for an oscillating body to interact with waves, when partly immersed in water. If a buoy sits on still water and experiences an external force, which is not from sea waves, it may generate waves due to the radiation force. On the other hand, if a buoy is assumed to be locked in a fixed position and in the path of an incident wave, it suffers from a scattering force or excitation force. In reality, both of these two interaction forces will also act on a buoy when it is unlocked.

Wave excitation force is considered to be the output of a linear system where the wave elevation is the input. In this thesis, the floating buoy is assumed to move only in one degree of freedom, known as heave. Hence, it is supposed that the buoy is fixed at one position along the wave path. The frequency domain expression for wave excitation force includes a transfer function as given in Equation 3.35, where $H(\omega)$ is the complex frequency response function which may be termed as the excitation force coefficient, and $\eta(\omega)$ is the wave elevation in the frequency domain. Based on the idea proposed in [76], the wave excitation force coefficient can be non-dimensionalised by dividing by the factor $\rho g \pi a^2$, and is plotted as shown in Figure 3.8. In this figure, k is wave number and is given by ω^2/g. This figure is only suitable when the draft is 1.88 times

the radius.

$$F_e(\omega) = H(\omega)\eta(\omega) \tag{3.35}$$

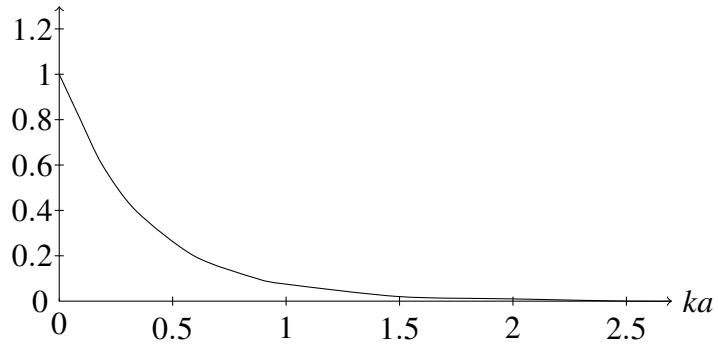

Figure 3.8: Non-dimension wave excitation force coefficient as a function of the product of wave number and radius.

The time domain expression, which includes an impulse response term $h(t)$, can be obtained by applying the Inverse Fourier Transform as shown in Equations 3.36 and 3.37. It can be seen from these equations that wave excitation force is an acausal system [77]. The present wave excitation force is affected by both past knowledge and future knowledge of the incident wave elevations. For time domain representation, the impulse response is provided in [73].

$$h(t) = \mathscr{F}^{-1}[H(\omega)] \tag{3.36}$$

$$f_e(t) = \int_{-\infty}^{\infty} h(\tau) * \eta(t-\tau) \tag{3.37}$$

Obtaining the time domain wave excitation force using Equation 3.37 increases the computation time due to the existence of the convolution term. A much faster method can be achieved by calculating the wave excitation force in the frequency domain and subsequently applying an Inverse Fourier Transform to the result as explained in Equation 3.38.

$$\begin{aligned} f_e(t) &= \mathscr{F}^{-1}[F_e(\omega)] \\ &= \mathscr{F}^{-1}[H(\omega)\eta(\omega)] \end{aligned} \tag{3.38}$$

Figure 3.9 provides an example of a time domain wave excitation force with a peak frequency of 0.225 Hz. During the first 100 seconds, the maximum force is around 30 kN which implies that small waves have been obtained. In general, a smaller peak frequency will result in a longer wavelength, a bigger wave period and a larger wave excitation force.

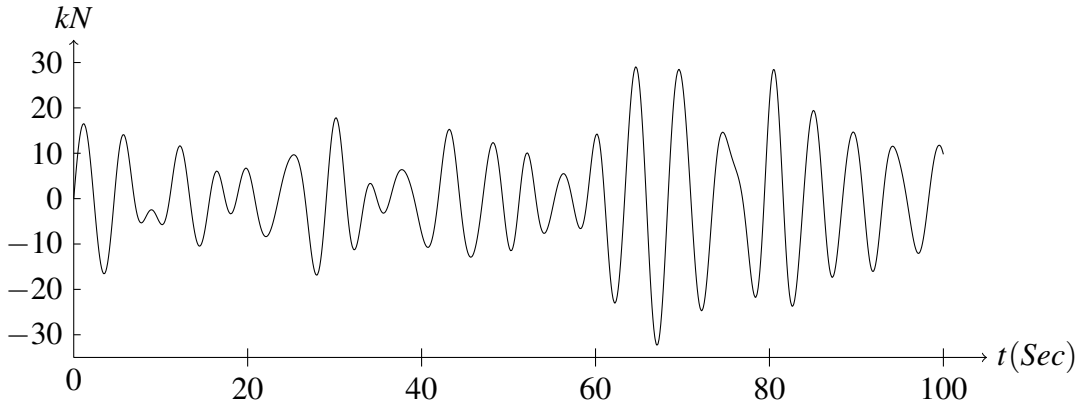

Figure 3.9: Time domain wave excitation force with peak frequency 0.225 Hz.

3.4.3 Radiation Force

In Equation 3.17, the radiation impedance is defined as a complex value where the real part is the added damping and the imaginary part is the added mass. The radiation force can be written by multiplying the radiation impedance with velocity as shown in Equation 3.39. From a different aspect, the added mass acts like the physical mass to contribute to energy storage, whereas the added damping acts like the real damping to contribute to energy extraction.

For a dry oscillator as given in Equation 3.32, the added mass and the added damping coefficients are unique due to no memory term, and obtained according to the input frequency. However, for a wet oscillator as given in Equation 3.30, calculation of the individual added mass and added damping coefficients for a specific frequency is not necessary, as a memory kernel is applied to represent the radiation impulse response which consists of added mass and added damping. Despite the fact that the added

mass and added damping parameters in a pure wet oscillator (no PTO force) are not that important, they are still needed in later chapters for calculating the ideal PTO force to achieve control. The (non-dimensional) graphs of the added mass and added damping coefficients, which are functions of the product of wave number and radius, are illustrated in Figures 3.10 and 3.11. k is the wave number and both of the graphs are normalized by $2\pi\rho a^3\omega/3$ [76].

$$\begin{aligned} F_r(\omega) &= Z_r(\omega)U(\omega) \\ &= B(\omega)U(\omega) + j\omega M(\omega)U(\omega) \end{aligned} \tag{3.39}$$

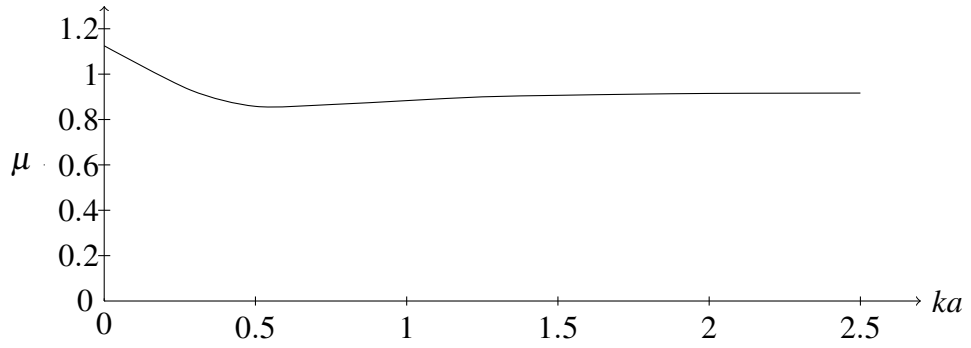

Figure 3.10: Non-dimensional added mass coefficient as a function of the product of wave number and radius.

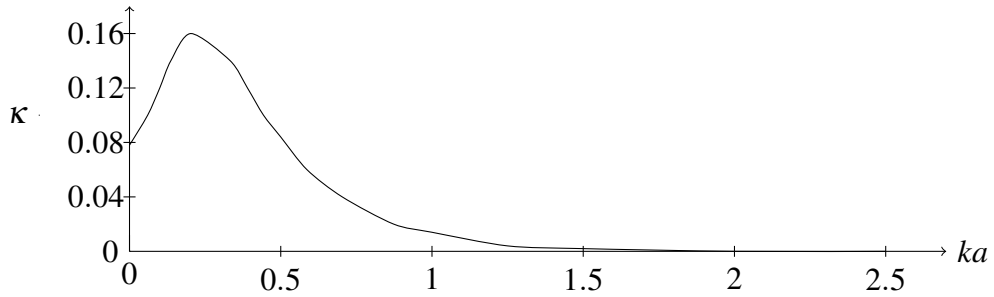

Figure 3.11: Non-dimensional added damping coefficient as a function of the product of wave number and radius.

Figure 3.12 [73] shows the dimensionless impulse response applied to a wet oscillator to calculate the memory term. As presented in Section 3.3.5, the wet oscillator is a causal system where $k(t) \neq 0$ when $t \geq 0$, hence, the impulse response has only the positive part. The wave excitation force coefficient, added mass coefficient and added

damping coefficient are all functions of frequency (although the graphs have been non-dimensionalised), therefore, all these parameters can only be applied in frequency domain equations or calculated with an individual frequency input. However, the radiation impulse response is a function of time and can only be applied to time domain expressions.

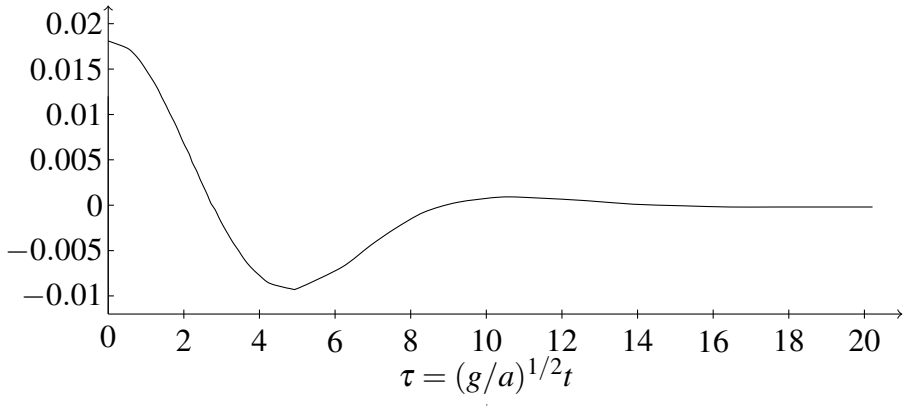

Figure 3.12: Impulse response function for a cylinder buoy where the scales are dimensionless. The dimensionless time on the horizontal scale is $(g/a)^{1/2}t$ and scale of the dimensionless impulse-response function is $\kappa_3/(\rho g \pi a^2)$

All the above parameters and impulse response graphs are suitable only for a cylindrical floating buoy which has a ratio between draft and radius of 1.88. For any other floating buoys that have different shapes or different draft and radius ratios, the hydrodynamic parameters can be calculated by using WAMIT, which is a professional and commercial software package for analysing wave interactions with offshore platforms and other structures or vessels [78].

3.5 Chapter Summary

This chapter details the linear WEC dynamics and provides some basic simulation results, such as wave elevation and wave excitation force, as tools for later chapters. Section 3.2 introduces the generation of irregular waves based on its energy spectrum and the Inverse Fourier Transform. Section 3.3 presents the basic oscillating model for

a WEC in ocean waves. This oscillating system is different from the traditional mass-spring-damper system due to the interaction between the water and the floating buoy. Section 3.4 provides the non-dimensional graphs for all hydrodynamic parameters, from which the excitation force coefficient, added mass coefficient, added damping coefficient and impulse response can be obtained. In conclusion, this chapter can be regarded as the beginning of a simulation model and preparation for implementing control systems.

Chapter 4

Control Methods of Point Absorber Wave Energy Converters

4.1 Introduction

Much research has been carried out in an effort to extract maximum power from the waves by controlling the WECs to achieve mechanical resonance such that the velocity of the generator is in phase with the wave excitation force [1]. Different control methods have been proposed by researchers with the aim of achieving a faster response. In regular waves, latching control can be applied to latch and unlatch the buoy at a specific time calculated from the wave frequency and the natural frequency of the buoy [20]. Reactive PTO force control is an alternative method to control the natural frequency of the buoy to make it move continuously with the waves, as described by Salter [28]. In previous work, reaction force control has been applied to a direct drive linear generator to extract maximum power in regular single frequency and multi-frequency waves [33, 34].

In irregular waves, control becomes non-causal which requires prediction of future waves. For latching control as proposed by Babarit [25, 26], short term prediction of the future excitation force is assumed. Wave prediction several seconds into the future has been described by Fusco in [45] by using information from the past. However, the error between prediction and reality increases with time. Also, Fuzzy Logic feedback control has been proposed by Schoen [79, 80], in which wave prediction also plays a significant role. Lopes [81] introduced another simple latching control which removes

the requirement of wave prediction by measuring the wave elevation for comparison with a pre-set threshold value to determine the unlatching instant.

In this chapter, reactive force control at the peak frequency of the wave spectrum (referred to here as reactive causal control where causal indicates no future information is required) is applied to control the WEC to extract the maximum power possible from irregular waves [23, 82]. Because of the near resonance between the WEC and the incoming waves, the motion displacement of the buoy is very large and may be unrealistic in practice. Therefore, an end-stop system is included in the model to constrain the motion displacement, hence to make the system more realistic. Work has been done by Eidsmoen [83] to restrict the amplitude of the buoy's motion, where an end-stop system is included using a large spring with damping. If an end-stop system is included, techniques to reduce the number of times that the end-stop is activated should be developed to avoid damage [84]. To implement reactive control, an extremely high PTO force is required. Both the real part of this force (damping) and the reactive part (analogous to spring and inertia) have large values. This force is typically much higher than the linear generator can provide, so the PTO force also needs to be restricted as introduced in Chapter 5.

This chapter begins with an introduction on the importance of control followed by a description of different control strategies. A new method to implement latching control in irregular waves is introduced, named sub-optimal latching control. PTO force control strategy is focused herein and in particular reactive force control. Different reactive force control strategies are compared through simulation results. At the end of this chapter, mechanical constraint is introduced to improve the system and make it more realistic.

4.2 Importance of Control for Point Absorber WECs

The ultimate objective of this thesis is to implement a control method onto a direct drive WEC to extract maximum power from irregular waves. The linear generator is normally fixed on a floating buoy which reacts with incoming waves to provide the reaction force for power generation. To achieve a higher power production without improving the WEC physical structure, a higher instant velocity must be obtained under some proposed control strategies. Optimal velocity can be obtained when mechanical resonance, between the floating buoy and ocean waves, occurs.

4.2.1 Mechanical Resonance

Most of the proposed WECs are designed to oscillate with incoming ocean waves according to their natural frequencies. The mechanical resonance phenomenon is defined as a mechanical system which can absorb more energy when the frequency of its oscillation matches the system natural frequency than it does at other frequencies. This theory can also be applied to extract maximum power from ocean waves by controlling the natural frequency of a floating body to match the frequency of ocean waves.

As stated above, energy conversion can be amplified if the oscillating body has the same frequency as the ocean waves, especially for some small devices with narrow bandwidth. A number of existing WECs have a large horizontal extension, such as a Pelamis WEC which has a full length design of about 180 m. Devices with such large horizontal dimensions have a broad bandwidth and are called *terminators*, *attenuators* or *linear absorbers*, thus energy extraction can be achieved irrespective of the wave frequency. There are several other WECs which employ small size floating buoys to interact with ocean waves. These floating buoys are called point absorbers, and have narrow bandwidth due to very small horizontal extensions compared to the predominant wavelength. Therefore, for point absorbers, any minor difference between the natural frequency and wave frequency means a significant drop in power conversion. In reality, due to the varying frequency of ocean waves, once the point absorber has

been designed, the natural frequency is fixed and cannot possibly meet every individual wave frequency, which implies the device would always operate off-resonance if there is no control system. Hence, it is imperative to apply an external force to make the floating buoy move in resonance with ocean waves, hence to maximize power production. Latching control strategy is regarded as an effective method which can be widely used in all different WECs. Reactive force control strategy is achieved by adjusting the oscillating frequency of the floating buoy, thus it is unnecessary for large scale WECs due to their broader bandwidths.

4.2.2 Case Study: Resonance of WECs

As described in the previous section, mechanical resonance occurs when the natural frequency of the oscillating buoy corresponds with the ocean waves frequency. For a conventional oscillating system, the natural frequency can be expressed as given in Equation 4.1,

$$\omega = \sqrt{K/m} \tag{4.1}$$

where K is the spring stiffness and m is the mass of the oscillating system. For an oscillating system in ocean waves, this equation still works, but the mass of the oscillating system should be the total mass, which is the sum of both physical mass and added mass. Therefore, the natural frequency of such a system can be expressed in Equation 4.2, where c is the buoyancy spring stiffness and $M(\omega)$ is the added mass.

$$\omega = \sqrt{c/(m+M(\omega))} \tag{4.2}$$

Dry oscillator resonance

In Section 3.3.5, a dry oscillator is defined as an oscillating system that operates in regular waves. Hence, no memory term is included, indicating that the velocity depends only on present input. For such a system, mechanical resonance can be simply achieved by designing a WEC that has a natural frequency the same as the frequency of regular waves. For a regular wave that has frequency 0.214 Hz with the peak value of wave

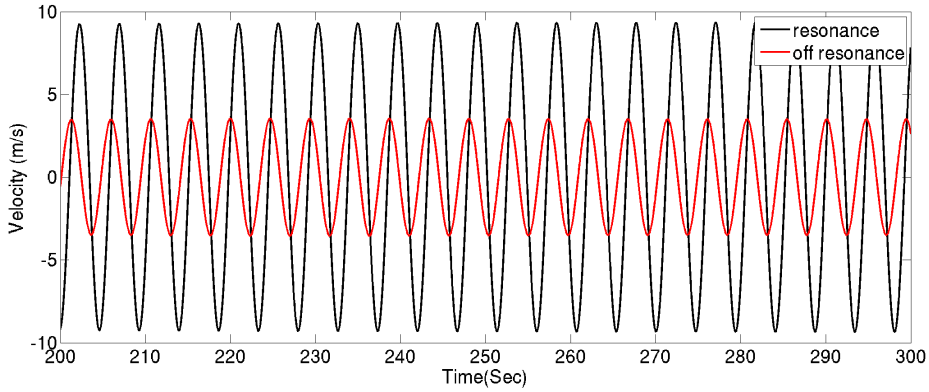

Figure 4.1: Velocity comparison for dry oscillator

excitation force 3×10^4 N, the results of velocity for two selected different size floating buoys are shown in Figure 4.1. The radius of the floating buoy is chosen as 2.2 m for mechanical resonance and 2 m for off-resonance. In this figure, it can be clearly seen that the velocity at resonance is much greater than the velocity at off-resonance, even though the 2 m floating buoy has a relatively smaller mass. It can be concluded that, in a dry oscillating system, control is not necessary unless the designed natural frequency of the floating buoy does not meet the frequency of regular waves as shown in the red line.

Wet oscillator resonance

Different from a dry oscillator, a wet oscillator has a memory term to indicate a causal system. In addition, as it is operating in irregular waves which are constantly varying in amplitude and frequency, mechanical resonance is impossible to be achieved without additional control systems. Figure 4.2 shows a comparison of velocities between two different size of buoys under irregular waves with peak frequency 0.214 Hz. The black line shows the velocity by designing the natural frequency of the floating buoy to be the same as the peak frequency of the ocean waves where the radius is 2.2 m. As exact mechanical resonance cannot be achieved, the black line is called *theoretical resonance* here to indicate the natural frequency is same as the peak frequency. The red line result shows another velocity when the buoy is designed to be off-resonance with the peak frequency with the radius 2 m. It can be seen that velocity is still larger

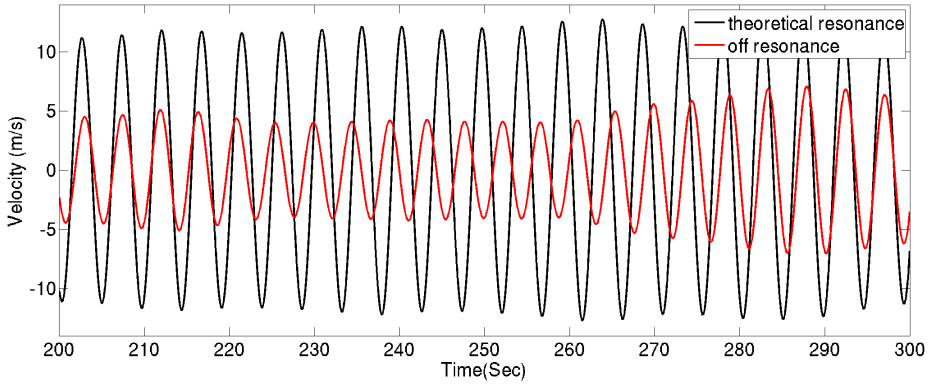

Figure 4.2: velocity comparison for wet oscillator

under theoretical resonance than off-resonance, even though mechanical resonance is not achieved.

4.2.3 Reality Considerations

The purpose of controlling a point absorber WEC to achieve mechanical resonance is to increase power production that benefits economic interests. Thus, once the device has been designed, it is expected to generate as much power as possible under appropriate control methods. However, the motion can become unrealistic due to the mechanical and electrical constraints and, hence, this need to be taken into account in the simulation work.

Amplitude

Any wave energy device has a specific length which implies the motion displacement cannot exceed its designed dimension. For a point absorber WEC which has been designed for a specific ocean area, it rarely reaches its designed oscillation amplitude without control, unless, in some cases, ocean waves become bigger or an unexpected storm arrives. Once a control system is applied, motion becomes optimal resulting in a large velocity and displacement. Large velocity is required to produce more power, whereas large displacement ideally is maintained to be small. However, displacement can become large and, sometimes, larger than the designed height of the point absorber

which makes the oscillating system unrealistic. Moreover, large displacement leads to a large reactive power which can exceed the capacity of the electrical machine. Hence, in reality, the amplitude has to be limited by employing end-stop systems to lock the buoy at both the upper and lower bounds.

Power capacity

Energy carried by ocean waves is transferred to the WEC in the form of the buoy's oscillation. This mechanical energy is subsequently captured by an electrical generator to be converted into electrical energy. Big ocean waves can create a large velocity of the oscillating buoy giving a large amount of available energy to be converted into electrical energy. This can result in large currents in the generator, which may exceed the designed rating. Therefore, power transfer has to be limited by means of limiting the current to protect the device.

4.3 Control Strategies

Control of WECs in wave energy engineering changes the natural motion of the wave energy device to extract more power. So far, no less than thirteen control methods had been proposed by Salter in [28]. Some of them use mechanical systems and others use electrical systems. Most of these control ideas are proposed only for theoretical analysis or computer simulation.

4.3.1 Development of Control

Control theory for wave energy engineering was first proposed by Budal in the mid-1970s [85]. The first idea proposed used a controllable PTO force to achieve optimum phase and optimum amplitude of the oscillation. The PTO force is derived from the generator which may operate as a motor depending on the relationship between the designed synchronous speed and the actual rotor speed [64]. This kind of control uses the reactive power to increase the active power output through mechanical resonance

so that power flow may be bidirectional, either from ocean waves to the grid or from grid to the ocean waves. In fact, real power always flows from ocean waves to the grid, but only reactive power may have a bidirectional flow. Because this control method is used to achieve the optimum phase with no power break, in many cases, the reactive control is also called continuous phase control.

A novel phase control idea was proposed later in 1978 by Budal, where the oscillating body is latched and unlatched at a specific time during one oscillation cycle to force it to move together with ocean waves [86]. As the buoy is locked firmly at a fixed position during part of the oscillating cycle, power generation cannot be continuous. Therefore, latching control is also called discrete control. It was later discovered that wave prediction plays a significant role in the performance of latching control [87]. This is because accurate information about future waves is required to decide when to lock the buoy and when to unlock. Generally speaking, wave prediction is important for both latching control and continuous control as is introduced later in this chapter.

4.3.2 Latching Control

> "The natural period of the buoy is shorter than the predominate wave periods. Thus, even outside resonance, approximate optimum phase is obtained by latching the buoy at an instant when its velocity is zero, and then releasing it at an instant such that the phase of its velocity will have the best possible match with the phase of the predicted excitation force" [27].

Latching control is perhaps the most widely used control strategy in wave energy engineering due to its simple mechanical structure and mature technology. To date, a number of published papers have modelled and tested latching control for different PTO systems such as hydraulic system and pneumatic system [24]. For a hydraulic system, latching control is achieved with a valve which controls the pressure of the fluid to adjust the motion of the ram, and hence the motion of the oscillating body. In a pneumatic system, latching control is achieved by adjusting the water level inside the chamber. Fast air flow into the chamber may cause high air pressure which can reduce the movement of the incoming water. On the contrary, slow air flow may speed up the

movement of the incoming waves. However, latching control strategy is rarely taken into account in direct drive systems. This is because power output is discontinuous during the latching periods as there is no short-term energy storage system.

Latching control could be easily applied to ocean wave energy if ocean waves maintained the same amplitude and the same wave period. Details of latching control in sinusoidal waves is provided by Greenhow [88]. In real sea conditions, latching control becomes more difficult to implement due to variable sea states, but some work has been carried out on the latching control of WECs in irregular waves. In the method proposed by Babarit [25, 26], short term prediction of the future excitation force is assumed.

The advantage of latching control is that a mechanical latching device is applied instead of a combined electric motor and generator, so that there is no reactive power flow, which implies energy conversion efficiency can be increased due to less electrical losses. However, by using a mechanical latching system, such as a braking system and a clutch system, the reliability is reduced.

4.3.3 Reactive Force Control

This control strategy introduces reverse power from the generator to provide additional force, hence changing the natural frequency of the wave system. This additional force is called mechanical reactive force and consists of an inertia force and a spring stiffness force. It is supplied by the generator which can be regarded as a part of the PTO system, hence, the generator must always be able to behave as a motor. There are two types of reactive force control, reactive loading control (or phase control) and complex conjugate control, depending on how to choose the reactive inertia force and reactive spring stiffness force.

Reactive loading control

The oscillating point absorber in ocean waves has both an inertia term which resists acceleration and a spring term which resists deflection. When there is no additional PTO force, it should oscillate according to its natural frequency. If ocean waves come to the body at the same frequency as its natural frequency, resonance occurs and the oscillating velocity can be maximized and the energy capture depends only on the choice of damping. If damping is given at the optimum value, theoretically all the energy carried by ocean waves can be extracted. However, real waves come at different frequencies which implies optimal velocity cannot be achieved all the time. Hence, some of the wave energy is stored temporarily as kinetic energy in inertia and potential energy in spring which can be fully returned to the ocean waves as wave reflection.

The introduction of reactive loading control is to curtail the energy stored in spring and inertia. This is achieved by introducing a phase shift into the PTO force to cancel a part of the spring and inertia and make the system look like a pure damper [28]. This will cause a reverse power flow to obtain a negative spring force and a negative inertia force. Hence, generators have to work as motors during part of the cycle. The power needed for the reactive force could be much bigger than for the damping force and may result in a significant electrical loss during the power transmission.

Complex conjugate control

Complex conjugate control is also related to reactive force control. Similar to reactive loading control, reactive force provided by the PTO force is also needed. However, the difference is that spring and inertia force can be almost fully cancelled by applying complex conjugate control. Therefore, maximum velocity can be obtained constantly to provide maximum power production. In irregular waves, the reactive force keeps on changing according to the wave's frequency to correspond with the changes of the inertia and spring forces. Normally, the PTO force required to achieve such a control strategy is extremely large, because it is the sum of inertia force, damping force and spring stiffness force. Hence, electrical loss reduction has to be taken into account

otherwise the net power recovered may be less than using other control strategies. As the reactive force is needed to respond quickly, it has to be implemented with the help of digital signal processors.

4.4 Latching Control Implementation

Latching control is applied to a mechanical system to temporarily hold the buoy's motion for a small time period and release the buoy to let it move in phase with the wave excitation force to achieve maximum power extraction. To implement latching control in regular waves, the natural frequency of the floating buoy has to be higher than the wave frequency as introduced above, so that the time to perform latching and unlatching can be calculated by comparing the frequencies. In irregular waves, the situation becomes more complicated, as ocean waves may come at various frequencies rather than only one frequency, and it is impossible to adjust the natural frequency of the floating buoy to make it higher than every incoming ocean wave. Hence, instead of using traditional optimal latching control for regular waves, a novel sub-optimal latching control is investigated in this section where future wave information is not needed.

4.4.1 Latching Procedures

Optimal latching control

The optimal latching control method can only be implemented to control a floating buoy which is operating in regular waves. Details are explained as shown in Figure 4.3. It can be seen that this method makes the oscillating velocity reach the peak value as the peak wave excitation force arrives. Before it can be implemented, the natural frequency of the floating buoy which is $2T_2$ in Figure 4.3 and the wave frequency which is $2T_1$ have to be known in advance to calculate the latching time Δt as shown. Therefore, the buoy is latched for Δt seconds at the beginning of each wave excitation force period, and then it is unlocked to move in phase with the wave excitation force

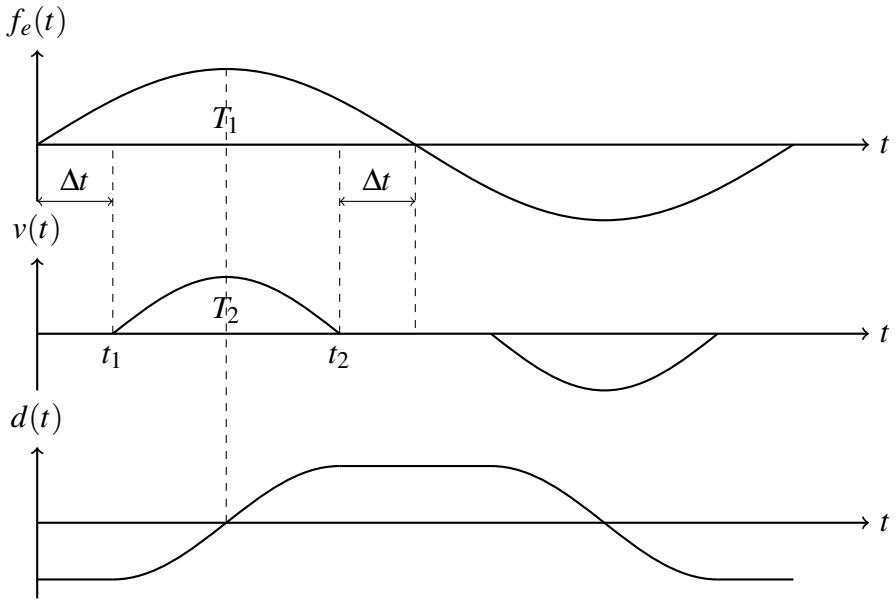

Figure 4.3: Optimal latching procedure for regular waves.

for T_2 seconds. The buoy's velocity drops to zero at t_2 seconds, whereas, the wave excitation force is not zero. At this instant, the buoy is locked again for $2\Delta t$ seconds before it can be unlocked again. The lower trace in Figure 4.3 shows the displacement information during the latching period. The buoy is locked at peak displacement rather than at the ocean surface. Details of such optimal latching control were presented in [5]. This optimal latching control strategy was also demonstrated in irregular waves in [89], based on the assumption that future wave information was known sufficiently far in the future.

Sub-optimal latching control

In irregular waves, optimal latching control strategy can only be achieved after obtaining the future wave information. As the technology for wave prediction is not mature enough and only the waves a few seconds into the future can be predicted, latching control can be only used to increase more power capture rather than achieve maximum power capture. Hence, sub-optimal latching control is introduced here where the peak oscillating velocity of the floating buoy does not occur at the peak wave excitation force.The sub-optimal latching control procedure is shown in Figure 4.4.

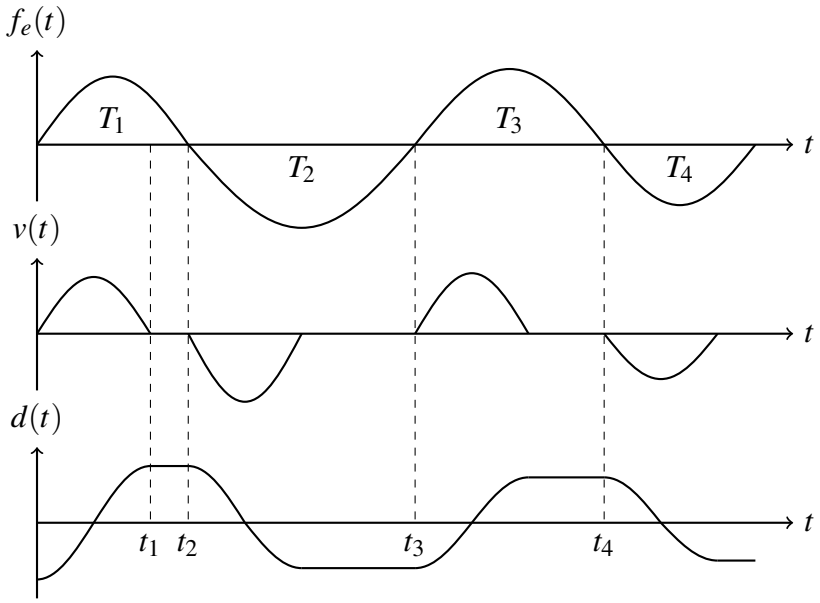

Figure 4.4: Sub-optimal latching procedure for irregular waves.

In sub-optimal latching control, the buoy is latched when its velocity vanishes, which is the same as with optimal latching control. The difference is that there is no way for sub-optimal latching control to calculate in advance how long the buoy should be locked, as wave frequency is not predicted. Instead, the buoy is released as soon as the wave excitation force changes direction with respect to the ocean surface. As shown in Figure 4.4, such control method forces the buoy to move in the beginning part of the oscillating periods T_1, T_2, T_3 and T_4, and then it is locked for the rest of the oscillating periods. The floating buoy oscillates according to its natural frequency which results in different latching times for different oscillating periods. The example shown in Figure 4.4 is based on an assumption that the buoy's natural frequency is higher than the wave frequency. There will almost always be some waves that come with a higher frequency than the buoy's natural frequency. If these waves approach, the buoy should be latched during these wave cycles, otherwise, it will oscillate against the wave excitation force.

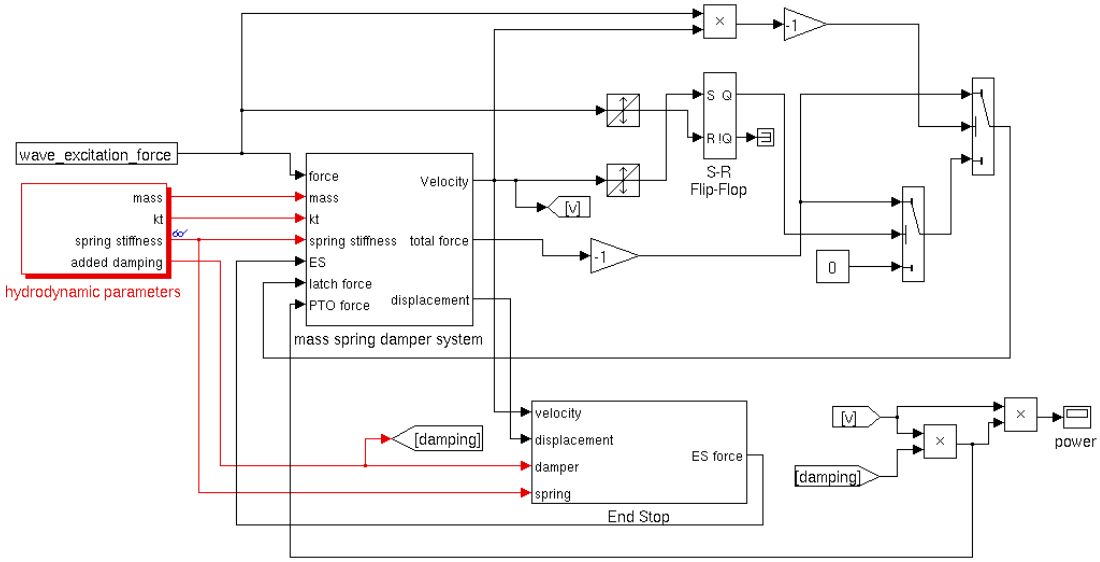

Figure 4.5: Simulink model of sub-optimal latching for irregular waves.

4.4.2 Simulation Implementation

Figure 4.5 shows the overall simulation model to implement sub-optimal latching control on a WEC in irregular waves. Hydrodynamic parameters are calculated in the sub-system as shown in Figure 4.7 and the results are subsequently input into the mass-spring-damper system block as shown in Figure 4.13. End-stop system is also included as shown in Figure 4.6. The latching system is represented by using a force which equals the negative value of the sum of all other forces applied on the WEC to make the total force zero. This latching force is then removed when the buoy is released. Velocity output is connected with a zero crossing block. If the velocity hits zero, the latching system is activated to supply latching force to the mass-spring-damper system. Wave excitation force is also compared with a zero crossing block to decide when to unlock the buoy. As soon as the wave excitation force changes direction, further comparison should be carried out to decide if the buoy natural frequency is higher than the wave frequency. However, this is not determined by comparing the frequencies directly because no wave prediction is included. Instead, this is achieved by comparing the directions of wave velocity and wave excitation force. If they have the same direction,

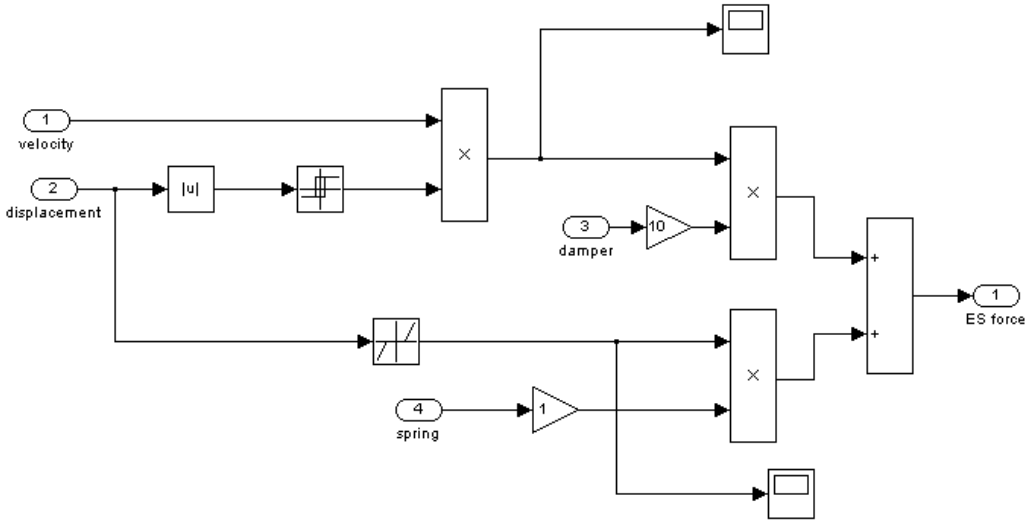

Figure 4.6: Simulink model of the end stop system.

the buoy should be unlocked immediately to let it move, otherwise, the latching system should always be activated. In a real system, velocity can be measured by a fixed sensor and wave excitation force can be calculated by measuring the wave elevation. For the sake of completeness, an end-stop system is included to make the system more realistic which is discussed in Section 4.6. The PTO system is also included in the system for simulating the power production.

4.4.3 Simulation Results

Figure 4.8 shows the results of a WEC under sub-optimal latching control. Wave excitation force is generated by selecting 0.18 Hz peak frequency and the radius of the floating buoy is chosen to be 2.2 m so that the natural frequency of the floating buoy is higher than the wave peak frequency. The generated wave excitation force is shown in Figure 4.8a and the corresponding buoy velocity is shown in Figure 4.8b. It can be seen that the velocity is discontinuously controlled to be nearly in phase with the wave excitation force. The WEC is moving according to its natural frequency no matter what the incoming wave is. As the WEC is operating in irregular waves where some of the waves may come at a higher frequency, during these periods, the buoy is latched for a relatively longer time as shown around 50 seconds and 90 seconds.

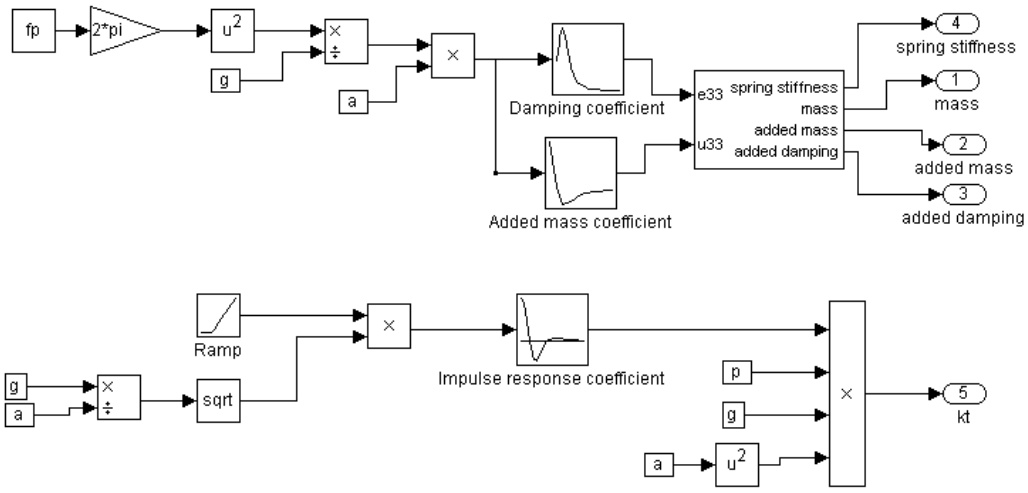

Figure 4.7: Hydrodynamic parameter block.

Therefore, there will be no power extracted when waves come at higher frequencies. Figure 4.8c shows the displacement under the sub-optimal latching control strategy. With end-stop systems, the displacement is successfully controlled within $\pm$ 4.136 m as is discussed in Section 4.6.

Figure 4.9 shows the instantaneous power output and average power output. It can be seen that the average output power extracted is around 40 kW with the peak instantaneous power about 150 kW.

4.5 Power Take-Off Force Control

The PTO force control uses additional force from the generator to control the motion of the WECs with the aim of achieving maximum power extraction. To implement the PTO force control, generators have to act as motors part of the time during the cycle. If only damping force is provided by the generators to allow only real power to be transferred to the system, the control method is called real control, whereas, if both damping force and reactive force are provided by the generator to allow some reactive power to be transferred in order to control the motion of the WECs, the control method is called reactive force control. As discussed in Section 4.3.3, there are two important

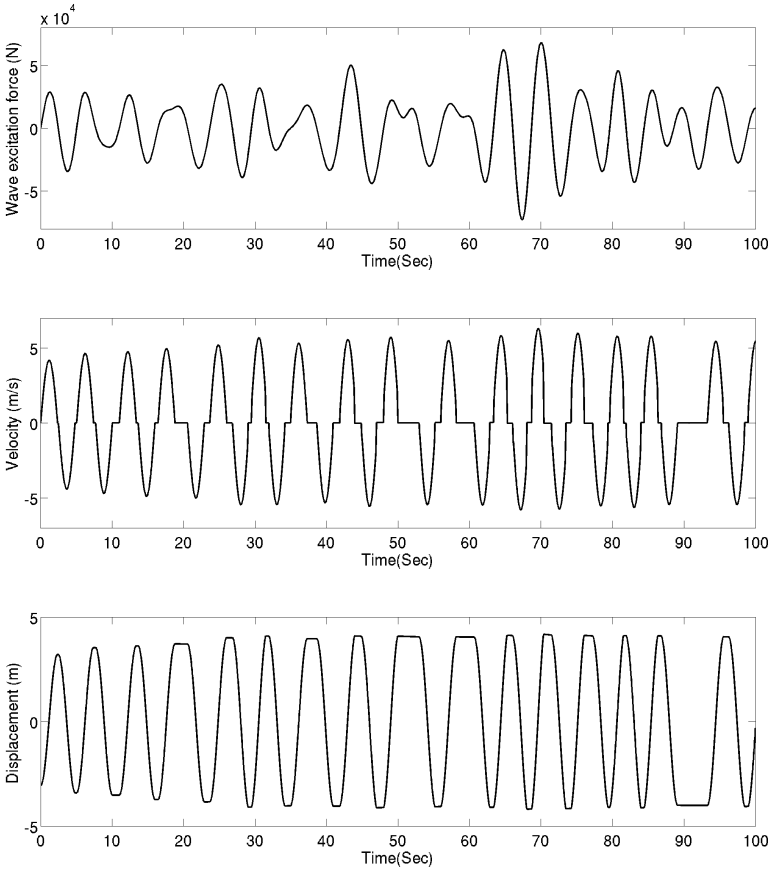

Figure 4.8: Sub-optimal latching control results, a) wave excitation force, b) velocity, c) displacement.

types of reactive force control method: reactive loading control and complex conjugate control. Reactive loading control provides a small amount of reactive force to cancel a part of the spring force and inertia force so that better performance can be achieved by adjusting the damping force. However, optimum velocity cannot be achieved by reactive loading control but only can be achieved by complex conjugate control, giving the optimum power extraction.

In this section, detailed classification of PTO force control is provided first, followed by different control procedures according to the classification. Finally, comparison of the different PTO force control strategies is discussed.

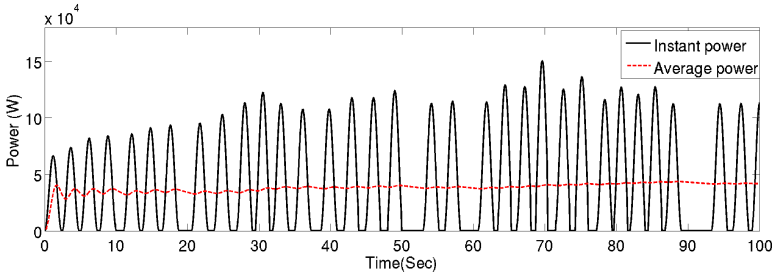

Figure 4.9: Power extraction under sub-optimal latching control.

4.5.1 Classification of Power Take-Off Control

The implementation of the control system is very important. All proposed WECs and the associated devices are costly, and proper control can improve performance of the equipment resulting in a good power production and hence good payback.

Figure 4.10 shows the energy flow from ocean waves to the electricity grid. Ocean waves carry mechanical energy thousands of kilometers until they approach the floating device. The first step of energy flow is the interaction of the energy carried by ocean waves with the primary interface. Some of the energy is converted into the kinetic energy of an oscillating buoy: this converted energy is called *intercepted energy*. However some of the energy cannot be intercepted by the first step: this unconverted energy is still carried by the ocean waves. Some of the waves carry part of the remaining energy to pass over the buoy and keep their original direction: these are called *transmitted waves*, and the energy carried by these waves is called *transmitted energy*. Other waves become separated by the floating buoy and travel in several directions which are different from the original direction: these are called *diffracted waves*, and the energy carried by such waves is called *diffracted energy*. To improve the performance of the first step entails intercepting as much energy as possible,while reducing transmitted and diffracted energy. This relies on designing the structure of the floating buoy to interact with complex ocean conditions.

The second step in the power flow is to extract as much power as possible from the intercepted power, and this extracted power is called *captured power*. As already discussed, the floating buoy has inertia and spring terms which can store some of the

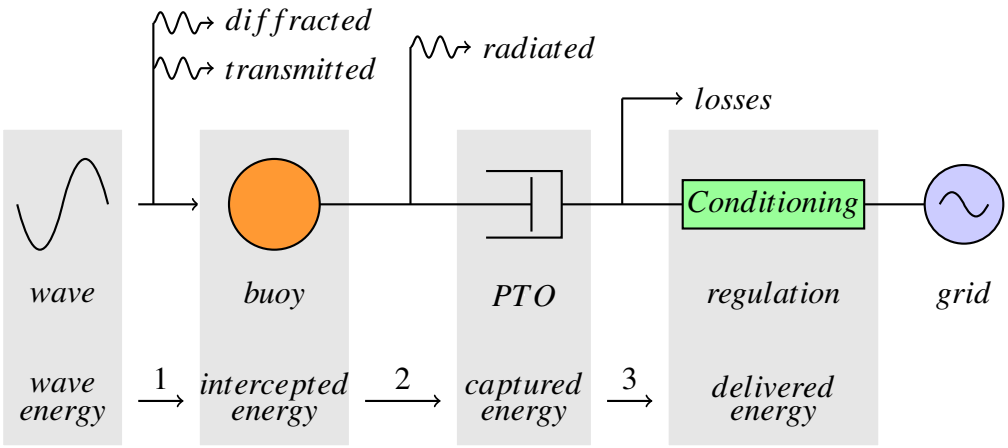

Figure 4.10: Power flow from ocean waves to grid and also the power losses.

power from ocean waves. This stored power can be extracted as real power or it can be returned to the ocean again. Uncaptured power can create new ocean waves which are called *radiated waves* and the power carried by radiated waves is called *radiated power*. So far, several control strategies have been applied to achieved maximum power capture from the intercepted power such as latching control. In this thesis, attention is focused on continuous control where the reactive PTO force is applied to control the WECs.

The final step of the power flow is power conditioning. Power from the WECs cannot be directly connected to the grid. The voltages and currents need to be regulated by applying a modern power electronics device, after which, power flow will meet the requirements of grid connection. Sometimes, in order to increase the conversion efficiency, power factor also needs to be controlled in this step. Moreover, if continuous control is required for the second step of power flow, the power electronic device is also required to control the currents to provide the desired force. In this thesis, direct drive PTO system is applied, hence, power conditioning should come at the final stage and is carried out fully by a power electronics device. However, for a buffered (hydraulic or pneumatic) PTO system, power conditioning is achieved by an accumulator or flywheel to provide a smooth power output. In this case power conversion comes in the final stage [23].

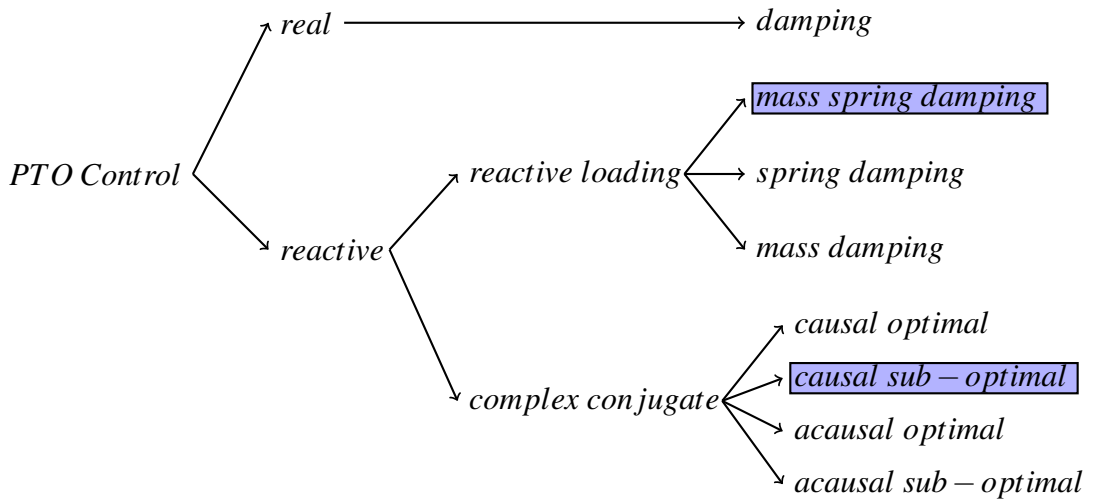

Figure 4.11: PTO force control classification for WECs.

Figure 4.11 shows a detailed classification of PTO force control. The PTO force control, also called reaction force control, uses the force from a generator to control the WECs. It can also be divided into two main categories which are real control and reactive control. If the force from the generator is a pure damping force, the control is called real control. If the generator force contains either spring term or inertia term, or both of these two terms, the control is called reactive control. For a pure damping control system, the amount of power extracted depends only on the choice of damping coefficient. Because there is no reactive force to cancel the inertia and spring terms in the system, most of the power is radiated back to the ocean waves. The advantage is that only a small rating generator (motor) is required as only a small amount of PTO force is required to achieve control.

Reactive force control aims to cancel some of the inertia term or spring term to achieve a better power extraction. As shown in Figure 4.11, the reactive force control can be further classified into reactive loading control and complex conjugate control. Let us look at the reactive loading control first. Based on the terms that need to be cancelled, this has three different control strategies as well. The mass-damping control requires the reactive force to provide some additional mass to cancel some of the inertia term, the spring-damping control requires the reactive force to provide some additional

spring to cancel some of the spring term, and the mass-spring-damping control requires both the additional spring and mass to cancel some of the spring and inertia terms in the system.

Another reactive force control is called complex conjugate control that applies impedance matching to obtain the required PTO force. As introduced in Section 3.3.5, the oscillating system can be divided into four types: memoryless system, causal system, anticausal system and acausal system.

- Causal optimal: This control idea is specially designed for regular waves. The PTO force is calculated by applying impedance matching at only one frequency (wave frequency): the control system is causal (no future information required). Wave energy can be absorbed completely, hence it is called optimal.
- Causal sub-optimal: As ocean waves become irregular, the oscillating motion is polychromatic. The PTO force is calculated based on the peak frequency of the energy spectrum to extract the most energy that can be extracted. The control system is still causal because only a single frequency (peak frequency) is required. However, power extracted is not maximum, hence it is a sub-optimal control.
- Acausal optimal: The PTO force is calculated by applying impedance matching at every frequency of the irregular wave excitation force, hence the control system is acausal (future information is required). If this control is implemented, power can be absorbed completely, so it is an optimal control.
- Acausal sub-optimal: The PTO force is calculated by applying impedance matching at several frequencies of the irregular wave excitation force. The control system is still acausal due to the requirement for future information. However, not all of the power can be extracted which results in a sub-optimal control.

In reactive loading control, if the PTO force is calculated by choosing the peak frequency, it is causal sub-optimal in the complex conjugate category as shown by the same colour blocks in Figure 4.11. Hence, we can say that complex conjugate control is reactive loading control taken to the limit [28].

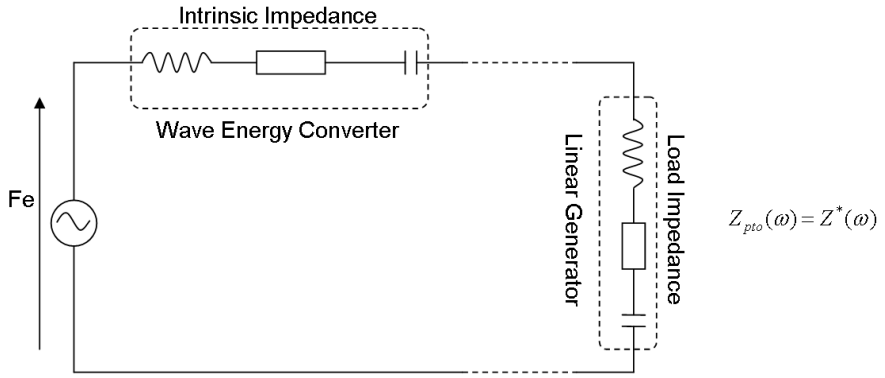

Figure 4.12: The electrical analogy of complex conjugate control.

PTO force control can also be divided into linear control and non-linear control. All the control strategies introduced above can be regarded as linear control. However, sometimes motion displacement may be very large by applying PTO control which can hit the preset end-stop systems. As the velocity is discontinuous when end-stops are activated, the control system becomes non-linear.

4.5.2 Complex Conjugate Control

Complex conjugate control is the ideal solution for controlling WECs, hence it is discussed first here. As introduced in Section 3.3.1, the mass-spring-damper system can be represented by an electrical circuit. If an external force (PTO force) is applied to the system, the whole circuit is shown in Figure 4.12. The wave excitation force is regarded as the voltage source. The mass, spring and damping terms of the oscillating system can be considered as the inductance, resistance and capacitance terms of the source. Hence, the intrinsic impedance is expressed in Equation 4.3 which has already been introduced in Section 3.3.3.

$$Z(\omega) = B(\omega) + j\left([m + M(\omega)] - \frac{c}{\omega}\right) \tag{4.3}$$

It is well known that in an electrical circuit, maximum power transfer from the source to the load is achieved by making the load impedance the complex conjugate of the source

impedance, known as *impedance matching*. If the load impedance is expressed as $Z_{pto}(\omega)$, the impedance matching is then given in Equation 4.4, where the superscript $*$ indicates complex conjugate.

$$Z_{pto}(\omega) = Z^*(\omega) \tag{4.4}$$

As introduced above, complex conjugate control has four different types based on the choice of the frequency. In this thesis, irregular waves are the incoming waves so that causal optimal control is not suitable. The two acausal control methods require future wave information which is not included in this thesis. Hence, only causal sub-optimal control is considered. The causal sub-optimal indicates that impedance matching is achieved by choosing only the peak frequency of the energy spectrum, which is expressed as ω_p. Hence, the impedance matching expression is rewritten in Equation 4.5.

$$Z_{pto}(\omega_p) = Z^*(\omega_p) \tag{4.5}$$

The simplest way to match the above equation is to give the PTO force impedance three terms, mass, spring and damping, to equal each of the terms of the intrinsic impedance. Hence, the PTO force impedance is given in Equation 4.6.

$$Z_{pto}(\omega_p) = j\omega m_{pto} + b_{pto} + c_{pto}/j\omega \tag{4.6}$$

By applying impedance matching, the three terms of PTO impedance are expressed in Equation 4.7, 4.8 and 4.9, where, $M(\omega_p)$ and $B(\omega_p)$ are added mass and added damping at the peak frequency, which indicates the PTO force coefficients are constants with no memory.

$$m_{pto} = -[m + M(\omega_p)] \tag{4.7}$$

$$b_{pto} = B(\omega_p) \tag{4.8}$$

$$c_{pto} = -c \tag{4.9}$$

As the PTO force control is causal and all the PTO force coefficients are constants, conversion of PTO force from the frequency domain to the time domain is simple and does not include any convolutions. The time domain PTO force is then given in Equations 4.10 and 4.11.

$$f_{pto} = m_{pto}\ddot{x}(t) + b_{pto}\dot{x}(t) + c_{pto}x(t) \tag{4.10}$$

$$f_{pto} = -[m + M(\omega_p)]\ddot{x}(t) + B(\omega_p)\dot{x}(t) - cx(t) \tag{4.11}$$

Simulation model description

The Simulink model of the mass-spring-damper system and PTO force system is shown in Figure 4.13. The wave excitation force is obtained in Matlab in the time domain by applying the IFFT on the PM spectrum and is then imported into the Simulink model. The hydrodynamic coefficients for added mass, added damping and impulse response data are stored in look-up tables to provide the corresponding coefficients with the frequency. Another sub-system block as shown in Figure 4.14 is used to calculate the required PTO force for controlling the WEC. The instantantaneous velocity, displacement and acceleration are three inputs for the block and the corresponding output is the PTO force. This calculated PTO force is fed back to the oscillating system based on Equation 3.28. The impulse response and velocity is convoluted to represent a causal system.

Simulation results

The simulation is commenced by selecting the peak frequency 0.214 Hz of the energy spectrum, and the radius of the buoy is 2.2 m such that the draft is 4.136 m. By applying complex conjugate control, the results of velocity, acceleration and displacement are shown in Figure 4.15.

From Figure 4.15a and Figure 4.15b, it can be seen that the buoy moves nearly in

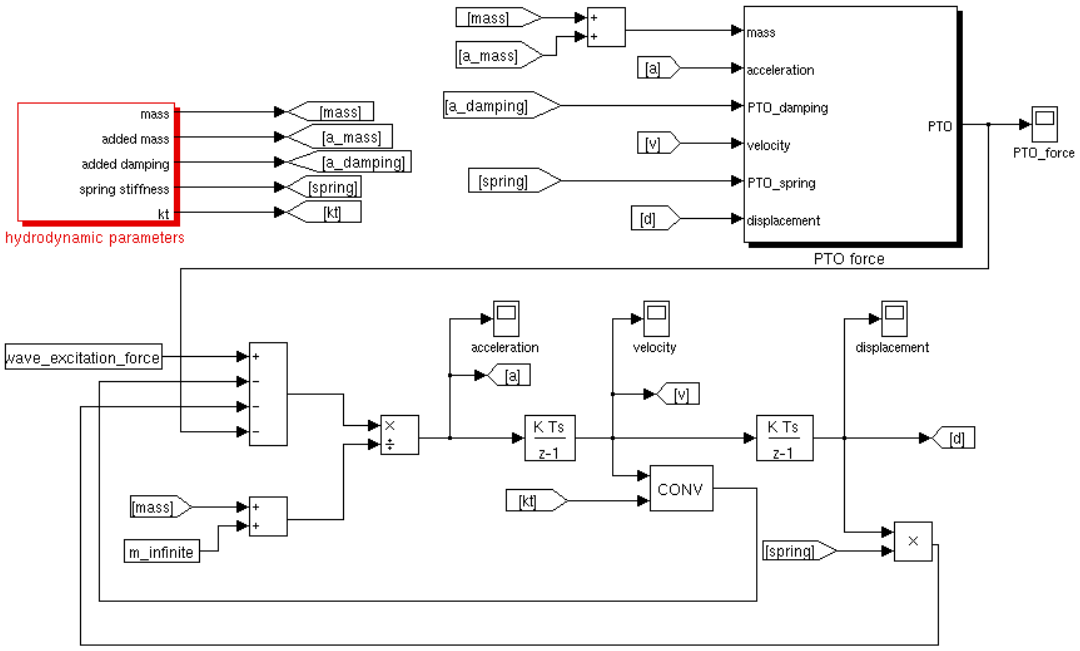

Figure 4.13: Simulink model for complex conjugate control.

phase with the wave excitation force, so that a large amount of wave power can be extracted. However, from Figure 4.16, it can be seen that there is still a very small phase difference between them because sub-optimal control is applied rather than optimal control. The choice for PTO force is only based on the single peak frequency rather than all of the frequencies.

Buoy displacement is shown in Figure 4.15d whose maximum value is 12.6 m, which

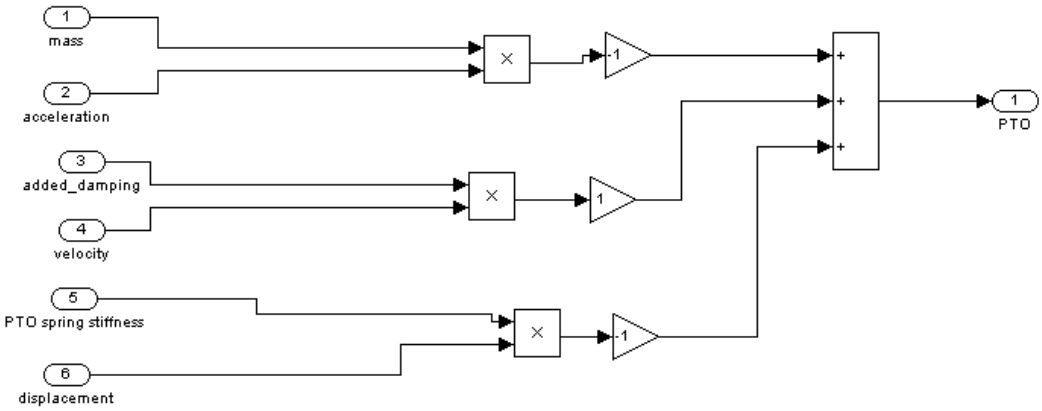

Figure 4.14: Power take off block.

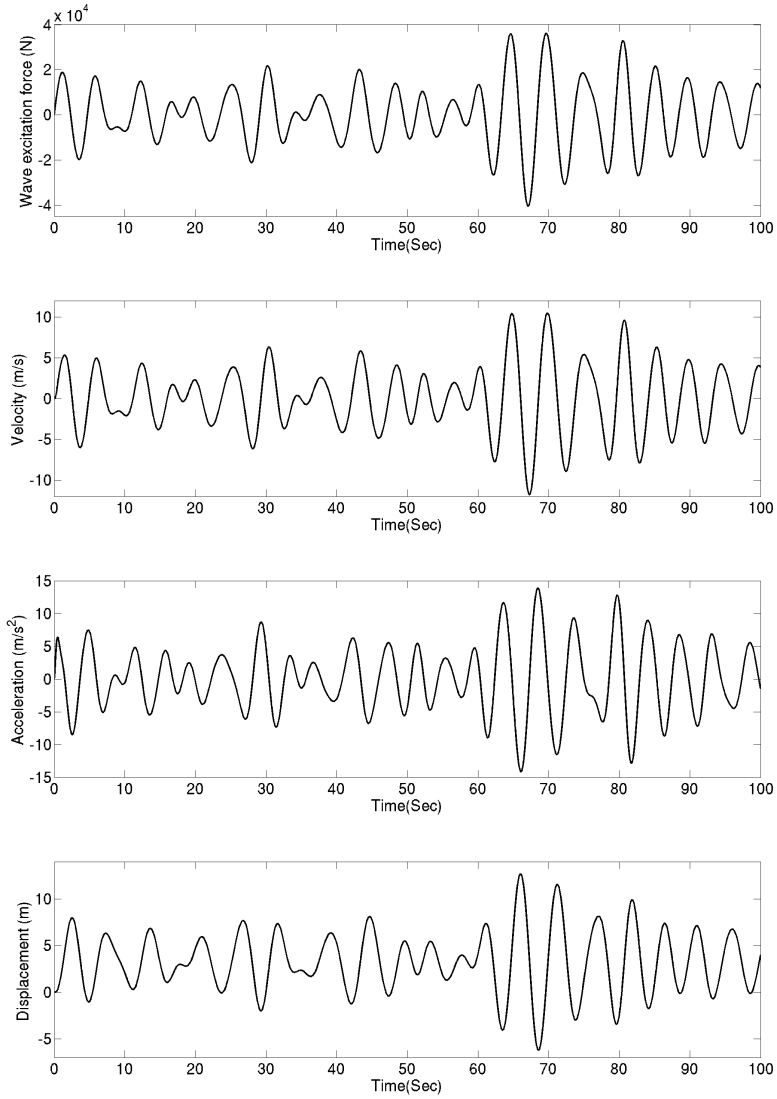

Figure 4.15: Complex conjugate control results, a) wave excitation force, b) velocity, c) acceleration, d) displacement.

is much greater than its draft. Thus the buoy would rise out of the water from the simulation results; however, the linear model is only valid when the model is partially submerged. Also, it can be seen that the buoy moves along an offset axis of symmetry about 3.28 m above the sea surface. This can be explained by Equation 4.12, obtained through combining Equations 3.28 and 4.11.

$$f_e(t) = [m_\infty - M(\omega_p)]\ddot{x}(t) + \int_0^t k(\tau)\dot{x}(t-\tau)d\tau + B(\omega_p)x(t) \tag{4.12}$$

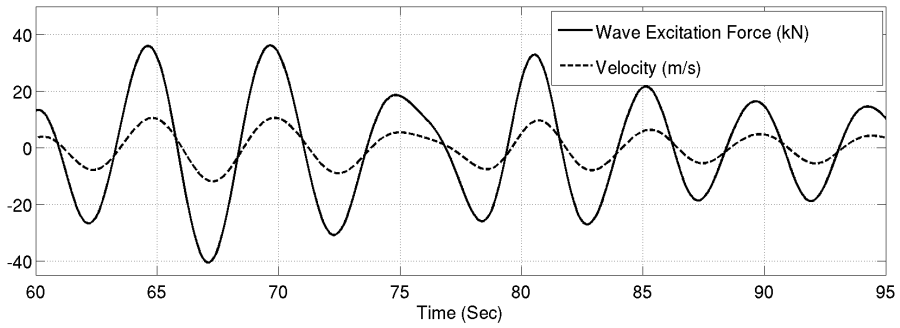

Figure 4.16: Phase shift between wave excitation force and velocity.

From this equation it can be seen that the coefficient of the displacement (referred here as spring stiffness coefficient) is zero. Hence, the value of the displacement will not affect the results of the velocity but will affect the value of the PTO force. As discussed in Section 3.4.3, when the point absorber operates in real seas, the value of $M(\omega_p)$ is almost the same as the value of m_∞, so that the coefficient of the acceleration $(m_\infty - M(\omega_p))$ is close to zero. This indicates that when the wave excitation force is applied to the point absorber, the change in acceleration is rapid. Thus, at the start of the simulation period, acceleration rises from zero to its maximum value very quickly. However, due to its large mass, the velocity of the buoy rises slowly and the displacement of the buoy therefore also rises slowly from zero. After this initial transient response, the buoy moves with a velocity proportional to the wave excitation force, as shown in Figure 4.15a and 4.15b. The acceleration and displacement are generally 180° out of phase. When the acceleration is at a maximum, displacement is at its minimum value. As a result, the mean value of displacement does not return to zero and instead the buoy oscillates about some non-zero offset displacement. This offset displacement will exist until either the generator hits the end-stop or the generator force is limited as described in Section 4.6. Alternatively, the buoy can be set initially to an offset position rather than zero. However, in practice this is impossible to implement because prediction of future waves is needed to calculate the offset value of the displacement.

Figure 4.17 shows the required PTO force to achieve complex conjugate control and the corresponding power extraction. In Figure 4.17a, the PTO force is always negative; this is due to the displacement offset as mentioned above. As spring force is the main

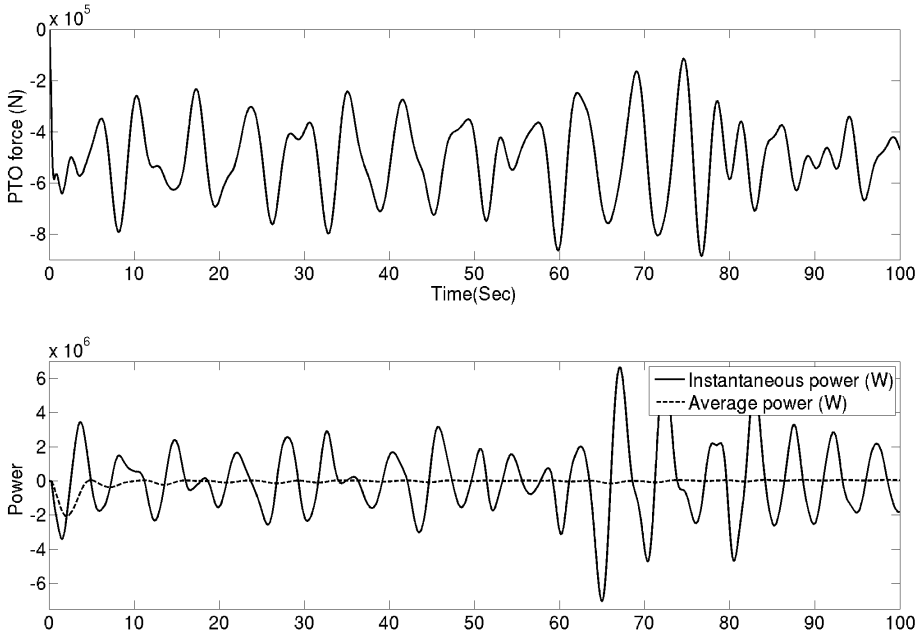

Figure 4.17: Complex conjugate control results, a) PTO force, b) power.

part of the PTO force, the offset displacement can result in the same sign of the PTO force. This phenomenon cannot occur in the real situation due to many constraints. Moreover, the non-positive PTO force does not result in a non-positive power flow; in fact, power flows bidirectionally.

The average extracted power in Figure 4.17b is approximately 40 kW and the peak instantaneous power is approximately 6.65 MW, which is almost 167.5 times the average extracted power. This implies a large amount of reactive power is required to achieve complex conjugate control which also means very low system efficiency. In addition, a huge generator and power converter system are required to provide such a big PTO force.

Simulation problems

The simulation results above show that the floating buoy does not oscillate along the axis of the water surface, instead, it oscillates along an offset axis of symmetry about 3.28 m above the surface. This is because the buoyancy spring is completely cancelled by the additional PTO spring stiffness as given in Equation 4.12, which means that

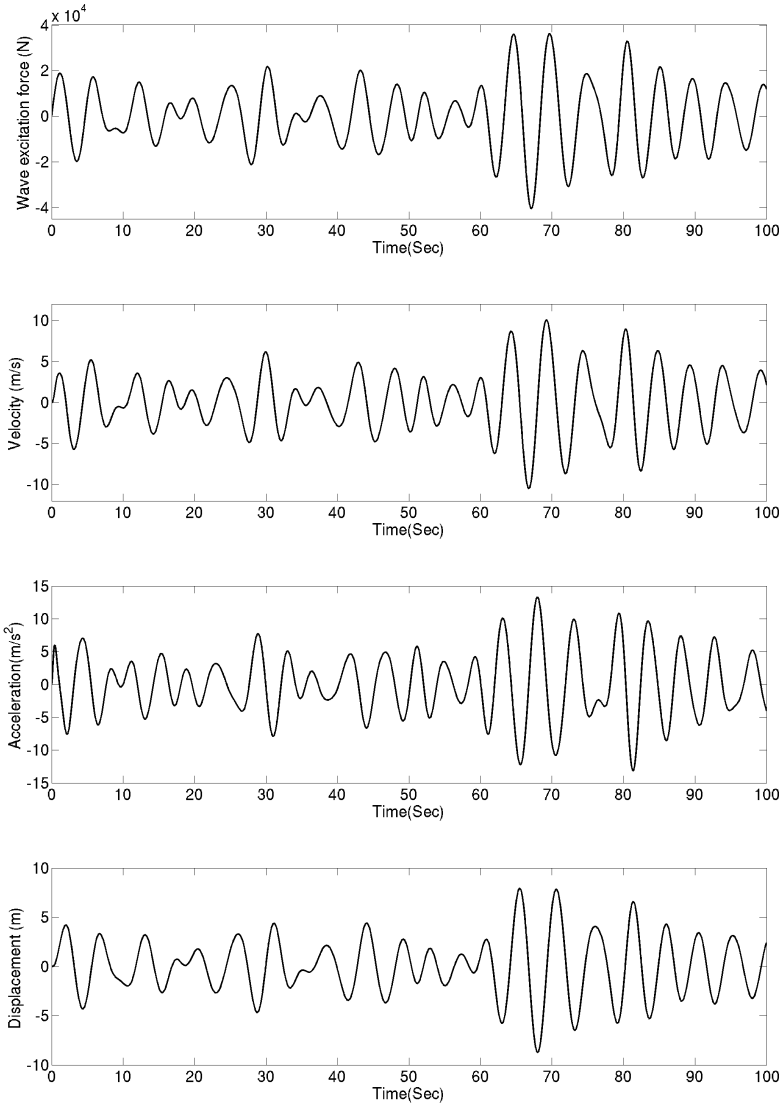

Figure 4.18: Complex conjugate control results with a new term for PTO spring, a) wave excitation force, b) velocity, c) acceleration, d) displacement.

the displacement of the oscillating buoy does not affect the acceleration and velocity. Only the PTO force is affected by the displacement offset, so that PTO force is always negative in the simulation results. Such a problem can theoretically be solved by introducing a small term spring into the PTO force to recreate the link between the motion and the displacement. Hence, a new PTO force is given in Equation 4.13,

$$f_{pto} = -[m + M(\omega_p)]\ddot{x}(t) + B(\omega_p)\dot{x}(t) - cx(t) + c_0 x(t) \tag{4.13}$$

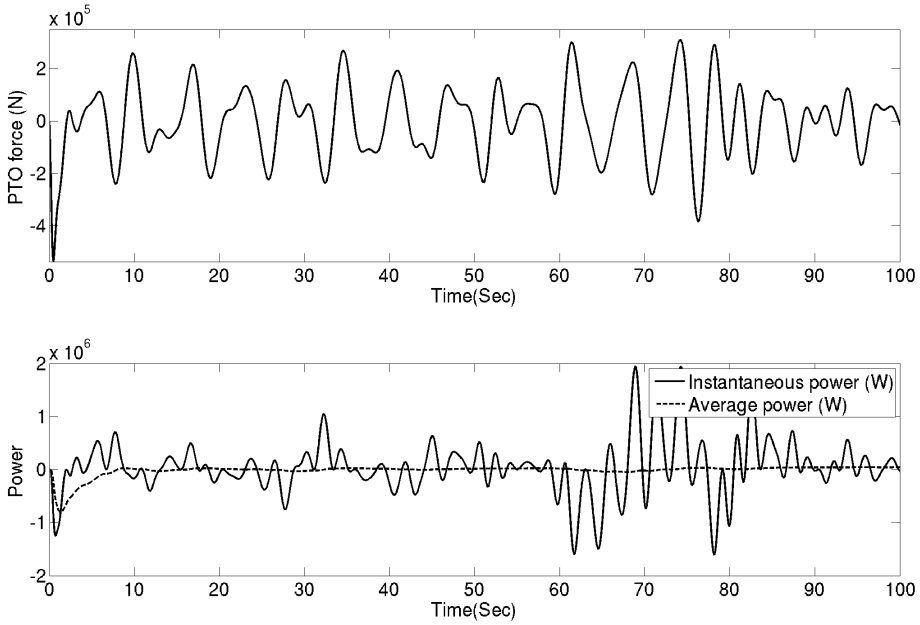

Figure 4.19: Complex conjugate control results with a new term for PTO spring, a) PTO force, b) power.

where c_0 is an extra spring term for PTO force and is very small. If c_0 is chosen to be five percent of c, a new set of results is achieved as shown in Figure 4.18. Peak frequency and buoy dimensions are maintained to be the same as in the previous simulation, which are 0.214 Hz and 2.2 m for the radius. By introducing the new term for PTO spring, the motion is slightly off-resonance with the wave excitation force, as explained in Figure 4.16, but it is hard to see from the figures above, hence they are still considered to be in phase. However, velocity drops a little bit compared to previous results where the maximum velocity is about 10.5 m/s in Figure 4.15b, whereas it is about 10 m/s in Figure 4.18b.

The significant difference from the previous results is that the buoy is now oscillating along the axis of symmetry with the ocean surface which implies that the relationship, based on Equation 4.13, between the oscillation motions and displacement is recreated. The additional PTO spring term could have been chosen to be even smaller than what has been chosen here to make the control much closer to complex conjugate control.

Figure 4.19 shows a new result of PTO force and power extraction after the new term PTO spring force is introduced. Because the oscillator is now moving up and down

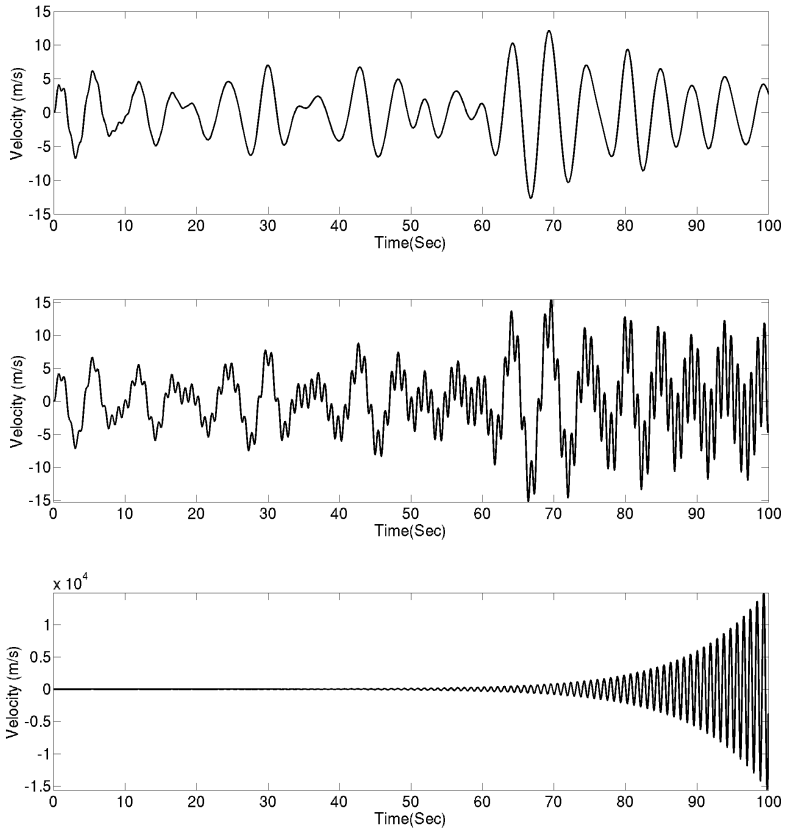

Figure 4.20: Comparison of velocity for different peak frequency, a) $\omega_p = 0.195$, b) $\omega_p = 0.194$, c) $\omega_p = 0.1935$

along the ocean surface, the PTO force in Figure 4.19a has both positive and negative values. If the transition part at the beginning is ignored, the peak negative PTO force is 383 kN which is much smaller compared to the 885 kN in the first simulation result, which indicates that the size of the generator could be selected much smaller by introducing a small PTO spring term into the system. In Figure 4.19b, the peak instantaneous power is 1.94 MW which is also much smaller than 6.65 MW in Figure 4.17b. The average real power extracted in these two results are almost identical due to the same PTO damping force and similar velocity. Hence, the advantage of introducing a small PTO spring force can significantly reduce the reactive force needed and can make the system more realistic than using complete complex conjugate control.

Another problem arises when bigger waves pass over the floating buoy. As seen from the results illustrated in Figure 4.20, the velocity of the oscillator increases when

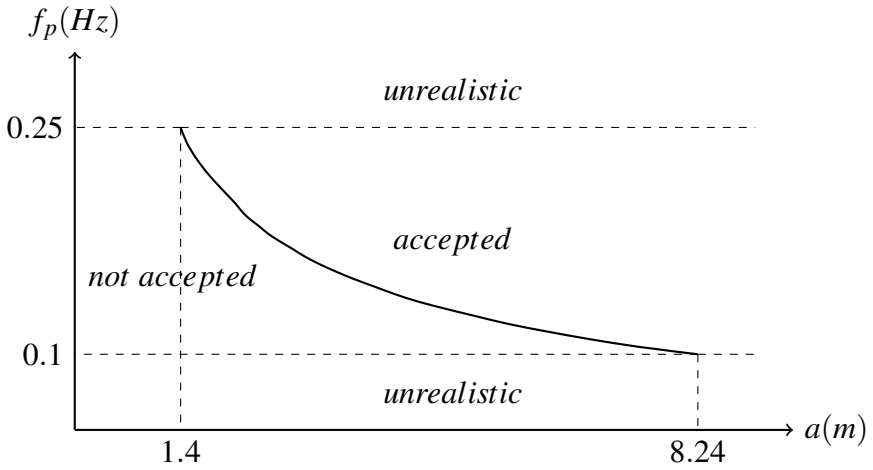

Figure 4.21: Choice method of buoy's dimension and peak frequency of the wave energy spectrum under complex conjugate control.

larger ocean waves arrive. The peak frequencies are chosen at 0.195 Hz, 0.194 Hz and 0.1935 Hz to increase the period of incoming waves, hence to increase the wave energy and the scale of ocean waves. Figure 4.20a shows the oscillating velocity at 0.195 Hz peak frequency. Some ripples appear in the first 10 seconds and then it becomes smooth. Hence, this frequency can be regarded as the border peak frequency for the selected WEC. When the peak frequency is chosen to be 0.194 Hz, the velocity waveform has a lot of ripples and velocity is bigger than the velocity at the border peak frequency. When the peak frequency is 0.1935 Hz, the velocity keeps on increasing, and eventually it would tend to be infinite which implies the WEC is out of control. Such a problem can only appear in simulation results due to the hydrodynamic model being assumed to be always valid even when the buoy is out of the water, and this cannot occur in reality due to physical limitations. Based on this result, every individual designed buoy under complex conjugate control has a border peak frequency.

Figure 4.21 indicates how to choose the size of a buoy for specific waves for computer simulation or in reality under complex conjugate control. The horizontal axis represents the radius of a floating buoy and the vertical axis represents the peak frequency of ocean waves. Normal waves have a range of period from 4 seconds to 10 seconds, so that any peak frequency which is greater than 0.25 Hz or smaller than 0.1 Hz can

be regarded as unrealistic. The area above the curve but between the two dashed lines is considered to be acceptable; nevertheless, the area below the curve and between the two dashed lines are considered to be unacceptable.

4.5.3 Reactive Spring Damping Control

Complex conjugate control needs the PTO force to provide three terms, mass, spring and damping as given in Equation 4.10. The presence of c_{pto} and m_{pto} cancels completely the inertia term and buoyancy term in the mass-spring-damper system. It must be emphasised that this is not the only solution for reactive force control. Any arbitrary value of c_{pto} and m_{pto} can be chosen to cancel part of the inertia term and buoyancy term. Also, some other solutions such as the absence of any term of the reactive force are of interest. In this section, the sub-optimal spring-damping control scheme is introduced when $m_{pto} = 0$. The reason why it is still called sub-optimal is because peak frequency is still used to calculate the PTO damping. Hence, the expression of PTO force is given in Equation 4.14.

$$f_{pto}(t) = b_{pto}\dot{x}(t) + c_{pto}x(t) \tag{4.14}$$

The PTO impedance in the frequency domain can now be given in Equation 4.15.

$$Z_{pto}(\omega_p) = b_{pto} + c_{pto}/j\omega \tag{4.15}$$

If impedance matching is still applied here, the PTO damping and PTO spring can be expressed in Equations 4.16 and 4.17.

$$b_{pto} = B(\omega_p) \tag{4.16}$$

$$c_{pto} = \omega_p^2[m + M(\omega_p)] - c \tag{4.17}$$

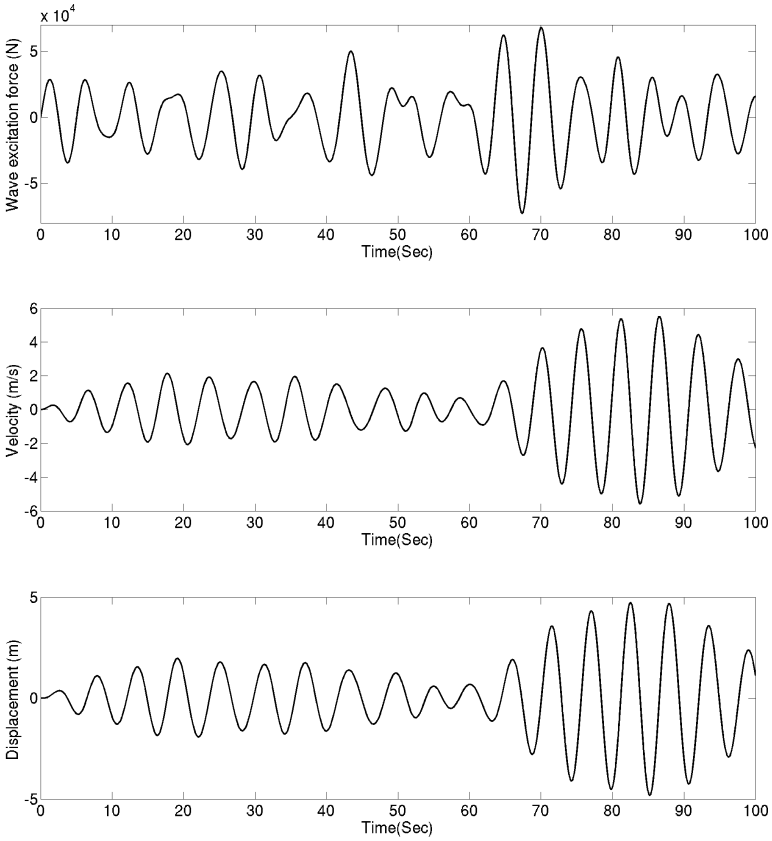

Figure 4.22: Simulation results under spring-damping control at 0.18 Hz peak frequency, a) wave excitation, b) velocity, c) displacement

Simulation: case one

The buoy's radius is chosen as 2.2 m and the peak frequency is selected as 0.18 Hz, which is smaller than the natural frequency of the oscillating system. For sub-optimal spring-damping control, acceleration does not contribute any PTO force, so it is not included in the results as shown in Figure 4.22.

For irregular waves, most energy is stored in the waves that come at the peak frequency; but many waves that come to the WEC have different frequencies. By applying spring-damping control, the natural frequency of the oscillating buoy is controlled to be the peak frequency. Hence, sometimes, the motion of the oscillating buoy is opposite to the wave excitation force, such as from 88 second to 100 second in Figure 4.23. It can be seen that there are still some resonance periods, such as from 65 second to 85 second in Figure 4.23. During these time periods, the velocity can be much bigger than the

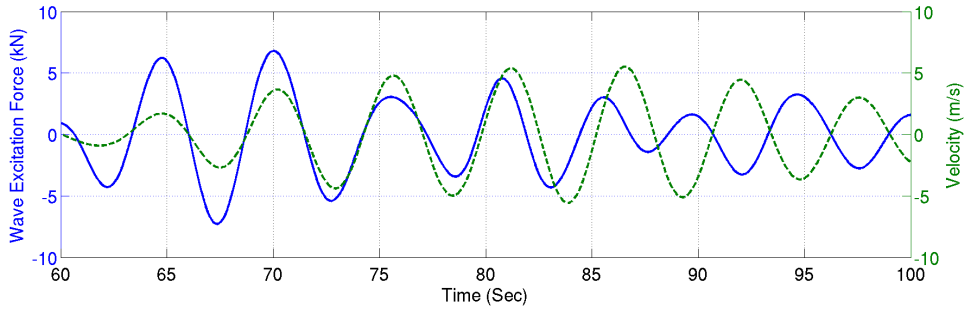

Figure 4.23: Phase difference between wave excitation force and velocity.

velocity at off-resonance which can result in greater power extraction.

Figure 4.24 shows the PTO force required to achieve spring-damping control and the power produced. The maximum PTO force is about 210 kN, the maximum instantaneous power is 640 kW and the average extracted power is 15.5 kW. The reactive force is needed only to keep the oscillating frequency the same as the peak frequency.

Simulation: case two

The buoy's radius is selected as 2.2 m and the peak frequency is selected as 0.214 Hz which is the same as the natural frequency of the oscillating system. In the last simulation case, most of the reactive force is used to adjust the natural frequency of the oscillating system to be the same as the peak frequency. Hence, in theory, this reactive force can be significantly reduced if the oscillating buoy's natural frequency is designed to be the same as the peak frequency.

The peak frequency selected in this case is smaller than the peak frequency in the first case, thus, energy carried by such irregular waves is smaller which results in smaller wave excitation forces, hence the velocity in Figure 4.25b is smaller than the velocity in case one.

The maximum PTO force required in this case is around 8 kN in Figure 4.26a. This is much smaller compared to case one which verifies the assumption above. Due to the better design of the WEC, no PTO spring force is needed in this case to achieve impedance matching, hence no reactive power should be needed as shown in Figure

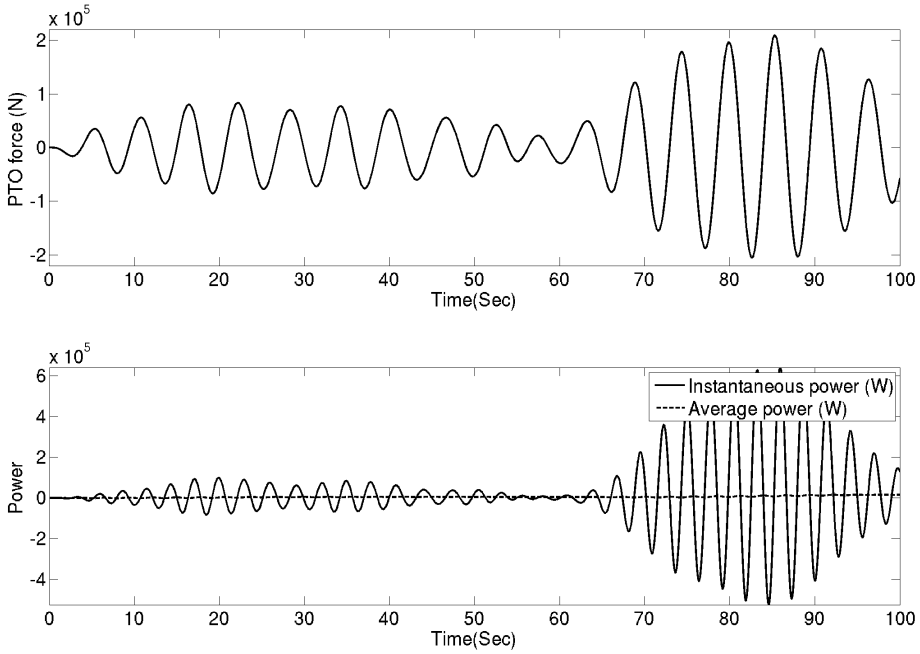

Figure 4.24: Spring-damping control results at $0.18\ Hz$ peak frequency, a) PTO force, b) power.

4.26b. It can be concluded that the design of the oscillating buoy plays a significant role in determining the system efficiency under causal sub-optimal spring damping control.

4.5.4 Reactive Mass Damping Control

Another possible solution for impedance matching is to omit the PTO spring term so that $c_{pto} = 0$. Such control is called sub-optimal mass-damping control. The PTO force expression is given in Equation 4.18.

$$f_{pto}(t) = m_{pto}\ddot{x}(t) + b_{pto}\dot{x}(t) \tag{4.18}$$

The PTO impedance in the frequency domain is now shown in Equation 4.19.

$$Z_{pto}(\omega_p) = b_{pto} + j\omega m_{pto} \tag{4.19}$$

By applying impedance matching, the PTO damping and PTO mass terms are ex-

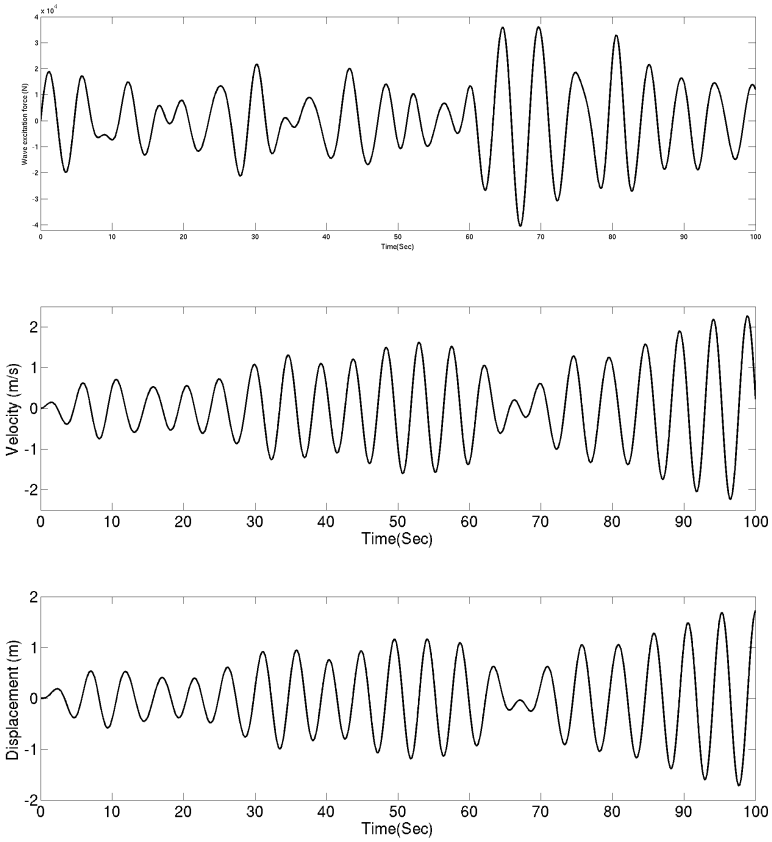

Figure 4.25: Simulation results under spring-damping control at $0.214\ Hz$ peak frequency, a) wave excitation, b) velocity, c) displacement

pressed in Equations 4.20 and 4.21.

$$m_{pto} = c/\omega_p^2 - (m + M(\omega_p)) \tag{4.20}$$

$$b_{pto} = B(\omega_p) \tag{4.21}$$

The results of applying mass-damping control to the oscillating system, whose natural frequency is designed to be the same as the peak frequency, will be exactly the same as by using spring-damping control. Since there is no reactive force in both cases, control requires no reactive force, which is called real control and is discussed in Section 4.5.5. Hence, in this section, only 0.18 Hz peak frequency is selected for analyzing simulation results. This control method also uses reactive force to control the natural frequency of the WEC to be the same as the peak frequency, hence the results of velocity and

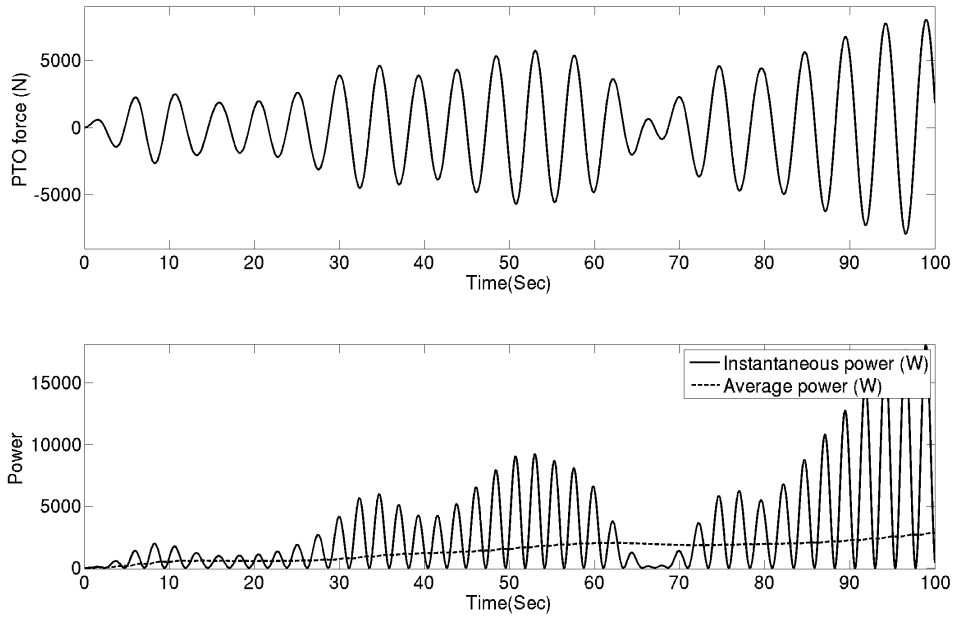

Figure 4.26: Spring-damping control results at 0.214 Hz peak frequency, a) PTO force, b) power.

displacement are quite similar to spring-damping control. Figure 4.27 provides only the required PTO force and the power extracted.

The waveforms of the PTO force and power in Figure 4.27 are very similar to Figure 4.24. However, the maximum PTO force and instantaneous power required to achieve mass-damping control are slightly smaller than using spring-damping control, which leads to less average real power extracted. In Figure 4.27, the instantaneous power extracted during the first 60 seconds is very small and then gets bigger. This is because the PTO force required in the first 60 seconds to control the device is less than the PTO force after 60 seconds. Apart from that, mechanical resonance may happen after 60 seconds. Hence, it cannot be concluded that the instantaneous power is increasing.

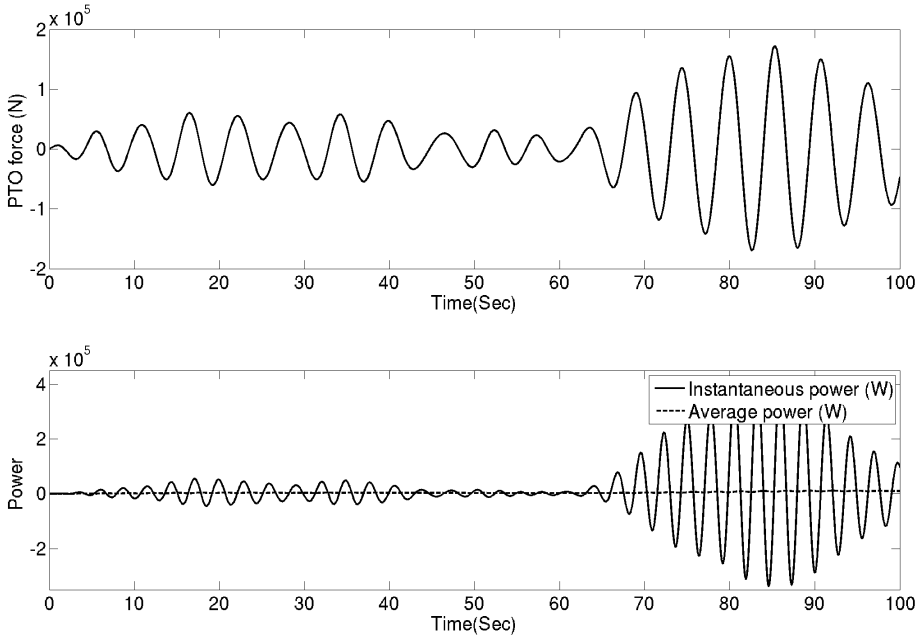

Figure 4.27: Mass-damping control results at 0.18 Hz peak frequency, a) PTO force, b) power.

4.5.5 Real Control

Real control is one of the most important reaction force control methods in which the PTO system only provides damping force, and hence, only real power is produced. This control method is very attractive for wave power engineers due to its simple implementation. The PTO force expression is given in Equation 4.22.

$$f_{pto}(t) = b_{pto}\dot{x}(t) \tag{4.22}$$

The PTO impedance contains only a real part:

$$Z_{PTO}(\omega_p) = b_{pto} \tag{4.23}$$

As there is no PTO reactance to cancel the intrinsic reactance, the optimum condition for PTO impedance is as shown in Equation 4.24 [23].

$$Z_{pto}(\omega_p) = |Z(\omega_p)| \tag{4.24}$$

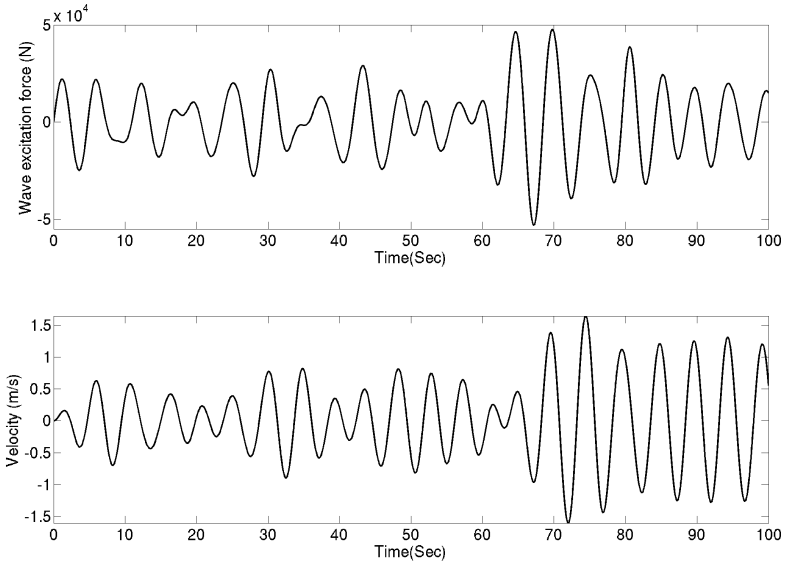

Figure 4.28: Simulation results under real control at 0.2 Hz peak frequency, a) wave excitation, b) velocity

Hence, the PTO damping coefficient is obtained in Equation 4.25.

$$b_{pto} = \sqrt{B^2(\omega_p) + (\omega_p[m + M(\omega_p)] - c/\omega_p)^2} \tag{4.25}$$

As there is no reactive force to cancel any part of the inertia force or the spring force, motion of the WEC is off-resonance with the wave excitation force, and the amplitude of the velocity is smaller compared to other control methods. If the buoy is designed to have its natural frequency corresponding to the peak frequency, the control results are very similar to spring-damping control case two in Section 4.5.3. Hence, a different simulation result is presented here by choosing 0.2 Hz for the peak frequency, so that the natural frequency of the oscillating system does not agree with the peak frequency. In this simulation only velocity needs to be considered.

The maximum PTO force required is around 25 kN in Figure 4.29a and all the force contributes to generate the real power. As the real power equals the product of PTO damping and velocity, hence, either increasing the velocity or the damping force will increase the power production. However, because the damping force is the only PTO force to adjust the motion of the WEC, there is a contradiction in that the increase of

damping force results in the reduction of velocity.

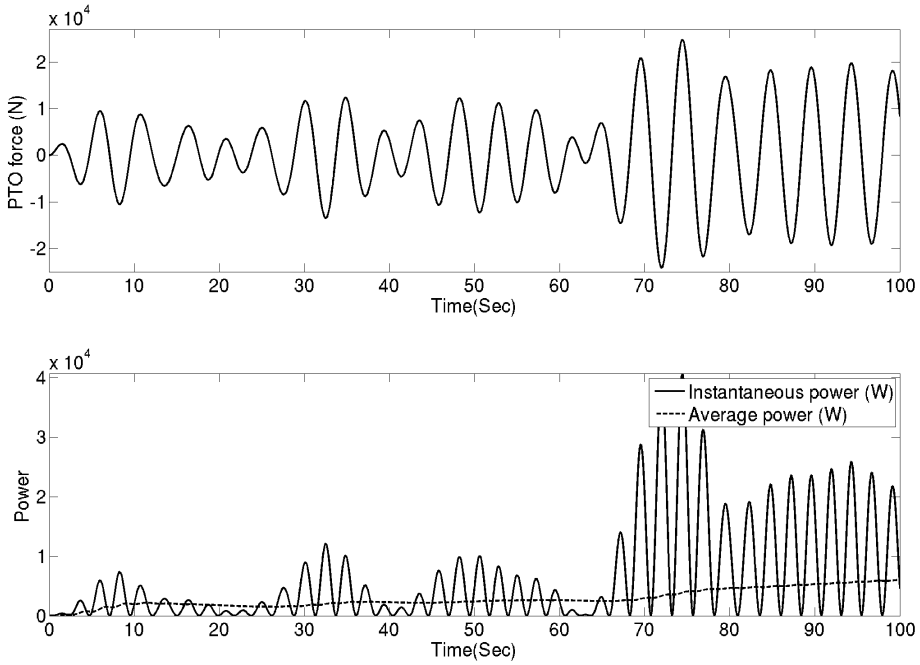

Figure 4.29: Real control results at 0.2 Hz peak frequency, a) PTO force, b) power.

4.5.6 Comparison Among Different Controls

In the last few sections, different reaction force control ideas have been proposed and the simulation results are provided. Reaction force control can be classified into reactive force control and real control. Velocity, hence power production, can be optimized by using complex conjugate control. For the real control method, velocity can only be controlled by adjusting the damping force, hence, it does not much affect power production which depends on the product of velocity and damping force rather than only velocity. Sub-optimal latching control is also proposed to obtain a higher velocity but with a discontinuous power output. Real power extraction by five different control methods are compared in Figure 4.30. It can be seen that complex conjugate always performs the best in real power extraction, but with a disadvantage of high reactive force required. Latching control extracts the second largest real power with no reactive power required. However, latching control produces discontinuous power output as no short term energy storage for direct drive linear generator system. The

other three reaction force control methods produce more or less the same real power, but in general, real control is the best due to there being no reactive power.

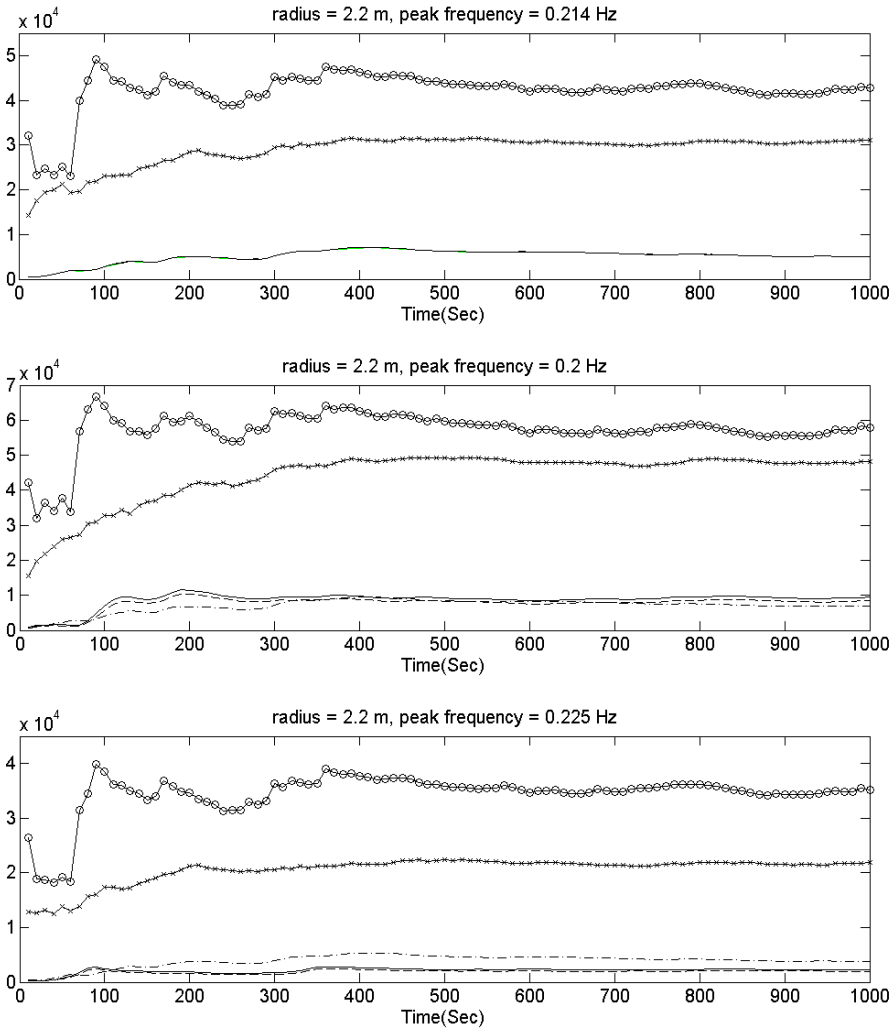

Figure 4.30: Real power extraction using five different control ideas, ○ is complex conjugate control, × is latching control, solid line is spring damping control, dashed line is mass damping control and dotted line is damping control.

For complex conjugate control as introduced in Section 4.5.2, average real power production is theoretically the maximum without performing wave prediction. The velocity of the WEC moves almost, but not quite, in phase with the wave excitation force. This slight phase difference is due to hydrodynamic parameters such as added mass and added damping being calculated based on the peak frequency of the wave spectrum. Theoretically, optimal control can be achieved if an effective method of predicting future incident waves is available, as the added mass and added damping

could then be adjusted depending on the provided frequencies. In practice, however, even with sub-optimal complex conjugate control, the maximum theoretical power extraction cannot be achieved with existing linear generator technologies.

As a large PTO force and reactive power is required for complex conjugate control, the reactive spring-damping and reactive mass-damping controls are investigated in Section 4.5.3 and Section 4.5.4. Both of these two methods apply PTO reactance to cancel part, but not all, of the intrinsic reactance. The advantage of applying these two methods is that the PTO force can be significantly reduced compared to complex conjugate control. These two methods both apply PTO force to change the natural frequency of the buoy to agree with the peak frequency of the wave energy spectrum. Although power extraction is not the maximum, most of the wave power that exists in peak frequency waves can be extracted due to resonance motion. For these two control methods, if the floating buoy is designed in advance to have its natural frequency the same as the peak frequency of the wave spectrum, the reactive force can be reduced to be very small or even zero.

Real control is particularly important in ocean wave energy engineering due to its simple implementation. However, velocity cannot be amplified because there is no PTO reactive force to cancel any part of either the inertia force or spring force. Therefore, the required PTO force is small in real control which can be easily achieved by existing linear generator technologies.

4.6 Mechanical Constraint

4.6.1 Mechanical Model

From the simulation results of causal sub-optimal complex conjugate control and sub-optimal latching control, the buoy's displacement is normally larger than the buoy's draft. Therefore, the WEC must be designed with amplitude constraints for when the incoming wave is large enough to drive the buoy over its draft. In the first AWS device,

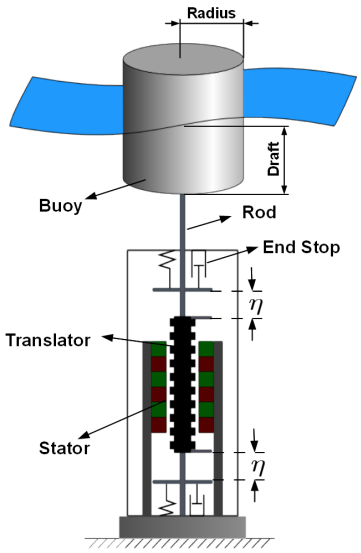

Figure 4.31: Direct drive WEC with an end-stop system. The connection rod means the buoy can only move in heave with other motions constrained

a water damper was used to provide an additional force when the WEC reaches its chosen end-stop point to prevent a heavy collision [90]. When operating freely in ocean waves the end-stops are rarely required due to the poor response of the system. However, for a WEC operating under reactive causal control, the displacement becomes very large as it approaches resonance. Here end-stops are added, each modelled as a combination of a spring stiffness term and a damping term as shown in Equation 4.26.

$$f_{es} = b_{es}\dot{x}(t) + c_{es}(x(t) - \eta) \tag{4.26}$$

The structure shown in Figure 4.31 is used to simulate the motion of the WEC in real waves; both the upper and lower boundaries need to be constrained because of the dimensions of the buoy and the finite length of the translator. Two end-stops with equal damping and spring characteristics are mounted at each end of the stroke. These two end-stop devices can dissipate and store the energy of the moving device so that a devastating collision is prevented. However, a large acceleration is created when the translator moves away from the end-stop due to the energy stored in the spring. This

can be avoided by choosing a larger damping term relative to the spring stiffness term, at a cost of greater energy dissipation.

In Equation 4.26, f_{es} is the end-stop force when the WEC approaches the end-stop point, b_{es} is the end-stop damping coefficient, c_{es} is the end-stop spring stiffness and η is the designed height for activating the end-stop system. Falnes points out in [11] that the oscillation amplitude can be equal to the design amplitude of the WEC (draft of the buoy), thus η (as shown in Figure 4.31) should be set to be slightly less than the draft to slow the system gradually rather than creating a huge deceleration.

4.6.2 Simulation Results

For simulation, the peak frequency is chosen as 0.214 Hz and the radius of the floating buoy is 2.2 m. The draft is calculated as 4.136 m which can be regarded as the upper and lower limits of the amplitudes. As the end-stop system needs some distance to decelerate the device, 3.5 m is chosen to activate the end-stop system. This activating position can be adjusted depending on the selection of the end-stop spring stiffness force and damping force.

The system becomes non-linear when end-stop systems are activated. The spring term of the end-stop stores part of the energy that exists in the moving WEC before coming to the end-stop. However, as a large spring force is required to stop the device in a short distance, the energy stored in the spring could be large. As soon as the wave excitation force becomes smaller than the spring force, the device accelerates rapidly to move in the opposite direction to the wave excitation force. When the device leaves the end-stop system (the velocity may be very high in the other direction), it decelerates rapidly first and then accelerates rapidly again under the wave excitation force. The result in Figure 4.32b is obtained by providing only a spring term in the end-stop system and is chosen to be half of the buoyancy spring stiffness. It is clearly seen that, between 62s and 72s, the velocity changes very quickly in both directions. Figure 4.32c shows that the device is not locked at the specific position when it approaches the end-stop systems, indicating an unstable system. Hence, the choice of the spring term must be

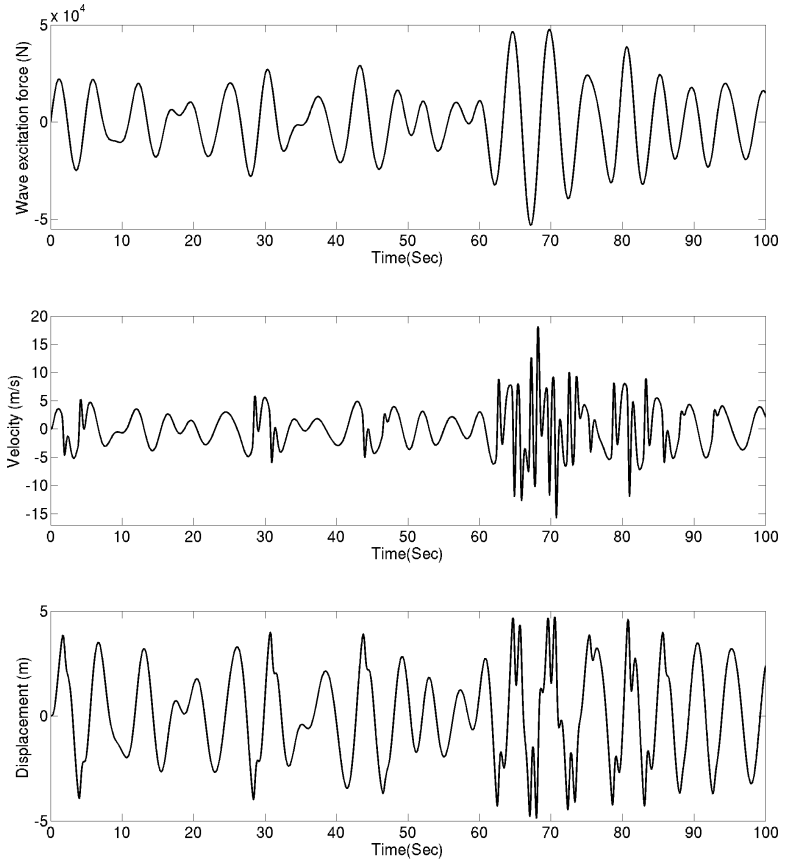

Figure 4.32: Simulation results under causal sub-optimal mass-spring-damping control with only spring force end-stop system at 0.214 Hz peak frequency, a) wave excitation force, b) velocity, c) displacement

carried out very carefully.

As a large end-stop spring leads to an unstable system, the end-stop force should include a small spring force and a relatively big damping force. If the end-stop system is given by choosing the spring stiffness force at 0.2 times the buoyancy spring stiffness force and the damping force is chosen to be 6 times the added damping force, the simulation results of velocity, displacement and PTO force required are as shown in Figure 4.33.

It can be seen from Figure 4.33a that velocity does not change very quickly at the end-stops because most of the energy dissipates through damping force. In Figure 4.33b, the displacement of the device is successfully controlled under 4.2 m which is more realistic than if there is no end-stop system. However, another problem arises when

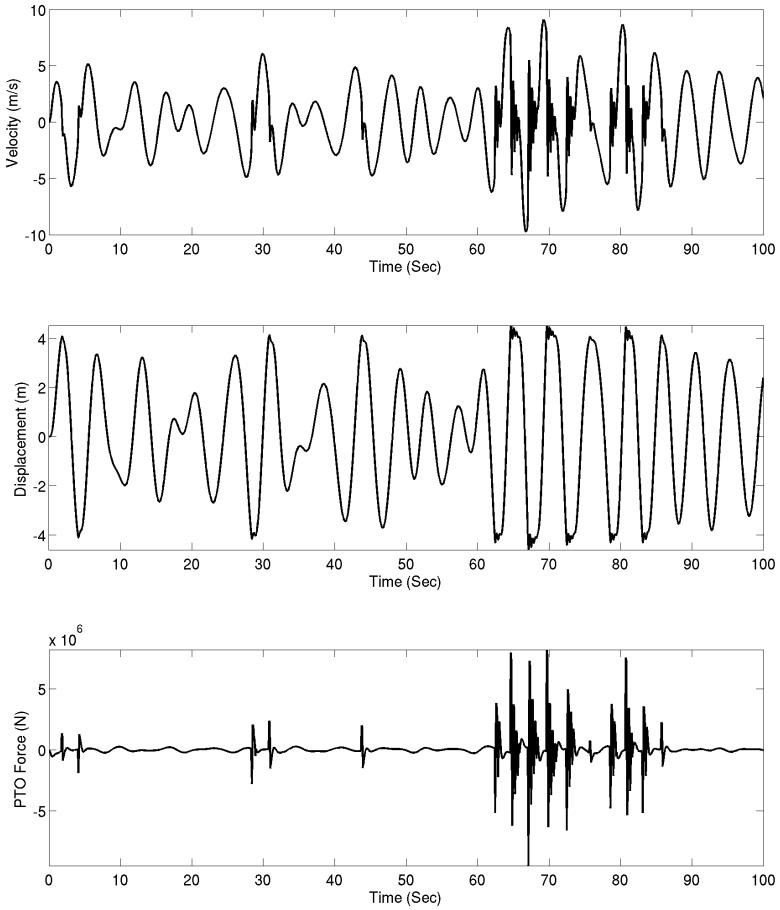

Figure 4.33: Simulation results under causal sub-optimal mass-spring-damping control with only spring and damping force for end-stop system at 0.214 Hz peak frequency, a) velocity, b) displacement, c) PTO force required

the end-stop system is added where the PTO force required to control the device is very large, as shown in Figure 4.33c. This is because there is a large acceleration when the buoy approaches the end-stop which is one of the important terms to calculate the required PTO force in causal sub-optimal mass-spring-damper control. Unfortunately, such a large amount of PTO force cannot be provided by any existing linear generator, hence, the generator force has to be limited which is discussed in Section 5.3.1. Such a problem would disappear if there is no mass term involved in the calculation of PTO force such as with causal sub-optimal spring-damping control or real control.

4.7 Chapter Summary

This chapter focuses on the control of point absorber WECs in irregular waves to extract the maximum power. An appropriate control system is very important to WEC due to the large investment of the system. To extract the maximum power, mechanical resonance where the buoy moves in phase with the wave excitation force should be achieved. There are several control strategies to achieve this resonance. Latching control is a very effective way, but as optimal latching control requires future wave prediction, only sub-optimal latching control method is discussed. Alternatively, PTO force control which applies the force from the generator can dispense with future wave prediction by applying casual sub-optimal control. By calculating the required PTO force through the peak frequency of the wave energy spectrum, near resonance occurs between the wave excitation force and the velocity. However, realistic considerations should be taken into account that the displacement of the device may be very large. Hence, displacement is constrained by introducing end-stop systems, but this creates a huge acceleration which results in an unrealistic PTO force. The PTO force constraint is discussed in Chapter 5.

Chapter 5

Linear Generator Control

5.1 Introduction

This chapter first describes the Air-Cored Tubular Machine (ACTM) and the corresponding simulation model. A method of choosing an appropriate limit for the available force is also described. By supplying the displacement, velocity and PTO force to the linear permanent-magnet generator model, the coil voltages are determined, as are the required currents to control the WEC. If an ideal power converter is assumed, the PTO force will be provided by the machine and fed back to the system. Amplitude constraint is also modelled by including the end-stop system. For a more realistic consideration, electrical loss of the electrical machine is also included. As the linear generator operates at the rated current most of the time under reactive force control, electrical loss is significant which directly reduces the net power production. Simulation results are provided to compare power extraction for the different control methods.

5.2 Simulation Model of Linear Generators

In order to extract power from waves as well as to achieve the reaction force control for a point absorber WEC, a linear generator that is directly coupled with the WEC is the simplest option. It can provide real force for generating real power and also the reactive force for controlling the buoy with the mean power zero. In the analysis of [5], the total force can be represented as the sum of two orthogonal components: the x directed component for the displacement and the orthogonal $\dot{x}$ component for the velocity.

This analysis is easily applied to spring-damping control in which the reactive force consists only of a spring stiffness force. Such analysis becomes more complicated in irregular waves, especially for causal sub-optimal mass-spring-damping control which contains an acceleration term, as the x directed component is for the combination of both displacement and acceleration.

Linear generators with a number of different topologies are available [31, 57], with no clear "winner" yet emerging from these choices. The particular topology chosen for the simulations presented here is the Air-Cored Tubular Machine (ACTM) [66]; however, the methods of force and EMF calculation for this machine are also applicable to other generator types. A linear variable reluctance permanent magnet machine is also developed and is described in Appendix B for completeness, although it is not used in the simulation. The following section of linear generator design is the work from Richard Corizer.

5.2.1 Air Cored Tubular Machine

The ACTM consists of two parts, the translator and the armature. The translator is made up of a series of axially magnetized permanent magnet discs with alternating polarity, separated by steel discs mounted on a central shaft. This slots into a second cylinder made up of circumferentially wound copper coils. A diagram of the arrangement is shown in Figure 5.1, and further details of its operation can be found in [66] and [62]. The machine has three phases, with all coils in a phase connected in parallel. It is further assumed that only coils overlapping the stator are active at any point, with the other coils being switched out of the circuit.

The particular design of the generator used is summarised in Table 5.1 with reference to the dimensions shown in Figure 5.1 and where D_C denotes the coil conductor wire diameter and p_f the number of translator poles.

The flux linkage in the coil windings is found at a number of positions by performing a 2D axisymmetric finite element simulation of the magnetic field around the translator. A polynomial is then fitted to the flux linkage (λ) versus displacement (x) and is

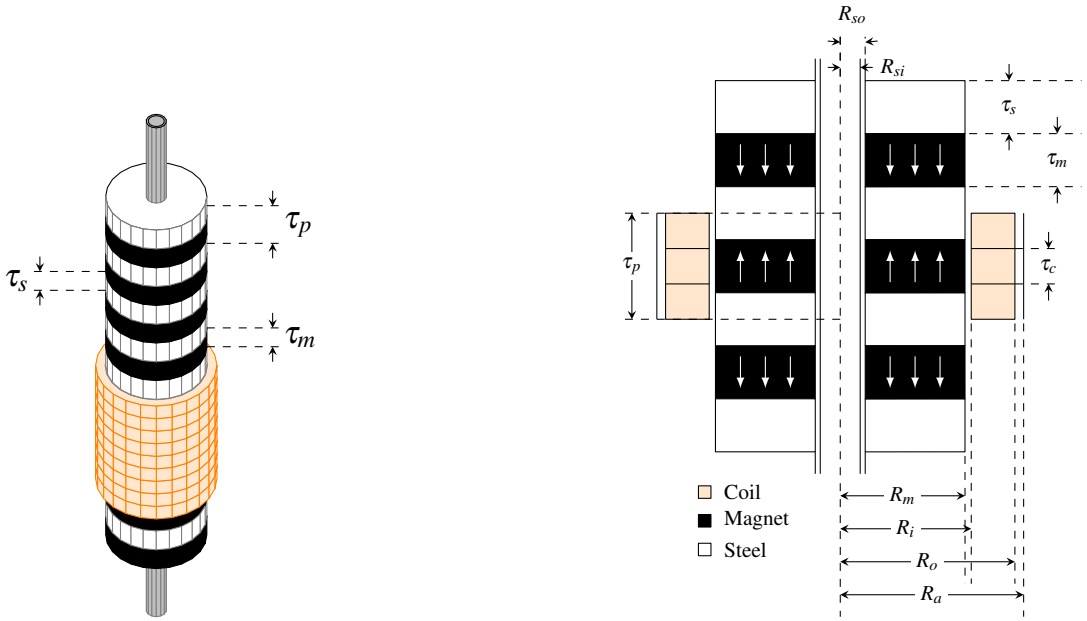

Figure 5.1: 3D view of the ACTM and cross-section of machine with dimensions.

Table 5.1: ACTM Design Variables

Dimension	Size	Dimension	Size
τ_p	133 mm	τ_c	36 mm
τ_s	36 mm	R_{si}	0 mm
τ_m	96 mm	R_{so}	39 mm
R_m	79 mm	N	4112
R_i	83 mm	p_f	38
R_o	126 mm	D_C	0.5 mm
R_a	133 mm		

assumed to be periodic over two poles. The EMF produced due to movement of the translator is the rate of change in the flux linkage with time and can then be calculated with knowledge of the velocity as in Equation 5.1.

$$\mathscr{E} = -\frac{\mathrm{d}\lambda}{\mathrm{d}t} = -\frac{\mathrm{d}\lambda}{\mathrm{d}x} \cdot \frac{\mathrm{d}x}{\mathrm{d}t} = -\frac{\mathrm{d}\lambda}{\mathrm{d}x} \cdot \dot{x}(t) \tag{5.1}$$

The value of $\frac{\mathrm{d}\lambda}{\mathrm{d}x}$ is simply the derivative of the polynomial and is evaluated at the current translator position.

The availability of this derivative also provides a convenient method of calculating the

PTO force given knowledge of the current in the armature coils. The force (F) exerted either on or by the generator is given in Equation 5.2, where P is the power in the generator electrical circuit. Here the power can be either positive or negative, where the sign indicates whether the power flow is into or out of the system (i.e. from the WEC or from the grid).

$$F = \frac{P}{\dot{x}(t)} \tag{5.2}$$

The instantaneous power in the generator/grid circuit is given by $P = i(t)v(t)$ where $v(t)$ is the voltage across the armature coils, i.e. the EMF, and $i(t)$ is the coil current. Therefore the PTO force is given by Equation 5.3 which leads to Equation 5.4.

$$\begin{aligned} f_{pto}(t) &= -\frac{i(t)v(t)}{\dot{x}(t)} \qquad (5.3) \\ &= -\frac{i(t)}{\dot{x}(t)}\mathscr{E} \\ &= -\frac{i(t)}{\dot{x}(t)}\left(-\frac{\mathrm{d}\lambda}{\mathrm{d}x}\dot{x}(t)\right) \\ &= i(t)\frac{\mathrm{d}\lambda}{\mathrm{d}x} \qquad (5.4) \end{aligned}$$

Clearly, this method is applicable to any machine for which the flux linkage can be specified with position, provided other forces can be neglected, e.g. tooth ripple forces in slotted machines. In practice, the derivative is easily estimated from experimental data for the purposes of this force calculation.

5.2.2 General Model Description

Figure 5.2 shows the simulation model of the entire system which includes the WEC and ACTM linear generator. The hydrodynamic parameters block was introduced in Section 4.5.2 where both the added mass and added damping coefficients are stored in the look-up tables. The mass-spring-damper system is the same as introduced in Section 4.5.2 but has been put into a sub-system which is called "mass spring damper". The ideal PTO force is calculated in the right top block. When the required PTO has been obtained, it is fed to the linear generator block as shown in orange. The first step

which is carried out in the linear generator block is to calculate the EMF voltages. Based on Equation 5.1, EMFs are calculated according to the provided velocity and displacement. Therefore, three inputs for the ACTM generator block are required, which are ideal PTO force, velocity and displacement of the oscillating buoy. The outputs of the generator block are the EMFs, the currents and the actual PTO force. The currents, here, are actual currents and the output PTO force is the actual force obtained from the actual currents. If there is no force limitation on the linear generator, the output currents should be the ideal currents to make the output PTO force the same as the desired PTO force.

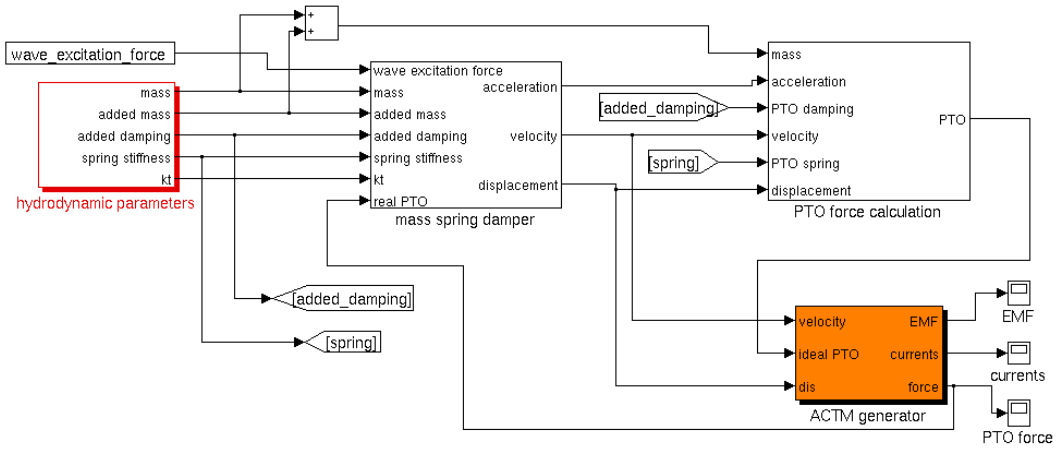

Figure 5.2: WEC system with PTO system and linear generator.

5.2.3 Simulation Results

It has already been established that by providing the ideal PTO force to the linear generator, the EMFs and required currents can be obtained, hence the PTO force. This generated force can be regarded as the actual force and is fed to the mass-spring-damper system to achieve control. The simulated linear generator, here, is assumed to be able to provide any force as required. The same test system is used as in Chapter 4 where the peak frequency is selected as 0.214 Hz and the radius of the floating buoy is chosen to be 2.2 m to make the natural frequency of the buoy the same as the peak

frequency of the energy spectrum. The whole oscillating system is under causal sub-optimal mass-spring-damping control.

Results in Figure 5.3 show the phase EMF and the required phase current according to the input PTO force. The velocity of the WEC is near resonance with the wave excitation force under causal sub-optimal mass-spring-damping as shown in Figures 5.3a and 5.3b. High velocity results in a big EMF output with the maximum amplitude 9700 volts as shown in Figure 5.3c, which occurs when the velocity reaches its peak value. The required phase current is shown in Figure 5.3d with the maximum 335 amperes.

5.3 Practical Considerations

5.3.1 Force Specification and Limits

As the ACTM used is three-phase, there is a wide choice in how to distribute the currents in each phase to give the required force. Therefore, to narrow this choice, the power electronic converter supplies or draws this current in phase with the voltage. In this case the force production can be distributed between phases in proportion to the values of $\frac{\mathrm{d}\lambda}{\mathrm{d}x}$ for each coil at a given position.

If the three coil currents are denoted as a three element vector, $\mathbf{C}$, and the instantaneous values of $\frac{\mathrm{d}\lambda}{\mathrm{d}x}$ for each phase as another three element vector, $\mathbf{L}$, suitable coil currents can then be found from Equation 5.5.

$$\mathbf{C} = \frac{f_{pto}(t)}{\max\left(\frac{\mathrm{d}\lambda}{\mathrm{d}x}\right)}\hat{\mathbf{L}} \tag{5.5}$$

The value of $\max\left(\frac{\mathrm{d}\lambda}{\mathrm{d}x}\right)$ can be determined in advance, and if the system is a 3-phase balanced circuit, the PTO force can be estimated from Equation 5.9 using the same

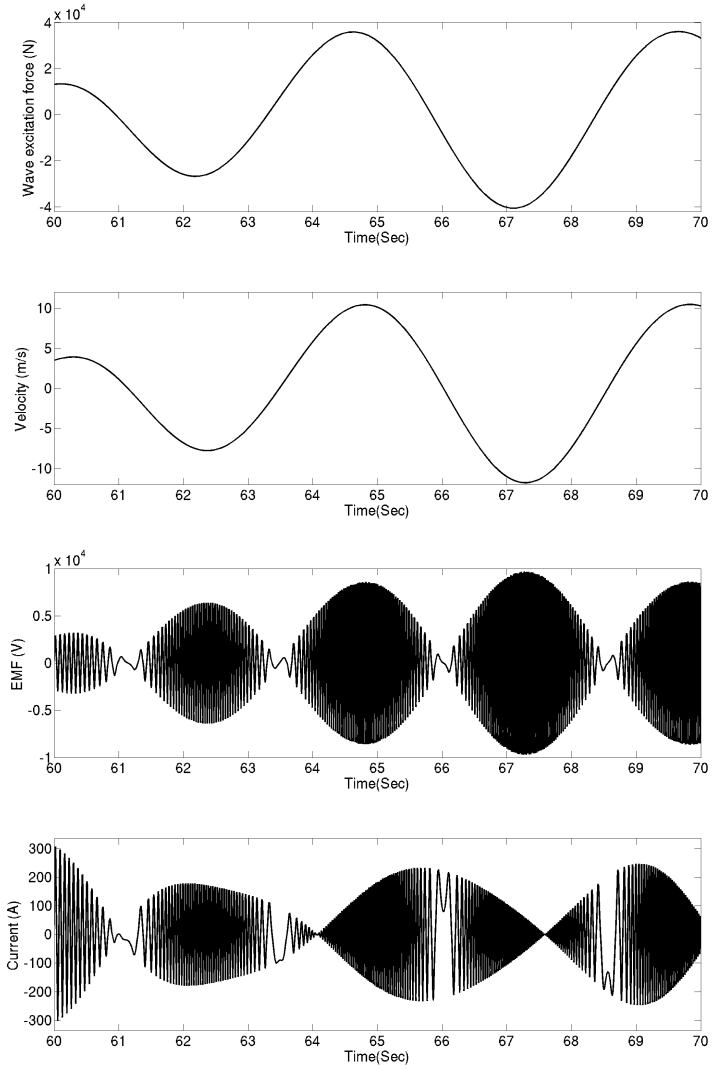

Figure 5.3: Simulation results of the linear generator under causal sub-optimal mass-spring-damping control, a) wave excitation force, b) velocity, c) phase EMF, d) phase current.

principle as applied in Equation 5.4.

$$P_{\mathrm{RMS}} = 3 I_{\mathrm{RMS}} V_{\mathrm{RMS}} \tag{5.6}$$

$$= 3 I_{\mathrm{RMS}} \frac{\hat{V}}{\sqrt{2}} \tag{5.7}$$

$$= 3 I_{\mathrm{RMS}} \frac{u(t) \max\left(\frac{\mathrm{d}\lambda}{\mathrm{d}x}\right)}{\sqrt{2}} \tag{5.8}$$

$$f_{pto} = \frac{P_{\text{RMS}}}{u(t)} \tag{5.9}$$

Using Equations 5.8 and 5.9 the PTO force can then be calculated in terms of the "instantaneous rms" current and the flux linkage derivative as shown in Equation 5.10. In general, the term "instantaneous rms" is defined here as the value the rms of the current or voltage waveform would have if the machine were maintained indefinitely at the instantaneous velocity at which the given voltage or current is experienced. If it is assumed that the current waveforms at a given velocity are approximately sinusoidal, or more specifically, that the flux linkage waveform with displacement is sinusoidal, the rms current required to give the desired force is then given by Equation 5.11. The required peak current in a cycle at the current velocity can be estimated from ($\hat{I} = \sqrt{2}I_{\text{RMS}}$), and the actual required currents in each coil are then given by Equation 5.12.

$$f_{pto} = \frac{3}{\sqrt{2}} I_{\text{RMS}} \max\left(\frac{\mathrm{d}\lambda}{\mathrm{d}x}\right) \tag{5.10}$$

$$I_{\text{RMS}} = \frac{\sqrt{2} f_{pto}}{3 \max\left(\frac{\mathrm{d}\lambda}{\mathrm{d}x}\right)} \tag{5.11}$$

$$\mathbf{C} = \frac{\sqrt{2} I_{\text{RMS}} \mathbf{L}}{\max\left(\frac{\mathrm{d}\lambda}{\mathrm{d}x}\right)} \tag{5.12}$$

However, Equation 5.12 assumes that the flux linkage in the coils with displacement, and its derivative, is a perfect sinusoid without harmonics. This is usually not the case and can result in a difference between the desired and calculated force. The correct currents can be found by dividing the desired PTO force by the actual force produced using the currents found using Equation 5.12 and multiplying the currents by this factor.

There are also practical limits on the current that can pass through any machine's coils without causing failure through heating of the windings due to resistive losses. This, therefore, places a limit on the maximum possible force that can be produced without damaging the generator. This current limit is best expressed as a maximum allowed

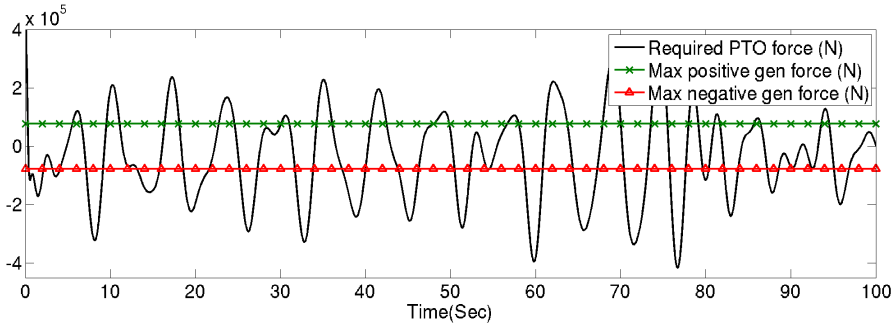

Figure 5.4: Comparison of the required PTO force and the actual PTO force that the linear generator can provide.

rms current density in the coil conductor, J_M. For the simulations presented here, a maximum rms current density of 7 A/mm^2 is permitted. If the desired PTO force results in an rms current requirement that exceeds this limit, the value of J_M, with the appropriate sign is used instead. However, if the linear generator is normally operating at over rating, design should be made according to the peak rather than the average.

Figure 5.4 demonstrates that for the majority of the time, the required PTO force needed to control the WEC, using sub-optimal mass-spring-damping control is greater than the generator can provide. The black line in the figure shows the desired PTO force, and the green line and the red line illustrate the maximum positive and negative forces that the linear generator can provide. In this example, a maximum PTO force of about 420 kN is needed during the first 100 seconds, which is in excess of five times the maximum force that can reasonably be provided by the linear generator. Therefore, causal sub-optimal mass-spring-damping control cannot be achieved by modern linear generator technologies.

5.3.2 Force Constraints

As the required force to achieve this control is excessive, the same control method has also been attempted but with the force limited as discussed in Section 5.3.1. When the generator force is constrained, the ideal PTO force can no longer be achieved, so the motion of the WEC and the wave excitation force are no longer kept in resonance, as shown in Figure 5.5. Although the overall motion is not in phase with the wave

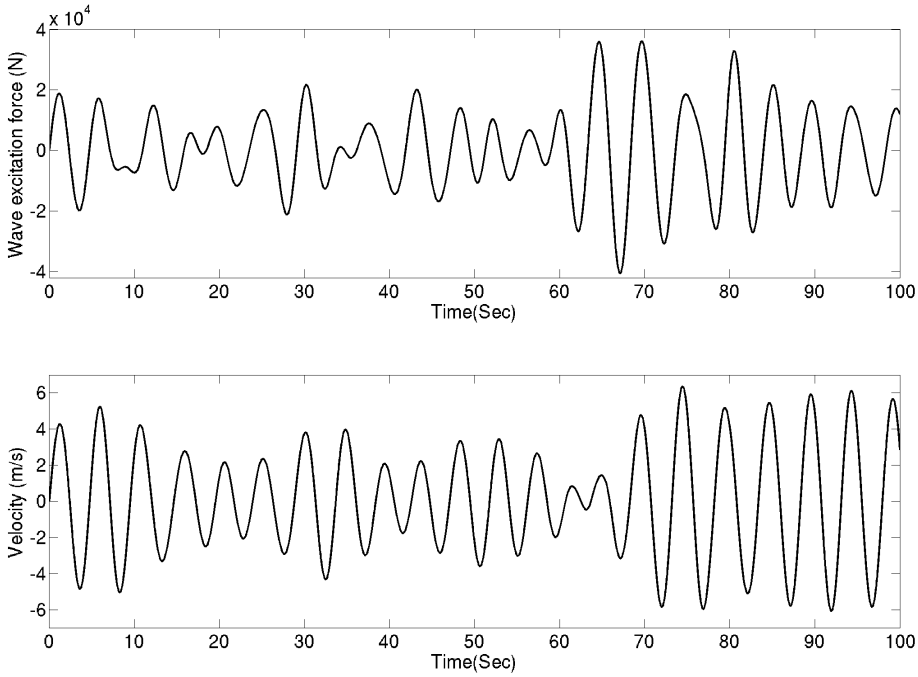

Figure 5.5: Simulation results of the WEC under causal sub-optimal mass-spring-damping control with force constraints, a) wave excitation force, b) velocity.

excitation due to insufficient PTO force provided, resonance still exists part of the time when the wave excitation force is not too big, such as the motion between 40 seconds and 60 seconds. The smaller PTO force required in this period can be provided by the linear generator, and short term resonance can still be achieved to extract as much power as possible.

Figure 5.6 shows the results of velocity, phase EMF and phase current under causal sub-optimal mass-spring-damping control with the linear generator force constraint. From Figure 5.6b it is clearly shown that the velocity is off-resonance with the wave excitation force in between 60 seconds and 70 seconds due to the force constraint. The maximum velocity is around 6 m/s which is significantly reduced compared to the velocity in Figure 5.3b. The reduced velocity results in a significant reduction in the EMFs as shown in Figure 5.6c. An important result is shown in Figure 5.6d where the maximum phase current is successfully controlled to be around 74.5 amperes due to the maximum PTO force constraint. The comparison between the required PTO force and actual PTO force the linear generator can provide after feeding the generator force

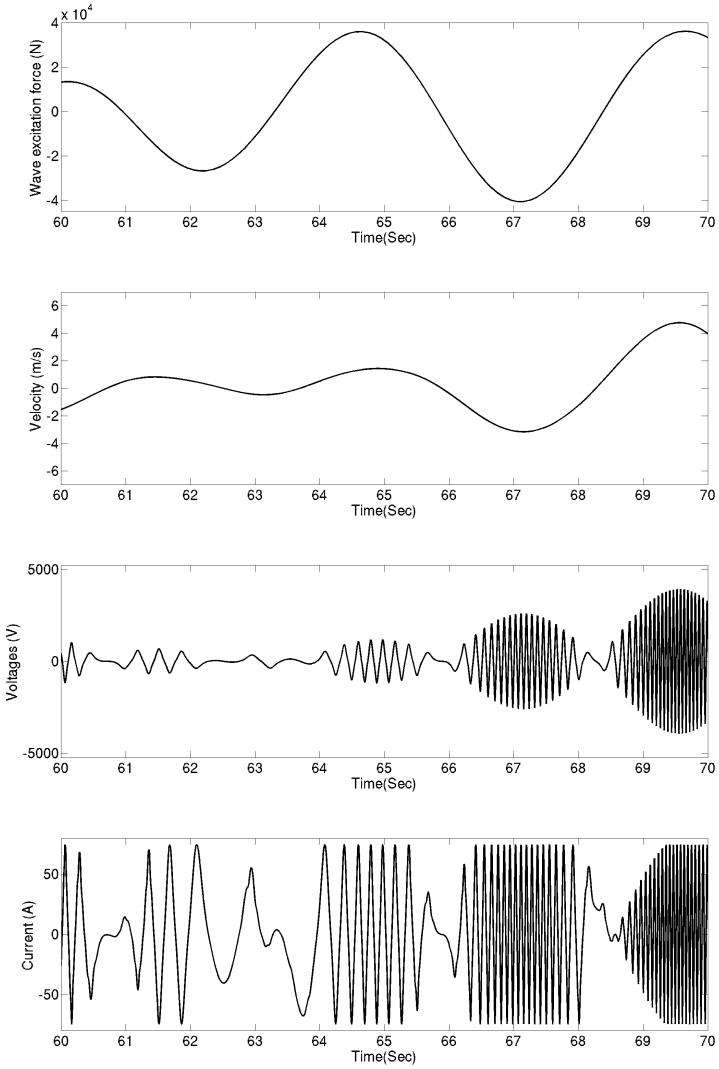

Figure 5.6: Simulation results of the linear generator under causal sub-optimal mass-spring-damping control with force constraint, a) wave excitation force, b) velocity, c) phase EMF, d) phase current.

to the control system is shown in Figure 5.7. Here, the required PTO force is no longer ideal as the input force is not kept at its required value anymore.

Under the generator force constraint, the oscillating displacement can be reduced significantly, but it is sometimes still bigger than the buoy's designed draft. Therefore, end-stop systems have to be included together with force constraint to make the system more realistic. Figure 5.8 shows the displacement comparison under force constraint: the black line represents the displacement without end-stop systems and the red dashed line represents the displacement with end-stop systems. It can be seen that, without

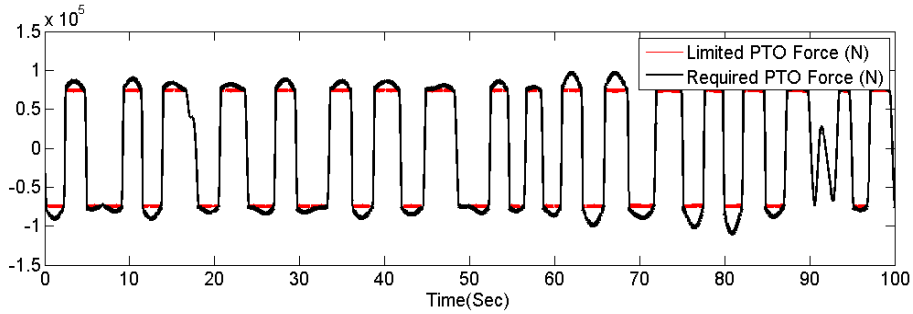

Figure 5.7: Comparison between required force and actual force the linear generator can provide.

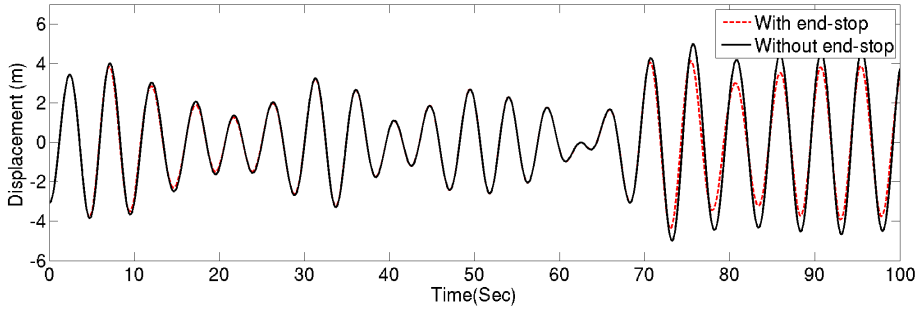

Figure 5.8: Comparison of displacement under force constraint: the black line is the displacement without end-stop systems and the red dashed line is the displacement with end-stop systems included.

end-stops, the maximum displacement under force constraint is around 5 m, which is much smaller than with no force limitation but still larger than the draft. By adding the end-stops, the maximum displacement is successfully controlled around 4 m.

Figure 5.9a shows that the generator force is limited to around 77 kN, and the velocity, acceleration and displacement of the WEC cannot be maintained at the desired values. As the optimal PTO force is determined dynamically, the required PTO force during force constraint diverges from the required force when using the ideal force as the simulation progresses. In this figure, there are several sections where the PTO force changes very sharply, such as at 5 s, 7.5 s, and between 70 s and 76 s. These rapid changes are produced by the large acceleration which is created when the end-stop systems are activated. Figure 5.9b shows that the instantaneous power flow either into or out of the system is often considerably greater than the mean power extracted during the entire simulation time.

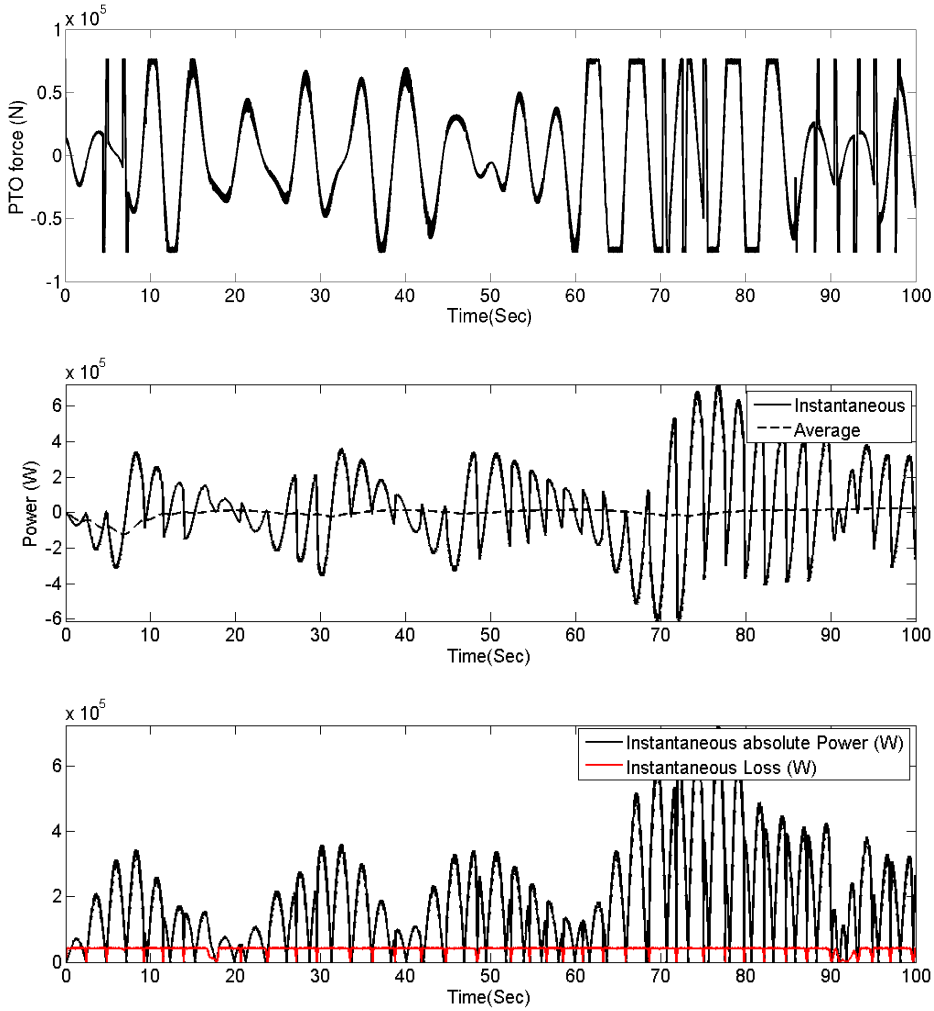

Figure 5.9: a) Actual PTO force under amplitude constraints, b) The instantaneous and average power under force and amplitude constraints, c)Instantaneous absolute power generated by linear generator and instantaneous power loss in linear generator.

5.3.3 Power Production

The average power production shown in Figure 5.9b is not the real average power extracted by the linear generator as electrical loss is not considered yet. In order to control the WEC, a large PTO force is required which leads to a large phase current from the generator, hence the electrical loss. Electrical loss is proportional to the square of currents and the resistance of the conducting line as given in Equation 5.13. To obtain the real average power extracted by the generator, electrical loss has to be subtracted from the average power. The instantaneous absolute power flow of the linear

generator and the instantaneous power loss in the linear generator is shown in Figure 5.9c.

$$P_{loss} = I^2 R \tag{5.13}$$

The reactive force required to achieve reaction force control is very large, and may result in a large negative power flow, as shown in Figure 5.9b. This mechanical reactive power is the analog of the reactive power required in reactive electrical circuits, but is distinct from the reactive electrical power drawn from the grid. In this thesis, the mechanical reactive force consists of the inertia and spring stiffness force. The total mechanical reactive force is generally much smaller than any component force that contributes to it due to the opposite signs of acceleration and displacement in a mass-spring-damper system. The existence of the mechanical reactive force can lead to a higher velocity and the production of a higher real, or mean, power output. The mechanical reactive power is used only to control the motion of the WEC, and the mean power used to perform this is zero, neglecting losses in the system. For this reason the reactive power is excluded from these results.

5.3.4 Multi-Connected Linear Generators

As modern technologies of linear generators cannot provide enough force to achieve causal sub-optimal mass-spring-damping control, it is proposed to have several linear generators connected together to obtain a larger force. Several problems do arise when several generators are connected. Firstly, the total mass increases by adding more generators. In this thesis, the mass of the floating device is calculated by combining the mass of the buoy and the generator. If the mass of the linear generators increases, the mass of the buoy has to be reduced to achieve a balance. Hence, not too many linear generators can be added as the overall designed mass will be exceeded. Secondly, as more linear generators are connected, the maximum possible current can be increased, hence the PTO force. When the PTO force approaches the desired PTO force, the buoy may move almost in phase with the wave excitation force to achieve near resonance. The displacement could be very big and exceed the maximum designed draft which can

	one generator	two generators	three generators
max velocity (m/s)	7.86	9.88	11.3
max displacement (m)	5.45	7.7	8.65
max instant power (kW)	741.98	1077.3	1287.6
extracted power (kW)	33.8	40.3	49.6
loss (kW)	15.05	12.22	10.15
net power (kW)	18.75	28.08	39.1

Table 5.2: Power comparison of multiple linear generators without amplitude constraint.

	one generator	two generators	three generators
max velocity (m/s)	5.327	5.419	5.498
max displacement (m)	4.082	4.084	4.086
max instant power (kW)	402.77	452.351	467.58
extracted power (kW)	21.29	21.43	21.37
loss (kW)	14.68	11.27	10.57
net power (kW)	6.6	10.16	10.8

Table 5.3: Power comparison of multiple linear generators with amplitude constraint.

lead to a contradiction. Finally, cost may increase with the number of linear generators and hence must be taken into account and compared with the power produced.

Table. 5.2 shows power production and other oscillating parameters by applying one generator, two generators and three generators. In this table, amplitude constraint is not taken into account. It shows that the average maximum extracted power is around 49.6 kW by using three generators. The net power output by using two generators is more than using only one generator, but not double, hence the cost of one more generator may not be economical.

In Table 5.3, amplitude constraint is considered. It is clear to see that the net power production is significantly curtailed. The net power extracted by two generators is still greater than using one, but only a slight increase when adding the third one. It can be concluded that the buoy's dimensions play a significant role in net power production.

5.4 Reaction Force Control Comparison

5.4.1 Notation Distinguishing

In the last section, causal sub-optimal mass-spring-damping control with both force and amplitude constraints are discussed. From the results, it can be seen that the maximum system efficiency of net power production is around 50%, which can only be achieved by applying two or three generators. Such a low efficiency is due to the large electrical loss from producing the large reaction force to achieve control. Other reaction force control methods as introduced in Section 4.5 are simulated in this section and their power production compared. For simplication, different control methods are represented by the following abbreviations:

- m, b, c control: This represents the causal sub-optimal mass-spring-damper control where the PTO force consists of a mass term, a spring term and a damping term.
- m, b, c, c control: This represents the causal sub-optimal mass-spring-damper control with both force and amplitude constrained.
- b, c control: This represents the causal sub-optimal spring-damper control where the PTO force consists of a spring term and a damping term.
- m, b control: This represents the causal sub-optimal mass-damper control where the PTO force consists of a mass term and a damping term.
- b control: This represents the real control where the PTO force consists of only a damping term.

5.4.2 Simulation Results

Different reaction force control methods are compared here under practical conditions. Practical conditions are only activated when applying causal sub-optimal m, b, c control due to the higher PTO force required and larger moving displacement when mechanical resonance occurs. Both one linear generator and two linear generators are considered for obtaining the results under m, b, c, c control. For other control methods,

Power (kW)	m,b,c,c (1)	m,b,c,c (2)	b,c	m,b	b
Peak Instant	453.099	480.26	112.91	105.642	41.57
Average Extracted	18.67	19.36	10.93	10.358	4.127
Average Loss	12.964	10.299	1.299	1.244	0.06
Average Net	5.7	9.062	9.63	9.11	4.067
Efficiency	30.5	46.8	88.1	87.95	98.55

Table 5.4: Comparison of the power extracted by four reaction force control methods, with limited PTO force and amplitude, where the buoy's radius is 2 m, peak frequency of the energy spectrum is 0.214 Hz and simulation time is 400 s.

the force required is small and within the capability of a single generator, thus only one machine is considered for other reaction force controls.

Buoy size consideration

Tables 5.4, 5.5 and 5.6 show the results of power production by choosing different size of floating buoy with a single peak frequency of energy spectrum 0.214 Hz. In Table 5.4 when the natural frequency of the floating buoy is bigger than the wave peak frequency, b, c control can extract more net power than other control methods. It can be seen that m, b, c, c control by using one generator extracts much less power power than b, c control. Even when two generators are used, the net power extracted is still smaller than b, c control due to large electrical losses.

In Table 5.5 where the buoy's natural frequency agrees with the waves peak frequency, the net power extracted by using m, b, c, c control with two generators is the largest. However, this is achieved at the cost of one more generator and which is unlikely to be economical. It also can be seen that the net power extracted by the other three control methods is almost the same due to no required reactive power to control the WEC when the natural frequency agrees with the peak frequency.

In Table 5.6 where the natural frequency of the floating buoy is smaller than the peak frequency, real control extracts the most net power. For this case, real control is the most efficient as it requires the least instantaneous power and has the least electrical loss to produce the most net power.

Power (kW)	m,b,c,c (1)	m,b,c,c (2)	b,c	m,b	b
Peak Instant	402.77	452.351	40.942	41.178	42.304
Average Extracted	21.29	21.43	8.673	8.701	8.572
Average Loss	14.68	11.27	0.152	0.151	0.147
Average Net	6.6	10.16	8.52	8.54	8.42
Efficiency	31	47.4	98.2	98.15	98.2

Table 5.5: Comparison of the power extracted by four reaction force control methods, with limited PTO force and amplitude, where the buoy's radius is 2.2 m, peak frequency of the energy spectrum is 0.214 Hz and simulation time is 400 s.

Power (kW)	m,b,c,c (1)	m,b,c,c (2)	b,c	m,b	b
Peak Instant	432.863	482.145	117.057	130.793	43.656
Average Extracted	20.466	20.755	7.779	8.29	8.189
Average Loss	16.758	13.154	1.66	1.676	0.161
Average Net	3.7	7.601	6.117	6.615	8.028
Efficiency	18.08	36.62	78.63	79.79	98.03

Table 5.6: Comparison of the power extracted by four reaction force control methods, with limited PTO force and amplitude, where the buoy's radius is 2.4 m, peak frequency of the energy spectrum is 0.214 Hz and simulation time is 400 s.

Peak frequency consideration

For the simulation results in this section, the radius of the floating buoy is fixed at 2.2 m with the natural frequency 0.214 Hz. Table 5.7 shows the extracted power by selecting the peak frequency 0.2 Hz where the predominant wave length is bigger than the waves natural frequency. As the wave length increases, the wave height also increases, hence the wave excitation force. Meanwhile, the PTO force required for causal sub-optimal m, b, c, control is larger which results in higher currents producing more electrical losses. It can be seen from Table 5.7 that real control is the optimal choice when the ocean waves become bigger.

Table 5.8 shows the extracted power when smaller waves are assumed. As introduced above, the PTO force required for causal sub-optimal control is reduced producing less electrical losses, hence, the net power extracted by causal sub-optimal m, b, c, c control is the most. When two linear generators are selected, the net power increases a small amount.

Power (kW)	m,b,c,c (1)	m,b,c,c (2)	b,c	m,b	b
Peak Instant	421.491	438.745	171.709	155.939	64.056
Average Extracted	24.577	25.645	13.243	12.246	11.688
Average Loss	19.694	17.271	3.84	3.677	0.218
Average Net	4.88	8.374	9.4	8.57	11.47
Efficiency	19.86	32.66	70.98	69.98	98.13

Table 5.7: Comparison of the power extracted by four reaction force control methods, with limited PTO force and amplitude, where the buoy's radius is 2.2 m, peak frequency of the energy spectrum is 0.2 Hz and simulation time is 400 s.

Power (kW)	m,b,c,c (1)	m,b,c,c (2)	b,c	m,b	b
Peak Instant	408.807	425.782	68.759	76.095	29.001
Average Extracted	18.083	18.059	3.256	3.789	6.452
Average Loss	11.197	8.235	0.726	0.76	0.1
Average Net	6.886	9.824	2.529	3.029	6.351
Efficiency	38.08	54.4	77.67	79.94	98.43

Table 5.8: Comparison of the power extracted by four reaction force control methods, with limited PTO force and amplitude, where the buoy's radius is 2.2 m, peak frequency of the energy spectrum is 0.225 Hz and simulation time is 400 s.

The results simulated from Table 5.4 to Table 5.8 indicate that ocean conditions and the size of the buoy should be taken into account before selecting the control strategy. Generally speaking, real control extracts more net power than other controls and has a higher efficiency. Here, efficiency is considered to be average net power divided by average extracted power. The average extracted power by real control is relatively small compared to other controls, because no reactive power is applied to optimize the motion. Hence, the required currents are small resulting in low electrical loss and high efficiency. For causal sub-optimal b, c control and causal sub-optimal m, b control, there is not a big difference in power production. The efficiency for these two control methods is lower than real control as some reactive power is needed.

There is no doubt that for causal sub-optimal m, b, c control under both force and amplitude constraints, the average extracted power is greater than other control methods. If the currents can be reduced, the net power output can be improved. When two linear generators are connected together, currents are shared by each generator which results in half of the total currents in each of the generators. It is well-known that electrical

loss is proportional to the square of currents as given in Equation 5.13. Hence, total electrical loss can be significantly curtailed. It can be seen from tables 5.4 to 5.8 that electrical loss by using two linear generators is rather less than using only one generator, but cost should be taken into account.

5.4.3 Performance Improvement

The above results show that the average power extracted by using causal sub-optimal m, b, c control under both force and amplitude constraints is much bigger than with other control methods. The reason net power production is smaller is due to large electrical losses. The required reactive force from the generator is always very large, and is likely to exceed the capability of a linear generator. Hence, such large reaction force has to be cut off by the force limit which makes the linear generator operate constantly at its full rating. This is an unstable state as the currents are always at the peak value producing a lot of heat. Therefore, performance improvement should aim to reduce electrical loss hence increase net power production and efficiency.

End-stop improvement

Net power production must be increased if the displacement is assumed to be large enough. In reality, an end-stop system must be installed to prevent unrealistic motion, as the WEC has to be at least partly submerged. If there is no end-stop system, oscillating displacement under causal sub-optimal m, b, c, c control can be very large from simulation results in Figure 4.15. This means the buoy moves out of the water, which is unrealistic. In the previous analysis, the end-stop system is set to be activated at 3.5 m and relative small end-stop damping and spring coefficients are used to decelerate the WEC. The buoy's draft is designed to be 1.88 times the radius and the height above the water when the floating buoy stays at the equilibrium position is the same as the draft. Hence, the maximum displacement is 4.136 m which indicates that there is 0.636 m deceleration distance. In the previous results, such long deceleration distance is necessary as only a small end-stop force is applied. When the floating buoy starts to decelerate

Power (kW)	m,b,c,c (1)	m,b,c,c (2)	b,c	m,b	b
Peak Instant	448.9	628.6	40.942	41.178	42.304
Average Extracted	23.7	24.06	8.673	8.701	8.572
Average Loss	12.6	7.23	0.152	0.151	0.147
Average Net	11.1	16.8	8.52	8.54	8.42
Efficiency	46.8	69.8	98.2	98.15	98.2

Table 5.9: Comparison of the power extracted by four reaction force control methods, with limited PTO force and amplitude, where the buoy's radius is 2.2 m, peak frequency of the energy spectrum is 0.214 Hz, the upper boundary is set at 4 m, the lower boundary is set at 7 m and simulation time is 400 s.

from 3.5 m, the power production in the following 0.636 m is affected by the slower velocity. In order to increase the power production, the end-stop activating point can be set slightly higher while the end-stop force should be set to be bigger to decelerate the buoy more rapidly. Moreover, the oscillating buoy can be fully submerged in the water. Hence, the bottom end-stop system can be set much lower to give the buoy enough distance to move in the water. If the upper boundary is set at 4 m and the lower boundary is set at 7 m, and a large end-stop damping is selected, Table 5.5 can be rewritten as Table 5.9.

After adjusting the end-stop activating point, the net power extracted by using causal sub-optimal m, b, c, c control is the highest among all reaction force control methods. Particularly, when two linear generators are applied, the net power production is significantly increased. Moreover, the efficiency is also increased marginally as shown in Table 5.9. Under the end-stop improvement, the buoy is decelerated rapidly in a small distance by the large end-stop force, which results in a huge acceleration, hence a huge PTO force which triggers force constraint together with amplitude constraint.

Combined control

Electrical losses can also be reduced by using a combined control method. For causal sub-optimal m, b, c, c control, the generator is always operating at the rated current as a big PTO force is required. This normally occurs when the wave excitation force is large. During these periods, motion of the WEC cannot be optimized due to the limited

Power (kW)	m,b,c,c (1)	m,b,c,c (2)	b,c	m,b	b
Peak Instant	402.650	427.688	40.942	41.178	42.304
Average Extracted	18.78	18.28	8.673	8.701	8.572
Average Loss	11.2	10.03	0.152	0.151	0.147
Average Net	7.58	7.42	8.52	8.54	8.42
Efficiency	40.36	40.6	98.2	98.15	98.2

Table 5.10: Comparison of the power extracted by four reaction force control methods, with limited PTO force and amplitude, where the buoy's radius is 2.2 m, peak frequency of the energy spectrum is 0.214 Hz, the threshold wave excitation force is 15 kN and simulation time is 400 s.

Power (kW)	m,b,c,c (1)	m,b,c,c (2)	b,c	m,b	b
Peak Instant	373.9	405.6	40.942	41.178	42.304
Average Extracted	21.2	20.99	8.673	8.701	8.572
Average Loss	13.76	9.55	0.152	0.151	0.147
Average Net	7.48	11.44	8.52	8.54	8.42
Efficiency	35.3	54.5	98.2	98.15	98.2

Table 5.11: Comparison of the power extracted by four reaction force control methods, with limited PTO force and amplitude, where the buoy's radius is 2.2 m, peak frequency of the energy spectrum is 0.214 Hz, the threshold wave excitation force is 25 kN and simulation time is 400 s.

available generator force; however, significant electrical loss is still created. Hence, it is considered that during large wave excitation force, real control can be used to replace the causal sub-optimal m, b, c, c control. To better compare the power production with the results shown in Table 5.5, the activating end-stop point is changed back to 3.5 m and the other parameters such as the buoy's dimensions and peak frequency are maintained to be the same. The threshold wave excitation force is selected to be 15 kN, 25 kN and 35 kN. This indicates that causal sub-optimal m, b, c, c control is selected when the wave excitation force is smaller than the selected threshold, otherwise real control is applied. From the results, it can be seen that power production is higher than with only single causal sub-optimal m, b, c, c control, but not by much.

Power (kW)	m,b,c,c (1)	m,b,c,c (2)	b,c	m,b	b
Peak Instant	382.9	395.9	40.942	41.178	42.304
Average Extracted	21.5	21.34	8.673	8.701	8.572
Average Loss	14.66	10.83	0.152	0.151	0.147
Average Net	6.85	10.52	8.52	8.54	8.42
Efficiency	31.9	49.3	98.2	98.15	98.2

Table 5.12: Comparison of the power extracted by four reaction force control methods, with limited PTO force and amplitude, where the buoy's radius is 2.2 m, peak frequency of the energy spectrum is 0.214 Hz, the threshold wave excitation force is 35 kN and simulation time is 400 s.

Power (kW)	m,b,c,c (1)	m,b,c,c (2)	b,c	m,b	b
Peak Instant	408.5	423.2	40.942	41.178	42.304
Average Extracted	22.4	22.8	8.673	8.701	8.572
Average Loss	12.85	7.98	0.152	0.151	0.147
Average Net	9.57	14.8	8.52	8.54	8.42
Efficiency	42.7	64.9	98.2	98.15	98.2

Table 5.13: Comparison of the power extracted by four reaction force control methods, with limited PTO force and amplitude, where the buoy's radius is 2.2 m, peak frequency of the energy spectrum is 0.214 Hz, and simulation time is 400 s. The PTO force is only damping when end-stop is activated.

Discontinuous control

In the previous simulation, a large PTO force exists constantly even when the WEC activates the end-stop. Power production is quite small during the time when the end-stop systems are activated, but with a large electrical loss. Therefore, to reduce electrical loss, the PTO force by using causal sub-optimal m, b, c, c control can be replaced by real control when the end-stop is activated. Table 5.13 shows that by reducing the electrical losses when the end-stop systems are activated, the net power production has been increased as well as the efficiency.

Control improvement

All three methods are introduced in order to improve the performance of causal sub-optimal m, b, c, c control. The end-stop improvement method forces the system to have a big end-stop force to decelerate the WEC quickly when the end-stops are activated. Hence, the oscillating displacement of m, b, c, c control is increased to amplify the power production. The other two methods aim to reduce the electrical loss by reducing the peak operating time. These three methods can be used together to increase power production.

- End-stop improvement: The activating point is set to be as close to the draft as possible, hence 4 m is selected.
- Combined control: The threshold wave excitation force is chosen to be 25 kN, such that m, b, c, c control is applied when the wave excitation force is smaller than 25 kN, otherwise, real control is applied.
- Discontinuous control: Real control is applied when the end-stop system is activated, otherwise, m, b, c, c control is applied.

Figure 5.10 shows the control procedures of the discussed control methods. The end-stop activating point is set to be 4 m, such that external end-stop force starts to act on the WEC when the displacement is over 4 m. Wave height is measured to calculate the wave excitation force. As the wave excitation force becomes greater than 25 kN, real control is applied, otherwise the end-stop system needs to be checked. If the end-stop is activated, real control is still applied, otherwise the causal sub-optimal m, b, c, c control is applied.

The buoy's radius is 2.2 m and the peak frequency is 0.214 Hz. Hence, the natural frequency of the floating buoy is the same as the waves' peak frequency. In the following results from Figure 5.11 to Figure 5.13, the left hand side results are for one linear generator and the right hand side results are for two linear generators connected together.

Figure 5.11 shows the results of velocity, acceleration and displacement of the floating buoy under causal sub-optimal m, b, c, c control with the control improvement. As

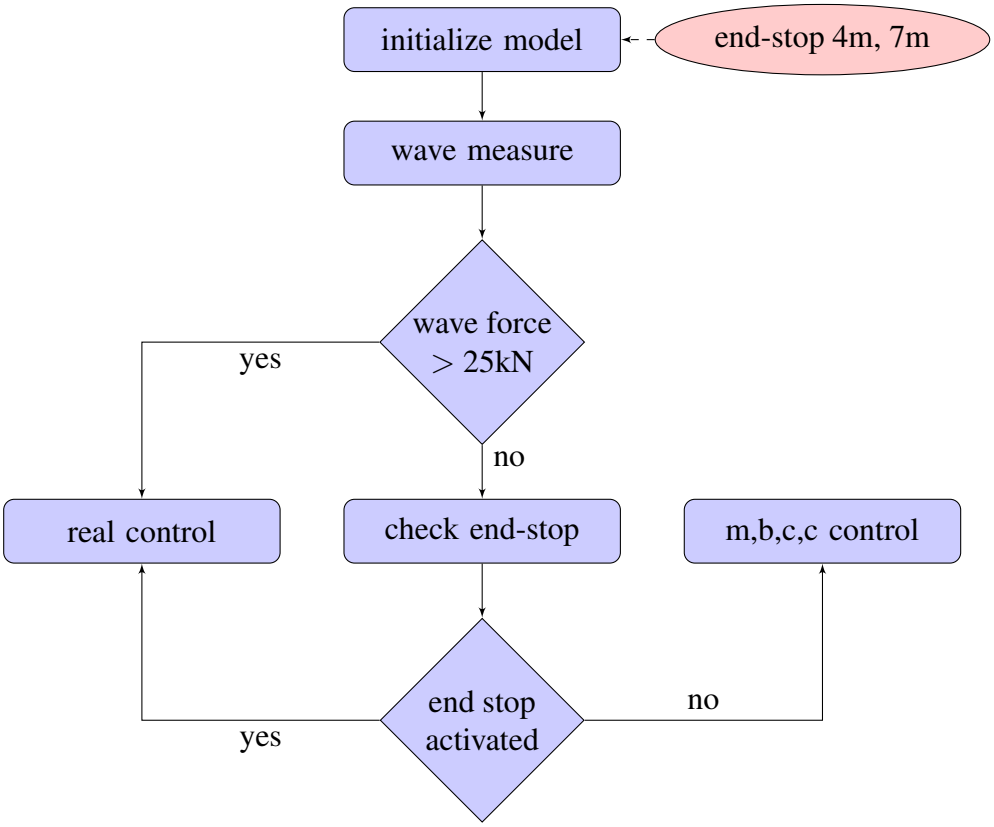

Figure 5.10: Control method flow chart to improve the power production

control is no longer sub-optimal, the velocity in Figure 5.11b is off-resonance with the wave excitation force. There are some short intervals where velocity is discontinuous due to the activated end-stop systems. The corresponding acceleration is shown in Figure 5.11c. Acceleration is extremely large when the end-stop system is activated. This is because the choice of the PTO spring and damping coefficient are large enough to decelerate the device very quickly. In Figure 5.11d, the buoy's upper displacement is successfully limited to around 4 m and the bottom displacement cannot reach the end-stop system. The results obtained by using one and two linear generators are very similar.

A ten second period from 350s to 360s is extracted from the results in Figure 5.11 to show the generated EMFs and currents. During this period, the end-stop has been activated several times which leads to a discontinuous velocity. Hence, the generated EMF, as shown in Figure 5.12b, is also discontinuous. The EMF drops rapidly as the

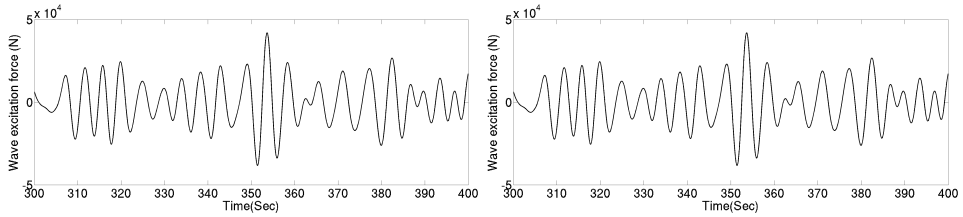

(a) Wave excitation force

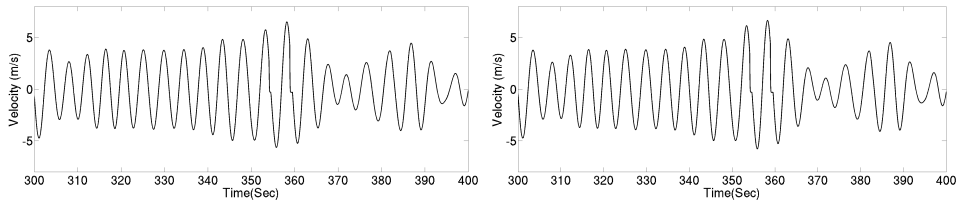

(b) Velocity

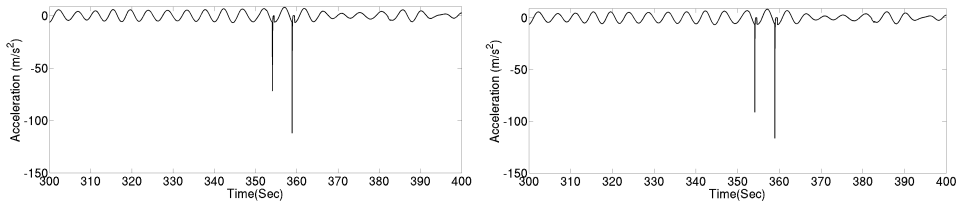

(c) Acceleration

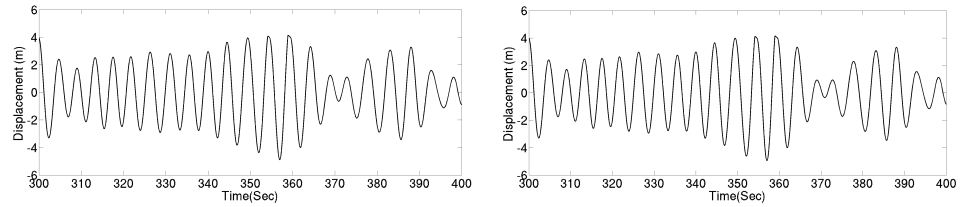

(d) Displacement

Figure 5.11: Control results under the improvement with one and two linear generators left graphs and right graphs respectively.

velocity decreases, and remains around zero when the end-stop system is operating. Figure 5.12c shows the current required to achieve control. It is clearly seen from the left figure, that amplitude of the current varies constantly: sometimes, the peak current is small and sometimes the peak current is very big which has then been cut off. This is because different control methods are switched in during different parts in this simulation. A smaller current indicates real control is applied and a large current indicates causal sub-optimal m, b, c, c control is applied. On the right hand side of Figure 5.12c, the current required cannot reach the cut off point as there are two linear

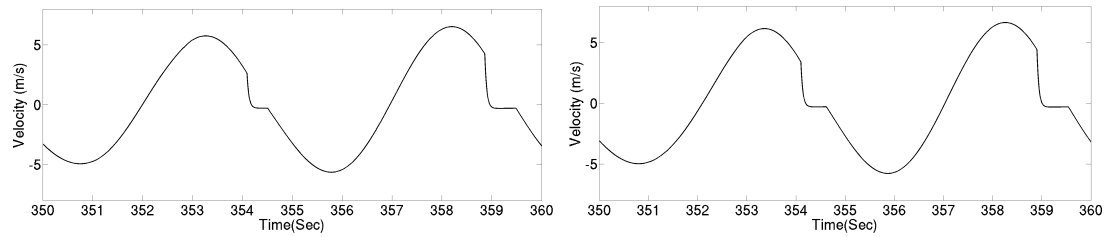

(a) Velocity

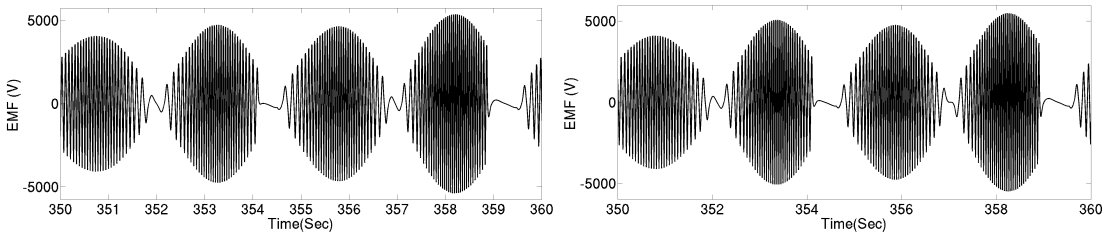

(b) Phase EMF

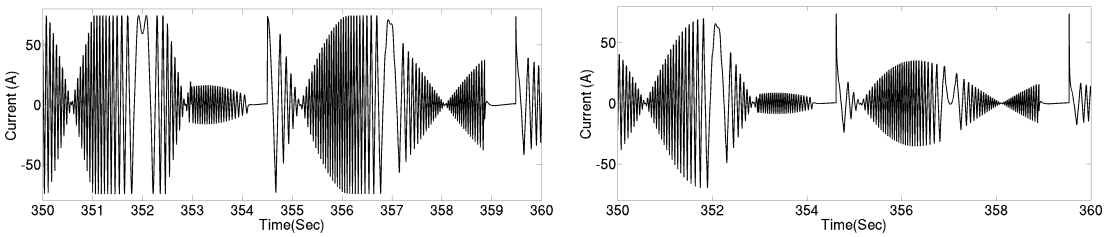

(c) Phase current

Figure 5.12: Control results under the control improvement with one and two linear generators left graphs and right graphs respectively.

generators, so the electrical losses are significantly curtailed.

Figure 5.13 shows the required PTO force and the power production. The control improvement aims to prevent the generator working always at its full rating. However, it is clearly shown that the generator is still working at the rated current for considerable periods producing a significant electrical loss. From Figure 5.13b, the instantaneous power is still very large compared to the average power extracted, which is inevitable because reactive power is still needed.

Table 5.14 shows the results of power production under causal sub-optimal m, b, c, c control with control improvement. In this table abbreviations are applied.

PF (Hz)	Radius (m)	NG	PI (kW)	AE (kW)	AL (kW)	AN (kW)	Efficiency
f_p=0.214	r=2	one	381.12	21.4	11.37	10.07	47.06
		two	513.7	22.34	6.47	15.87	71.4
	r=2.2	one	448.9	23.7	12.6	11.1	46.8
		two	628.64	24.06	7.23	16.83	69.95
	r=2.4	one	403.89	21.72	14.13	7.59	34.9
		two	572.14	22.28	8.78	13.51	60.64
f_p=0.225	r=2	one	374.5	19.06	8.88	10.16	53.31
		two	438.81	19.55	4.78	14.76	75.5
	r=2.2	one	446.56	19.94	9.78	10.17	51
		two	506.55	20.05	5.2	14.85	74.06
	r=2.4	one	357.12	17.63	11.44	6.19	35.11
		two	399.35	17.81	6.39	11.41	64.07
f_p=0.2	r=2	one	415.84	23.15	14.86	8.29	35.81
		two	784.15	25	9.7	15.3	61.2
	r=2.2	one	455.98	26.44	16.07	10.37	39.22
		two	827.23	27.91	11	16.91	60.59
	r=2.4	one	453	26.1	16.75	9.35	35.82
		two	814.32	27.56	12.61	14.96	54.28

Table 5.14: Simulation results by applying causal sub-optimal m, b, c, c control under control improvement (PF-Peak Frequency, NG-Number of Generators, PI-Peak Instantaneous Power, AE-Average Extracted Power, AL-Average Loss, AN-Average Net Power)

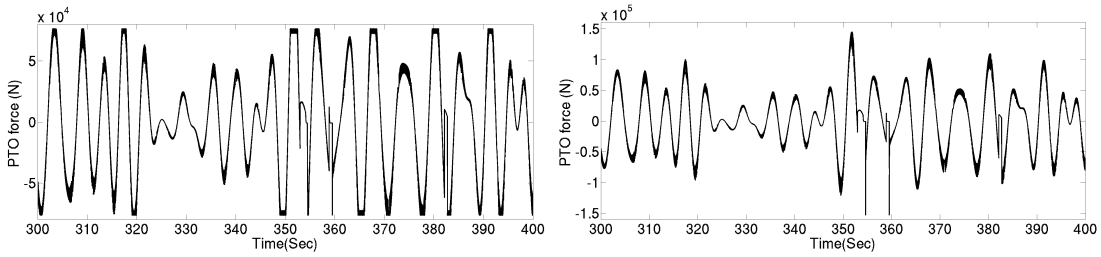

(a) PTO force

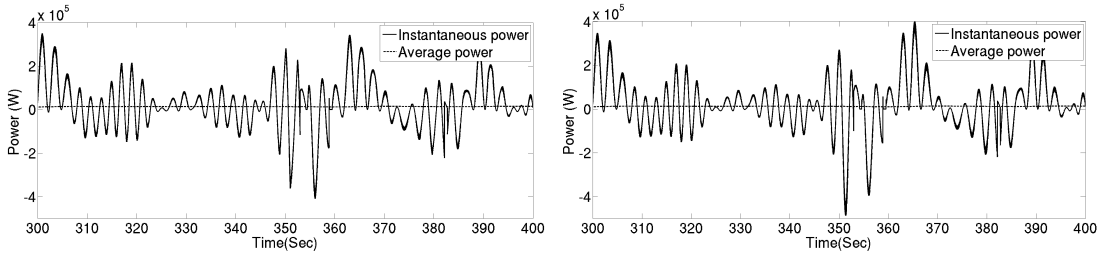

(b) Power

Figure 5.13: Control results under the improvement with one and two linear generators left graphs and right graphs respectively.

Compared with previous results, it can be seen that the average net power production under causal sub-optimal m, b, c, c control is more than with the other reaction force control methods, especially when two linear generators are used together. The most net power extracted, 16.91 kW, is when the peak frequency is 0.2 Hz, radius is 2.2 m and two linear generators are applied. However, this does not indicate that the discussed configuration of the WEC and the ocean waves is the optimum, because the wave energy spectrum of this peak frequency possesses more energy than other illustrated wave energy spectrum, so that more energy extraction is reasonable. The best efficiency occurs when the peak frequency is selected to be 0.225 Hz and net power extracted is still satisfactory. Hence, causal sub-optimal m, b, c control under practical conditions is suitable for small energy ocean waves.

5.5 Chapter Summary

This chapter describes the control of a direct drive linear generator to extract the maximum power possible under practical constraints from irregular waves, without any system for predicting the incoming waves. In this study, this was achieved by using reactive causal control to calculate the required PTO force provided by the linear generator. The machine used in this paper is the ACTM and is used to calculate the EMF voltage as well as the currents. However, if reactive causal control is applied, the PTO force required is much larger than the linear generator can provide. Hence, the PTO force needs to be limited. In addition to the force constraint, displacement amplitude is also limited by using an end-stop device. As the machine is always operating at the rated current, electrical loss is significant. The final section focuses on means to reduce electrical loss. Under several control improvements which include end-stop improvement and combined control methods, net power extraction is increased. However, the most effective means of reducing the electrical loss is to use two linear generators connected together to share the currents. It can be seen from the results that power extraction by using two generators is alway approximately double the net power production of other control methods.

Chapter 6

Control of Power Converters

6.1 Introduction

Most papers on power converters for renewable energy focus on the applications for wind energy due to its increasing output power production [91], [92]. A back-to-back power converter is the most common solution for a wide range of power output. Several solutions for the design of back-to-back power converter have been proposed depending on system requirements, such as the generator type. Research on power converter design and control for wave energy system is becoming more important with the growing maturity of wave power [93], [94].

In order to implement force control in this work, the linear generator is connected to a two level back-to-back power converter system, consisting of an active rectifier, an inverter and a common dc rail. The active rectifier (also called a regenerative rectifier) is a highly developed and mature technology with a wide industrial acceptance [95]. The dc rail can either exploit an inductance to produce the current source version or a high capacitance to produce the voltage source version. Both of them can be implemented in applications with a power range from a few kilowatts up to several megawatts. In previous work (especially for regular waves) [71], the active rectifier is used to control the phase currents to be in phase with the no-load phase voltage to achieve unity power factor and maximum power transfer from the linear generator to the grid. In this chapter, a voltage source PWM rectifier is used to set the appropriate reaction force on the buoy so that it moves in resonance with irregular waves, where the frequency and amplitude are continuously varying, to extract the maximum power

from the ocean waves. The most widely used modulation techniques are conventional carrier-based PWM and space vector modulation, both requiring a fixed value of modulation index. For the carrier-based modulation technique, a reference sinusoidal signal needs to be created, hence it is also called sinusoidal PWM (SPWM). However, in this application, irregular phase currents are required and need to be controlled, therefore the conventional PWM technique with a single modulation index is no longer applicable. Hence, two novel control methods based on the carrier-based PWM technique are presented here.

The first method introduced here is called the continuous varying average voltage method which is used to control the "instantaneous average" voltage to follow the reference voltage obtained by defining the duty ratio for each switching cycle. The other method is called the various modulation index method. This method requires the voltages at the mid-point of all three phase legs, which are calculated by using the EMFs and the voltage drops across the conducting lines. By using the traditional relationship between dc link voltage and the voltages at the mid-point of the three legs, a reference modulation index waveform is created. This waveform is compared with the triangular carriers to generate the control signals. These two PWM techniques degrade the system performance due to some uncertain parameters, hence feedback current control and a PI controller are employed to improve the performance.

6.2 Power Converter

In this work, a linear machine is used to convert the mechanical energy carried by ocean waves directly into electrical energy. Ocean waves force the WEC to move up and down to drive its directly coupled translator. The reciprocating movement of the translator has a low frequency due to the low frequency of the ocean waves. As there is no accumulator connected to the direct drive linear generator for short term energy storage, the electrical output is varying in both voltage and frequency depending on the magnitude and frequency of the incoming waves, when operating in real sea

conditions. Reaction force control is regarded as an effective way to control the WEC, which requires variable currents to provide the desired PTO force to achieve maximum power production. Therefore, power conditioning is required to achieve reaction force control, and to convert it into constant voltage and frequency that can be connected to the grid. An appropriate power converter is required to achieve the necessary power conditioning.

6.2.1 Rectification and Inversion

Rectification

For a direct drive linear generator, power conversion from a variable voltage and frequency to a fixed voltage and frequency for network connection can be achieved through rectification followed by inversion. A rectifier is the device to convert the ac power to dc. A diode bridge (or passive rectifier) as shown in Figure 6.1a, is widely used in wind power for a permanent magnet synchronous generator (PMSG) as no reactive power is needed in such a generator and active power flows uni-directionally from the PMSG to the grid via the power converter [92].

Apart from passive rectifiers, other rectifiers that can employ full control include the three phase, phase controlled bridge rectifier, as shown in Figure 6.1b, consisting of six thyristors (silicon controlled rectifier). This rectifier is able to control the current and hence the energy flow. However, these naturally commutated converters produce high harmonics and reactive power. In some applications, energy needs to flow in the reverse direction, for instance, in locomotives, cranes and the application discussed in this thesis. In all these applications, the rectifier has to play a role to deliver energy back to the power supply. One such rectifier is the active rectifier shown in Figure 6.1c. There are several types of controllable switches for the active rectifier, such as the insulated gate bipolar transistor (IGBT), the integrated gate-commutated thyristor (IGCT) and the gate turn-off thyristor (GTO). The six switches of this three phase active rectifier are controlled using the PWM technique. One vital requirement is to ensure that two switches in the same leg cannot be switched on together to prevent a

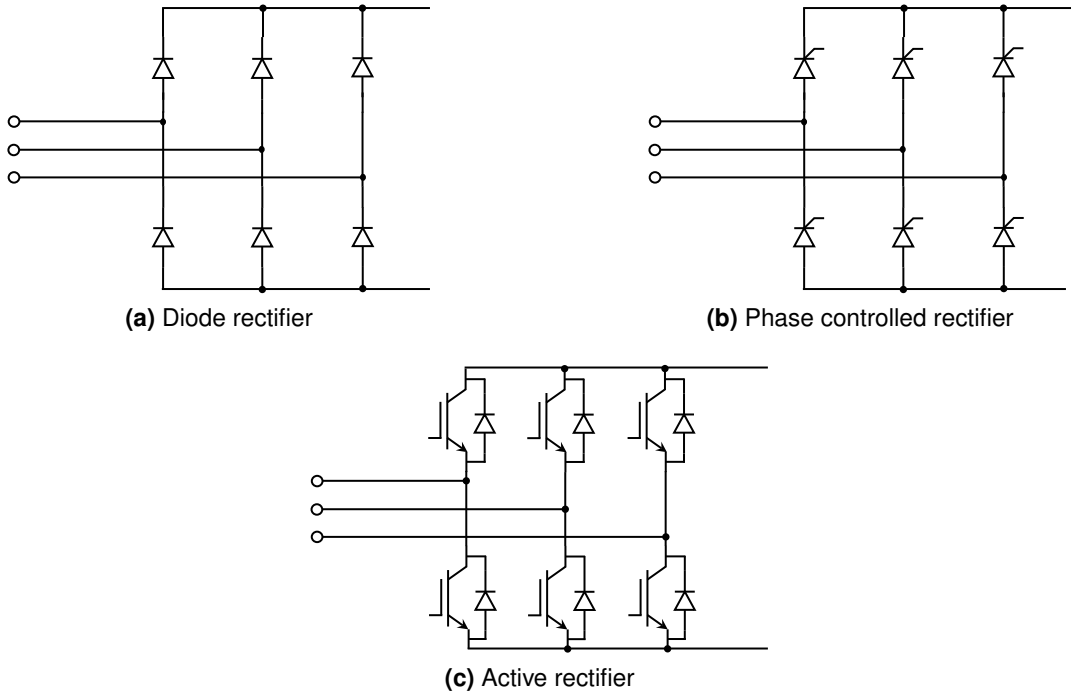

(a) Diode rectifier

(b) Phase controlled rectifier

(c) Active rectifier

Figure 6.1: Three phase electrical rectifiers.

short circuit. Simulink provides a built-in PWM generator for such an active rectifier for both carrier based PWM control and space vector PWM control.

6.2.2 Inversion

The inversion process converts the dc output (after the rectification) into an ac output with a controlled frequency and amplitude that can be connected to the grid or to supply three phase electrical machines. Recently, fast development of wind energy has led to the demand for high power converter topologies, and converters up to 5 MW have been proposed for permanent magnet generators [96]. Normal two-level power converters can only be used to deal with low voltage designs limited by the device rating, with a 1700 V IGBTs required to handle 690 V ac voltages. Multi-level modular power converter can be used in higher voltage rating applications [97].

There are two types of inverters: the voltage source inverter (VSI) and the current source inverter (CSI). The VSI, as shown in Figure 6.2b can be used together with an active rectifier or passive rectifier and a dc capacitor to form a back-to-back power

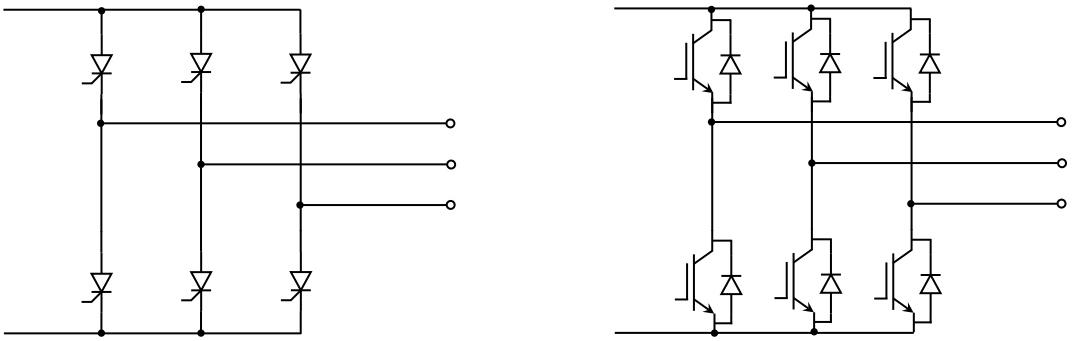

(a) Current source inverter **(b)** Voltage source inverter

Figure 6.2: Three phase electrical inverters.

converter where the VSI maintains the dc link voltage to be constant and controls the output voltage. In modern technologies, most of the high power converters are VSI. Compared with VSI configuration, the PWM CSI, as shown in Figure 6.2a, provides a simple topology solution and excellent performance of grid integration [22]. The CSI can be used together with a phase controlled bridge rectifier or a passive rectifier with a inductor in the dc link.

6.2.3 Back-to-Back Converter

In Section 6.2.2, two types of power converters, based on either the voltage source converter or the current source converter are introduced. In this work, the back-to-back power converter system consists of a voltage source active rectifier and a VSI connected by a common dc link, as shown in Figure 6.3. Such a configuration is able to deliver the required power to the grid and to control the generator three phase currents, hence the PTO force. In this thesis, IGBTs are used for constructing the back-to-back converter. In this configuration, the rectifier is used to control the generator line currents, the dc link capacitor is used for short term energy storage, and the inverter is used to maintain the voltage across the capacitor to be constant.

An important feature of the back-to-back converter is its rapid response. Appropriate control algorithms for both the rectifier and the inverter can be generated by using PWM, and are used to switch the IGBTs to achieve the desired voltages and currents.

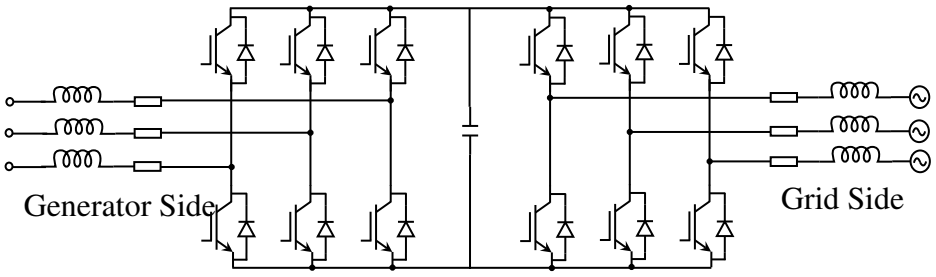

Figure 6.3: A back-to-back converter used for wave power.

6.3 Rectifier Control

6.3.1 Simulation Model

The complete system, as shown in Figure 6.4, includes the mechanical interface and the power electronics. Hydrodynamic coefficients are stored in look-up tables in the top left block, and hydrodynamic parameters such as added mass, added damping, spring stiffness and impulse response are calculated based on information provided previously, where the required draft of the buoy is 1.88 times the buoy's radius. These hydrodynamic parameters are used in the mass-spring-damper system to determine the actual acceleration, velocity and displacement, which are then imported into the PTO calculation block to generate the ideal PTO force based on causal sub-optimal control methods. The required PTO force is then provided to the linear generator block which determines the required currents in each coil. The correct total current for the given number of active machine poles is then supplied to the control system. In this case thirty-eight poles are used, with all active machine coils in a phase connected in parallel. Along with the calculated required currents, the EMFs are also generated. The electrical parameters such as resistance and inductance for both the linear generator and the conducting lines are also included. The calculated required currents are then achieved through control of the active rectifier. The control signals are generated in a subsystem according to the measured line voltages and required currents, and are fed to the rectifier. Here, the primary focus is on current control and therefore, for convenience, the dc link capacitor and inverter are replaced by a battery in the simulation model.

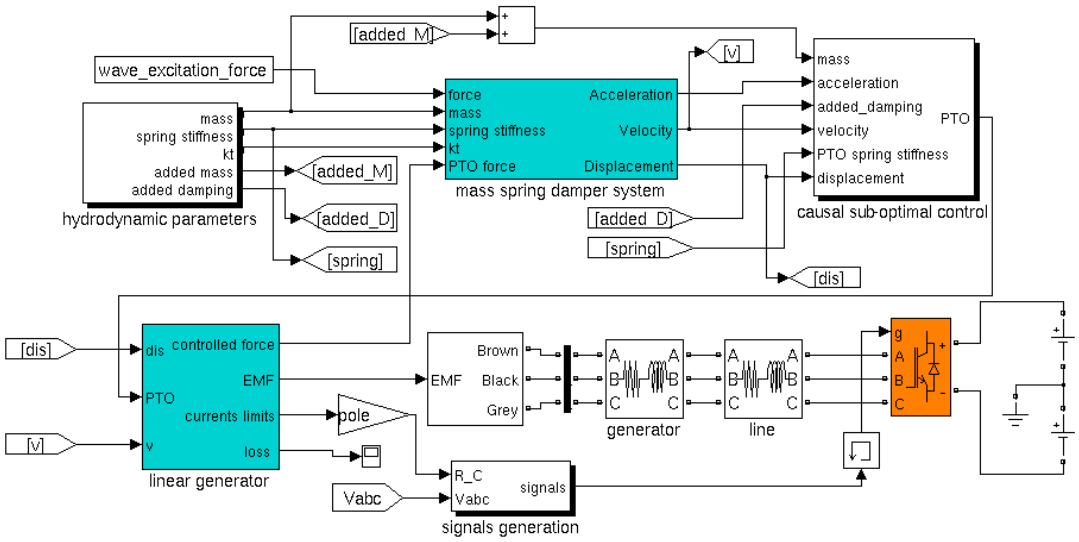

Figure 6.4: Simulation model of the entire system.

6.3.2 Continuous Varying Average Voltage Method

The generator side converter is an active rectifier with an appropriate control algorithm. PWM control methods have been extensively studied during the past few decades. Carrier-based PWM and space vector PWM are two important methods for computing the duty ratio of the switches. However, both these methods have to determine the modulation index and phase shift. For carried based PWM control, these parameters are used to form a pre-established reference which is compared with the triangular carrier to calculate the switching information for the IGBT gates. This reference is either a sinusoidal voltage or a sinusoidal current waveform. Details of carrier-based PWM and space-vector PWM can be found in [72].

With irregular waves, the variation of amplitude and frequency implies that it is impossible to have a fixed modulation index and phase shift. Hence, a short-term current control method has to be used. Through knowledge of the linear generator coil EMFs, the required currents, and the electrical parameters such as the resistance and inductance for both the linear generator and the conducting line and the voltage drop between the linear generator and the power converter can be obtained. The required voltages at the midpoint of each leg, $v_i'(t)(i = a,b,c)$, can then be calculated using

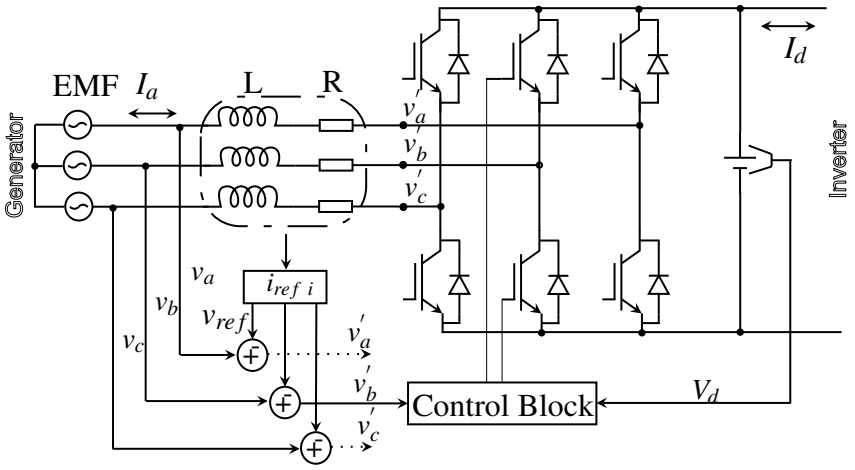

Figure 6.5: Active rectifier control concept for following the required currents.

Equation 6.1, where $v_i(t)(i = a,b,c)$ is the generator EMF, L_g is the inductance of the linear generator, R_g is the resistance of the linear generator, L_l is the inductance of the conducting line, and R_l is the resistance of the conducting line. Hence, the whole control procedure and control signals generation are shown in Figure 6.5.

$$v'_i(t) = v_i(t) - (L_g + L_l)\frac{\mathrm{d}i_{ref\ i}(t)}{\mathrm{d}t} - (R_g + R_l)i_{ref\ i}(t) \tag{6.1}$$

$$R = R_g + R_l \tag{6.2}$$

$$L = L_g + L_l \tag{6.3}$$

The generator no load EMF voltages can be measured directly. Line inductance and resistance must be known in advance in order to calculate the voltages drop V_{ref} across them. Hence, the desired voltages at the midpoints of all three legs are obtained and fed into the control algorithm. In addition, the dc link voltage is measured and compared with the required voltages of the midpoints to generate the required control signals.

As stated at the beginning of this section, conventional PWM methods do not work in this situation. In order to control random currents, the IGBT duty ratio can be determined by a novel continuously varying average voltage method. Figure 6.6a shows

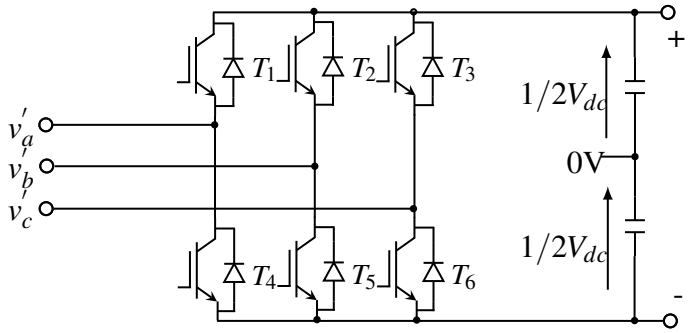

(a) Currents control rectifier

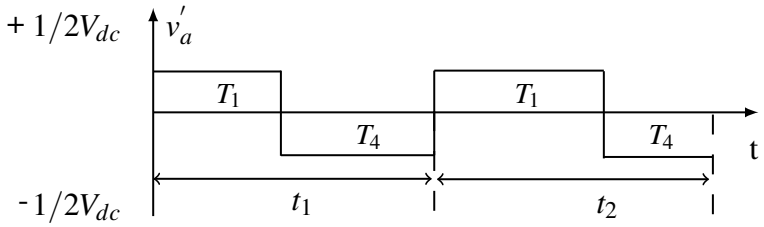

(b) Phase average voltage, v'_a during t_1 and t_2 switching cycles

Figure 6.6: Control of three phase electrical rectifiers.

the three phase rectifier used to control the currents, and Figure 6.6b shows the phase average voltage which can be calculated from the duty ratio and the dc link voltage.

In Figure 6.6a, a single dc link capacitor is represented by two capacitors of equal value for ease of understanding. The mid-point is connected to ground such that the average across each of these capacitors to be $V_{dc}/2$. Figure 6.6b shows the average phase voltage v'_a, which is controlled by the switch duty ratio. If switch T_1 is chosen as the example, the relationship between the voltage at the mid-point of the leg and the dc link voltage is expressed in Equation 6.4.

$$v'_a = \frac{1}{2}V_{dc} \cdot D_1 + (-\frac{1}{2})V_{dc} \cdot (1 - D_1) \tag{6.4}$$

Hence, the duty ratios for switches T_1, T_2 and T_3 are given in Equation 6.5, 6.6 and 6.7.

$$D_1 = \frac{v'_a}{V_{dc}} + 0.5 \tag{6.5}$$

$$D_2 = \frac{v_b^{'}}{V_{dc}} + 0.5 \tag{6.6}$$

$$D_3 = \frac{v_c^{'}}{V_{dc}} + 0.5 \tag{6.7}$$

Here, $v_a^{'}$, $v_b^{'}$ and $v_c^{'}$ represent the voltage at the mid-points of each leg, and D_1, D_2 and D_3 represent the required duty ratios of switches T_1, T_2 and T_3 respectively. The other switches, T_4, T_5 and T_6 should always be in the opposite states of T_1, T_2 and T_3 respectively.

Figure 6.7 shows the simulation model to generate the control signals under the continuous varying average voltage method. Ideal currents are calculated and input into this subsystem. The resistance and inductance of both the generator and the conducting lines are known so the voltage drop can be calculated. As all the poles in the generator are connected in parallel, the total resistance and inductance is calculated by using the single pole resistance and inductance divided by the number of poles. The EMFs are measured and also imported into this subsystem to calculate the required voltages at the mid-point of all three legs. By giving the dc link voltage, the required duty ratios can be calculated. All the above calculations in the simulation are based on the system sample time "T_f", which is also the switching period. The duty ratio of each switch can then be determined. However, even though the duty ratio has been decided, the system still does not know precisely when to switch on and when to switch off, hence, another sample time "T_s", which is much smaller than T_f, has to be selected to decide the switching time in a T_f cycle. In this application, T_f is selected to be 0.4 ms and hence the sampling frequency is 2.5 kHz. The explanation of these two sample times is shown in Figure 6.8.

From these results shown in Figure 6.9, it is clear that the controlled current follows the required current. However, the simulation process is very slow due to the very small value of T_s. Therefore, an improved method is discussed in Section 6.3.3.

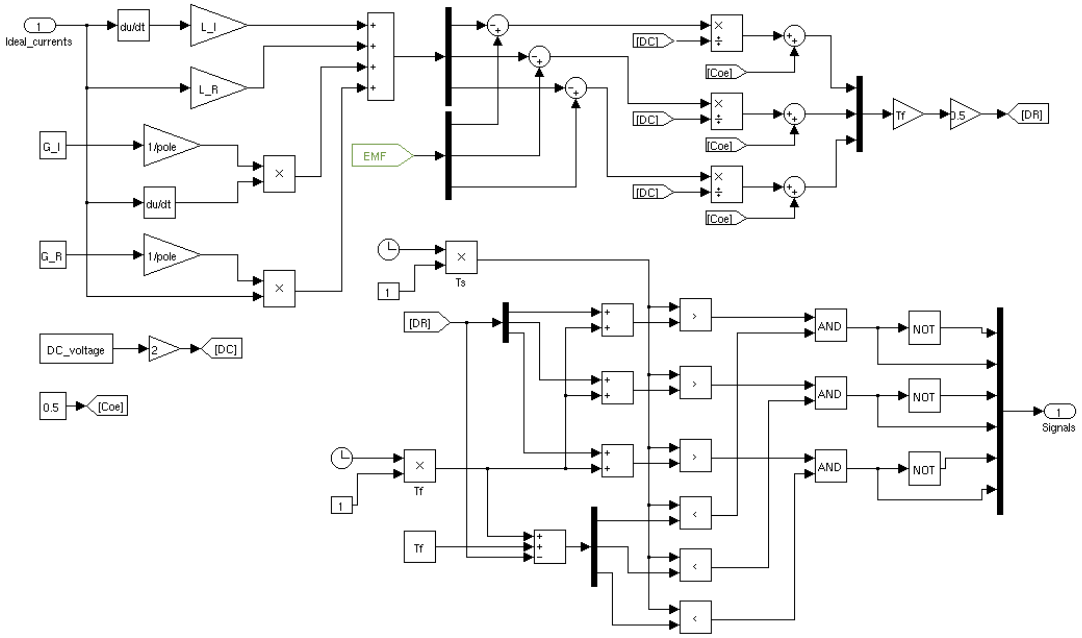

Figure 6.7: Simulation model of the generation of the control signals by the continuous varying average voltage method.

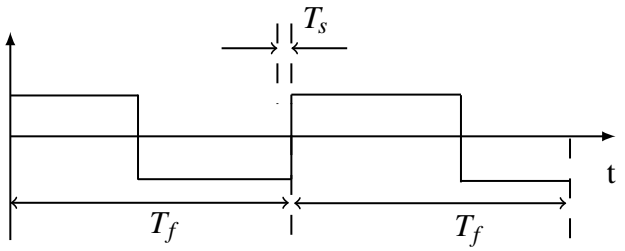

Figure 6.8: Explanation of two selected sample times in continuous varying average voltage method.

6.3.3 Various Modulation Index Method

The existing PWM control algorithms are only suitable for regular sinusoidal waves where a sinusoidal voltage (or current) reference is created and compared with a high frequency triangular carrier to generate the control signals. As the peak value of the triangular waveform is set at unity, the amplitude of the reference sinusoidal waveform is the modulation index m. In this thesis, the currents required to set the desired PTO force are irregular, where both amplitude and frequency vary with time. The comparison between a single sinusoidal reference and the carrier is not suitable for achieving

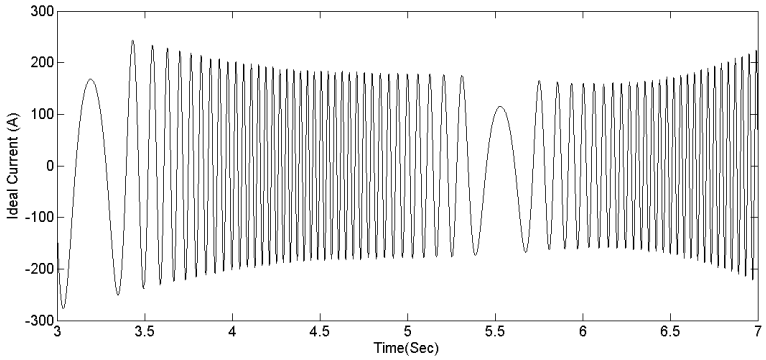

(a) Ideal phase current

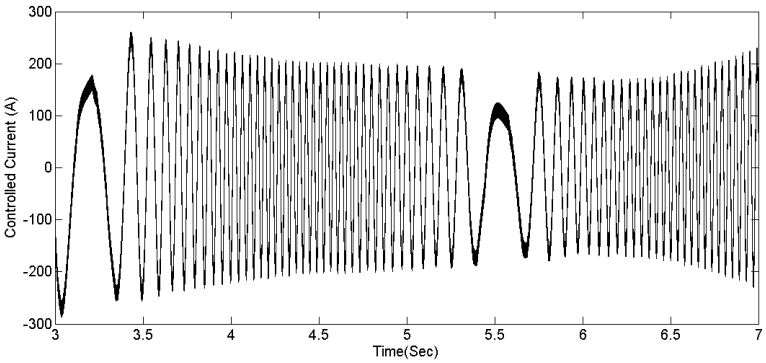

(b) Controlled phase current

Figure 6.9: Simulation results of ideal and controlled phase current under continuous varying average voltage method.

random current control. Instead, a variable modulation index reference is created to generate the control signals. The well-known equation relating the peak ac voltage for a three phase inverter, the dc voltage and the modulation index is given in Equation 6.8. $\hat{\mathbf{v}}_i$ is the peak value of the sinusoidal voltage, and the modulation index m is given in Equation 6.9, where $\hat{\mathbf{v}}_{ref}$ is the peak value of the reference signal, and $\hat{\mathbf{v}}_{car}$ is the peak value of the triangular carrier signals. Figure 6.10 shows the traditional PWM theory.

$$\hat{\mathbf{v}}_i = m \cdot \frac{V_{dc}}{2} \ (i = a,b,c) \tag{6.8}$$

$$m = \frac{\hat{\mathbf{v}}_{ref}}{\hat{\mathbf{v}}_{car}} \tag{6.9}$$

In this thesis, the required voltages at the midpoint of each leg, referred to as $v_i^{'}$, are

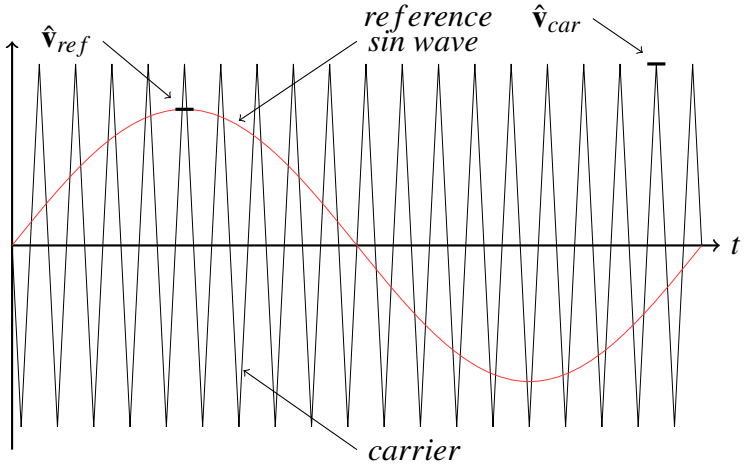

Figure 6.10: Explanation of carrier based PWM control and the modulation index.

irregular so the frequency and amplitude are constantly changing. Thus a new method has to be introduced instead of using Equation 6.8 and Equation 6.9.

Figure 6.11, shows an irregular voltage waveform at the midpoint of one of the legs. Two example points a and b at times t_1 and t_2 on the irregular waveform are selected where their vertical coordinates are the voltages required. If the traditional PWM control algorithm is applied to achieve the desired results, point a and b must be the peak points of the desired voltage waveforms. Therefore, two different sinusoidal waveforms can be selected which pass through points a and b at their peak values, as shown by the red and blue lines in Figure 6.11. Hence, the traditional PWM control method can be rewritten as in Equations 6.10, 6.11 and 6.12.

$$m_1 = v_{t1} \cdot \frac{2}{V_{dc}} (i = a,b,c) \tag{6.10}$$

$$m_2 = v_{t2} \cdot \frac{2}{V_{dc}} (i = a,b,c) \tag{6.11}$$

$$m_n = v_{tn} \cdot \frac{2}{V_{dc}} (i = a,b,c) \tag{6.12}$$

For any time t_n there will be a sinusoidal waveform corresponding to the instantaneous value of the irregular waveform, with a peak value of the same amplitude occurring at the same time. There is, therefore, also a corresponding modulation index to form a

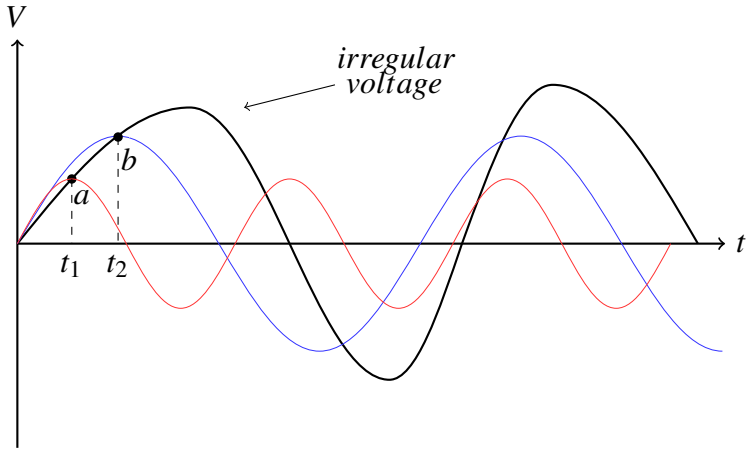

Figure 6.11: Explanation of how each point on a irregular voltage waveform can be expressed by the peak value of a regular wave.

reference sinusoidal wave to obtain the required voltage at the specific time. The dc link voltage is a constant, which results in the calculated modulation indices (m_1,m_2.....m_n) having the same shapes as the sinusoidal waveforms (v_{t1},v_{t2}.....v_{tn}). The modulation index should be between zero and one, with the peak of the carrier being defined as unity. Hence, the reference sinusoidal waveforms can be obtained using Equations 6.13, 6.14 and 6.15.

$$v_{ref1}(t) = m_1 sin(\omega_1 t) \tag{6.13}$$

$$v_{ref2}(t) = m_2 sin(\omega_2 t) \tag{6.14}$$

$$v_{refn}(t) = m_n sin(\omega_n t) \tag{6.15}$$

Figure 6.12 illustrates how the PWM signals can be generated by applying different modulation indices. From the above analysis, for each given voltage on the voltage waveform as shown in Figure 6.11, such as v_{t1} or v_{t2}, there should be a corresponding reference sinusoidal waveform to compare with the triangular carrier at the specific time, such as t_1 or t_2, to obtain the control signals. Generally, each reference sinusoidal waveform defines only one point on the waveform and another reference voltage waveform has to be chosen to determine the next required voltage. Therefore, to obtain a required voltage waveform such as that shown in Figure 6.11, a number of reference sinusoidal waveforms are required. However, it is not necessary to generate a large

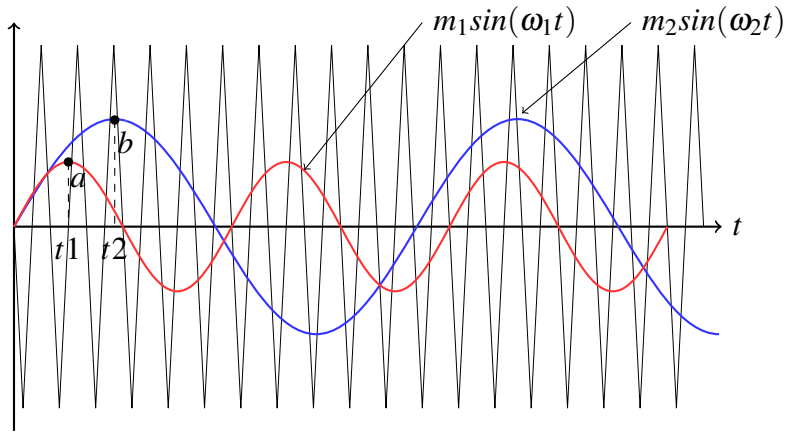

Figure 6.12: Explanation of variable modulation indices control.

number of reference waveforms. As shown in Figure 6.12, only the points at the peak values of the reference waveforms are used to calculate the required voltages. If the peak of the triangular carrier is unity, those points can be regarded as the modulation indices of different reference sinusoidal waveforms, and the control signals are generated by the comparison between the variable modulation indices and the carrier signals. These modulation indices are a function of time which can be expressed in Equation 6.16, where $v_i^{'}(t)$ is the instantaneous required voltage rather than the peak voltage.

$$m(t) = 2 \cdot \frac{v_i^{'}}{V_{dc}} (i = a, b, c) \tag{6.16}$$

The required voltages at the midpoint of each leg, $v_i'(t)(i = a, b, c)$ as shown in Figure 6.6a, can then be calculated using Equation 6.1 and the control signals generation is shown in Figure 6.13.

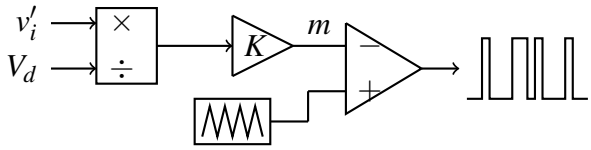

Figure 6.13: Control algorithm of various modulation index method

The simulation model of the control algorithm using the various modulation index method is shown in Figure 6.14. The first part for calculating the voltages at the mid-

point of all three legs is the same as the continuous varying average voltage method. After obtaining these voltages, the variable modulation indices are then calculated to be the reference waveform. This waveform is then input into the PWM signal generator to achieve the control signals.

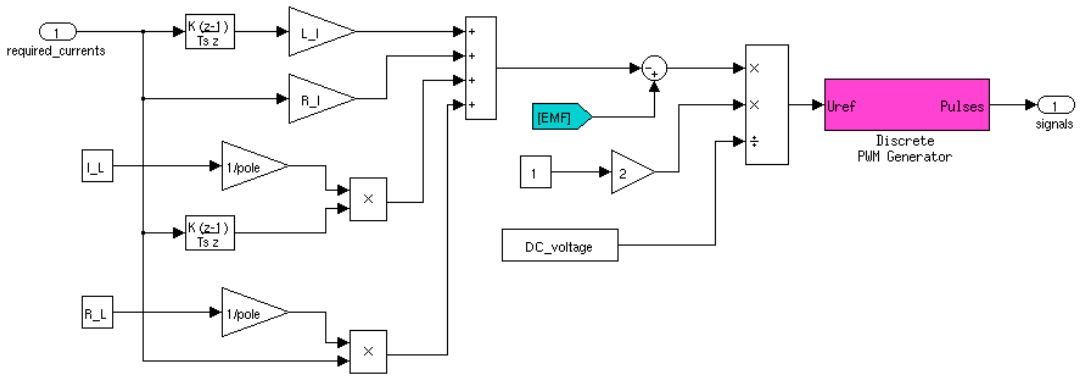

Figure 6.14: Simulation model of the signals generation by various modulation index method.

Figure 6.15 shows the power converter control results based on the variable modulation index method. It can be seen from Figure 6.15b that current control has a good performance during high frequency periods but a bad performance during low frequency periods. Low frequency currents are required when the generator's EMFs are small; therefore the required voltages at the mid-point of each leg are small compared to the dc link voltage which lead to small modulation indices (almost zero) as shown in Figure 6.15c. Hence, the sensitivity of the whole system is reduced to react to small changes. As the current cannot be controlled during low frequency periods, the required PTO force cannot be obtained during such periods as shown in Figure 6.15a.

6.3.4 Control Implementation and Improvement

For the current control applications in Section 6.3.2 and Section 6.3.3, the control method can be shifted from controlling currents directly to controlling the voltages, hence called voltage mode control [95, 98]. Therefore, in this particular situation, an active voltage-source rectifier is applied to implement reaction force control of a

direct drive linear generator to extract maximum power from irregular waves. The operation of the voltage source rectifier requires a constant dc voltage source, which is maintained by the grid inverter. By measuring the EMFs from the linear generator, the control voltages can be obtained from the required line currents, the line impedance and the impedance of the filters. These voltages can, therefore, be controlled by the straightforward relationship between line voltage and dc link voltage. The varying required voltages lead to varying modulation indices, and hence, degrade the system performance, which employs current feedback and PI regulator to improve performance. Traditional PI controllers are used to control the active and reactive power [22, 99]. However, in this section, it only acts as a current regulator as a large reactive power is needed to achieve reaction force control, and hence inevitably results in a low power factor.

The active rectifier feedback control to achieve sub-optimal reaction force control is shown in Figure 6.16. The main function of this control scheme is to control the generator three-phase currents to provide the required PTO force. The building of the control system starts by creating a reference model using the dynamic response of the mechanical system. When ocean waves meet the WEC and apply a wave excitation force on the mechanical interface, dynamic parameters such as acceleration, velocity and displacement can be sensed and are the inputs to the control system. Velocity and displacement can be easily obtained by installing sensors, and the acceleration can be calculated via the recorded history of the past values of the velocity. From the sensed values, the desired PTO force can be calculated. This PTO force is directly provided by the linear generator and hence the required three-phase currents can be obtained through knowledge of the linear generator. In this process, the resistance change due to increased temperature is ignored.

The modulation index waveform is the reference which is compared with the triangular carriers. This waveform is not sinusoidal, but the SPWM technique is still applicable to generate the gating signals. If the system is operating always in the assumed ideal condition, the currents can be controlled to the required value as expected with no

Table 6.1: System parameters for the simulations.

Mechanical		Electrical	
Peak frequency	0.214Hz	dc link voltage	10kV
Buoy radius	2.2m	Line and generator resistance	6.36Ω
Buoy height	8.272m	Line and generator inductance	0.1534H
Submerged height	4.136m	Number of poles	38
Mass	64.4×10^3kg	Switching frequency	2.5kHz

steady state error. However, in reality, some conditions change as the system operates, such as machine temperature, so the control system cannot perform as desired. A feedback control loop is necessary to maintain regulation by providing some type of compensation. In this application, actual phase currents are measured to compare with the reference currents. A current difference is generated and delivered to the PI controller. Voltage control through adjusting the modulation index can be used to compensate for the current error. It should be noted that the voltages increase as the modulation index is increased.

Major system parameters are listed in Table 6.1. By providing the appropriate PTO force (calculated under desired sub-optimal control) for the oscillating system, the WEC moves almost in phase with the wave excitation force, as shown in Figure 6.18, so the theoretical maximum power extraction without performing wave prediction is almost achieved.

Figure 6.19 shows the linear generator phase induced EMF and required phase current for achieving the desired PTO force. For reaction force control, both real force (damping force) which contributes real power generation and reactive force (spring force and inertia force) which contribute reactive power generation are needed. Reactive power (mechanical) is used to control the motion of the buoy and the instantaneous power may be much larger than the average power. In Figure 6.19, the induced EMF and required phase current are exactly in phase before 2.5 seconds, and 180 degrees out of phase for the next period. Hence, it can be seen that power flows from the generator to the grid and later from the grid to the generator, and changes every period, which implies the linear machine acts as both a generator and a motor during the reaction

force control process.

As the required force to achieve this level of control is excessive, the same form of control has also been attempted but with the force limited as discussed in Section 5.3.1. When the generator force is constrained, the motion of the WEC and the wave excitation force are no longer kept in resonance. Figure 6.20 shows the required current comparison of the system with no force constraint and under force constraint.

Figures 6.21 and 6.22 show the power converter control results based on the control theory developed in Figures 6.16 and Figure 6.17. A feedback current loop and PI regulator are included in the system to increase the accuracy of the whole system. It can be seen that the phase current is successfully controlled to follow the required current in Figure 6.21b to give the desired PTO force as shown in Figure 6.21a. As modulation indices are calculated in advance and are tuned based on these calculated values as shown in Figure 6.21c, the system response is significantly improved for high frequency periods. In Figure 6.22, the system is tested to control the required phase current when the generator force is constrained.

It can be observed from Figure 6.21c that the modulation indices are negative some of the time. This is very different from the traditional PWM control where the modulation index can only run between 0 and 1. In this control method, each point on the waveform of modulation indices in Figure 6.21c represents only a single point on the generated reference sinusoidal waveform as introduced in Figure 6.11 and Figure 6.12.

6.4 Chapter Summary

This chapter introduced the control of a back-to-back power converter to provide the required PTO force to control the WEC. As the WEC is operating in irregular waves, the required currents are irregular. Hence, traditional PWM control algorithm is no longer suitable in this case. Two novel control methods, continuously varying average voltage control and various modulation index control, are introduced in this chapter. The simulation results show that reaction force can be controlled to follow the required

PTO force by both these two methods. However, by using the continuously varying average voltage method, the sample time has to be kept very short which results in a long calculation time. Although voltages at the mid-points of all of the three legs are controlled to provide the required currents, the minimum dc link voltage in this simulation is 10 kV, therefore it is likely that multi-level converters would be used.

The system performance is degraded because variable voltages in both amplitude and frequency are required. A feedback current loop and PI controller are included to provide a much better performance and faster response.

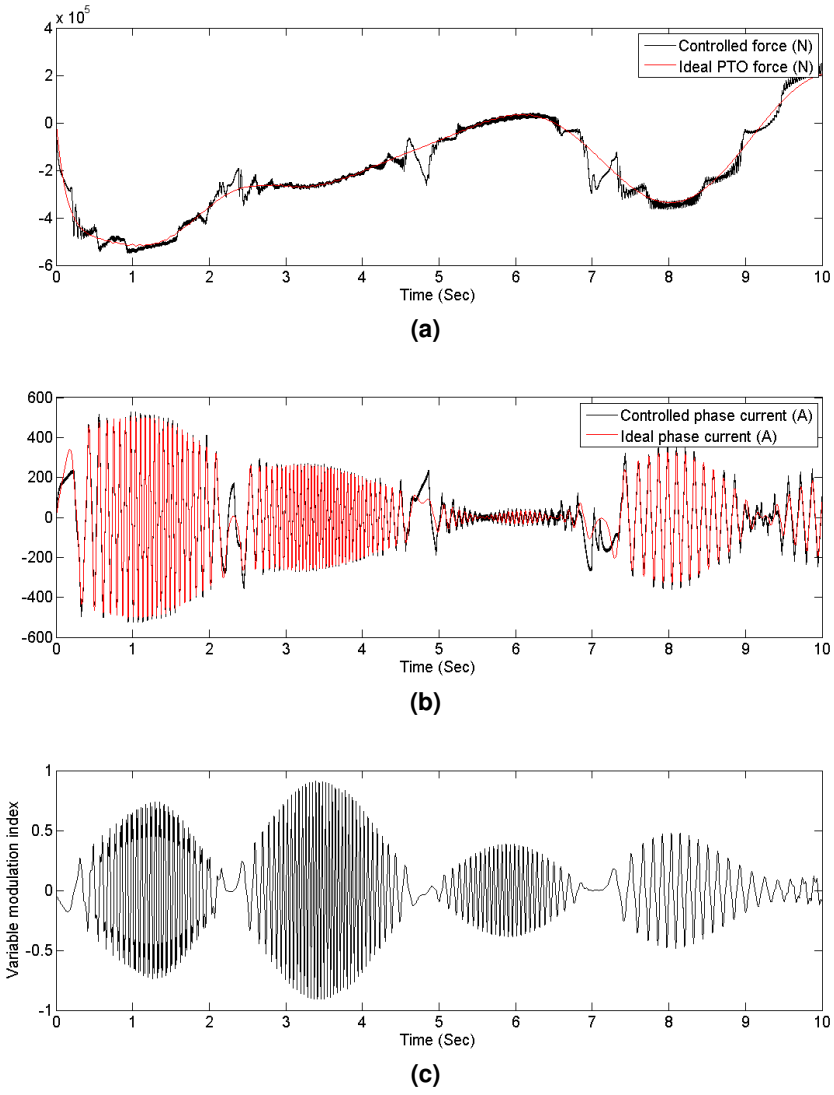

Figure 6.15: a) Comparison between controlled force and desired force. b) Comparison between controlled current and reference current. c) Modulation indices to control the phase current.

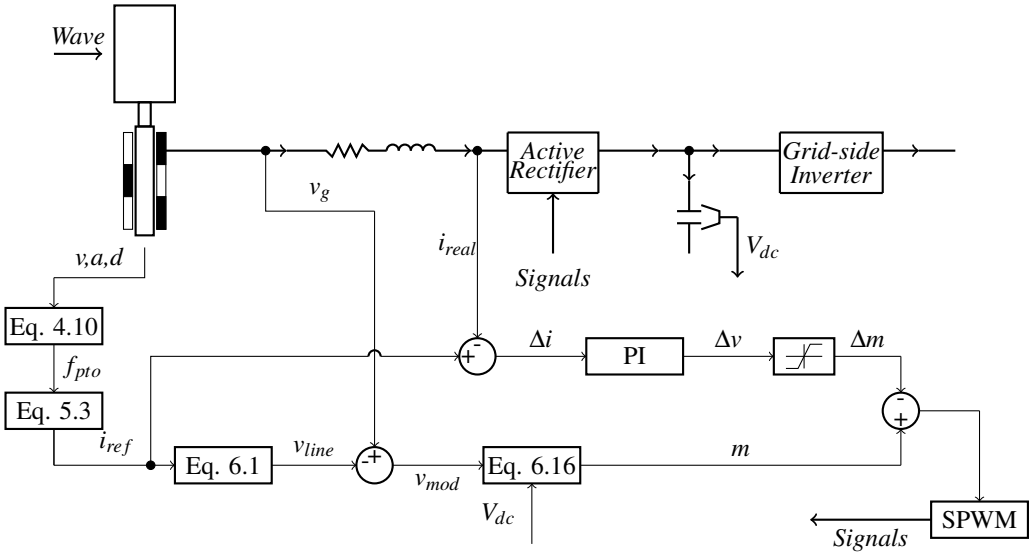

Figure 6.16: Block diagram of active rectifier feedback control scheme implementation.

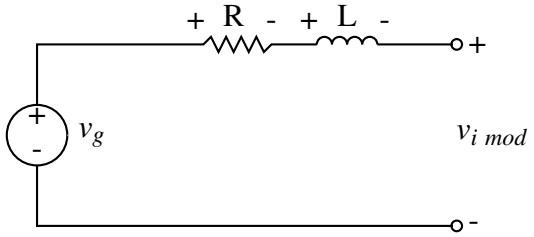

Figure 6.17: Equivalent circuit of the linear generator.

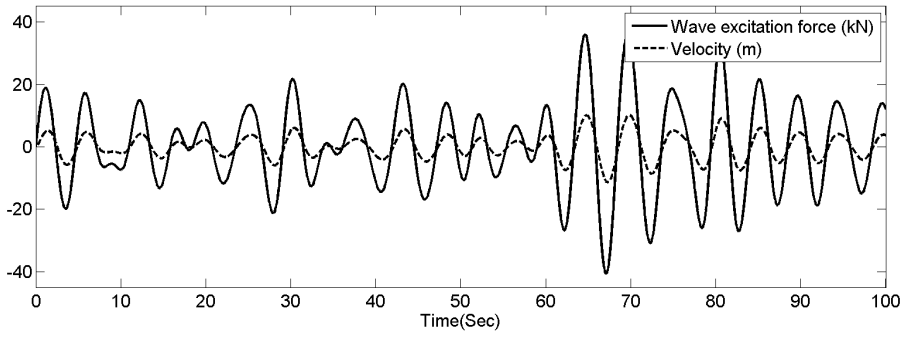

Figure 6.18: Relationship between velocity of the WEC and the incoming wave excitation force.

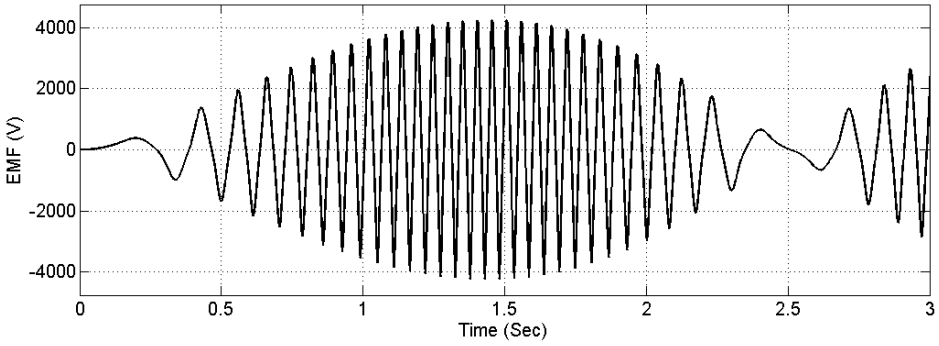

(a)

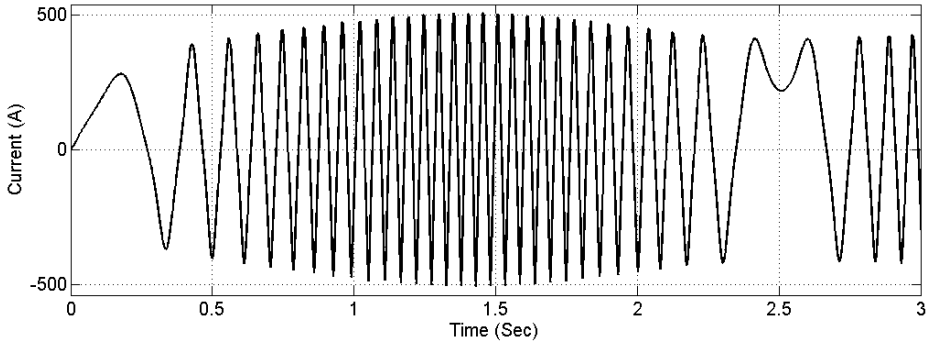

(b)

Figure 6.19: a) Phase induced EMF voltage under sub-optimal control. b) Required phase current under sub-optimal control.

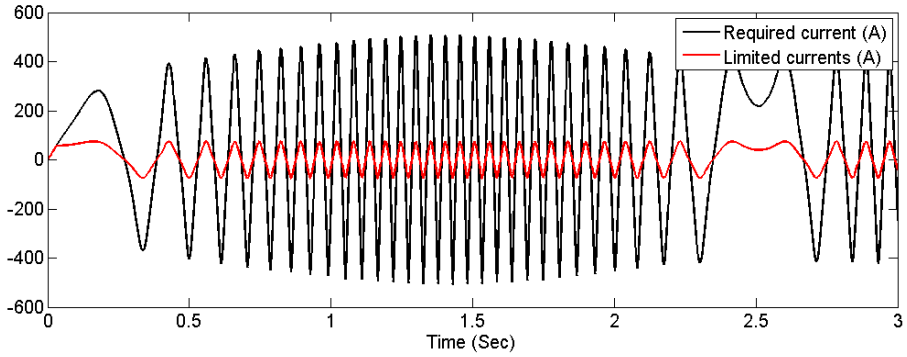

Figure 6.20: The required phase current to achieve reaction force control and actual current a linear generator can provide.

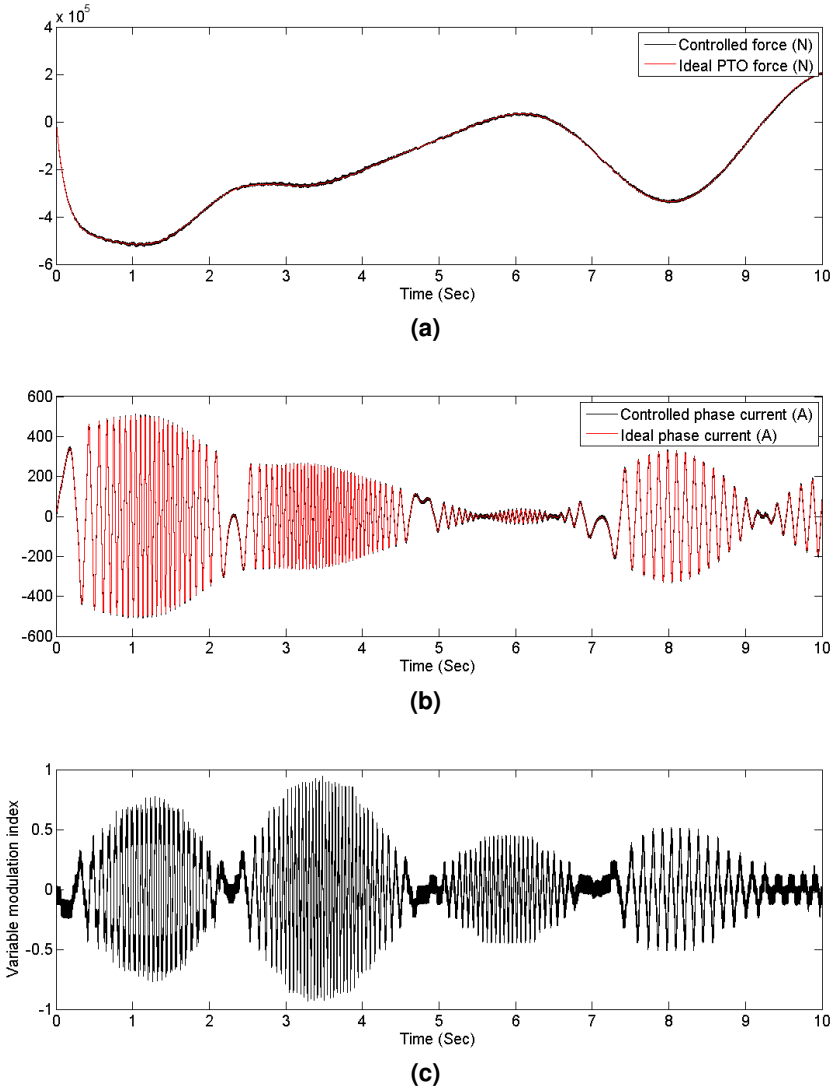

Figure 6.21: a) Comparison between controlled force and desired force. b) Comparison between controlled current and reference current. c) Modulation indices to control the phase current.

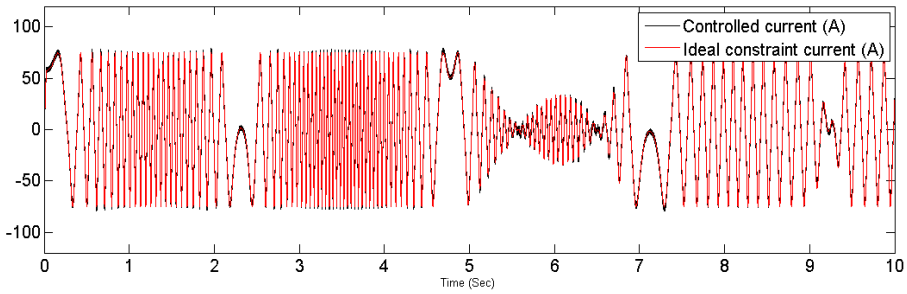

Figure 6.22: Ideal current under force constraint and the corresponding controlled current.

Chapter 7

Discussion and Interpretation

7.1 Introduction

This thesis introduces reaction force control of a direct drive linear generator in real sea conditions to extract maximum possible power. Chapters 3-6 have discussed ocean wave generation, control strategies, linear generator control and power converter control, and some simulation results have been provided. Experimental work cannot readily be carried out due to the cost of providing real ocean conditions. This chapter will collate the previous chapters and provide some discussion on the simulation results.

7.2 Ocean Wave Generation

In this thesis, random ocean wave generation is from the PM spectrum. This traditional PM spectrum describes ocean wave energy with respect to the frequency. To achieve time domain ocean waves, the Inverse Fourier Transform has to be applied. However, this procedure is difficult to carry out in Simulink, because Simulink runs the program in the time domain. Thus, as soon as the programme starts to be compiled, all the parameters have to be functions of time. Unfortunately, the procedures of Inverse Fourier Transform are to deal with all parameters in the frequency domain. Hence, the frequency domain PM spectrum and the Inverse Fourier Transform procedures are carried out in Matlab. Subsequently, the wave excitation force can be obtained in the time domain and imported into the Simulink model.

During the process of the Inverse Fourier Transform as explained in Section 3.2.2, T is chosen as the time period. During this time period, N points are selected to carry out the Fourier Transform and thus these points are called sample points. Hence, the sample frequency can be obtained as $f_s = N/T = 1/\Delta t$. As f_s is fixed in this work, the time period T should change according to the selected sample number N. Therefore, in the simulation process, random waves can be generated to any second as required by simply changing N.

Several methods can be used to solve the DFT, but normally, with a huge amount of calculation. In order to increase the calculating speed, the FFT is proposed and applied in Matlab as an effective way to reduce the calculation time. The FFT is based on the complex DFT as introduced in Section 2.3.3. The well-known Inverse Fourier Transform is expressed in Equation 7.1 which can be regarded as the opposite calculation of Equation 2.14.

$$x[n] = \sum_{k=0}^{N-1} X[k] e^{j2\pi kn/N} \tag{7.1}$$

The IFFT equation in Matlab is expressed in Equation 7.2, which is slightly different from the traditional Equation 7.1. An important difference is that the exponent has been changed from kn to $(k-1)(n-1)$. It can easily be seen that the notation in Matlab cannot be zero, thus, $x[n]$ starts with $x[1]$ rather than $x[0]$. However, the calculation has to be maintained the same as the traditional expression, hence, $(k-1)(n-1)$ when $k = 1$ and $n = 1$ can give the same expression as the original equation shown in Equation 7.1. Another difference is that the IFFT in the Matlab expression has a coefficient $1/N$, which has to be compensated by multiplying by a coefficient N to recover the time domain.

$$x[n] = (1/N) \sum_{k=1}^{N-1} X[k] e^{j2\pi(k-1)(n-1)/N} \tag{7.2}$$

7.3 Latching Control

Latching control was investigated in this work as an effective way to improve power production. When a floating buoy is operating in regular waves, optimal latching control can be implemented to extract maximum power by controlling the oscillating velocity to reach its peak value as the peak wave excitation force arrives. For irregular waves, such optimal latching control can only be applied when wave prediction is included, providing the incoming wave period so that the specific latching and unlatching time can be determined. As ocean wave prediction techniques are still under investigation and the current technology is not mature, it is necessary to find a solution to achieve latching control without future wave information. In this thesis, sub-optimal latching control is proposed to extract "more power" rather than "maximum power". Instead of latching and unlatching the buoy at a specific time, in sub-optimal latching control, the buoy is unlatched as soon as the wave excitation force changes its direction with respect to the ocean surface, and it is latched when the oscillating velocity is zero. Therefore, the maximum velocity occurs earlier than the peak wave excitation force.

The uncertainty of future waves brings a big challenge to sub-optimal latching control. The ocean waves may come at different frequencies. If the waves come always at a frequency which is smaller than the natural frequency of the buoy, sub-optimal latching control can be implemented well to control the motion. In reality, it it likely that there will be some waves with a higher frequency than the buoy natural frequency. For these waves, the wave excitation force changes its direction with respect to the ocean surface before the oscillating velocity becomes zero. Hence, for a short time, the oscillating buoy is moving against the wave excitation force. Afterwards, the buoy is locked down when its velocity approaches zero. As the wave excitation force changes direction again, the buoy will start to move against the wave excitation force under either gravity or the buoyancy spring stiffness force, because it is locked at the maximum position. Such motion continues until another higher frequency wave comes, which maybe a long time. The problem has been solved as discussed in Section 4.4.1, by latching the buoy a bit longer when the velocity is moving in the opposite direction to the wave

excitation force.

From the simulation results in this work, it can be concluded that latching control performs better than reaction force control due to smaller required currents. This is based on the assumption that the peak frequency of the waves is smaller than the natural frequency of the oscillating buoy. However, in real sea conditions, a series of small waves with high frequencies may come to the floating buoy. If that occurs, the buoy may be latched most of the time and thus produce low average power. This problem does not occur with reaction force control, as such control changes the buoy's natural frequency to suit different incoming waves.

7.4 Reaction Force Control

7.4.1 Theoretical Reaction Force Control

Reaction force control uses the force from the linear generator to control the WEC to extract as much power as possible from ocean waves. In this thesis, four different reaction force control methods are introduced which are:

- Real control
- Reactive spring damping control
- Reactive mass damping control
- Complex conjugate control

Three of them use reactive power to provide an additional inertia force (or spring force) leading to a negative power flow, hence, these control methods are also called reactive force control. The mechanical reactive force consists of the inertia force and the spring stiffness force, or possibly just one of them. The existence of the mechanical reactive force can lead to a higher velocity and the production of higher real, or mean, power output. The mechanical reactive power is used only to control the motion of the WEC, and the mean power used to perform this is zero, disregarding losses in the system. As wave prediction is not included, only peak frequency of the energy spectrum is used to

calculate the PTO force. Hence, it is here also called causal sub-optimal reactive force control. Apart from the three reactive force control methods, real control in which only damping is used is also included.

According to simulation results, complex conjugate control is theoretically the best control method to extract maximum power. By adjusting the PTO impedance to be the same as the complex conjugate of the intrinsic impedance, resonance between the velocity of the WEC and the wave excitation force can be achieved. As causal sub-optimal reactive force control is applied, perfect mechanical resonance cannot be achieved, only near resonance. Nevertheless, high velocity, acceleration and displacement are achieved as shown in Figure 4.15. The displacement under the complex conjugate control has an offset such that the floating buoy does not oscillate symmetrically along with the ocean surface. This causes a huge PTO force which is always negative, and a very large instantaneous power as shown in Figure 4.17. In this case, although the PTO force is always negative, it does not mean that the power flow is always negative. The offset displacement can be solved by introducing a small PTO spring stiffness term to make the total spring stiffness coefficient non-zero. With this small change, the velocity is still near resonance with the wave excitation force, the displacement can move symmetrically along with the ocean surface as shown in Figure 4.18, and the peak PTO force and peak instantaneous power flow are significantly curtailed as shown in Figure 4.19, but with only a very small change in average power production which can be disregarded.

From the results, the peak instantaneous power is about 1.94 MW. As the mean reactive power is zero, the average power extracted is only produced by the damping force and is about 50 kW. Hence, peak instantaneous power is about 40 times the average power. This large peak to average power ratio implies a big linear machine and converter system is required to produce a relatively low average power. To compare with a real case, for example, the first AWS prototype in 2004 produced a maximum peak power of 2 MW with a maximum average power 1 MW [53]. However, this high power output assumes that no reactive force is required to control the WEC, thus,

damping force is the only reaction force. To produce such a high peak power with high average power under only damping force, the generator has to be very big to interact with huge waves. In addition, the generator is assumed to operate in regular waves where the natural frequency of the floating device matches the frequency of the waves. Hence, the information above of the first AWS machine is only for ideal conditions. Shek [5] used reactive force to control the WEC in regular waves, where the maximum peak instantaneous power required to control the buoy is about 10 times the average power: this ratio changes depending on the design of the floating device. If the natural frequency differs greatly from the wave frequency, this ratio increases, otherwise the ratio decreases if the difference is small. When the natural frequency of the floating device is similar to the wave frequency, the maximum peak instantaneous power is twice the average power because no reactive power is required. This agrees with the results for the first AWS device discussed above.

Apart from the complex conjugate control with large PTO force and large instantaneous power, other reaction force control methods are also investigated. The reactive spring-damper control, which was applied by Shek [5], operates well in regular waves as long as the floating buoy is perfectly designed. In irregular waves, as discussed in this thesis, the spring-damper control can only be used to adjust the natural frequency of the floating buoy to be the same as the peak frequency of ocean waves, which is different from complex conjugate control where the natural frequency of the floating buoy is controlled to agree with the frequency of each individual incoming wave. Similarly to the regular waves case, reactive force can be significantly reduced when the natural frequency of the floating device is designed to be close to the waves' peak frequency. If the buoy is perfectly designed with the natural frequency equal to the peak frequency, such control can be regarded as real control where only damping force is required as shown in Figure 4.26. Similarly, the reactive mass-damper control also controls the natural frequency of the device to meet the peak frequency of the waves. The extracted power is very similar to that using spring-damper control. Based on these two control methods, the required PTO force and peak instantaneous power can be significantly

reduced compared with complex conjugate control. The real control is another reaction force control method which requires only damping force and produces only real power. Indeed, this control method can also be combined with latching control.

7.4.2 Practical Reaction Force Control

From the simulation results, the average power extracted by causal sub-optimal mass-spring-damping control can be as much as 10 times greater than other reaction force control methods and several times greater than latching control. However, the instantaneous power required to achieve this control method is very high. Such a high peak instantaneous power indicates that the linear generator must be very overrated. A highly overrated machine is economically unrealistic, therefore the instantaneous power has to be limited. Moreover, the displacement under such control is very large due to mechanical near resonance between the WEC and the wave excitation force, and the peak excursion can be over the designed draft of the floating device which implies the device moves out of the water. When the buoy is out of the water, the discussed hydrodynamic analysis is no longer applicable. Hence, an end-stop system must be installed to prevent large excursions. It can be concluded that pure causal sub-optimal mass-spring-damping control cannot be achieved with linear generators and oscillating devices, much less acausal optimal control. For reaction force control, future wave prediction allows interesting simulations to be carried out but is not suitable for realistic situations.

In this work, an end-stop system is applied to prevent the floating buoy moving out of the water under complex conjugate control. The end-stop system can also be used to prevent the translator from exceeding its maximum excursion and causing a loss of interaction between the stator coils and the translator. When operating freely in ocean waves or even with spring damping control, mass damping control or damping control, the floating device should oscillate within the design limit and the end-stops are rarely required due to the poor response of the system, unless there is a large incident wave. Hence, the end-stop system can be considered as a protection device.

However, for a WEC operating under sub-optimal mass-spring-damping control, the end-stop system is frequently activated as it approaches resonance, and thus has to employ a large damper together with a large spring to prevent damage to the WEC. The end-stop system starts to operate when the buoy hits the design limits, so that measurement of the displacement has to be included. Problems arise for causal sub-optimal mass-spring-damping control when the end-stop system is activated. As the PTO force consists of mass term, damping term and spring term, the PTO inertia force can be extremely large due to the large deceleration. If a force limit is not included, such a large force would cause large currents in the generator which would be likely to damage the machine. Hence, as well as displacement limits considerations, force limit has to be considered.

Linear generator force is constrained by limiting the rms current density. It is difficult to define a precise value because the rms current density can be allowed to be higher if the current rarely reaches the peak value; conversely, it has to be lower if the current reaches the peak value frequently. A direct drive linear generator for ocean wave engineering is designed to operate under the sea water and the cold sea water can be used to cool the machine. In this work, the rms current density of the ACTM machine is chosen to be 7 A/mm^2 which is higher than normal. With this limitation, the machine is assumed to work normally, but electrical losses have to be taken into account if real conditions are modelled, as they contribute noticeably to net power production. If no amplitude limitation is considered, the net power extracted is approximately 18.75 kW as shown in Table 5.2. As one linear generator cannot provide the PTO force required, two or three linear generators connected together are simulated. As more generators are connected together, the electrical losses are significantly reduced which results in a higher net power production as shown in Table 5.2.

The results in Table 5.3 show the net power production is greatly reduced by introducing the amplitude constraint. Hence, future work should be focused on designing a floating buoy with the same physical mass but a longer draft. If the radius and the buoyancy spring stiffness force are reduced, the PTO spring stiffness can be reduced.

Also, a longer draft allows a larger moving displacement to produce more power. If such a design is carried out, the hydrodynamic parameters must be recalculated.

Due to amplitude and generator force constraints, it is difficult to tell which reaction force control method is the best as shown from the results in Section 5.4. From these results, the control method should be selected depending on the dimension of the buoy as well as the peak frequency. However, causal sub-optimal mass-spring-damping control with both force and amplitude constraints can be improved by removing one side of the end-stop system as well as by combining the control methods as discussed in Section 5.4.3. The results in Table 5.14 show that the net power extracted with this control method and using two linear generators is normally twice that when using other control methods.

7.5 Power Converter Control

After determining the PTO force based on the machine model, the required currents from the generator can be obtained. These currents have varying amplitudes and frequencies thus presenting a challenge to traditional PWM control. In Chapter 6, two rectifier control methods are introduced to control these variable currents. By using causal sub-optimal control, the peak EMF is about 5000 volts which requires the dc link voltage to be at least 10 kilovolts to achieve proper control.

Both control methods proposed in Chapter 6 require a high switching frequency. However, for continuous varying average voltage method, another higher frequency is required to calculate the exact switching time based on the duty ratio calculated. Results are more accurate if a higher frequency is selected, but a high frequency slows down the computing time considerably. For the various modulation index method, only the switching frequency is chosen which makes the computing time much faster.

There are two converters to control; the active rectifier and the grid side inverter. In direct drive linear generators, the active rectifier can be controlled in order to control the reaction force, to control the velocity of the floating buoy or to control the current to

be in phase with the input EMF to obtain unity power factor. The purpose for reaction force control is to achieve the desired PTO force to optimize the power production as discussed in this thesis. For this purpose, both EMFs and currents are varying due to the continuously varying velocity. If the active rectifier is controlled to keep the current in phase with the input EMFs to achieve unity power factor in irregular waves, control becomes more complicated as the working principal is different from a conventional rotary machine. For a rotary machine, the rotating speed is constant most of the time, so that the details of output EMFs, such as amplitude and frequency, can be easily measured. In a linear generator, although the amplitude of EMFs can be easily measured they are continuously changing, and the phase angle is very difficult to obtain. Hence, in order to control the linear generator to make it run at unity power factor, a phase angle reference has to be established accurately.

For inverter side control, the most popular method is to measure the instantaneous output power from the generator and apply feedforward control to regulate the dc link voltage and achieve unity power factor to the grid. However, in reaction force control, this is difficult to implement because a large amount of reactive power is needed from the grid side. More work is required to achieve this.

7.6 Challenges and Improvement

In this work, if no practical considerations are taken into account, the simulation results show that maximum power extracted from irregular waves, where there is no future wave information, can be achieved by causal sub-optimal mass-spring-damper control. For this, although the specific wave elevation is not required, the energy peak frequency is needed. If the future wave elevation is available, acausal optimal mass-spring-damper control can be achieved. Theoretically, absolute mechanical resonance can be achieved under acausal optimal control, but this presents a big challenge to wave prediction techniques. However, in reality, the PTO force required under acausal optimal control would be extremely large, beyond the scope of modern linear genera-

tors. Also, the absolute mechanical resonance would cause large motion displacement which has to be limited by end-stop systems (or other mechanisms). Due to these limitations, acausal optimal control can not be achieved, which makes future wave prediction unnecessary for pure reaction force control. However, as the performance of reaction force control under practical constraints is not as good as expected, a hypothesis can be proposed that latching control can be applied together with reaction force control. For smaller waves, reaction force control performs better than latching control; conversely, latching control may perform better than reaction force control when bigger waves approach. Hence, under this hypothesis, wave prediction is still necessary to determine whether the incoming waves are big or small. Also, optimal latching control requires wave prediction to decide the latching and unlatching times.

For reaction force control, electrical losses have to be considered. The results in Section 5.4.2 show electrical losses are significant due to large coil currents being required. With the existence of these electrical losses, the net power extracted under causal sub-optimal mass-spring-damper control could be smaller than other control methods, although the power recovered (from ocean waves) is much larger. Hence, the reduction of the electrical losses sets a challenge to machine designers. This can be achieved by reducing the resistance of the linear generator coils. Equation 7.3 gives the relationship between the resistance and line parameters, where, R is the resistance, ρ is the electrical resistivity, l is the length of the conducting coils and A is the cross-section area of the coils. Hence, by enlarging the cross-section area of the conducting coils, resistance can be significantly reduced, but at the cost of increasing the physical mass. If the electrical losses can be significantly reduced, power extraction under causal sub-optimal mass-spring-damping control can be much better than other control methods.

$$R = \rho \frac{l}{A} \tag{7.3}$$

It is simple to conclude that, with causal sub-optimal mass-spring-damper control, the net power extracted could be larger if the end-stops are activated less frequently or the required PTO force is smaller than the capability of the linear generator. In other

words, this sub-optimal control method may be suitable for small waves with higher peak frequency which is confirmed from Table 5.8. From this result, the peak frequency is chosen to be higher than the natural frequency of the floating buoy, which indicates a smaller significant wave height. Hence, this control method may be suitable for areas which have smaller ocean waves, such as the east coast of China. However, further work has to be carried out to test this.

Inverter control also presents a significant challenge to electrical engineers to maintain the dc link voltage to be constant. The required output power from the generator needs to be determined. This power is resolved into real power and reactive power which are used to determine the inverter control parameters. It is well known that the modulation index can be used to control the real power and phase can be used to adjust the reactive power. Most previous research has focused on calculating the modulation index and phase angle based on dqo transformation, which requires fixed frequency and amplitude information. This method does not work for a linear generator in irregular waves as the phase angle is very difficult to obtain. Hence, a new method needs to be developed to control the inverter for specific use in this thesis.

Chapter 8

Conclusions

8.1 Introduction

The majority of WECs that have been proposed for wave energy engineering employ a hydraulic or pneumatic interface between the wave device and the generator. The advantages of these mechanical PTO systems are that electricity production can be smoothed and a control system can be easily designed. A direct drive PTO system is a recent technology which uses a linear electrical generator to convert the energy from sea waves into electrical energy without any mechanical interfaces. Due to the simple mechanism, power transfer efficiency and reliability can be significantly increased. Among all existing prototypes of wave energy conversion systems, the point absorber WEC can most easily be connected to a linear generator and electricity is generated based on the reciprocating motion with the ocean waves.

This project investigated the reaction force control of a direct drive linear generator to extract maximum possible power from irregular waves, which is a continuation of the work of Shek [5]. Unlike hydraulic and pneumatic systems, a direct drive system can only be controlled by either latching or reaction force from the linear generator. As ocean waves approach the WEC, the reciprocating motion produces a linear generator output with variable amplitude and frequency. The power electronics equipment is connected directly with the linear generator to convert the output to an acceptable form of electricity for network connection. An active rectifier is used to control the armature currents to provide the required currents for controlling the motion.

Unlike reaction force control in regular waves, optimal control is difficult to achieve

even with knowledge of the future waves. Sub-optimal control is, instead, used by understanding the peak frequency of the energy spectrum, but the requirement of knowing actual wave elevations for future waves is not now necessary. The performances of reaction force control have been proven through the simulation results presented.

It can be seen from the results that power can be optimized by reaction force controls, especially under complex conjugate control. However, if physical size and linear generator current rating are considered, power output under complex conjugate is not always larger than real control but with a very high peak to average ratio which is not very economic. Therefore, unless a better generator is designed with less electrical losses, complex conjugate control is not suitable to control direct drive linear generator. It can also been seen that continuous varying average voltage method and various modulation index method are both developed with current feedback PI controller to get the required currents to achieve the reaction force control.

8.2 Conclusion

Irregular ocean waves are generated by converting the frequency domain energy spectrum into a time domain wave excitation force using the random phase method. The scale of ocean waves can be achieved by choosing the peak frequency, with a smaller frequency indicating larger ocean waves.

This project describes the reaction force control of a direct drive linear generator to extract the maximum possible power from irregular waves, with a constraint on the available PTO force, without any system for predicting the incoming waves. Sub-optimal latching control and four different reaction force methods are presented and simulation results are provided. Theoretically, with no future wave information, maximum power extraction is achieved by applying causal sub-optimal mass-spring-damper control to determine the desired PTO force based on the peak frequency of the incident wave spectrum. However, the desired PTO force is much larger than the selected ACTM can provide, so that the force has to be constrained through limiting the currents.

Moreover, amplitude of the motion is large under causal sub-optimal mass-spring-damper control method, and sometimes may exceed the design draft. Thus, an end-stop system is included to limit the displacement. By these two constraints, net power extraction is significantly reduced and may be smaller than other reaction force control methods in some cases, due to large electrical losses and amplitude limitation. Net power production and efficiency can be improved by introducing two control methods together, whereby real control is used when the incoming wave excitation force is large enough, and causal sub-optimal mass-spring-damper control is used when the wave excitation force is small. By choosing bigger end-stop spring and damping coefficients to give the device more space to move, net power production is also increased. In addition to these two modifications, improvement can also be achieved by connecting two linear generators together to provide a larger force. As the linear generators are connected, armature currents are shared by both of them which results in less electrical losses.

After determining the required generator currents, the power converter is controlled to obtain them through PWM control. The traditional PWM method of constructing the current or voltage template signal is not suitable for random currents with varying frequency and amplitudes. Therefore, two novel control algorithms were introduced. The first method is called continuous varying average voltage method which uses the duty ratio to calculate the exact switching time. As a higher frequency is needed, the computational time required is extended. This drawback is overcome by introducing the varying modulation indices method. For this method, the reference waveform is generated by using varying modulation indices to generate the PWM signals, which are then fed to the IGBT gates to achieve the required control. In addition, a feedback current loop and PI controller are employed to improve performance.

With both force and amplitude limitations, control is no longer the conventional causal sub-optimal mass-spring-damper control, as the motion of the WEC is out of phase with the incoming waves. However the recovered power is still much larger than using other reaction force control methods. By implementing the control algorithms

presented here, machine losses become large as a large reactive force is required. A more suitable machine design, optimized to produced large forces, could be used to increase the efficiency of the energy conversion. Although significant improvements to the extracted power can be achieved through reaction force control, there will inevitably be huge mechanical reactive power flows relative to the net power extracted, presenting a difficult challenge for wave energy engineers.

8.3 Future Work

There are many other realistic conditions under reaction force control that need to be taken into account in the future. Reaction force control can also be improved to extract more power from irregular waves through the following listed points.

In real sea conditions, waves will not always come at only one peak frequency. To make the system more realistic, consideration of non-stationarity is required that wave energy spectral density is changing with time. In that case, JONSWAP spectrum should be modelled. As spectrum changes all the time, a mean value can be used instead to achieve reaction force.

From the simulation results, full complex conjugate control does not perform very well. The net power extracted is considerably reduced due to the excessively high currents and electrical losses. Latching control is an alternative method to achieve mechanical resonance which leads to discontinuous power flow. For latching control, the natural frequency of the floating buoy cannot be continuously adjusted to match the ocean waves, therefore, the buoy's natural frequency must be designed to be higher than most of the incoming waves. However, irregular ocean waves will not always come in low frequencies which may force the buoy to be continuously locked for extensive periods. For high frequency ocean waves, causal sub-optimal mass-spring-damper control is more suitable. Hence, further work can be undertaken to extract more power by combining the two control methods together so that latching control is

activated when big waves arrive and causal sub-optimal mass-spring-damper control is activated when small waves arrive.

Energy storage is required, but this presents a big challenge to direct drive WECs, because sub-optimal controls produce a discontinuous power output. For sub-optimal latching, power output is zero when the floating buoy is latched, whereas, for causal sub-optimal mass-spring-damping control, power output is also discontinuous due to the end-stop systems. An electrical power converter can only provide a very short-term energy storage even when a big capacitor is selected. Hence, future work has to be carried out to find out a way to achieve short-term energy storage for direct drive systems.

From the results in this thesis, the draft of the floating buoy and the capability of the linear generator play a significant role in extracting net power under causal sub-optimal mass-spring-damping control. Future work can be carried out by designing a long draft floating buoy to reduce the times of activating the end-stops, hence increasing the power generation. In addition, using a bigger linear generator to provide more force with less electrical loss is an effective way to increase power production.

Inverter control is a major challenge for electrical engineers. Previous research on controlling inverters has focused on rotating machines where both amplitude and frequency are nearly constant most of the time, hence the dqo transformation can be applied to calculate the modulation index and phase angle to control both real power and reactive power. For this work, a linear generator is used to provide a varying voltage output whose amplitude and frequency are continuously changing. Hence, previously proposed techniques are no longer applicable to this case and a new control method requires to be developed.

Experimental work should be carried out on a linear generator test rig for optimising power production under reaction force control with irregular excitation force or on a small scale linear generator in a wave tank. For a linear generator test rig, it is not simple to control the translator drive to simulate irregular waves. This would require a complex drive system with computer control. In a wave tank, irregular waves can be

generated by controlling paddle displacement. However, for most narrow wave tanks, such as a wave flume, only single direction irregular waves can be generated. Indeed, the generation of irregular waves at one point is the combination of all waves come from different directions and what needs to be considered are only wave amplitude and frequency. The depth of existing wave tanks is too shallow so some hydrodynamic parameters may differ from real seas such as the relationship between wave frequency and wave numbers. The final test should be carried out in real seas, but device installation and testing requirements will necessitate considerable investment. Moreover, unpredictable ocean conditions might also create considerable difficulties.

Appendix A

Pierson-Moskowitz Spectrum

In this thesis, PM spectrum is used to generate random sea waves. Because of peak frequency of the spectrum is applied to implement reaction force control, the PM spectrum has to be simplified by using peak frequency. The typical PM spectrum equation is expressed below.

$$S(\omega) = \frac{\alpha g^2}{\omega^5} exp\left[-\beta\left(\frac{\omega_0}{\omega}\right)^4\right] \tag{A.1}$$

Hence, based on Eq. (A.1) the ideal PM spectrum is plotted as shown in Fig. A.1.

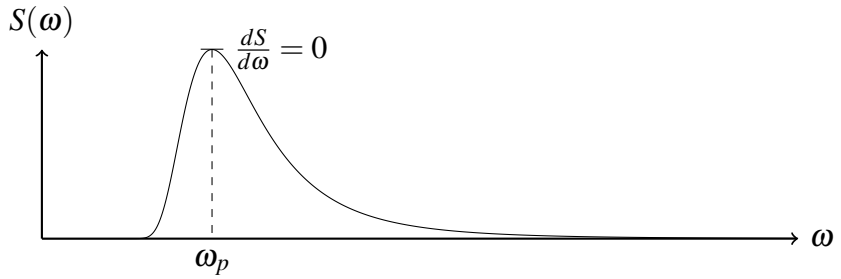

Figure A.1: Pierson-Moskowitz Spectrum.

The peak frequency can be calculated based on $\frac{dS}{d\omega} = 0$.

$$\frac{dS}{d\omega} = -5 \times \frac{\alpha g^2}{\omega^6} exp\left[-\beta\left(\frac{\omega_0}{\omega}\right)^4\right] + \left(-4 \times \frac{\alpha g^2}{\omega^5} \times -\beta \frac{\omega_0^4}{\omega^5} \times exp\left[-\beta(\frac{\omega_0}{\omega})^4\right]\right) \tag{A.2}$$

$$= -5 \times \frac{\alpha g^2}{\omega^6} + 4 \times \frac{\alpha g^2}{\omega^5} \times \frac{\beta \omega_0^4}{\omega^5} \tag{A.3}$$

$$= -5 \times \frac{\alpha g^2}{\omega^6} + 4 \times \frac{\alpha \beta g^2 \omega_0^4}{\omega_{10}} \tag{A.4}$$

$$= 0$$

Where, $\alpha = 8.1 \times 10^{-3}$, $\beta = 0.74$, hence,

$$\omega_p = \omega = (\frac{4}{5} \times \beta)^{1/4} \cdot \omega_0 = 0.877\omega_0 \tag{A.5}$$

After obtaining peak frequency, the original equation can be rewritten as shown in Eq. (A.6).

$$S(\omega) = \frac{\alpha g^2}{\omega^5} exp\left[-\frac{5}{4}\left(\frac{\omega_p}{\omega}\right)^4\right] \tag{A.6}$$

Appendix B

Variable Reluctance Linear Permanent Magnet Machine

The topology described here is a variable reluctance linear permanent magnet machine based on the introduction in Chapter 2.5.2. The methods of calculating the electromagnetic force and EMF voltages, shown below, are provided by Plinder in [100].

The no-load voltages are given below.

$$E_a = -N_t \frac{\pi}{\tau_p} \Phi sin\left(\frac{\pi}{\tau_p}\right) \frac{dx}{dt} \tag{B.1}$$

$$E_b = -N_t \frac{\pi}{\tau_p} \Phi sin\left(\frac{\pi}{\tau_p} - \frac{2}{3}\pi\right) \frac{dx}{dt} \tag{B.2}$$

$$E_c = -N_t \frac{\pi}{\tau_p} \Phi sin\left(\frac{\pi}{\tau_p} - \frac{4}{3}\pi\right) \frac{dx}{dt} \tag{B.3}$$

The linear generator EMFs expressed above are functions of the position, where N_t is the number of turns around a tooth, Φ is the flux in the tooth and τ_p is the pole pitch. The three EMFs have a 120° phase shift with each other.

After obtaining the PTO force from simulation model, the current can be expressed in Eq. (B.4), where the current leads the EMF voltage with an angle ϕ.

$$f_{pto} = \frac{3}{2} \cdot \frac{\pi}{\tau} N_t \Phi I cos\varphi \tag{B.4}$$

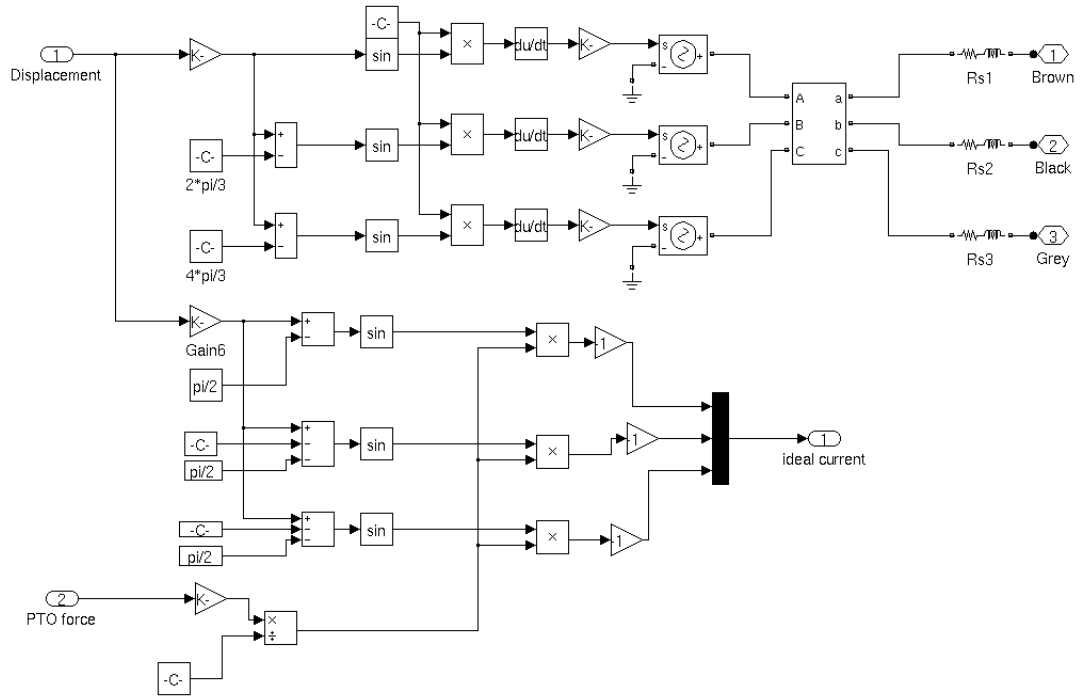

Figure B.1: Simulation model of variable reluctance linear permanent magnet machine

Hence, the phase currents can be obtained below. The three phase currents have a 120° phase shift with each other.

$$i_a = -Isin\left(\frac{\pi}{\tau_p}x + \phi\right) \tag{B.5}$$

$$i_b = -Isin\left(\frac{\pi}{\tau_p}x - \frac{2}{3}\pi + \phi\right) \tag{B.6}$$

$$i_c = -Isin\left(\frac{\pi}{\tau_p}x - \frac{4}{3}\pi + \phi\right) \tag{B.7}$$

The simulation model is implemented as shown in Fig. B.1. Displacement from mass-spring-damper is one of the inputs for calculating the EMFs. Ideal PTO force is the other input to calculate the required currents to control the WEC. The results of wave excitation force, velocity, EMFs and required are shown in Fig. B.2 and Fig. B.3.

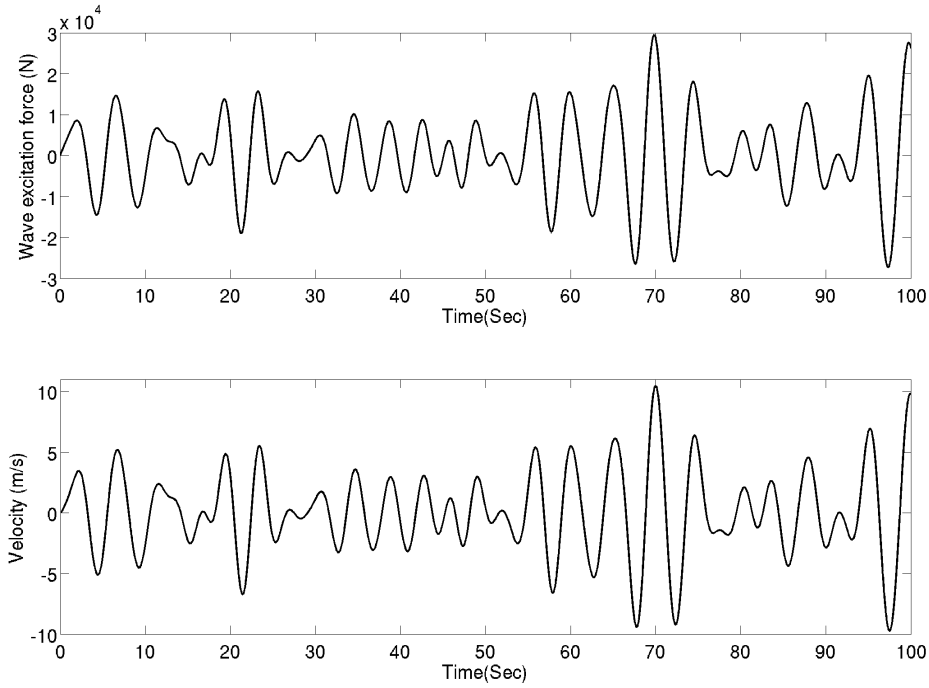

Figure B.2: Simulation results of a variable reluctance linear generator under causal sub-optimal mass-spring-damping control, a) wave excitation force, b) velocity.

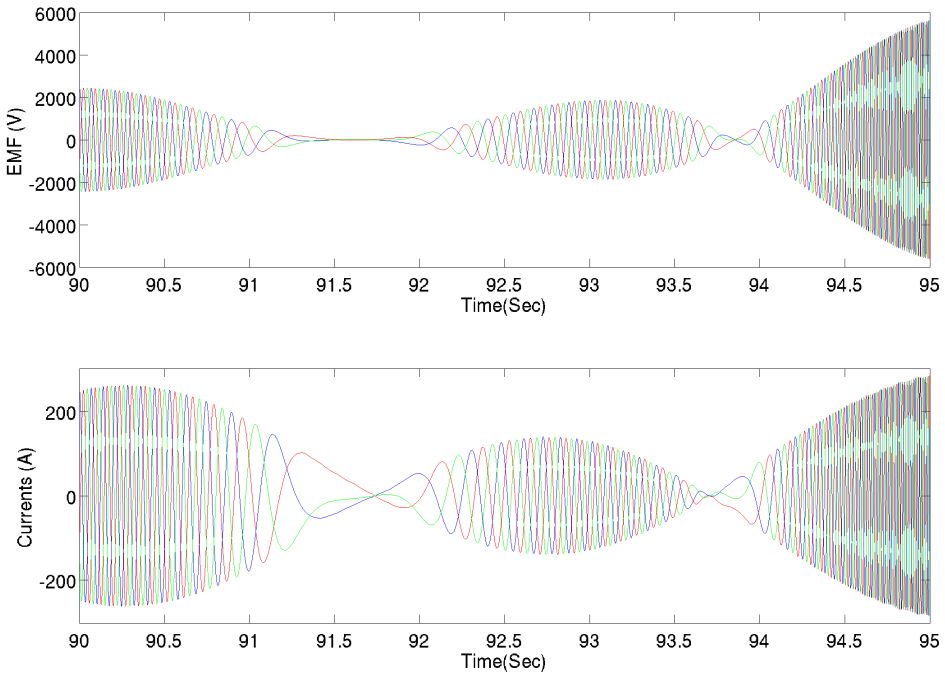

Figure B.3: Simulation results of a variable reluctance linear generator under causal sub-optimal mass-spring-damping control, a) EMFs, b) required currents.

Appendix C

Publications

Details of Published Papers

B. Li, R. Crozier and E. Macpherson, “Reactive Causal Control of a Linear Generator in Irregular Waves for Wave Power System”, 9th European Wave and Tidal Energy Conference (EWTEC 2011), Southampton, UK, September, 2011.

B. Li, D.E. Macpherson, and J.K.H. Shek, “DIRECT DRIVE WAVE ENERGY CONVERTER CONTROL IN IRREGULAR WAVES”, IET Renewable Power Generation Conference (RPG 2011), Edinburgh, UK, September, 2011.

Reactive Causal Control of a Linear Generator in Irregular Waves for Wave Power System

Bin Li
Institute for Energy Systems
The University of Edinburgh
Edinburgh, EH9 3JL, UK
E-mail: b.li@ed.ac.uk

Richard Crozier
Institute for Energy Systems
The University of Edinburgh
Edinburgh, EH9 3JL, UK
E-mail:r.crozier@ed.ac.uk

Ewen Macpherson
Institute for Energy Systems
The University of Edinburgh
Edinburgh, EH9 3JL, UK
E-mail: Ewen.Macpherson@ed.ac.uk

***Abstract*—This paper proposes the reactive control of a wave energy converter (WEC) to extract power from a direct drive linear generator in irregular waves. By introducing reactive control at a single frequency, the motion of the WEC is generally in phase with the incoming waves without the need for wave prediction. The power take-off (PTO) force is provided by an air-cored tubular machine which is directly coupled to the WEC. The model of a WEC with reactive control is only linear when no amplitude or force constraints are required; these must be added to the model to see how it works in sea states that excite a resonance response. With these constraints, the motion between the buoy and waves becomes out of phase and the system is non-linear. A Matlab/Simulink time domain model is used to analyze and simulate the system.**

***Index Terms*—wave energy converter, reactive causal control, irregular waves, linear generator, power take-off force**

I. Introduction

Most designs for WECs include a hydraulic (or pneumatic) interface between the wave device and the generator, but a direct drive PTO system is an alternative method first adopted by Archimedes Wave Swing (AWS), a commercial company, to achieve higher energy conversion efficiency [1]. A direct-drive WEC normally includes a low speed linear generator and a power converter system to interface the variable generator voltage and frequency to the grid.

Much research has been carried out seeking to extract maximum power from the waves by controlling the effective load impedance to match the complex conjugate of the source impedance such that mechanical resonance occurs, with the velocity of the generator in phase with the wave excitation force [2]. Different control methods have been proposed by researchers with the aim of achieving resonance. In regular waves, latching control can be applied to latch and unlatch the buoy at a specific time calculated from the wave frequency and the natural frequency of the buoy [3]. Reactive PTO force control is an alternative way to control the natural frequency of the buoy to make it move continuously with the waves, as has been described by Salter [4]. Shek applied reactive PTO force control for extracting power from regular waves and multi-frequency waves [5], [6].

In irregular waves, control becomes non-causal which requires prediction of future waves. For latching control as proposed by Babarit [7], [8], short term prediction of the future excitation force is assumed. Wave prediction several seconds into the future has been described by Fusco in [9] by using information from the past. However, the error between prediction and reality increases with time. Also, Fuzzy Logic feedback control has been proposed by Schoen [10], [11], in which wave prediction also plays a significant role. Lopes [12] introduced another simple latching control which removes the requirement of wave prediction by measuring the wave elevation for comparison with a pre-set threshold value to determine the unlatching instant.

In this paper, reactive control at the peak frequency of the wave spectrum (referred to here as reactive causal control where causal indicates no future information is required) is applied to control the WEC to extract the maximum power that can be extracted from irregular waves [13], [14]. Because of the near resonance between the WEC and the incoming waves, the motion displacement of the buoy is very large and may be unrealistic in practice. In reality, displacement is limited because of geometry and an end-stop system is applied. Work has been done by Eidsmoen [15] to restrict the amplitude of the buoy's motion, where an end-stop system is included using a large spring with damping. If an end-stop system is included, techniques to reduce the number of times that the end-stop is activated should be developed to avoid damage [16]. To implement reactive control, an extremely high PTO force is required. Both the real part of this force (damping) and the reactive part (analogous to spring and inertia) have large values. This force is typically much higher than the linear generator can provide, so the PTO force needs to be restricted as well.

This paper first describes a simulation of the reactive causal control with displacement limits, and then a model of one possible linear generator, the Air-Cored Tubular Machine (ACTM), is presented. A method of choosing an appropriate limit on the available force is also described. By supplying the displacement, velocity and power take-off (PTO) force to the linear permanent-magnet generator model, the coil voltages are determined, as are the required currents to control the WEC. If an ideal power converter is assumed, the PTO force will be provided by the machine and fed back to the system.

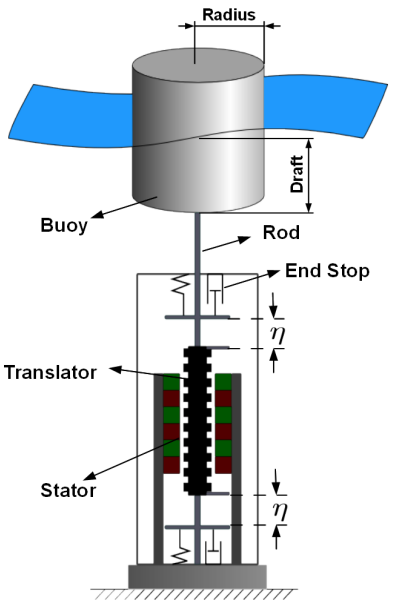

Fig. 1. Direct drive wave energy converter with an end-stop system. The connection rod means the buoy can only move in heave with other motions constrained.

II. Control of Wave Energy Converter

As shown in Fig. 1, the WEC is a submerged vertical cylinder with only one degree of freedom (DoF), i.e. under the wave excitation force, the buoy is constrained to move in heave motion only. The model shown in Fig. 1 is used to simulate the motion of the WEC in real waves; both the upper and lower boundaries need to be constrained because of the dimensions of the buoy and the finite length of the translator. Two end-stops with equal damping and spring characteristics are mounted at each end of the stroke. These two end-stop devices can dissipate and store the energy of the moving device so that devastating collision is prevented. However, a large acceleration is created when the translator moves away from the end-stop due to the energy stored in the spring. This could be avoided by choosing a larger damping term relative to the spring stiffness term, at a cost of greater energy dissipation.

A. Wave Energy Converter Control

If a PTO force is not included, the WEC is considered to be an oscillator and the typical equation in the frequency domain of a single degree of freedom oscillating buoy is of the form shown in (1) [17].

$$F_e(\omega) = i\omega[m + M(\omega)]U(\omega) + B(\omega)U(\omega) + \frac{c}{i\omega}U(\omega) \quad (1)$$

Here, loss between the buoy and surrounding fluid (drag, viscosity and friction) and between translator and end-stops is not modeled. $F_e(\omega)$ is the wave excitation force, $M(\omega)$ and $B(\omega)$ are the added mass and damping, c is the buoyancy spring stiffness and $U(\omega)$ is the velocity in the frequency domain.

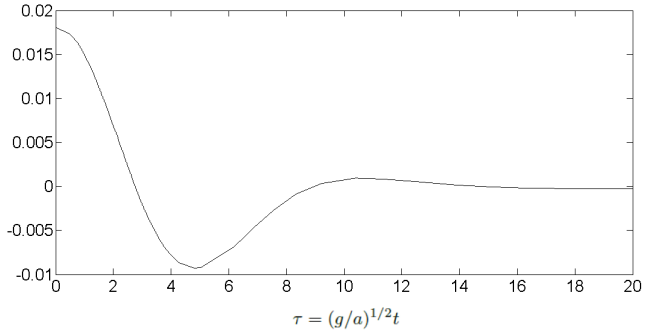

Fig. 2. Impulse response function for cylinder buoy where the scales are dimensionless. The dimensionless time on the horizontal scale is $(g/a)^{1/2}t$ and scale of the dimensionless impulse-response function is $\kappa_3/(\rho g a^2)$ [19]

The intrinsic impedance $Z(\omega)$ can be expressed in (2).

$$Z(\omega) = B(\omega) + i\omega(m + M(\omega)) - i\frac{c}{\omega} \quad (2)$$

In order to control the WEC to extract as much power as possible, the PTO impedance should be the complex conjugate of the intrinsic impedance [18]. According to (2), the intrinsic impedance varies with the frequency of the waves which implies the PTO force ought to be a function of this frequency to complete so called optimal control. However, optimal control is impractical because future wave prediction is difficult to obtain and often inaccurate. In this study sub-optimal control is applied by using the peak frequency of the wave spectrum. The PTO impedance is chosen to equal the value of the intrinsic impedance at this peak frequency ($Z_{pto} = Z^*(\omega_p)$) which has three terms; mass, damping and spring stiffness. ω_p is the peak frequency of the wave spectrum. Here, the PTO force in the time domain can be written as:

$$f_{pto}(t) = -(m + M_p)a(t) + B_p u(t) - cx(t) \quad (3)$$

where M_p and B_p are added mass and added damping at the peak frequency.

If the Inverse Fourier Transform is applied to (1) and PTO force control is included, the time domain equation of WEC control is obtained in (4).

$$f_e(t) = [m + m_\infty]a(t) + \int_0^t k(\tau)u(t-\tau)d\tau + cx(t) + f_{pto}(t) \quad (4)$$

Here, m_∞ is the value of added mass at infinite frequency. The convolution term contains a causal impulse response $k(t)$ corresponding to the force that is caused by the radiated waves generated by the oscillating buoy. Falnes [19] gives a typical impulse response function of a floating vertical cylinder in Fig. 2, in which the draft of the buoy should be 1.88 times the radius of the buoy: this relationship is applied here in this model.

B. Amplitude Restriction

The wave energy converter must be designed with amplitude constraints for when the incoming wave is large enough to

drive the buoy over its draft. In the first AWS device, a water damper was used to provide an additional force when the WEC reaches its chosen end-stop point to prevent a heavy collision [20]. When operating freely in ocean waves the end-stops are rarely required due to the poor response of the system. However, for a WEC operating under reactive causal control, the displacement becomes very large as it approaches resonance. Here we add end-stops, each modelled as a combination of a spring stiffness term and damping term as shown in (5).

$$f_{es} = b_{es}u(t) + c_{es}(x(t) - \eta) \tag{5}$$

In (5), f_{es} is the end-stop force when the WEC approaches the end-stop point, b_{es} is the end-stop damping coefficient, c_{es} is the end-stop spring stiffness and η is the designed height for activating the end-stop system. Falnes points out in [21] that the oscillation amplitude can be equal to the design amplitude of the WEC (draft of the buoy), thus η (as shown in Fig. 1) should be set to be slightly less than the draft to slow the system gradually rather than creating a huge deceleration.

III. Linear Generator

Linear generators with a number of different topologies are available [22], [23], with no clear winner yet emerging from these choices. The particular topology chosen for the simulations presented here is the Air-Cored Tubular Machine (ACTM) [24], however the methods of force and EMF calculation for this machine are also applicable to other generator types.

The ACTM consists of two parts, the translator and armature. The translator is made up of a series of axially magnetized permanent magnet discs with alternating polarity, separated by steel discs mounted on a central shaft. This slots into a second cylinder made up of circumferentially wound copper coils. A diagram of the arrangement is shown in Fig. 3, and further details of its operation can be found in [24] and [25]. The machine has three phases with all coils in a phase connected in parallel. It is further assumed that only coils overlapping the stator are active at any point, with the other coils being switched out of the circuit.

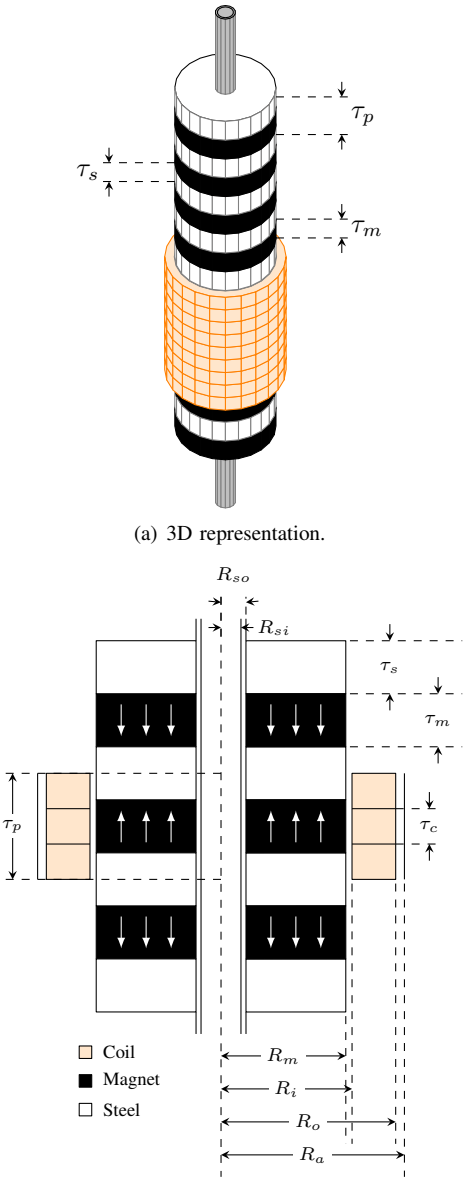

(a) 3D representation.

(b) 2D cross-section with relevant dimensions.

Fig. 3. 3D view of ACTM and cross-section of machine with dimensions.

A. EMF and Force Calculation

The flux linkage in the coil windings is found at a number of positions by performing a 2D axisymmetric finite element simulation of the magnetic field around the translator. A polynomial is then fitted to the flux linkage (λ) versus displacement (x) and assumed to be periodic over two poles. The EMF produced due to movement of the translator is the rate of change in the flux linkage with time and can then be calculated with knowledge of the velocity as in (6).

$$\text{EMF} = -\frac{d\lambda}{dt} = -\frac{d\lambda}{dx}\cdot\frac{dx}{dt} = -\frac{d\lambda}{dx}\cdot\dot{x} \tag{6}$$

The value of $d\lambda/dx$ is simply the derivative of the polynomial, introduced previously, evaluated at the current translator position.

The availability of this derivative also provides a convenient method of calculating the PTO force given knowledge of the current in the armature coils. The force (F) exerted either on or by the generator is given in (7) where P is the power in the generator. Here the power can be either positive or negative where the sign indicates whether the power flow is into or out of the system (i.e. from the WEC or from the grid).

$$F = \frac{P}{\dot{x}} \tag{7}$$

The instantaneous power in the generator/grid circuit is given by $P = i(t)v(t)$ where $v(t)$ is the voltage across the armature

coils, i.e. the EMF, and $i(t)$ is the coil current. Therefore

$$\begin{aligned} f_{pto}(t) &= -\frac{i(t)v(t)}{\dot{x}} \\ &= -\frac{i(t)}{\dot{x}}\,\text{EMF} \\ &= -\frac{i(t)}{\dot{x}}\left(-\frac{d\,\lambda}{d\,x}\,\dot{x}\right) \\ &= i(t)\,\frac{d\,\lambda}{d\,x} \end{aligned} \tag{8}$$

Clearly this method is applicable to any machine for which we can specify the flux linkage with position, provided other forces can be neglected, e.g. tooth ripple forces in slotted machines.

B. Force Specification and Limits

Using the method described in Sec. III-A we can determine the force on the translator by solving the circuit and determining the current in the coils to yield the passive take-off force. Alternatively, if we assume we have a power electronic converter capable of supplying or drawing the necessary current, we can instead obtain a desired force by specifying the required value of $i(t)$. It is this assumption which is made here.

As the ACTM used is three-phase, we have a wide choice in how to distribute the currents in each phase to give the required force. Therefore, to narrow this choice, it is further assumed that the power electronic converter supplies or draws this current in phase with the voltage. In this case the force production can be distributed between phases in proportion to the values of $d\,\lambda/d\,x$ for each coil at a given position.

However, there are practical limits on the current that can pass through any machine's coils without causing failure through heating of the windings due to resistive losses. This, therefore, places a limit on the maximum possible force that can be produced without damaging the generator. This current limit is best expressed as a maximum current density in the coil conductor, J_M. The formula in (9) can be used to find the currents in each phase that keep the phases balanced while maintaining this limit in any coil, where A_C is the cross-sectional area of the coils, $\mathbf{C}$ is a vector containing the instantaneous values of the three coil currents, $||\mathbf{C}||_\infty$ is the infinity norm of the coil current vector (i.e. the maximum value of the absolute value of each vector element), $\text{sgn}(\mathbf{C})$ is a vector containing the sign of each element of $\mathbf{C}$, and $\mathbf{I_3}$ is a 3×3 identity matrix.

$$\mathbf{C}_{\text{lim}} = \text{sgn}(\mathbf{C})\,\mathbf{I_3}\,|\mathbf{C}|\,\frac{J_M A_C}{||\mathbf{C}||_\infty} \tag{9}$$

This formula is applied only when the magnitudes of any of the coil currents exceed J_M. Equation (9) could easily be used for a greater number of phases given an appropriately sized identity matrix. For the simulations presented here, a maximum current density of 10 A/mm^2 is permitted. For a constant sinusoidal current waveform this is an rms current density of 7.1 A/mm^2, or rms current of 1.38 A. It should be noted that the current will not be sinusoidal however, and more detailed calculations may be required to choose an appropriate limit in future.

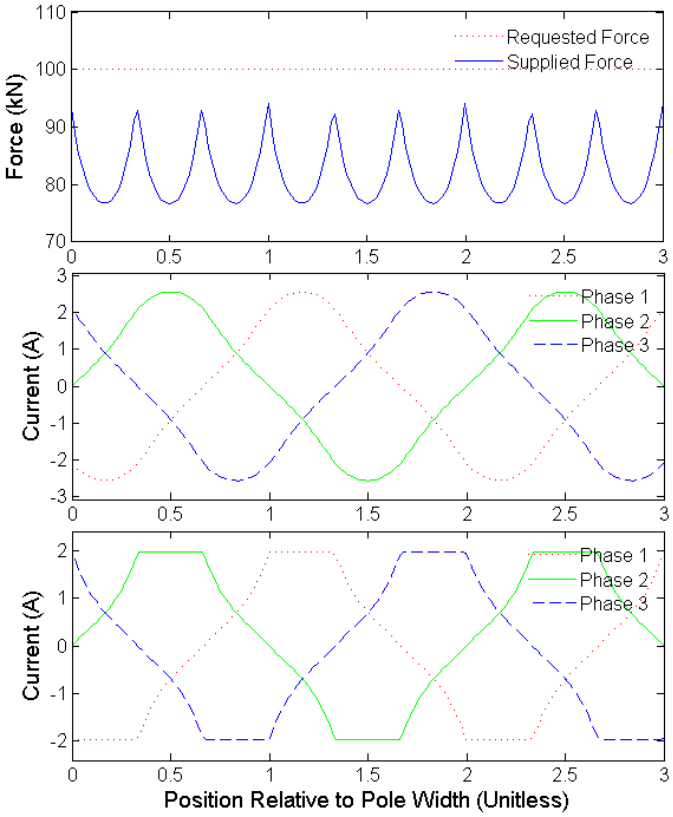

Fig. 4. Graphs of the requested and resulting limited force (top), the currents required to supply the requested force (middle) and the limited currents (bottom), all versus the displacement of the translator relative to one pole width.

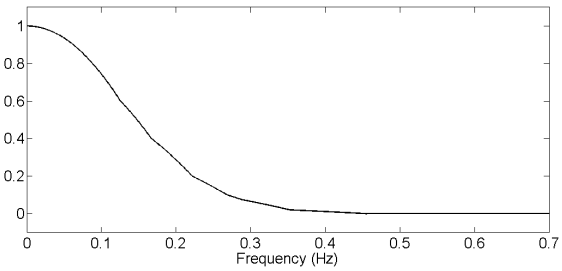

Fig. 5. Non-dimensional wave excitation coefficient

The result of using the instantaneous values of J_M to determine the maximum possible force is that this maximum force changes with the displacement of the coils relative to the translator pole as shown in Fig. 4. For the example machine used here, the maximum possible force varies between 94 kN and 77 kN.

IV. Simulation Results

Simulation of the fully developed sea is based on the typical PM spectrum that gives the relationship between wave energy

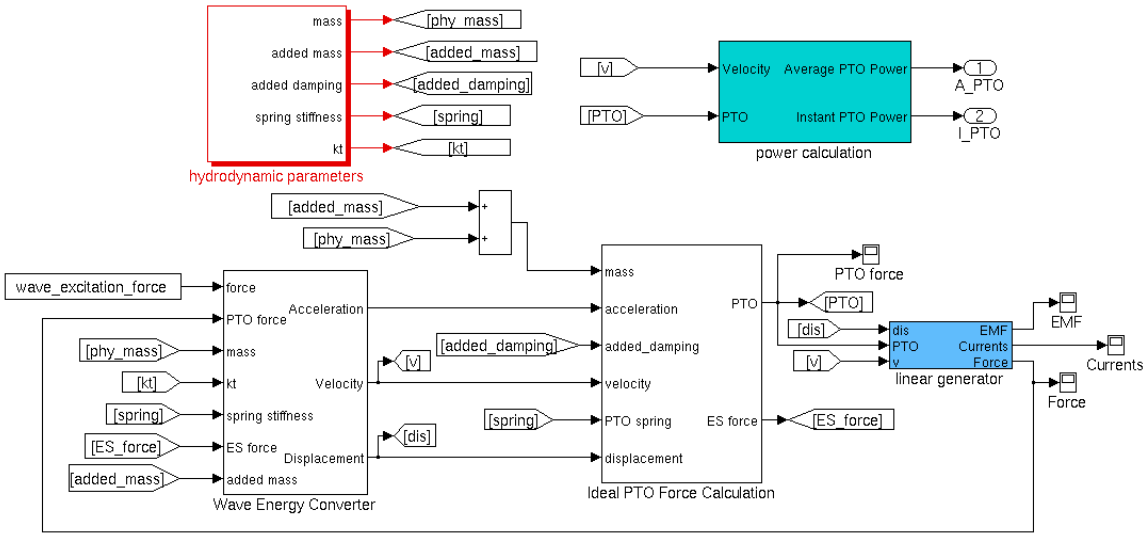

Fig. 6. Simulink model of the whole system

density and frequency [26]. The wave energy spectrum can be obtained from (10) where $\alpha = 0.0081, \beta = 0.74, \omega_0 = g/U_{19.5}$, where $U_{19.5}$ denotes the wind speed at a height of 19.5 m above the water level.

$$S(\omega) = \frac{\alpha g^2}{\omega^5} exp(-\beta(\frac{\omega_0}{\omega})^4) \tag{10}$$

An Inverse Fourier Transform is applied to find the time domain random wave elevation. In order to make the magnitudes before and after the Inverse Fourier Transform identical, a discrete wave energy spectrum is obtained in (11) by giving the sample frequency f_s and the resolution of the spectrum N.

$$\sigma^2(f_i) = S(i \cdot \Delta f) \cdot \Delta f \tag{11}$$

Here, Δf is the frequency interval and expressed by f_s/N. Based on equation (12), the wave excitation force can be calculated in the frequency domain. The Inverse Fast Fourier Transform (IFFT) technique is then applied to derive the random wave excitation force in the time domain [27].

$$F_e(\omega) = \kappa_3(\omega)\rho g \pi a^2 A(\omega) \tag{12}$$

Here, κ_3 is the non-dimensional wave excitation coefficient. In Fig. 5, a is the radius of the WEC and A is the wave elevation in the frequency domain.

A. Reactive Causal Control

The Simulink model of the entire system is shown in Fig. 6. The wave excitation force is obtained in Matlab in the time domain by applying the Inverse Fourier Transform and is then imported into the Simulink model. The hydrodynamic coefficients for added mass, added damping and impulse response data are stored in look-up tables to provide the corresponding coefficients with the frequency. There are two subsystem blocks to indicate the motion of the WEC and the calculation of the required PTO force to control the buoy based on equation (4). The real-time displacement and velocity are given to the linear generator as well as the calculated PTO force. If an ideal power converter to control the currents is assumed, the outputs from the linear generator are the coil voltages (EMFs), the currents and the actual PTO force. The block in the top right corner calculates the average and instantaneous powers.

From wave measurements, the wavelength (the distance between prominent crests) is around $50 - 100m$ [28]. The wavelength L in this paper is chosen to be $50m$ and the peak frequency is $f_p = 0.1768\ Hz$.

For the point absorber, its horizontal extent should be much smaller than the wave length. In this study the radius of the buoy is chosen to be 3 m such that the draft is 5.64 m (as describe in Sec.II-A) . The resulting motion is shown in Fig. 7.

From Fig. 7(a), it can be seen that the buoy moves nearly in phase with the wave excitation force, so that a large amount of wave power can be extracted. However, there is still a very small phase difference between them because sub-optimal control is applied rather than optimal control.

$$f_e(t) = [m_\infty - M_p]a(t) + \int_0^t k(\tau)u(t-\tau)d\tau + B_p u(t) \tag{13}$$

The buoy displacement is shown in Fig. 7(b): it can be seen that its maximum value is 13 m which is much greater than its draft. Thus the buoy would rise out of the water, but the linear model is only valid when the model is partially submerged. Also, it can be seen that the buoy moves along an offset axis of symmetry about 2.5 m above the sea surface. This can be explained by equation (13), obtained through combining equations (3) and (4). From this equation we can see that the coefficient of the displacement (referred here as

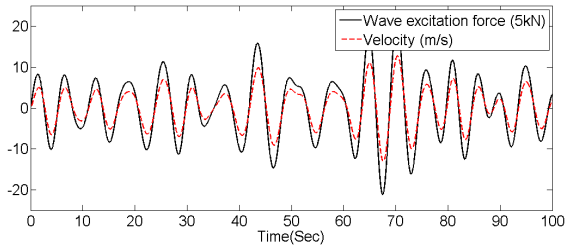

(a)

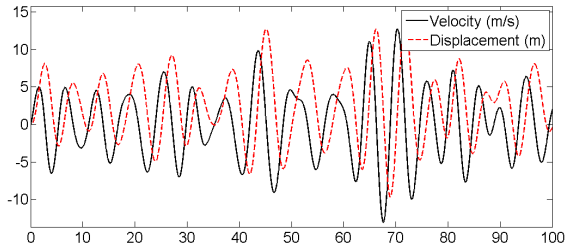

(b)

Fig. 7. a) The velocity of the buoy in blue dashed line and the wave excitation force in black solid line are in phase b) Motion parameters with displacement in blue dashed line and the velocity in black solid line

spring stiffness) is zero. Hence, the value of the displacement will not affect the results of the velocity but will affect the value of the PTO force. As discussed in the paper, when the point absorber operates in real seas, the value of M_p is almost the same as the value of m_∞, so that the coefficient of the acceleration $(m_\infty - M_p)$ is close to zero. This indicates that when the wave excitation force is applied to the point absorber, the change in acceleration is very fast. Thus, at the beginning of the simulation period, acceleration rises from zero to its maximum value very quickly. However, due to its large mass, the velocity of the buoy rises slowly and the displacement of the buoy therefore also rises slowly from zero. After this initial transient response, the buoy moves with a velocity proportional to the wave excitation force, as shown in Fig. 7(a) and the acceleration and displacement are generally $180°$ out of phase. When the acceleration is at a maximum, displacement is at its minimum value. As a result, the mean value of displacement does not return to zero and instead the buoy oscillates about some non-zero offset displacement. This offset displacement will exist until either the generator hits the end-stop or the generator force is limited as described in Sec.II-B. Alternatively, the buoy can be set initially to an offset position rather than zero. However, in practice this is impossible to implement because prediction of future waves is needed to calculate the offset value of the displacement.

From Fig. 8, the maximum required PTO force to control the buoy is calculated to be approximately $1000\ kN$, which is about 13 times greater than the generator can provide. Hence, both the force and the displacement need to be constrained in reality.

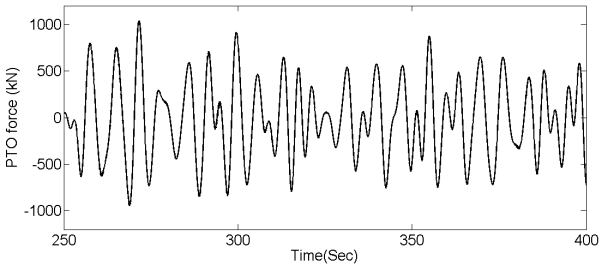

Fig. 8. Ideal PTO force to implement reactive causal control

B. Force and Amplitude Constraints

Fig. 10(a) shows the buoy's displacement with the generator currents (and hence forces) limited to the values specified in Sec. III-B, but with no end-stop system. It can be observed that the maximum displacement is still over 6 m, and therefore still requires an end-stop system.

Fig. 9 and Fig. 10 present results with both the force constraint and the end-stop system included to limit the large displacement. Based on equation (5), a position needs to be set as a reference when the end-stop will be activated. In this paper, the reference point is set to $5\ m$ to give the buoy a small distance to come to a stop.

If the end-stop system starts to operate, the velocity of the buoy decreases very quickly: the large deceleration results in a rapid increase in the PTO force as the reactive control algorithm contains a term proportional to acceleration. If there is no limit on the force (as described in the previous section), the currents needed will be extremely high for a short period. Thus both the force and the amplitude constraints are required to work together. In Fig. 10(a), the blue dashed line indicates the displacement with end-stops in place. It can be seen that the maximum amplitude is successfully restricted to around $5.2\ m$.

The force and currents in Fig. 9 indicate that they are limited successfully to the desired values in Sec.III-B. It can be observed that the controlled PTO force moves from a very high value to a very low value very quickly; this is because the input ideal force is much bigger than the force shown in Fig. 9, so the change between $-80\ kN$ and $80\ kN$ will happen quickly.

Fig. 10(b) shows the relationship between velocity and wave excitation force under constraints. It can be seen that motion of the buoy is out of phase with the wave excitation, but near resonance still occurs some of the time to extract more power. Fig. 10(c) shows the ratio of peak-to-average power, the average power extracted using reactive causal control with both force and amplitude limits is about $37\ kW$ and the maximum instantaneous power is about $500\ kW$. Neither of these figures include losses in the generator, which could be considerable. Reactive control requires negative power from the generator. For regular wave control as described in [5], the peak instantaneous power is about 5 times the average power, therefore the generator and power converter must be overrated.

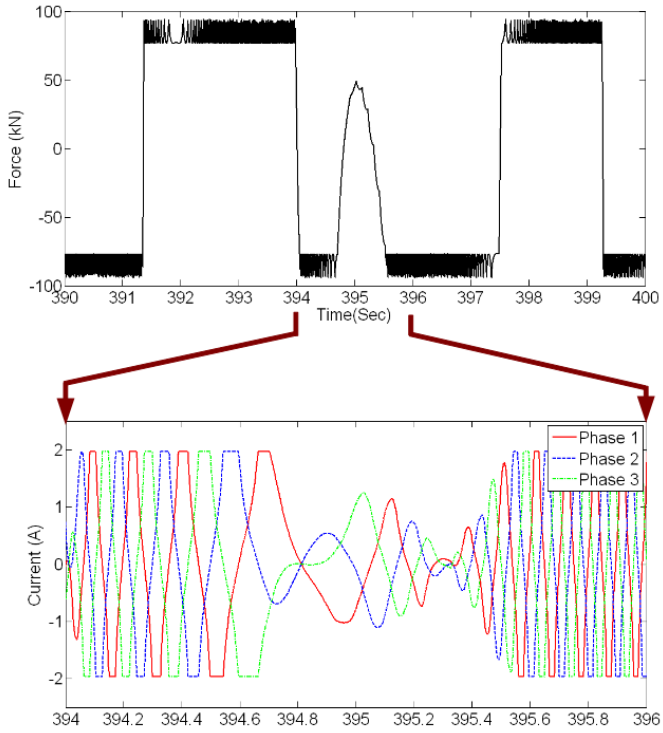

Fig. 9. PTO force and currents generated from linear generator under constrains

Hence, if force constraint is taken into account in Shek's work, the ratio between instantaneous power and average power will be smaller than 5. However, in irregular wave control discussed in this paper, instantaneous power is about 13.5 times of the average power.

Fig. 11 shows a comparison between reactive causal control and damping control. In this case, the average energy extracted using causal sub-optimal control with limits is about 3 times greater than using only damping control. If the simulation were extended, it is likely that this rate will increase as the average reactive power required for controlling in the first 400 seconds of this simulation happens to be negative but will tend to zero as time increases. In contrast, for damping control, because no reactive force is needed, the average power extracted is always positive.

It can also be seen that although the average power extracted using PTO force limitations is increased when compared with damping control, it is significantly reduced from that extracted without force limitations. Hence, an optimised machine that can produce a much larger force, or the same force with reduced losses, than the one used in this paper is highly desirable. However, as a larger force is produced, the electrical losses will increase which presents a difficult challenge to the linear generator designer.

V. Conclusion

This paper describes the control of a direct drive linear generator to extract the maximum possible power under practical constraints from irregular waves, without any system for

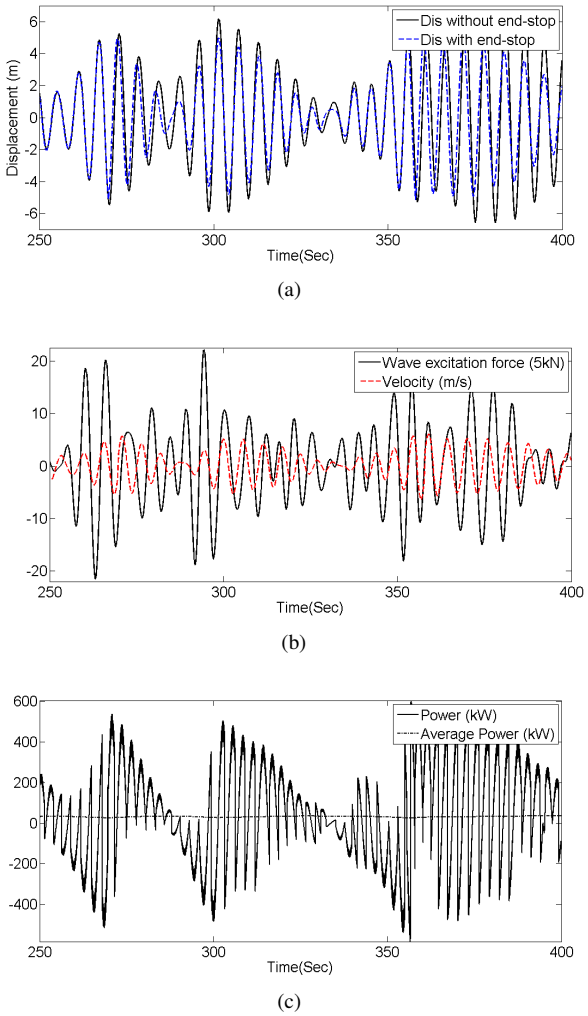

Fig. 10. a) The comparison between displacement with end-stop (blue dashed line) and displacement without end-stop (black solid line) b) The relationship between wave excitation force and velocity under both force and amplitude constraints c) Power extraction with instantaneous power (solid line) and average power (dashed line)

predicting the incoming waves. In this study, this was achieved by using reactive causal control to calculate the required PTO force provided by the linear generator. The machine used in this paper is the ACTM and is used to calculate the EMF voltage as well as the currents. However, if reactive causal control is applied, the PTO force required is much larger than the linear generator can provide. Hence, the PTO force needs to be limited. In addition to the force constraint, the displacement amplitude is also limited by using an end-stop device.

Future work will take into account the machine losses, which could be very significant. In this paper, due to the required forces to achieve resonance being very large, the machine is constantly operated at more than 100% of its rated power, an unsustainable mode of operation. A more suitible machine design, optimised to produce large forces, could be used to increase the efficiency of the energy conversion.

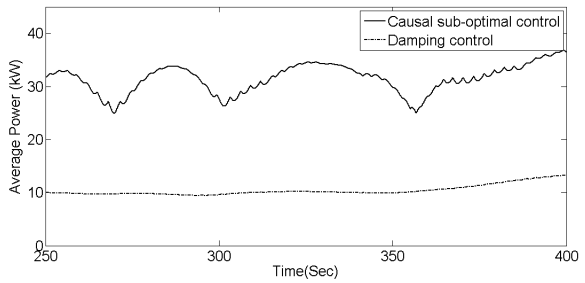

Fig. 11. Comparison of average power extracted between using causal sub-optimal control with force and displacement limits, and damping control

ACKNOWLEDGMENT

The first author is financially supported by the SuperGen Marine Energy Research Programme. The authors also like to acknowledge Jonathan Shek, Ally Price and David Forehand for their invaluable advice and help.

REFERENCES

[1] Feng Wu, X.P. Zhang, Ping Ju, and M.J.H. Sterling, "Optimal Control for AWS-Based Wave Energy Conversion System", *Power Systems, IEEE Transactions on*, vol. 24, no. 4, pp. 1747–1755, 2009.

[2] J Falnes, "A review of wave-energy extraction", *Marine Structures*, vol. 20, no. 4, pp. 185–201, October 2007.

[3] A Falcao, "Phase control through load control of oscillating-body wave energy converters with hydraulic PTO system", *Ocean Engineering*, vol. 35, no. 3-4, pp. 358–366, March 2008.

[4] S H Salter, J R M Taylor, and N J Caldwell, "Power conversion mechanisms for wave energy", *Proceedings of the Institution of Mechanical Engineers, Part M: Journal of Engineering for the Maritime Environment*, vol. 216, no. 1, pp. 1–27, January 2002.

[5] J.K.H. Shek, D.E. Macpherson, M.A. Mueller, and J Xiang, "Reaction force control of a linear electrical generator for direct drive wave energy conversion", *IET renewable power generation*, pp. 17–24, 2007.

[6] J.K.H. Shek, D.E. Macpherson, and M.a. Mueller, "Experimental verification of linear generator control for direct drive wave energy conversion", *IET Renewable Power Generation*, vol. 4, no. 5, pp. 395, 2010.

[7] A Babarit and A.H Clement, "Optimal latching control of a wave energy device in regular and irregular waves", *Applied Ocean Research*, vol. 28, no. 2, pp. 77–91, April 2006.

[8] A Babarit, G Duclos, and A Clement, "Comparison of latching control strategies for a heaving wave energy device in random sea", *Applied Ocean Research*, vol. 26, no. 5, pp. 227–238, July 2004.

[9] Francesco Fusco and John V Ringwood, "Short-Term Wave Forecasting for Real-Time Control of Wave Energy Converters", *IEEE Transactions on Sustainable Energy*, vol. 1, no. 2, pp. 99–106, July 2010.

[10] MP Schoen, J Hals, and Torgeir Moan, "Wave prediction and fuzzy logic control of wave energy converters in irregular waves", *Control and Automation, 2008*, pp. 767–772, 2008.

[11] Marco P. Schoen, Jorgen Hals, and Torgeir Moan, "Robust control of heaving wave energy devices in irregular waves", *2008 16th Mediterranean Conference on Control and Automation*, , no. 1, pp. 779–784, June 2008.

[12] M.F.P. Lopes, J. Hals, R.P.F. Gomes, T. Moan, L.M.C. Gato, and A.F.de O. Falcão, "Experimental and numerical investigation of non-predictive phase-control strategies for a point-absorbing wave energy converter", *Ocean Engineering*, vol. 36, no. 5, pp. 386–402, April 2009.

[13] A.A.E. Price, C.J. Dent, and A.R. Wallace, "On the capture width of wave energy converters", *Applied Ocean Research*, vol. 31, no. 4, pp. 251–259, October 2009.

[14] AAE Price, "New Perspectives on Wave Energy Converter Control", *Engineering*, , no. March, 2009.

[15] H. Eidsmoen and Norges Institutt Fysikk, *Simulation of a tight-moored amplitude-limited heaving-buoy wave-energy converter with phase control*, Division of Physics, Norwegian University of Science and Technology, 1996.

[16] Jorgen Hals, Johannes Falnes, and Torgeir Moan, "Constrained Optimal Control of a Heaving Buoy Wave-Energy Converter", *Journal of Offshore Mechanics and Arctic Engineering*, vol. 133, no. 1, pp. 011401, 2011.

[17] AAE Price and CJ Dent, "Frequency domain techniques for numerical and experimental modelling of wave energy converters", *European wave and tidal energy*, 2009.

[18] D. V. Evans, "A theory for wave-power absorption by oscillating bodies", *Journal of Fluid Mechanics*, vol. 77, no. 01, pp. 1, April 1976.

[19] Johannes Falnes, "Ocean waves and oscillating systems", *System*, 2002.

[20] Duarte Valério, Mário J.G.C. Mendes, Pedro Beirão, and José Sá da Costa, "Identification and control of the AWS using neural network models", *Applied Ocean Research*, vol. 30, no. 3, pp. 178–188, July 2008.

[21] J Falnes, "Optimum control of oscillation of wave-energy converters.", *International Journal of Offshore and Polar*, , no. June, 2002.

[22] M. A. Mueller and N. J. Baker, "Direct drive electrical power take-off for offshore marine energy converters", *Proceedings of the I MECH E Part A Journal of Power and Energy*, vol. 219, pp. 223–234, 2005, doi:10.1243/095765005X7574.

[23] H. Polinder, B. C. Mecrow, Dickinson P.G. A. Jack, and M. A. Mueller, "Conventional and tfpm linear generators for direct-drive wave energy conversion", *Energy Conversion, IEEE Transaction on*, vol. 20, no. 2, pp. 260–267, 2005, 0885-8969.

[24] N. J. Baker, M. A. Mueller, and E. Spooner, "Permanent magnet air-cored tubular linear generator for marine energy converters", in *Power Electronics, Machines and Drives, 2004. (PEMD 2004). Second International Conference on (Conf. Publ. No. 498)*, M. A. Mueller, Ed., 2004, vol. 2, pp. 862–867.

[25] Baker J., *Linear generators for direct drive marine renewable energy converters*, PhD thesis, University of Durham, 2003.

[26] Willard J. Pierson and Lionel Moskowitz, "A Proposed Spectral Form for Fully Developed Wind Seas Based on the Similarity Theory of S. A. Kitaigorodskii", *Journal of Geophysical Research*, vol. 69, no. 24, pp. 5181–5190, 1964.

[27] Steven W. Smith, *The Scientist & Engineer's Guide to Digital Signal Processing*, California Technical Pub., 1997.

[28] R. H Stewart, "Introduction to Physical Oceanography", *American Journal of Physics*, vol. 65, no. 10, pp. 1028, 1997.

DIRECT DRIVE WAVE ENERGY CONVERTER CONTROL IN IRREGULAR WAVES

B. Li, D.E. Macpherson, and J.K.H. Shek

Institute for Energy Systems, School of Engineering, The University of Edinburgh, UK.
E-mail: B.Li@ed.ac.uk

Keywords: Direct drive, irregular waves, reactive control, power converter

Abstract

This paper describes causal sub-optimal control of a direct drive linear generator to extract the maximum power from real sea conditions without wave prediction. The reaction force required to control the buoy to move in phase with the ocean waves is provided by the linear generator. After determining the power take-off force based on the model of a machine, the required currents from the generator can be obtained. These currents have varying amplitudes and frequencies thus presenting a challenge to traditional Pulse Width Modulation control. In this paper, a continuously varying average voltage method is presented where the average voltage for each switching cycle is determined by pre-calculated duty ratio to meet the required voltages before coming into the power converter. Using Matlab/Simulink, simulated results of the power converter current control are presented.

1 Introduction

Most designs for wave energy converters include a hydraulic (or pneumatic) interface between the wave device and the generator to smooth electricity production. However, this mechanical interface will reduce the power transfer efficiency and the reliability [11]. A direct drive power take-off (PTO) system is an alternative method first adopted by Archimedes Wave Swing (AWS), a commercial company, to achieve higher energy conversion efficiency [13]. A direct-drive wave energy converter normally includes a low speed linear generator directly coupled with the wave device, and a power converter system to interface the variable generator voltage and frequency to the grid. With no mechanical interface, mechanical energy loss is zero and maintenance requirements can be significantly curtailed [6].

Maximum power conversion is achieved by mechanical resonance where the velocity of the generator is in phase with the wave excitation force. The AWS mechanically pumps the water in/out to change the air pressure and volume to achieve resonance. This mechanical reaction is usually very slow so that rapid response control is not able to be carried out [13]. An alternative technique, latching control, was verified by Babarit [1] to be an effective way to control a wave energy converter in both regular and irregular waves; the ratio between power extracted with control and without control in irregular waves can reach approximately 300% when the peak frequency is 0.07Hz. Latching control concentrates on determining the critical moment to lock and unlock the wave energy converter so that wave prediction plays a vital role. As for reaction control, resonance occurs by controlling the effective load impedance to match the complex conjugate of the source impedance [4]. Shek developed linear generator reaction force control in both regular and multi frequency waves [12]. This paper attempts to show how reactive control at the peak frequency of the wave spectrum (referred to here as reactive causal control where causal indicates no future information required) can be applied in irregular waves to extract maximum power. Currents with varying amplitudes and frequencies are controlled to obtain the desired PTO force.

In order to implement the control, the linear generator is connected to a power converter system consisting of back-to-back converters with a common DC rail. In previous work (for regular waves), the rectifier is used to control the phase currents to be in phase with the no-load phase voltage to achieve maximum power transferred from the linear generator to the grid [2], [11]. In this paper, an active rectifier with Pulse Width Modulation (PWM) control is used to set the appropriate reaction force on the buoy such that it moves in resonance with irregular waves, where the frequency and amplitude are continuously varying. Most PWM systems employ either carrier-based PWM or space vector modulation that requires a fixed value of modulation index [14]. However in this application, irregular phase currents are required and need to be controlled, so that the conventional PWM technique is no longer applicable. Hence, a novel continuously varying average voltage method is presented to control the “instantaneous average” voltage to follow the reference average voltage which is obtained by defining the duty ratio for each switching cycle.

2 Reaction Force Control in Irregular Waves

Figure 1 shows the direct drive linear generator with the power converter system. The active front-end rectifier connected directly to the generator controls the reaction force to achieve mechanical resonance. The inverter connected to the grid maintains the DC link voltage to be constant.

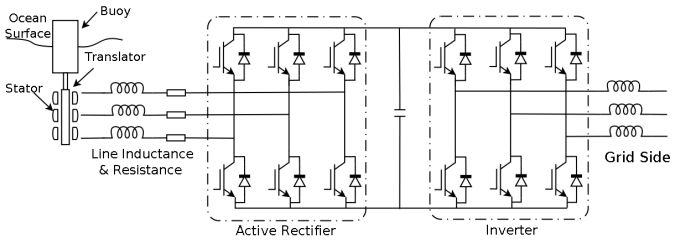

Figure 1: The direct drive linear generator and back-to-back power converter system.

2.1 Control of wave energy converter

In this paper, the wave energy converter is assumed to be a solid semi-immersed body with only one degree of freedom, known as heave. The typical equation of an oscillating system under wave excitation force in the frequency domain is of the form shown in equation (1) [8].

$$F_e(\omega) = i\omega[m + M(\omega)]U(\omega) + B(\omega)U(\omega) + \frac{c}{i\omega}U(\omega) \tag{1}$$

Here, loss between the buoy and the surrounding fluid (drag, viscosity and friction) is not modelled. $F_e(\omega)$ is the wave excitation force, $M(\omega)$ and $B(\omega)$ are the added mass and damping, c is the buoyancy spring stiffness and $U(\omega)$ is the velocity in the frequency domain.

The intrinsic impedance $Z(\omega)$ is expressed in equation (2).

$$Z(\omega) = B(\omega) + i\omega(m + M(\omega)) - i\frac{c}{\omega} \tag{2}$$

To extract maximum power from the waves, the PTO impedance should be equal to the complex conjugate of the intrinsic impedance [3]. As the intrinsic impedance in (2) is a function of frequency, the PTO impedance should vary with the frequency of the waves. Hence, in order to obtain a real-time PTO impedance to apply full optimal control, future information is needed regarding the frequency of the incoming waves. Current technology for wave prediction can be achieved only several seconds into the future and is not very accurate. In this paper, the PTO impedance is calculated by choosing the peak frequency of the incoming waves, which lead to sub-optimal control. According to $Z_{pto}=Z^*(\omega_p)$, the PTO force can be expressed in the time domain as shown in (3), in which PTO force consists of three terms: inertia force (mass term), a damping term and a spring stiffness term.

$$f_{pto}(t) = -(m + M_p)a(t) + B_p u(t) - cx(t) \tag{3}$$

Here, ω_p is angular peak frequency, and M_p and B_p are added mass and added damping at the peak frequency respectively. Hence, the time domain equation of the wave energy converter motion under the PTO force is expressed in (4).

$$f_e(t) = [m + m_\infty]a(t) + \int_0^t k(\tau)u(t-\tau)d\tau + cx(t) + f_{pto}(t) \tag{4}$$

where, m_∞ is the value of added mass at infinite frequency. There is a convolution term, acquired through an Inverse Fourier Transform, which indicates that the system has a memory of the past state. Therefore, it can be interpreted that this is a causal system; where the motion of the wave energy converter is affected by past and present inputs and states. In equation (4), k(t) is an impulse response which depends on the parameters of the floating buoy. A typical impulse response function is chosen as shown in Fig. 2 based on [5], which requires the draft of the buoy to be 1.88 times the buoy's radius.

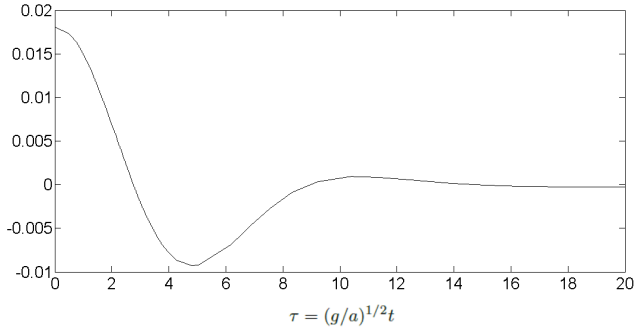

Figure 2: Impulse response function for cylindrical buoy where the scales are dimensionless.

2.2 Linear generator

Several linear generator topologies are available, with no common consensus as to which is the best [7], [9]. The topology chosen here is a linear permanent-magnet (PM) machine. The methods of calculating the electromagnetic force and EMF voltages, shown below, are provided by Polinder in [10]. The specific methods can be applied to other linear electrical machines.

$$EMF = -Nt\frac{\pi}{\tau_p}\Phi\sin\left(\frac{\pi}{\tau_p}\right)\frac{dx}{dt} \tag{5}$$

$$f_{pto} = \frac{3}{2}\cdot\frac{\pi}{\tau_p}N_t\Phi I\cos\varphi \tag{6}$$

The linear generator EMF (one phase) expressed in (5) is a function of the position, where, N_t is the number of turns around a tooth, Φ is the flux in the tooth and τ_p is the pole pitch. The EMFs of the other two phases are shifted by 120 degrees. In (6), the generator reaction force is a function of current I which can be decomposed into three phase current as shown in equation (7).

$$i = -I\sin\left(\frac{\pi}{\tau}x + \varphi\right) \tag{7}$$

The current leads the EMF voltage with an angle φ. i is the phase current in one phase and the other two phase currents are lagging and leading the above phase current by 120 degrees.

3 Current Control

To control the incoming currents and DC link voltage, a power converter which consists of two back-to-back converters with a common DC rail is used. The generator side converter has to be an active rectifier with control algorithm. The conventional PWM method has been studied during the

past decades in most current control schemes. Carrier-based PWM and space-vector PWM are two important methods to compute the duty ratio of the switches. However, both of these methods have to determine the modulation index and phase shift. These parameters are used to form a pre-established template which is used to compare with the triangular carrier to calculate the switching information of the IGBT gates. This template is a sinusoidal voltage or current waveform. Details of carrier-based PWM and space-vector PWM can be found in [14].

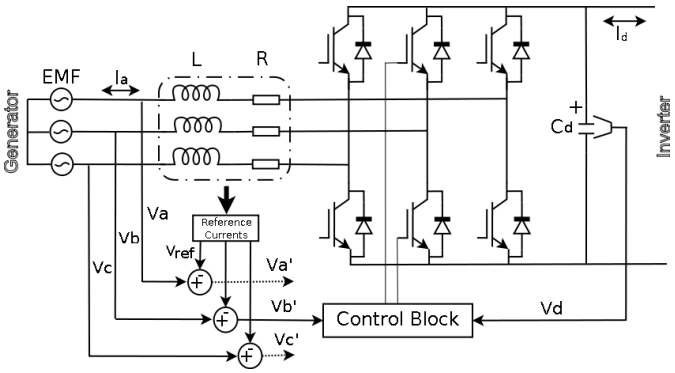

Figure 3: Current control method of active rectifier

As for irregular waves, the variation of amplitude and frequency implies that it is impossible to have a fixed modulation index and phase shift. Hence, a short-term current control method has to be taken into account. After understanding the ideal currents, ideal voltages across the line inductance and resistance can be obtained, such that the required voltages at the midpoint of each leg $v'_i(t)(i=a,b,c)$ can be computed by using the voltages from generator $v_i(t)(i=a,b,c)$ to subtract the voltages across line inductance and resistance which is given in equation (8).

$$v'_i(t) = v_i(t) - L\frac{di_i(t)}{dt} - Ri_i(t) \quad (8)$$

Here, R is the line resistance and L is the line inductance. $i_i(t)(i=a,b,c)$ is phase current.

The whole procedure of current control is illustrated in Fig. 3. No load EMF voltages can be measured directly from the generator. Line inductance and resistance are known beforehand in order to calculate the voltages drop V_{ref} across them. Hence, the desired voltages at the midpoints of all three legs are obtained and fed into the control algorithm. Apart from that DC link voltage is measured and compared with the required voltages of the midpoints to generate control signals.

As stated at the beginning of this section, a conventional PWM method does not work in this situation. In order to control random currents, the duty ratio is still needed and will be determined by a novel continuously varying average voltage method. Figure 4(a) shows the three phase rectifier used to control the currents, and figure 4(b) shows the phase average voltage calculated by applying duty ratio and DC link voltage.

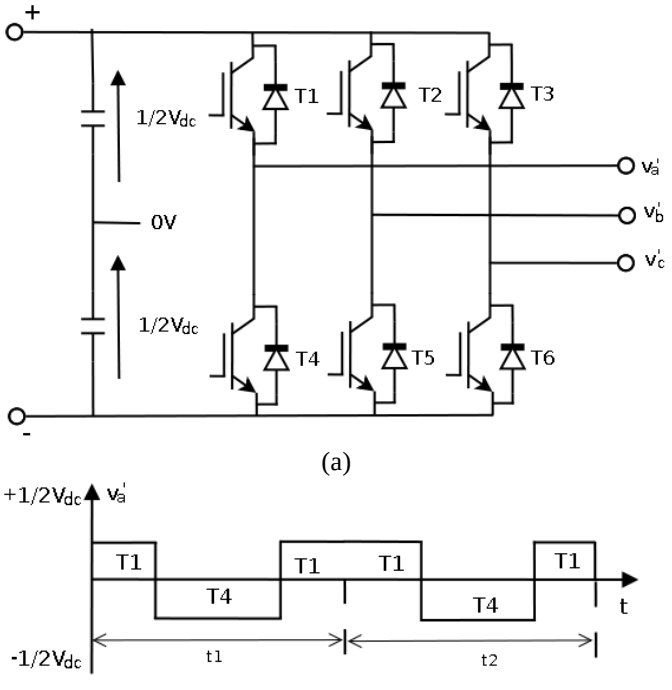

Figure 4: a) Currents control rectifier b) Phase average voltage, v'_a during t1 and t2 switching cycles

In Fig. 4(a), a single DC link capacitor can be represented by two capacitors of equal value for ease of understanding. The mid point is connected to ground to allow the voltage across each of these capacitors to be $V_{dc}/2$. Fig. 4(b) shows the average phase voltage v'_a, which is controlled by the duty ratio, which determines when two switches are on and off. This can be expressed in equation (9).

$$v'_a = \frac{1}{2}V_{dc}\cdot D + (-\frac{1}{2})V_{dc}(1-D) \quad (9)$$

Here, v_a represents phase voltage and D represents the duty ratio of one switching cycle. Equation (9) can be simplified to obtain the relationship between the phase voltage and DC link voltage as shown in equation (10).

$$v'_i(t) = (D-0.5)V_{dc} \quad (10)$$

4 System Model

The whole system can be simply divided into two parts; a mechanical model and an electrical model. Within the electrical model, there is also a generator model and a power electronics model of the power converter. Models of those two parts are designed and linked together in Matlab/Simulink.

In Fig. 5, the wave excitation force is generated in Matlab by applying the Inverse Fourier Transform to the Pierson-Moskowitz (PM) spectrum and importing this into a Simulink model. A hydrodynamic parameters block is used to calculate mass, buoyancy spring stiffness, added mass, added damping and the impulse response. By providing hydrodynamic

parameters to a mass-spring-damper system, acceleration, velocity and displacement of the wave energy converter are obtained. Together with the added mass, added damping and spring stiffness from the hydrodynamic calculation, the ideal PTO force is also obtained. The required PTO force is used in the electrical model to calculate ideal currents based on (6) and (7) and are delivered into the control block to generate control signals. Meanwhile, the EMF voltages are also simulated in the electrical model using the displacement. This paper focuses on active rectifier control, with a DC link voltage that is assumed to be constant. Therefore, a battery is used in the DC link instead of a capacitor to represent that the voltage is constant.

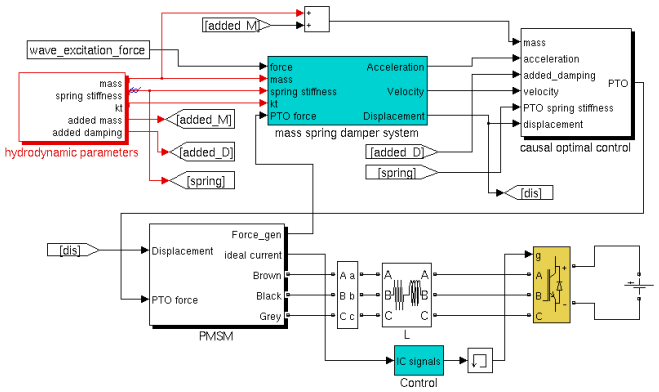

Figure 5: Simulink model for the whole system

The duty ratios of the three phases are the parameters that need to be updated frequently. In other words, the duty ratio will be different for each time period. For controlling currents as accurately as possible, a very short cycle is needed, where tf=4e-4s. Hence, the switching frequency is 2.5kHz. After defining the switching frequency, another frequency which is called here the “judging frequency” has to be determined. This frequency should be much higher than the switching frequency. This is because if a duty ratio has been calculated in one cycle, the judging frequency has to be used to decide when to switch on and when to switch off. Hence, a higher judging frequency can reduce the difference between the calculated value and the simulation value. In addition, if signals are generated to control the IGBTs, controlled voltages will respond in the next time period which we call ‘time delay’. Because this time delay is inevitable, its influence needs to be kept as small as possible which can be achieved by increasing the judging frequency. Hence, another sample time ts=20e-7 is chosen here which could also be considered to be a time delay.

5 Results

The simulation is carried out by assuming that the measurement of the wind speed at the height of 19.5m is known, which is represented by the peak frequency. The wave length is not taken into account so the wave energy capture device can be considered to be a point absorber. Apart from that the wave energy converter is limited to move up and down in a single degree-of-freedom. The cylinder floating buoy has a height 1.88 times that of the radius in order to meet the hydrodynamic requirement.

Fig. 6 shows the velocity of the wave energy converter under the causal sub-optimal control. By inputting the calculated PTO force into the system, the velocity of the wave energy converter moves nearly in phase with the wave excitation force so that a large amount of wave power can be extracted. However, there is still a very small phase difference between them because sub-optimal control is applied rather than optimal control. Meanwhile, other parameters such as displacement and acceleration are also obtained which can be used to calculate the desired PTO force.

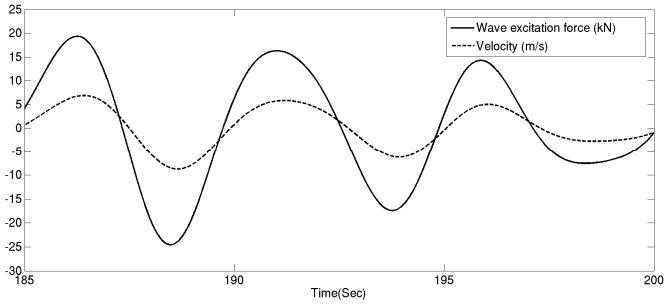

Figure 6: Wave excitation force and its corresponding velocity

As the displacement and ideal PTO force are known, the EMF voltages can be obtained in Fig. 7. It is easy to see that the EMF voltages have different amplitudes and different frequencies as a consequence of random displacement input. Fig. 7 illustrates that the peak voltage for a single phase in the first 200 seconds is around 7000 volts. Hence, the DC link voltage needs to be set to at least double the peak voltage. This can be calculated from equation (10) where the phase voltage is half of the DC link voltage if the duty ratio is 1. It also shows that the cycle with higher peak voltage has higher frequency.

Fig. 8 gives a clear result showing one phase of the controlled current in 8(b) following its corresponding ideal current in 8(a). The amplitude of the ripple is about 10A which depends on the switching frequency and the line inductance. The higher the switching frequency, the better the results can be obtained. However, as the switching frequency increases, the

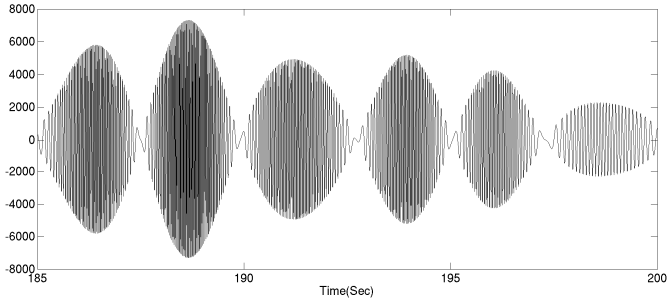

Figure 7: Single phase of EMF voltage

judging frequency also has to increase in order to maintain a small time delay. This creates a large amount of data stored

into the computer memory. In this particular simulation, as the switching frequency is 2.5kHz, the judging frequency is set to be 200 times of the switching frequency; system

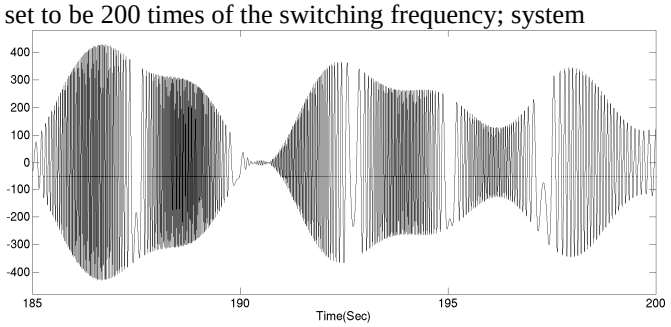

(a)

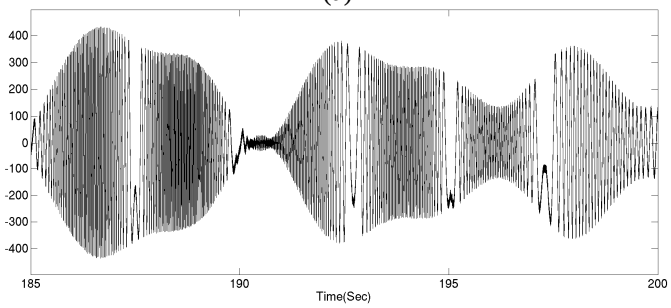

(b)

Figure 8: a) Required current b) Controlled current

memory can only deal with about 15 seconds data. As shown in Fig. 8, all of data before 185 seconds has been deleted. During the period between 185 seconds and 200 seconds, the required current has a peak value of about 400A which implies a big PTO force is generated to control the wave energy converter.

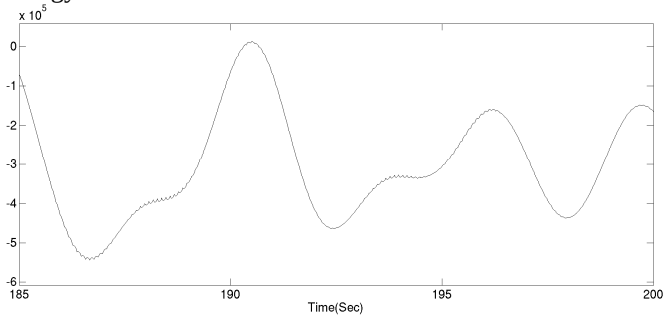

(a)

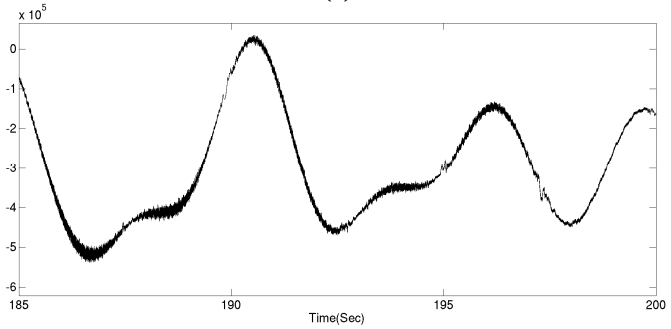

(b)

Figure 9: a) Required PTO force b) Controlled PTO force

Fig. 9 shows that the controlled PTO force follows the required force. In order to complete causal sub-optimal control, a large reaction force is needed that will contribute a huge reactive power production as shown in Fig. 10. The average power and instantaneous power are shown for 200 seconds with the ideal PTO force applied. The instantaneous power produced by the linear generator has a peak value of about 4000kW, whereas the average power is of around 40kW. Therefore, to complete causal sub-optimal control, a large amount of reactive power (100 times the average power extracted) needs to be supplied.

6 Discussion

Although Fig. 6 shows very good results where the velocity of the WEC and the wave excitation force are in phase, there is still a small phase difference when looking closely. This is because the hydrodynamic parameters such as added damping

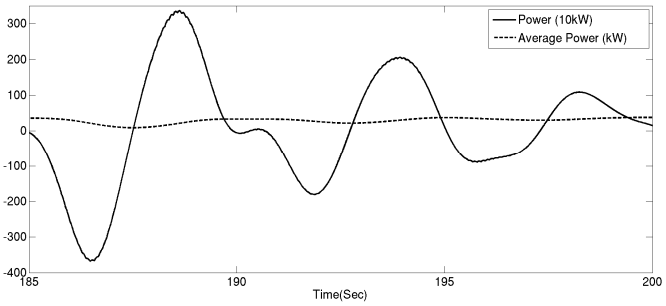

Figure 10: Power production under causal sub-optimal control

and added mass for generating the PTO force are calculated using the peak frequency of the wave spectrum. Such a phase difference can be reduced by applying optimal control, but future information of waves needs to be known beforehand. However, in reality, the phase difference cannot be removed completely; because future wave prediction is not easy to be obtained and is not accurate if indeed it is possible.

In Fig. 7, the period of the EMF voltage depends on the input displacement where one period of the voltage waveform is decided by the time between one wave crest and the adjacent wave trough. Therefore, the frequency of the EMF voltage varies with the frequency of the wave displacement. The amplitude of the EMF voltage varies with the rate of change of the wave displacement which is expressed as dx/dt. In the result, the peak voltage generated is about 7000 volts which requires the DC link voltage to be at least 14000 volts to achieve control. However, modern techniques in power converter manufacture can only sustain a DC link voltage of up to 6000 volts [15]. As shown in Fig. 8, the maximum current used to control the wave energy converter is more than 400A, which is much higher than the linear generator can provide. Hence, both the linear generator and power converter have to be overrated in order to achieve the desired result.

In Fig. 10, a lot of reactive power is needed to control the wave energy converter which is illustrated as negative power, especially when the wave height is large. At the beginning, this huge negative power makes the average power drop to

zero and even to a negative value which means that the power consumed is bigger than power extracted. For the control in regular waves by Shek [8], PTO spring stiffness is calculated and used to maintain the natural frequency of the wave energy converter to meet the wave frequency. Hence, as long as the buoy's natural frequency is designed to be the same as the dominant wave frequency, the PTO spring stiffness can be kept at a very small value, even zero. In addition the PTO spring stiffness is the only reactive force which is used to control the WEC in regular waves, so that reactive power can be reduced and even eliminated. In contrast to regular waves, to control the wave energy converter in irregular waves, the reactive force is made up by two terms which are mass term and spring stiffness term. Both of these two reactive forces consume a huge amount of reactive power. That is why the peak instantaneous power in Fig. 10 can be hundreds of times more than the average power extracted. Moreover, the PTO spring stiffness force equals the physical spring stiffness force, so that the buoy's size can be designed to be smaller in order to reduce the spring stiffness force. However, once the buoy's size is reduced to an acceptable size, the displacement will increase to a value where the buoy is moving out of the water surface. Therefore, future work has to concentrate on displacement limitation of the buoy and force limitation of the generator to prevent overrating of both the linear generator and power converter.

7 Conclusion

The work presented has focused on causal sub-optimal control of a linear generator in irregular waves to extract maximum power, which includes mechanical analysis on the control of the wave energy converter and control algorithm of the electrical power converter. A linear PM machine is applied for modelling, with both EMF voltage and current calculations. The simulation results show that reaction force can be controlled to follow the required PTO force based on the continuously varying average voltage method. Although voltages at the midpoints of all of the three legs are controlled to provide the required currents, the electrical power converter implemented in this paper has to be considerably overrated. In addition, the linear generator in this simulation is assumed to be able to provide overrated currents as well, because of a large reactive force demand. Overrating can be solved by setting a limit for the buoy displacement and linear generator force limitation in future investigation.

Acknowledgements

The first author is financially supported by the SuperGen Marine Energy Research Programme. The authors also like to acknowledge Ally Price, Richard Crozier and David Forehand for their invaluable advice and help.

References

[1] A. Babarit, G. Duclos, and A. Clement, "Comparison of latching control strategies for a heaving wave energy device in random sea," *Applied Ocean Research*, vol. 26, Jul. 2004, pp. 227-238.

[2] P. Brooking. "Power conditioning of the output from a linear vernier hybrid permanent magnet generator for use in direct drive wave energy converters," *Generation, Transmission and*, 2005, pp. 673-681.

[3] D.V. Evans, "A theory for wave-power absorption by oscillating bodies," *Journal of Fluid Mechanics*, vol. 77, Apr. 1976, pp. 1-25.

[4] J. Falnes, "Optimum control of oscillation of wave-energy converters," *International Journal of Offshore and Polar Engineering*, 2002.

[5] J. Falnes, "Ocean waves and oscillating systems," Cambridge University Press, 2002.

[6] R. Henderson, "Design, simulation, and testing of a novel hydraulic power take-off system for the Pelamis wave energy converter," *Renewable Energy*, vol. 31, Feb. 2006, pp.271-283.

[7] M.A. Mueller and N.J. Baker, "Direct drive electrical power take-off for offshore marine energy converters," *Proceedings of the Institution of Mechanical Engineers, Part A: Journal of Power and Energy*, vol. 219, Jan. 2005, pp. 223-234.

[8] A. Price and C. Dent, "Frequency domain techniques for numerical and experimental modelling of wave energy converters," *European Wave and Tidal Energy*, 2009.

[9] H. Polinder, B.C. Mecrow, A.G. Jack, P.G. Dickinson, and M.A. Mueller, "Conventional and TFPM Linear Generators for Direct-Drive Wave Energy Conversion," *IEEE Transactions on Energy Conversion*, vol. 20, Jun. 2005, pp. 260-267.

[10] H. Polinder, J.G. Slootweg, M.J. Hoeijmakers, and J.C. Compter, "Modeling of a linear pm machine including magnetic saturation and end effects: maximum force-to-current ratio," *IEEE Transactions on Industry Applications*, vol. 39, Nov. 2003, pp. 1681-1688.

[11] L. Ran, M.A. Mueller, C. Ng, P.J. Tavner, H. Zhao, N.J. Baker, S. McDonald, and P. McKeever, "Power conversion and control for a linear direct drive permanent magnet generator for wave energy," *IET Renewable Power Generation*, vol. 5, 2011, pp. 1-9.

[12] J.K.H. Shek, D.E. Macpherson, M.A. Mueller, and J. Xiang, "Reaction force control of a linear electrical generator for direct drive wave energy conversion," *IET Renewable Power Generation*, 2007, pp. 17-24.

[13] F. Wu, X.P. Zhang, P. Ju, and M.J.H. Sterling, "Optimal Control for AWS-Based Wave Energy Conversion System," *Power Systems, IEEE Transactions on*, vol. 24, 2009, pp. 1747–1755.

[14] K. Zhou and D. Wang, "Relationship between space-vector modulation and three-phase carrier-based PWM: a comprehensive analysis [three-phase inverters]," *IEEE Transactions on Industrial Electronics*, vol. 49, 2002, pp. 186-196.

[15] AVX High Power Capacitors for Power Electronics, AVX Corporation, pp. 15-22, available online, http://www.avx.com/docs/catalogs/trafim.pdf.

Bibliography

[1] J Falnes. A review of wave-energy extraction. *Marine Structures*, 20(4):185–201, October 2007.

[2] International Energy Agency. World Energy Outlook 2009. Technical report, Technical report, IEA/OECD, Paris, France, 2009.

[3] International Energy Agency. Status and research and development priorities 2003: Wave and marine current energy. *International Energy Agency*.

[4] World Energy Council. Survey of Energy Resources Interim Update 2009. *Energy*, 2009.

[5] J K H Shek. *Reaction Force Control of a Linear Electrical Generator for Direct Drive Wave Energy Conversion*. PhD thesis, 2009.

[6] World Energy Council. 2010 Survey of energy resources. Technical report, 2010.

[7] Sustainable Development. Ocean Energy Conversion in Europe. *Renewable Energy*, 2006.

[8] T.W Thorpe. A brief review of wave energy. (May), 1999.

[9] J. G. Vining and A. Muetze. Economic Factors and Incentives for Ocean Wave Energy Conversion. *2007 IEEE Industry Applications Annual Meeting*, pages 756–763, September 2007.

[10] K. Budar and J. Falnes. A resonant point absorber of ocean-wave power. *Nature*, 256(5517):478–479, 1975.

[11] J Falnes. Optimum control of oscillation of wave-energy converters. *International Journal of Offshore and Polar*, (June), 2002.

[12] R P M Parker, G P Harrison, and J P Chick. Energy and carbon audit of an offshore wave energy converter. *Proceedings of the Institution of Mechanical*

Engineers, Part A: Journal of Power and Energy, 221(8):1119–1130, January 2007.

[13] International Energy Agency. Energy Technology Perspectives. *Energy*, 2010.

[14] G. Dalton and B.P. Ó Gallachóir. Building a wave energy policy focusing on innovation, manufacturing and deployment. *Renewable and Sustainable Energy Reviews*, 14(8):2339–2358, October 2010.

[15] The Scottish Government. THE SALTIRE PRIZE PROGRAMME. Technical Report March, 2010.

[16] Waveplam. Non-technological Barriers to Wave Energy Implementation. (March), 2009.

[17] Lewis Wave Power Limited. Environmental Scoping Report. (May), 2011.

[18] AWS. New Investment for AWS Ocean Energy.

[19] P. Ricci, J. Lopez, M. Santos, P. Ruiz-Minguela, J.L. Villate, F. Salcedo, and A. Falcao. Control strategies for a wave energy converter connected to a hydraulic power take-off. *IET Renewable Power Generation*, 5(3):234, 2011.

[20] A Falcao. Phase control through load control of oscillating-body wave energy converters with hydraulic PTO system. *Ocean Engineering*, 35(3-4):358–366, March 2007.

[21] D. Valério, P. Beirao, MJG Mendes, and J. Sa da Costa. Comparison of control strategies performance for a Wave Energy Converter. In *Control and Automation, 2008 16th Mediterranean Conference on*, pages 773–778. IEEE, 2008.

[22] J Dai, D Xu, and B Wu. A Novel Control Scheme for Current-Source-Converter-Based PMSG Wind Energy Conversion Systems. *IEEE Transactions on Power Electronics*, 24(4):963–972, April 2009.

[23] AAE Price. *New Perspectives on Wave Energy Converter Control*. PhD thesis, 2009.

[24] J Falnes and P M Lillebekken. Budal ' s latching-controlled-buoy type wave-power plant. In *5th European Wave Energy Conference*, pages 233–244, 2003.

[25] A Babarit, G Duclos, and A Clement. Comparison of latching control strategies

for a heaving wave energy device in random sea. *Applied Ocean Research*, 26(5):227–238, July 2004.

[26] A Babarit and A.H Clement. Optimal latching control of a wave energy device in regular and irregular waves. *Applied Ocean Research*, 28(2):77–91, April 2006.

[27] J Falnes. Optimum control of oscillation of wave-energy converters. *International Journal of Offshore and Polar*, (June), 2002.

[28] S H Salter, J R M Taylor, and N J Caldwell. Power conversion mechanisms for wave energy. *Proceedings of the Institution of Mechanical Engineers, Part M: Journal of Engineering for the Maritime Environment*, 216(1):1–27, January 2002.

[29] P Nebel. Maximizing the efficiency of wave-energy plant using complex-conjugate control. *ARCHIVE: Proceedings of the Institution of Mechanical Engineers, Part I: Journal of Systems and Control Engineering 1991-1996 (vols 205-210)*, 206(49):225–236, 1992.

[30] NJ Baker and MA Mueller. Direct drive wave energy converters. *Revue des Energies Renouvelables*, pages 1–7, 2001.

[31] H. Polinder, B.C. Mecrow, A.G. Jack, P.G. Dickinson, and M.A. Mueller. Conventional and TFPM Linear Generators for Direct-Drive Wave Energy Conversion. *IEEE Transactions on Energy Conversion*, 20(2):260–267, June 2005.

[32] M.A. Mueller. Electrical generators for direct drive wave energy converters. *IEE Proceedings - Generation, Transmission and Distribution*, 149(4):446, 2002.

[33] J.K.H. Shek, D.E. Macpherson, M.A. Mueller, and J Xiang. Reaction force control of a linear electrical generator for direct drive wave energy conversion. *IET Renewable Power Generation*, pages 17–24, 2007.

[34] J.K.H. Shek, D.E. Macpherson, and M.A. Mueller. Experimental verification of linear generator control for direct drive wave energy conversion. *IET Renewable Power Generation*, 4(5):395, 2010.

[35] AAE Price and CJ Dent. Frequency domain techniques for numerical and

experimental modelling of wave energy converters. *European wave and tidal energy*, 2009.

[36] R. H Stewart. Introduction to Physical Oceanography. *American Journal of Physics*, 65(10):1028, 1997.

[37] W J. Pierson and L Moskowitz. A Proposed Spectral Form for Fully Developed Wind Seas Based on the Similarity Theory of S. A. Kitaigorodskii. *Journal of Geophysical Research*, 69(24):5181–5190, 1964.

[38] K. Hasselmann, TP Barnett, E. Bouws, H. Carlson, DE Cartwright, K. Enke, JA Ewing, H. Gienapp, DE Hasselmann, P. Kruseman, and Others. Measurements of wind-wave growth and swell decay during the Joint North Sea Wave Project (JONSWAP). *Ergnzungsheft zur Deutschen Hydrographischen Zeitschrift Reihe*, 8(12), 1973.

[39] Qiuying Guo and Zunyi Xu. Simulation of deep-water waves based on JONSWAP spectrum and realization by MATLAB. *Geoinformatics, 2011 19th International . . .*, 22:1–4, 2011.

[40] F.M. Monaldo and R.C. Beal. Real-time observations of Southern Ocean wave fields from the Shuttle Imaging Radar. *IEEE Transactions on Geoscience and Remote Sensing*, 33(4):942–949, July 1995.

[41] R Allard, T Campbell, S Chen, and J Cook. The Navy's coupled atmosphere-ocean-wave prediction system. *OCEANS*, 2010.

[42] J.L Forsber. On-line identification and prediction of waves. *Hydrodynamics of Ocean-Wave Energy Utilization, Berlin*, pages 185–193, 1986.

[43] F Fusco and J Ringwood. A study on short-term sea profile prediction for wave energy applications. 2009.

[44] F Fusco. Short-term wave forecasting with AR models in real-time optimal control of wave energy converters. *ISIE), 2010 IEEE International Symposium on*, pages 2475–2480, 2010.

[45] F Fusco and J V Ringwood. Short-Term Wave Forecasting for Real-Time Control of Wave Energy Converters. *IEEE Transactions on Sustainable Energy*, 1(2):99–106, July 2010.

[46] S.W. Smith. *The Scientist and Engineer's Guide to Digital Signal Processing*. California Technical Pub., 1998.

[47] J.W. Cooley and J.W. Tukey. An algorithm for the machine calculation of complex Fourier series. *Math. Comput*, 19(90):297–301, 1965.

[48] J Twidell. Wind Energy-The Facts. *Wind Engineering*, 1, 2009.

[49] SIEMENS. Siemens to deliver first direct wind turbines in the UK for Community Windpower. Technical Report April 2011, 2011.

[50] L. Ran, M.A. Mueller, C. Ng, P.J. Tavner, H. Zhao, N.J. Baker, S. McDonald, and P. McKeever. Power conversion and control for a linear direct drive permanent magnet generator for wave energy. *IET Renewable Power Generation*, 5(1):1–9, 2011.

[51] H. Polinder, B.C. Mecrow, a.G. Jack, P.G. Dickinson, and M.a. Mueller. Conventional and TFPM Linear Generators for Direct-Drive Wave Energy Conversion. *IEEE Transactions on Energy Conversion*, 20(2):260–267, June 2005.

[52] R Henderson. Design, simulation, and testing of a novel hydraulic power take-off system for the Pelamis wave energy converter. *Renewable Energy*, 31(2):271–283, February 2006.

[53] H. Polinder, M.E.C. Damen, and F. Gardner. Linear PM Generator System for Wave Energy Conversion in the AWS. *IEEE Transactions on Energy Conversion*, 19(3):583–589, September 2004.

[54] http://www.maritimejournal.com/features101/marine-renewable-energy/a_simpler_form_of_wave_power.

[55] P.C.J. Clifton, R.A. McMahon, and H.-P. Kelly. Design and commissioning of a 30 kW direct drive wave generator. *5th IET International Conference on Power Electronics, Machines and Drives (PEMD 2010)*, pages MO245–MO245, 2010.

[56] JRM Taylor and I Mackay. The design of an eddy current dynamometer for a free-floating sloped IPS buoy. In *Marine Renewable Energy Conference (MAREC)*, pages 67–74, 2001.

[57] M A Mueller and N J Baker. Direct drive electrical power take-off for

offshore marine energy converters. *Proceedings of the Institution of Mechanical Engineers, Part A: Journal of Power and Energy*, 219(3):223–234, January 2005.

[58] A.F.O. Falcão. The shoreline OWC wave power plant at the Azores. In *Proc. 4rd European Wave Power Conference*, number December, pages 42–28, 2000.

[59] http://goodcleantech.pcmag.com/news-and-events/279986-mit-to-test-innovative-wave-power-system.

[60] E. Spooner and MA Mueller. *Comparative study of linear generators and hydraulic systems for wave energy conversion.* Harwell Laboratory, Energy Technology Support Unit, 2001.

[61] E Spooner and MA Mueller. Comparative study of linear generators and hydraulic systems for wave energy conversion. 2001.

[62] NJ Baker. *Linear generators for direct drive marine renewable energy converters.* PhD thesis, 2003.

[63] J Lu and W Ma. Research on End Effect of Linear Induction Machine for High-Speed Industrial Transportation. *IEEE Transactions on Plasma Science*, 39(1):116–120, 2011.

[64] M S. Sarma. *Electric Machines Steady-State Theory and Dynamic Performance.* West Publishing Company, second edi edition, 1994.

[65] MR Harris and B.C. Mecrow. Variable reluctance permanent magnet motors for high specific output. In *Electrical Machines and Drives, 1993. Sixth International Conference on (Conf. Publ. No. 376)*, pages 437–442. IET, 1993.

[66] NJ Baker, MA Mueller, and E. Spooner. Permanent magnet air-cored tubular linear generator for marine energy converters. In *Power Electronics, Machines and Drives, 2004.(PEMD 2004). Second International Conference on (Conf. Publ. No. 498)*, volume 2, pages 862–867. IET, 2004.

[67] R Crozier, H Bailey, M Mueller, Ed Spooner, P Mckeever, and A Mcdonald. Hydrodynamic and Electromechanical Simulation of a WEC with a Novel Non-Linear PTO. In *9th European Wave and Tidal Energy Conference*, 2011.

[68] MR Harris, GH Pajooman, and SM Abu Sharkh. The problem of power factor in VRPM (transverse-flux) machines. In *Electrical Machines and Drives, 1997*

Eighth International Conference on (Conf. Publ. No. 444), volume 2004, pages 386–390. IET, 1997.

[69] S Bernet, R Teichmann, A. Zuckerberger, and P.K. Steimer. Comparison of high-power IGBT's and hard-driven GTO's for high-power inverters. *Industry Applications, IEEE Transactions on*, 35(2):487–495, 1999.

[70] J.K.H. Shek, D.E. Macpherson, and M.A. Mueller. Power conversion for wave energy applications. *5th IET International Conference on Power Electronics, Machines and Drives (PEMD 2010)*, pages MO242–MO242, 2010.

[71] PRM Brooking and MA Mueller. Power conditioning of the output from a linear vernier hybrid permanent magnet generator for use in direct drive wave energy converters. *Generation, Transmission and*, pages 673–681, 2005.

[72] K Zhou and D Wang. Relationship between space-vector modulation and three-phase carrier-based PWM: a comprehensive analysis [three-phase inverters]. *IEEE Transactions on Industrial Electronics*, 49(1):186–196, 2002.

[73] Johannes Falnes. *Ocean waves and oscillating systems.* Cambridge University Press, 2002.

[74] G. Payne. Guidance for the experimental tank testing of wave energy converters. *supergen-marine.org.uk*, 2008.

[75] G Thomas. Dimensional analysis applied to electricity and mechanics. *Physics Education*, 14(2):116, March 1979.

[76] H Eidsmoen. Hydrodynamic parameters for a two-body axisymmetric system. *Applied Ocean Research*, 17(2):103–115, 1995.

[77] J Falnes. On non-causal impulse response functions related to propagating water waves. *Applied Ocean Research*, 17(6):379–389, December 1995.

[78] http://www.wamit.com/.

[79] MP Schoen, J Hals, and Torgeir Moan. Wave prediction and fuzzy logic control of wave energy converters in irregular waves. *Control and Automation, 2008*, pages 767–772, 2008.

[80] M P. Schoen, J Hals, and T Moan. Robust control of heaving wave energy

devices in irregular waves. *2008 16th Mediterranean Conference on Control and Automation*, (1):779–784, June 2008.

[81] M.F.P. Lopes, J. Hals, R.P.F. Gomes, T. Moan, L.M.C. Gato, and A.F.de O. Falcão. Experimental and numerical investigation of non-predictive phase-control strategies for a point-absorbing wave energy converter. *Ocean Engineering*, 36(5):386–402, April 2009.

[82] A.A.E. Price, C.J. Dent, and A.R. Wallace. On the capture width of wave energy converters. *Applied Ocean Research*, 31(4):251–259, October 2009.

[83] H. Eidsmoen and I Fysikk, N. *Simulation of a tight-moored amplitude-limited heaving-buoy wave-energy converter with phase control.* Division of Physics, Norwegian University of Science and Technology, 1996.

[84] J Hals, J Falnes, and T Moan. Constrained Optimal Control of a Heaving Buoy Wave-Energy Converter. *Journal of Offshore Mechanics and Arctic Engineering*, 133(1):011401, 2011.

[85] K Budal and J Falnes. A system for the conversion of sea wave energy. *British Patent No. 1522661*, 1978.

[86] J Falnes and K Budal. Wave power conversion by point absorber. *Norwegian Maritime Research*, 6, No.4:2–11, 1976.

[87] K Budal and J Falnes. Interacting point absorbers with controlled motion. In *Power From Sea Waves*, pages 381–399. Academic Press London, 1980.

[88] M Greenhow. Optimal heave motion of some axisymmetric wave energy devices in sinusoidal waves. *Applied Ocean Research*, 19(3-4):141–159, August 1997.

[89] A. Babarit, G. Duclos, and A.H. Clément. Comparison of latching control strategies for a heaving wave energy device in random sea. *Applied Ocean Research*, 26(5):227–238, July 2004.

[90] D Valério, J.G.C. Mendes, M, P Beirão, and J Sá da C. Identification and control of the AWS using neural network models. *Applied Ocean Research*, 30(3):178–188, July 2008.

[91] M Liserre and M Molinas. Overview of multi-MW wind turbines and wind parks. , *IEEE Transactions on*, 58(4):1081–1095, 2011.

[92] F. Blaabjerg and M. Liserre. Power electronics converters for wind turbine systems. *Energy Conversion Congress*, pages 281–290, September 2011.

[93] Z Nie, P C. J. Clifton, and R A. McMahon. Emulation and power conditioning of outputs from a Direct Drive Wave Energy Converter. *2008 IEEE International Conference on Sustainable Energy Technologies*, pages 1129–1133, November 2008.

[94] M Molinas, O Skjervheim, P Andreasen, T Undeland, J Hals, T Moan, and B Sorby. Power electronics as grid interface for actively controlled wave energy converters. *2007 International Conference on Clean Electrical Power*, pages 188–195, May 2007.

[95] J R Rodríguez, J W Dixon, J R Espinoza, J Pontt, and P Lezana. PWM Regenerative Rectifiers : State of the Art. *Power*, 52(1):5–22, 2005.

[96] A Faulstich and JK Stinke. Medium voltage converter for permanent magnet wind power generators up to 5 MW. *Power Electronics and*, pages 1–9, 2005.

[97] CH Ng, MA Parker, Li Ran, and PJ Tavner. A multilevel modular converter for a large, light weight wind turbine generator. *Power Electronics,*, 23(3):1062–1074, 2008.

[98] E Pepa. *Adaptive control of a step-up full-bridge DC-DC converter for variable low input voltage applications.* PhD thesis, 2004.

[99] Y Xiao, B Wu, and SC Rizzo. A novel power factor control scheme for high-power GTO current-source converter. , *IEEE Transactions on*, 34(6):1278–1283, 1998.

[100] H. Polinder, J.G. Slootweg, M.J. Hoeijmakers, and J.C. Compter. Modeling of a linear pm machine including magnetic saturation and end effects: maximum force-to-current ratio. *IEEE Transactions on Industry Applications*, 39(6):1681–1688, November 2003.